

UNIVERSITÀ
DEGLI STUDI
DI TORINO

Doctoral Dissertation
Doctoral Program in Bioengineering and Medical-Surgical Sciences (30th Cycle)

Nonlinear and factorization methods for the non-invasive investigation of the central nervous system

Daniele Rimini

* * * * * *

Supervisor
Prof. Marco Knaflitz

Doctoral Examination Committee:
Prof. Sandro Fioretti, Referee, Università Politecnica delle Marche
Prof. Simona Ferrante, Referee, Politecnico di Milano

Politecnico di Torino
2018

Declaration

I hereby declare that, the contents and organization of this dissertation constitute my own original work and does not compromise in any way the rights of third parties, including those relating to the security of personal data.

Daniele Rimini

2018

* This dissertation is presented in partial fulfillment of the requirements for Ph.D. degree in the Graduate School of Politecnico di Torino (ScuDo).

In loving memory of my father

Acknowledgment

First and foremost, I would like to thank my supervisor, Prof. Marco Knaflitz, for his insight and guidance during time I spent at Politecnico di Torino. I am grateful for his insightful teachings, his dedication to my work, and for his helpfulness in all the moments. I would also like to thank Prof. Valentina Agostini for supporting me in experiments and for helping me at every stage of my PhD.

I am grateful to Prof. Filippo Molinari and dr. William Liboni, for their guidance and for these years of fruitful collaboration.

I would like to thank all my colleagues at Biolab, professors and students: in these years, I have learned a lot from all of them.

I acknowledge physiotherapists at San Camillo Hospital in Turin, particularly dr. Marco Trucco, and the Società Italiana di Ossigeno-Ozono Terapia (SIOOT), particularly dr. Vincenzo Simonetti, for their collaboration.

I would like to acknowledge Fondazione San Paolo di Torino for the financial support.

Last but not least, I remain indebted to my beloved family and friends for sustaining me always, in good as well as hard moments.

Abstract

This thesis focuses on the functional study of the Central Nervous System (CNS) with non-invasive techniques. The work focuses on two different aspects: nonlinear aspects of the cerebrovascular system, and the muscle synergies model to describe motor control strategies. The main objective of this thesis is to propose novel protocols, post-processing procedures or indices to enhance the analysis of cerebrovascular system and human motion analysis with noninvasive devices or wearable sensors in clinics and rehabilitation.

One the one hand, we investigated cerebrovascular system with nonlinear methods. Some physiological systems are characterized by nonlinearity: for instance, neurovascular coupling showed nonlinearity between excitatory and inhibitory neuronal processes, due to the many feedback circuits of circulatory system. Near-infrared Spectroscopy (NIRS) was adopted as a method of measuring blood oxygenation at the level of microcirculation, whose modification reflects cerebrovascular response to neuronal activation. NIRS signal is nonlinear and nonstationary. Indeed, it describes nonlinear phenomena and it is characterized by time-varying chromophore concentration. We adopted Empirical Mode Decomposition (EMD) to decompose signal into a finite number of simple functions, called Intrinsic Mode Functions (IMF). For each IMF, we computed entropy-based features to characterize signal complexity and variability. Nonlinear features of the cerebrovascular response were employed to characterize two different kind of treatments: psychotherapy and ozonetherapy. As for the psychotherapy, we administered eye movement desensitization and reprocessing (EMDR) and we compared two groups of patients suffering by post-traumatic stress disorder: the first group performed therapy with eye movements, the second without. NIRS analysis with EMD and entropy based features revealed a different cerebrovascular pattern between the two groups, that may indicate the efficacy of the psychotherapy administered with eye movements. Secondly, we administered ozone autohemotherapy to two groups of subjects: healthy subjects and a group of patients suffering by multiple sclerosis (MS). We monitored the microcirculation with NIRS from oxygen-ozone injection up 1.5 hours after therapy, and 24 hours after therapy. We observed that, after 1.5 hours after the ozonetherapy, oxygenation levels improved in both groups, that may indicate that ozonetherapy reduced oxidative stress level in MS patients. Furthermore, we observed that, after

ozonetherapy, autoregulation improved in both groups, and that the beneficial effects of ozonetherapy persisted up to 24 hours after the treatment in MS patients.

On the other hand, we investigated how CNS controls musculoskeletal system. Due to the complexity of musculoskeletal system, CNS adopts strategies to control efficient execution of motor tasks. A model of motor control are muscle synergies, defined as functional groups of muscles recruited by a unique central command. Human locomotion was the object of investigation, due to its importance for daily life and the cyclicity of the movement. Firstly, by exploiting features provided from statistical gait analysis, we investigated consistency of muscle synergies in human locomotion. We demonstrated that synergies are highly repeatable within-subjects. Our results reinforce the hypothesis of modular control in human motor performance. Secondly, in locomotion, we distinguish principal from secondary activations of electromyography. Principal activations are necessary for the generation of the movement. Secondary activations generate supplement and non-necessary movements, for instance slight balance correction. We investigated the difference in the motor control strategies underlying muscle synergies of principal (PS) and secondary (SS) activations. We found that PS and SS are different in terms of muscle weights vector, activation signal, and consistency. PS are constituted by a few modules with many muscles each; SS are described by many modules, between eight and ten for each subject, with one or two muscles each. Furthermore, amplitude of activation signals of PS is higher than SS. Finally, both weight vectors and activation signals of PS are more consistent and flexible than SS. Our results demonstrated that muscle synergies, which reflect motor control, vary according to the task. Finally, muscle synergies were adopted to investigate the efficacy of rehabilitation of stiffed-leg walking in lower back pain (LBP). A pilot study was conducted in San Camillo Hospital, Torino. We recruited a group of patients suffering from non-specific LBP stiffening the leg at initial contact. Muscle synergies during gait were extracted before and after rehabilitation. Our results showed that muscles recruitment and consistency of synergies improved after the treatment, showing that the rehabilitation may affect motor control strategies.

Contents

List of Tables vii

List of Figures ix

1. Introduction 1

1.1 Aims of the work 1

1.2 Thesis organization 3

Part I 5

2. Background: NIRS fundamentals and the prefrontal cortex 7

2.1 Introduction 7

2.2 NIRS Fundamentals 7

2.3 Measurements principles 10

2.4 The prefrontal cortex 13

3. Empirical mode decomposition and entropy-based metrics 17

3.1 Introduction 17

3.2 Empirical mode decomposition 18

3.2.1 Traditional EMD 18

3.2.2 Alternative EMD algorithms 21

3.3 Entropy and entropy-based features 25

3.3.1 Shannon entropy 25

3.3.2 Sample Entropy 25

3.3.3 Fuzzy Entropy 27

3.3.4 Permutation Entropy 30

3.3.5 Hurst Exponent 31

4. Effect of Ocular Movements During Eye Movement Desensitization and Reprocessing (EMDR) Therapy: a Near-Infrared Spectroscopy Study 33

4.1 Introduction 33
4.2 Material and Methods 35
4.2.1 Patients recruitment 35
4.2.2 EMDR Protocol 36
4.2.3 NIRS data recording 38
4.2.4 Data analysis 39
4.2.5 Statistical analysis 41
4.3 Results 43
4.3.1 wEM – woEM angular coefficients 45
4.3.2 wEM – woEM percentage of positive angular coefficients 46
4.3.3 Unsupervised analysis - PCA 47
4.3.4 Supervised analysis – MANOVA 51
4.4 Discussion 53
4.5 Conclusion 54
5. Cerebrovascular pattern improved by ozone autohemotherapy: an entropy-based study on multiple sclerosis patients 55
5.1 Introduction 55
5.1.1 General overview of ozone therapy 55
5.1.2 The action of ozone on microcirculation pathologies 57
5.1.3 Ozone therapy in the multiple sclerosis 57
5.2 Material and methods 59
5.2.1 Patients demographics 59
5.2.2 Experimental protocol 60
5.2.3 Primary end-point: effect of ozone autohemotherapy on cerebral patterns 60
5.2.4 Secondary end-point: short- and long-term effects of ozone on cerebral autoregulation 64
5.2.5 Statistical Analysis 65
5.3 Results 65

5.3.1 Time Changes in Brain Oxygenation....65
5.3.2 Frequency Changes in NIRS Signals....68
5.3.3 Signals' entropy and HE changes....70
5.3.4 24 hours monitoring....74
5.4 Discussion....75
5.4.1 Primary end-point: effect of ozone autohemotherapy on cerebral patterns....76
5.4.2 Secondary end-point: 24-hours effects of ozone on cerebral autoregulation....79
5.4.3 Study limitations and further perspectives....79
5.5 Conclusion....80
Part II....81
6. Background: from motor control problem to the muscle synergies definition 83
6.1 The motor control problem....83
6.2 The equilibrium point hypothesis and spinal force fields....84
6.3 Spinal motor modules and muscle synergies....87
7. Muscle synergies extraction method....93
7.1 Blind source separation....93
7.2 Basic Nonnegative Matrix Factorization algorithm....95
7.3 Checking the quality of muscle synergies: the VAF criterion....96
7.4 Application of NMF to extract muscle synergies....97
8. Muscle synergies during locomotion: consistency of muscle weights and activation signals....101
8.1 Introduction....101
8.2 Material and Methods....103
8.2.1 Subjects....103
8.2.2 Recording system and signal acquisition....103
8.2.3 Statistical gait analysis....105

8.2.4 Muscle synergies extraction....107
8.2.5 Synergy consistency....108
8.2.6 Shared muscle synergies....110
8.2.7 Data analysis....110
8.3 Results....111
8.3.1 Number of extracted muscles synergies and analysis of synergy consistency....112
8.3.2 Shared motor functions and their muscle synergies consistency..114
8.3.3 Characteristic subject-specific synergies....117
8.4 Discussion....119
8.4.1 Methodological observations....119
8.4.2 Five motor functions: coherence with literature and biomechanics....120
8.4.3 Consistency of shared and subject-specific muscle synergies....120
8.5 Conclusion....121
9. Muscle synergies of principal and secondary activations during gait....123
9.1 Introduction....123
9.2 Material and methods....124
9.2.1 Principal and secondary activations algorithm....124
9.2.2 Data analysis....129
9.3 Results....131
9.3.1 Muscle synergies of a representative subject....131
9.3.2 Number of synergies and reconstruction VAF....137
9.3.3 Number of muscles within synergies....137
9.3.4 Synergies flexibility and consistency....138
9.4 Discussion....139
9.5 Conclusion....141
10. Clinical cases of muscle synergies analysis in lower back pain patients after one-month physiotherapy rehabilitation....143

10.1 Introduction 143
10.2 Material and methods 145
10.2.1 Participants and experimental setup.....145
10.2.2 Enrollment 146
10.2.3 Physiotherapy protocol 147
10.2.4 Muscle synergies.....148
10.2.5 Data analysis 149
10.3 Results 151
10.3.1 Enrollment 151
10.3.2 Rehabilitation.....152
10.3.3 Muscle synergies.....154
10.4 Discussion.....159
10.5 Conclusion.....161
11. Conclusions.....163
12. References.....167

List of Tables

Table 4-I. VOC and initial and final SUD for wEM and woEM patients. P is the significance of the Wilcoxon signed rank test between the scores at the beginning and at the end of the therapy. *: P<0.05 43

Table 4-II. Summary demographic data. Trauma severity has been categorized as low (t) or severe (T).....44

Table 4-III. two-sample t-test of mean percentage of positive slopes of wEM and woEM groups.....46

Table 4-IV. Significant variables after ANOVA analysis. R stands for right hemisphere, L stands for Left hemisphere.....48

Table 4-V. T-test comparing the scores of the Component 1 and Component 2 of wEM vs woEM groups in pre-RECALL and RECALL periods. The significance threshold is 0.05. First component significantly separates wEM from woEM subjects in both pre-RECALL and RECALL periods. Data are reported as mean ± standard deviation. 49

Table 4-VI. Most significant variables after Wilk's Lambda analysis. The values of the variables are reported as mean ± standard deviation. In variable names, R stands for right, L stands for left hemispheres. 51

Table 5-I. Relative concentration of O_2Hb and HHb in the analysis windows. The first window (baseline) is taken as reference.....68

Table 5-II. Relative power in the LF band for the O2Hb and HHb signals in the analysis windows. 69

Table 5-III. Numerical values of the three most discriminant features in the 1st, 4th, and 7th analysis windows. The first three rows are relative to controls, the

bottom three rows to the MS patients. Increasing values of sample entropy and decreasing values of the Hurst exponent are observable. * : $p < 0.05$.....72

Table 8-I. Cosine similarity for the weights and cross-correlation coefficients for the activation signals for the five shared muscle synergies. Data are reported as mean ± standard deviation. 117

Table 8-II. Intra-subject consistency of muscle weights and activation signals across subgroups of GCs, principal muscles recruited, and biomechanical functions of the subject-specific muscle synergies. Data are reported as mean ± standard deviation.....118

Table 9-I. Number of synergies according to the number of dominant muscles for PS and SS modalities. Data are reported as mean ± standard deviation. 137

Table 10-I. Results of the knee joint kinematic of the patients investigated during enrollment stage. Each subject is labelled progressively from S1 to S8. For each subject, the following parameters are reported: angle at initial contact (a_i), peak angle at first knee extension (a_p), knee excursion at first extension (a_p - a_i), and knee range of motion (ROM). In last column, it is reported if the subject met the threshold criteria to be enrolled in the following stages.....152

Table 10-II. Results of the physiotherapy tests adopted to evaluate patients in pre-treatment and post-treatment phases. 152

Table 10-III. Gait parameters obtained from gait analysis before and after rehabilitative treatment. 154

Table 10-IV. P-values for the Wilcoxon rank sum test for VAF pre-treatment vs. post-treatment when 3 to 8 synergies are adopted to reconstruct original EMG signal.....155

Table 10-V. Wilcoxon rank sum test p-values for CS pre- and post-treatment. 158

List of Figures

Figure 2-1. Absorption spectra of oxygenated (red) and deoxygenated (blue) hemoglobin in the infrared bandwidth. 9

Figure 2-2. Schematic representation of three NIRS acquisition modalities: (A) Continuous wave, (B) Time resolved, and (C) Frequency resolved (from Bakker et al., 2012). 11

Figure 3-1. EMD decomposition process. For a nonlinear signal x(t) (black line) the maxima (blue dots) and minima (green dots) are computed. The envelop of maxima (dotted blue line) and the envelop of minima (dotted green line) are computed with a cubic spline. Finally, the mean of the envelopes (m(t), red line) is subtracted to x(t) to obtain the first IMF. 20

Figure 3-2. First IMF for the signal showed in Figure 3-1. It can be observed that the slow frequencies trend has been removed. 20

Figure 3-3. Adaptive EMD of a strongly nonlinear signal. (A) Original signal obtained from the superposition of a chirp signal and a linear trend. (B) and (C). The IMFs with the separate signals. 24

Figure 3-4. A generic time series of N points for the computation of SampEn for m=2 and a generic positive value r. Dotted horizontal lines indicate distance r around data points h(1), h(2), and h(3). Two data points of the time series match if the absolute distance between them is lower than r. Black filled dots represent data point matching with h(1). Similarly, red and green points match with h(2) and h(3) respectively. Consider the two components sequence (h(1), h(2)) and the three components sequence (h(1), h(2), h(3)). There are 4 sequences matching with sequence (h(1), h(2)), and three sequences matching with sequence (h(1), h(2), h(3)). Then, the number of matching sequences is repeated for the next two-components sequence (h(2), h(3)) and three components (h(2), h(3), h(4)). The calculation is repeated for the next N-m+1 sequences to compute the ratio between the number of two components sequences and the three components sequences. The negative natural logarithm of this ratio provides the SampEn of the time series. It

indicates the probability that sequences that match each other for the first two data points will also match for the next point. (Modified from Costa, 2005). 27

Figure 3-5. Exponential fuzzy function with different parameter choices. (a) Exponential function with fixed n=2 and r varying in the range 0.1-0.3. (b) Exponential function with fixed r = 0.2 and n varying between 1 and 5. For a certain distance between two vectors d, a value between 0 and 1 is given according to an exponential symmetric curve (from Chen 2007). 30

Figure 4-1. NIRS probes placement on patient forehead. Detectors are placed medially with respect to emitters. Detectors are placed 2 cm away from midline and 1 cm from supraorbital ridge. 38

Figure 4-2. Right hemisphere O_2Hb and HHb slopes for pre-RECALL and RECALL. Subjects are numbered from 1 to 10 for wEM group and from 1 to 9 for woEM group. Data are reported as mean ± standard error. 45

Figure 4-3. Mean percentage of positive angular coefficients of O_2Hb (A) and HHb (B) in pre-RECALL and RECALL periods for wEM and woEM groups. * : $P < 0.05$. Data are reported as mean ± standard error. 47

Figure 4-4. Eigenvalues applied to the dataset consisting of 6 variables for pre-RECALL (left panel) and RECALL (right panel) summarized in Table IV. The first two eigenvalues are higher than 1 (horizontal filled line). Therefore, these two eigenvalues were adopted to represent the subjects in a reduced domain of two principal components. 48

Figure 4-5. PCA representation of the subjects in the hyperplane of principal components 1 and 2. Top panel: pre-RECALL. Bottom panel: RECALL. White circles represent wEM subjects, black circles those in the woEM group. The black lines represent the projection of the original variables in the hyperplanes. In variable names, R stands for right hemisphere, L stands for Left hemisphere. 50

Figure 4-6. Representation of the subjects in the hyperplane of the first and second Canonical Variables. Upper panel shows the pre-RECALL periods, bottom panel represents the RECALL periods. The subjects of wEM group are represented with white markers. The subjects of the woEM group are represented with black markers. One Canonical Variable well separates the two groups. 52

Figure 5-1. (A) Time course of the concentration of O_2Hb during baseline. (B) CW transform of the signal. The gray zone represents the LF band. The gray rectangle depicts the LF band. (C) Corresponding instantaneous SE derived from

the CW transform. The time course of the SE was averaged to compute a single value for each signal. 63

Figure 5-2. Boxplot showing the time evolution of the average concentration of O_2Hb (A) and HHb (B) in the seven analysis windows. All the values are normalized and scaled w.r.t. the first window. Controls are depicted in white, MS patients in gray. +: outlier values. 67

Figure 5-3. Changes in the power associated to the LF band compared to the overall signal power. Controls are depicted in gray, MS patients in white. The vertical bars superimposed to the histogram represent the standard error. (A) Power in the LF band for the O_2Hb. (B) Power in the LF band for the HHb. +: outlier values. 69

Figure 5-4. Results of the empirical mode decomposition applied to the HHb signal acquired in baseline conditions (A) and at the end of the monitoring (B) from a MS subject. The upper panels report the HHb time course; then the three IMFs are depicted. It can be observed that in panel (B) the IMFs are characterized by random bursts and changes, which make the signals less predictable. 72

Figure 5-5. Representation of the MANOVA analysis for the subjects in three windows during therapy: (A) baseline (window 1); (B) end of the blood reinfusion (window 4); (C) end of monitoring (window 7). Controls are represented by white squares, MS patients by black circles. In (A) the subjects belong to two different groups ($p = 1.9 \cdot 10\text{-}4$), whereas in (B) and (C) the hypothesis that the subjects belong to the same group cannot be rejected ($p > 0.5$). 73

Figure 5-6. BHI values for O_2Hb (top) and HHb (bottom) for Control and SM-RR groups. BHI has been computed at three different time points: at the beginning of therapy (BHI_0), 1.5 hours after reinjection ($BHI_{1.5\text{-hours}}$), and 24 hours after therapy ($BHI_{24\text{-hours}}$). 75

Figure 6-1. Fields of static forces associated with electrical stimulation of a spinal cord site in a deafferented frog. Forces were measured for different hindlimb's positions at the ankle level in two conditions: at resting state and after electrical stimulation of the spinal cord. (a) spatial locations of force recording; (b) force vector fields. Each arrow represents the vectoral summation between force vectors at resting state and after electrical stimulation condition respectively. It can be observed that vectors point towards an equilibrium-point (black filled dot) (from Bizzi et al., 2002). 86

Figure 6-2. Linear superposition of electric fields of stimulation in frog's spinal cord for two couples of muscles. (Left) stimulus of sartorius (SA) and gastrocnemius (GA)(upper); co-stimulation of SA and GA (&) and vector sum (+). (Right) Stimulation of Vastus intermedius (VI) and GA (upper); co-stimulation of VI and GA (&) and vector sum (+). It can be observed that co-stimulation electric fields are the linear combination of the stimulation of the single muscles. (Copyright 1994 National Academy of Sciences).....87

Figure 6-3. A schematic representation of motor patterns generation. Telencephalon and brain stem neural circuitry generate activation signals, and are continuously modulated by sensory and proprioceptive feedbacks. Supraspinal signals are sent to neuronal circuitry in the spinal cord to generate movement. CPGs generate rhythmic signals modulating motoneurons signaling on effector muscles. Interneurons are cyclically influenced by the CPG but are not part of the rhythm generation process itself of the CPG. Spinal circuitry is modulated by feedback information coming from proprioceptive and cutaneous reflex systems. F= flexor, E=extensor. (from Rossignol et al., 2006).....89

Figure 6-4. Scheme of muscle synergies formation for human locomotion. Supraspinal descending commands recruit motor modules, located at spinal level. From the combination of the motor modules with descending commands, the muscle synergies are generated. In this example, four motor modules are recruited to form four muscle synergies to describe motor subtasks of gait cycle. Individual muscle activations, recorded by EMG, are given by the linear combination of the four muscle synergies. In this manner, biomechanics behavior is fully described by nervous systems elements (from Ting et al., 2015). 91

Figure 7-1. Scheme of a BSS system. Observations [$y_1(t)$, $y_2(t)$,…, $y_I(t)$] are the output of a mixing system where the source signals [$x_1(t)$, $x_2(t)$,…, $x_J(t)$] are unknown.....94

Figure 7-2. A schematic representation of NMF decomposition. A source matrix V, of dimensions m×t, is decomposed as a combination of non-negative matrices W, of dimension m×n, and H, of dimension n×t.....95

Figure 7-3. Example of muscle synergies extraction. Reported data are taken from 3 gait cycles of a representative healthy subject. (A) Original EMG for 12 muscles of the lower limb and the trunk after preprocessing (filtering, rectification, envelop). (B) Muscle synergies obtained with NMF. Muscle synergies are a linear combination of non-negative vectors of muscle weightings and activation signals. The number of synergies can vary from 1 to the number of muscles. In this case,

muscle synergies are computer for 3,4, and 5 set of synergies. (C) For each synergy, the Variance Accounted For (VAF) measures the correlation between original EMG and data obtained from synergies (reconstructed EMG). In this case, 5 synergies reconstruct original EMG with a VAF>90%. (D) Superposition of original EMG (Black line) and reconstructed EMG with 3, 4, and 5 synergies. 99

Figure 8-1. EMG probes positioning in lower limb and trunk.....104

Figure 8-2. Schematic representation of the walking path. Subjects walked from point A to point B at their natural pace, then turned back and proceeded in the opposite direction.....105

Figure 8-3. Scheme of HFPS foot switches signals sequence. (A): the timing of foot switches is reported for the gait phases. A black dotted circle indicates the switch is closed. (B): the four-levels signal obtained by the configurations of foot-switches. In the stance phase can be recorded three sub-phases, that are Heel-contact, Flat foot contact, and Push off. 106

Figure 8-4. Scheme of the entire experimental processing, from data acquisition to muscle synergies parameters extraction. 110

Figure 8-5. Onset/Offset EMG activation intervals of the tibialis anterior of a representative subject relative to 163 GCs of her walking trial. In each row, the black bars represent the EMG activation intervals within stride. 112

Figure 8-6. Number of synergies satisfying the VAF > 90% criterion of each subgroup of GCs for a representative subject. 113

Figure 8-7. Analysis of the consistency of muscle synergies in a representative subject. (A) Muscle synergy weights: each bar represents weights of a subgroup of 10 concatenated GCs. The black line represents the average across bars. (B) Muscle synergy activation signals: each line represents activation signal of a subgroup of 10 concatenated GCs. (C) Cosine Similarity for the weights of each synergy. (D) Cross-Correlation coefficient for the activation signals of each synergy. Data are reported as mean ± standard error of the mean. 114

Figure 8-8. Weights (left) and coefficients (right) of the common muscle synergies across subjects. Muscle labels are reported below the weight plots. Data are reported as mean ± standard deviation. 116

Figure 9-1. Results of CIMAP clustering algorithm for tibialis anterior muscle of a representative subject. Each grey bar represents the activation interval in percent of GC. Activation intervals are clustered according to number and duration of onset/offset intervals. Principal activations (green bar) are those common to all

clusters prototypes extracted with the CIMAP algorithm, while secondary activations (red bar) are those present only in a subset of clusters. 126

Figure 9-2. Example of activation masks applied to the EMG of a representative GC. The mask for original (blue line, panel A), principal activations (green line, panel B), and secondary activations (red line, panel C), are superimposed to the EMG of the tibialis anterior. Black line represents the EMG included in the mask, grey line represents the EMG excluded for the specified activation modality. ...128

Figure 9-3. Muscle weights and activation signals for a representative subject. (A) muscle synergies obtained from original EMG signal. (B) muscle synergies obtained after principal activations processing. Black lines represent mean weights across subgroups of GCs.....133

Figure 9-4. Secondary activations muscle synergies for a representative subject. One to two muscles are recruited within each muscle weight vector (Left), and activation signal have low amplitude (Right). Black lines represent mean weights across subgroups of GCs.....134

Figure 9-5. Muscle synergies consistency measurements for the representative subject. For the muscle weights, it has been adopted cosine similarity (Left panel), while for the activation signals it has been adopted zero lag cross-correlation (Right panel). Consistency measurements have been reported for OS (A), PS (B), and SS (C) Data are reported as mean ± standard error. Each bar represents the mean consistency measurement between the same synergy of all subgroups of GCs. Measures have been labeled according to the muscle weights vectors or activation signals (Figure 9-3 and Figure 9-4). 136

Figure 9-6. Within-subject cross-VAF for synergies obtained from original EMG (OS), principal activation (PS), and secondary activation (SS). +: outlier subject. 138

Figure 10-1. Flow chart of the study. At each stage, n patients were analyzed. 145

Figure 10-2. Comparison of knee joint kinematic between good (A) and stiff-legged (B) initial contact. Black line is the mean knee joint goniometry of all recorded gait cycles. 2-A reports the parameters adopted to define knee extension at initial contact: a_i is the angle at initial contact, a_p is the peak angle at first extension, and a_p - a_i is the difference between the two parameters. 147

Figure 10-3. Comparison between reference synergy (black) and a representative LBP subject (red). Top figure reports the muscle weights and bottom

the activation signals. A good similarity between the two synergies reflects in the high cosine similarity ($CS_{LBP\text{-}Control}$ = 0.98). 151

Figure 10-4. Mean knee joint angle pre-treatment (red) and post-treatment (blue) in the LBP patients. Black circles indicate knee angle at the initial contact and peak angle at first knee extension. 153

Figure 10-5. VAF of the synergies for the patients submitted to rehabilitation before (red line) and after (blue line) rehabilitation. Data are reported mean ± standard error. 155

Figure 10-6. Weights and Coefficients for the motor functions of the three subjects before (red line) and after (blue line) rehabilitation.....157

Figure 10-7. CS of the motor functions of the three patients before (red) and after (blue) the rehabilitation. 158

Chapter 1

Introduction

1.1 Aims of the work

In last decades, non-invasive investigation of the central nervous system (CNS) has been increasingly gained interest. It involves an interdisciplinary research integrating methods from neuroscience and engineering to analyze neurological functions and to design solutions to problems associated with neurological limitations and dysfunctions. Despite this research area is relatively new, the field is developing rapidly, and it requires continuous updates. Actually, relevant neural processes cannot be directly recorded, and even if one had an opportunity to get information about activity of all neurons within the human body, it is not at all obvious what to do with these hypothetical recordings. The logic of the functioning of the CNS cannot be deduced from knowledge about functioning of all its elements. This makes CNS something like “physics of unobservable”, because relevant variables are not directly accessible for measurement (M. Latash and Zatsiorsky 2015). Particularly, there are two main areas are of interest: cerebrovascular system and motor control. The first consists of investigating cerebral activity by stimuli by means of the neurovascular coupling. The latter refers to the processes adopted by the CNS to coordinate muscles and limbs activity to perform a motor task.

Cerebrovascular system can be intended both nonlinear and nonstationary. Traditionally, the randomness in biological signals has been ascribed to noise or interactions between very large numbers of constituent components (Akay 2000). However, it has been demonstrated that some physiological systems are

characterized by nonlinearity: neurovascular coupling, for instance, showed nonlinearity between excitatory and inhibitory neuronal processes, due to the many feedback circuits of circulatory system. Also, the neurovascular response to a cognitive task and somatosensory stimulation reveled nonlinear components in neurovascular coupling. Cerebrovascular system can be explored by means of Near-Infrared Spectroscopy (NIRS). NIRS is a non-invasive functional technique that monitors cerebral metabolism and hemodynamics by measuring relative concentrations of oxy and deoxy-hemoglobin in the brain. It is based on measurement of infrared light intensity absorption that reflects the different oxygenation condition of the underlying tissue (Scholkmann et al. 2014). NIRS has been widely adopted to investigate cognitive processes (León-Carrion et al. 2008), to differentiate pathological conditions (K Sakatani et al. 1998), and to localize cerebral lesions (Van Haren et al. 2013).

Motor control aims at describing the interactions between the CNS, the body, and the environment during the production of voluntary and involuntary movements. Indeed, the motor control problem takes origin from the redundancy of the musculoskeletal system, that is a motor task can be performed in many ways. Furthermore, hierarchic levels of motor action construction mask upper level of motor control, and the interaction with environment do not allow a direct measurement of central commands generating movements. Particularly, the way CNS coordinates muscles and limbs to act together in motor tasks remains unsolved. A hypothesis is that CNS works in terms of movement efficacy to reduce system complexity. To this aim, groups of motor units and muscles are recruited with a single central command: this model is named muscle synergy. Muscle synergies are adopted to model many human activities, in healthy and pathological conditions. One of the most studied activity, for its importance in daily life activities, is locomotion. It is characterized by a cyclicity of movements and it requires a hard activity of force and balance control, and a rapid muscles-joints coordination. For these reasons, the description of locomotion by means of muscle synergies may provide insightful information how movements are generated and controlled. In recent years, many works explored muscle synergies in the human walking. They revealed the main muscle groups and activation timing of the synergies. Also, they investigated how muscle synergies adapt to biomechanical and environmental constraints and how they reduce the complexity of motor control. However, certain aspects have not been investigated yet, and methodological aspects limit their employment and generalization. This part of the

thesis work aims to deal with some of these aspects to improve the comprehension of motor control by means of muscle synergies. Particularly, two aspects are explored: the consistency of muscle synergies during a single task, and the difference in the motor control strategies between needed and auxiliary movements.

Then, the main objective of this thesis is to propose novel protocols, post-processing procedures or indices to enhance the cerebrovascular system and human motion analysis performed with noninvasive devices or wearable sensors in clinics and rehabilitation.

1.2 Thesis organization

The present thesis is divided in two parts: the first part focuses on the studies of the cerebrovascular system with NIRS. The second part describes studies on motor control problem and muscle synergies.

Part one is dedicated to study the cerebral microcirculation by means of nonlinear analysis of NIRS signals. Chapter 2 summarizes the basic concepts of NIRS methodology and the main methods implemented to acquire the signals. Furthermore, the chapter provides a summary of the function of prefrontal cortex in integrating information and executing actions, to underline the importance of investigating this cerebral area due to its involvement in all human activities. Chapter 3 describes the nonlinear methods adopted to study the NIRS signal. Particularly, Empirical Mode Decomposition (EMD) is a method adopted to extract the so called Intrinsic Mode Functions, that are characterized to have a single frequency component. EMD is based on the empirical analysis of the evolution of the signal, rather than mathematically defined theory, hence it is suitable to analyze nonlinear signals. The chapter also describes some entropy-based metrics. Entropy is a concept translated from thermodynamics to the information theory. From the first definition of entropy applied to information theory, called Shannon entropy, other measures of entropy have been developed to describe the periodicity and complexity of a signal. EMD and entropy metrics described in Chapter 3 have been applied to study NIRS signals in two different fields: neuropsychology and ozone therapy. Chapter 4 describes the application of nonlinear analysis of NIRS signal to study the effects of ocular movements in a psychotherapy called Eye Movement Desensitization and Reprocessing (EMDR). Chapter 5 the nonlinear analysis of

NIRS signals evidences the modification of cerebrovascular patterns during ozone therapy in multiple sclerosis patients.

Part two is devoted to study muscle synergies. An introduction chapter (Chapter 6) provides the background to the muscle synergies theory. It describes how the muscle synergy concept raised from the motor control problem. Also, it defines some basic keywords and concepts, that are the redundancy of degrees of freedom, the equilibrium point hypothesis, the role of central pattern generator, and the definitions of motor module and muscle synergy. Chapter 7 provides an overview of the factorization method adopted to extract muscle synergies from EMG signal, called nonnegative matrix factorization. Chapter 8 describes the experimental setup and protocol. Muscle synergies are extracted during a 5 minutes walking of young healthy subjects by integrating the statistical gait analysis, a tool that in a user-independent manner filters out atypical gait patterns. Finally, the chapter focuses on how the synergies are consistent within-subject. Chapter 9 introduces the concept of principal and secondary activations: principal activations are those necessary to execute the movement, whereas secondary activations are auxiliary to the movement. This chapter studies the difference of muscle synergies underlying principal and secondary activations. Finally, Chapter 10 is a pilot study of the effect of rehabilitation on the muscle synergies of patients suffering from lower back pain with stiffed leg walking. It is worth to be observed that, in the second part, the work described in each chapter is based on the methods and measurements defined in the previous chapters. That is, Chapter 8 describes experimental protocol, sample description, and methods adopted to extract muscle synergies. Chapter 9 and Chapter 10 also adopted the same dataset and protocol. Similarly, algorithm described in Chapters 9 to compute principal activations is also adopted in Chapter 10 to study muscle synergies in lower back pain patients. Therefore, this second part of the thesis is intended as a whole, and, where required, a reference to previous chapters for a full description of the methods is provided.

Part I

Chapter 2

Background: NIRS fundamentals and the prefrontal cortex

2.1 Introduction

The Near Infrared spectroscopy (NIRS) is a technique, which allows measuring the oxygenation of the brain tissue (Gersten 2015). It uses intensity changes of scattered light related to regional blood volume and oxygenation changes in brain cortex (neurovascular coupling). The main advantages of adopting this technique in medical imaging are: it is non-invasive and portable. It is safe, since it does not adopt ionizing radiation, and it is rapid and continuous. However, it is affected by several limitations: scattering limits spatial resolution to nearly 1 cm. Light penetration is limited to brain cortex in adult. NIRS provides no absolute measurements, hence NIRS monitoring is limited to protocols evaluating the response to external stimuli. Finally, it is contaminated by systemic hemodynamic signals. For these reasons, it is still adopted mainly at research level (Strangman, Boas, and Sutton 2002).

The history of NIRS applied to biological tissues is relatively recent: it was firstly applied by Frans Jobsis in 1977, who showed how the average hemoglobin-oxyhemoglobin equilibrium can be effectively and continuously recorded (Jobsis 1977). A major contribution to early works on NIRS was provided by Britton Chance (L. Z. Li et al. 2014): in the late eighties, he started working on *in vivo* NIRS, mainly with Nioka (Tamura et al. 1988) and Leigh (Chance, Leigh, et al.

1988). Chance then published with Patterson and Wilson the first work on time-resolved optical spectroscopy. That work made it possible to measure scattering and absorption coefficients in biological tissue, giving birth to the diffusive biomedical photonics (Patterson, Chance, and Wilson 1989). Then, in early nineties, different groups started exploring cerebral function in adult and newborn infants brain by using NIRS (Hoshi and Tamura 1993b; Hoshi and Tamura 1993a; Chance et al. 1993; Kato et al. 1993; A. Villringer et al. 1993; von Siebenthal, Bernert, and Casaer 1992). In the last twenty years, NIRS have been increasingly used in behavioral and cognitive development in infants and children, psychiatric conditions, stroke, and brain injury (Ferrari, Norris, and Sowa 2012; Davies et al. 2015; Boas et al. 2014).

This chapter briefly introduces basic concepts of NIRS and the methods of measuring modification in concentration of tissue oxygenation. The chapter concludes with a short introduction to the functions of prefrontal cortex, since it is the investigated area in the studies of the next chapters.

2.2 NIRS Fundamentals

The basics and main characteristics of NIRS can be summarized as follows:

1) human tissues are relatively transparent to light in the NIRS spectral window (650 – 1000 nm)

2) NIR light is either absorbed by pigmented compounds (chromophores) or scattered in tissues

3) NIR light is able to penetrate human tissues, since the dominant factor in its tissue transport is scattering, which is typically about 100 times more probable than absorption. Approximately, 80% of the total attenuation of NIR light in tissue is due to scattering, and the remaining 20% to absorption.

4) the relatively high attenuation of NIR light in tissue is mainly due to the chromophore hemoglobin, the oxygen transport red cell protein. Hemoglobin is located in small vessels (1 mm diameter) of microcirculation, such as capillary, arteriolar and venular beds. NIRS is weakly sensitive to blood vessels > 1mm because they completely absorb the light. Given the fact that arterial blood volume fraction is approximately 30% in human brain, the NIRS technique offers the

possibility to obtain information mainly concerning concentration oxygenation changes occurring within the venous compartment.

Hemoglobin is the most influential absorber, whose absorption characteristics depends on its oxygenation level. Other absorbers (e.g. water) contributing to overall attenuation, are assumed to remain relatively constant in concentration. The absorption spectrum of hemoglobin depends on its level of oxygenation. Oxygenated (O_2Hb) and deoxygenated (HHb) hemoglobin show different behavior when tissue is irradiated by an electromagnetic field in the infrared bandwidth. **Figure 2-1** evidences how adsorption spectra of oxygenated (red) and deoxygenated (blue) hemoglobin are different. Hence, by comparing sent versus emitted light intensities, it is possible monitoring separately the modification in concentration of O_2Hb and HHb.

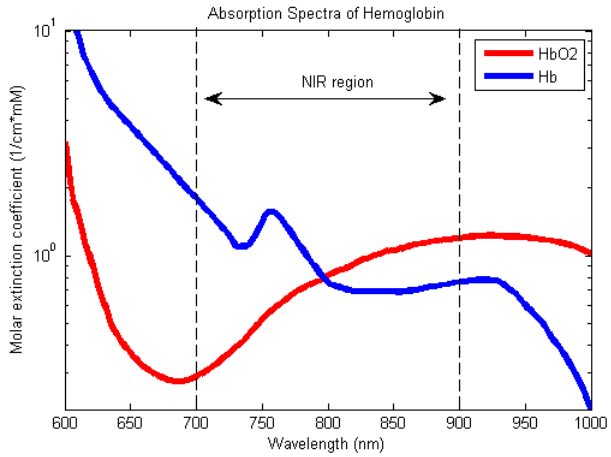

Figure 2-1. Absorption spectra of oxygenated (red) and deoxygenated (blue) hemoglobin in the infrared bandwidth.

NIRS signal modifies when neural activity changes after a stimulus. Change in neuronal activity is detected through the measurement of Cerebral Blood Flow (CBF). CBF is adopted as an index of neuronal activity based on the concept of a relationship, called neurovascular coupling, existing between local brain metabolic variations and CBF variations (Gsell et al. 2000). Neuronal activity is fueled by glucose metabolism, so when neural activity increases after a stimulus, glucose and oxygen consumption from the local capillary bed increases too. Subsequently, the reduction in local glucose and oxygen concentration stimulates local arteriolar

vasodilation, which increases local CBF (Bunce et al. 2006). Within several seconds, the increased CBF carries oxygen to the area by means of oxygenated hemoglobin in the blood. The carried oxygen is higher than the oxygen consumption rate ($CMRO_2$). It results in an overabundance of cerebral blood oxygenation in active areas (Ances et al. 2001) and a slight reduction in HHb in the cerebral vessels (Kaoru Sakatani et al. 1998).

2.3 Measurements principles

Three main categories of near-infrared light spectrometers have been developed: continuous wave, time domain and frequency domain spectrometers. **Figure 2-2** schematizes principles of the three main categories of NIRS (Bakker et al. 2012).

Continuous wave (CW) NIRS instruments are the earliest and most common commercial NIRS devices. CW instruments generally employ a multiple discrete wavelength source or a filtered white light source. They measure the light attenuation by using a photomultiplier, photodiode or an avalanche photodiode detector (Delpy and Cope 1997; Scholkmann et al. 2014).

The Modified Beer-Lambert Law (MBLL) is generally adopted to measure modification in concentration of O_2Hb and HHb (Owen-Reece et al. 1999; Arno Villringer and Obrig 2002). According to traditional Beer-Lambert Law, light attenuation in a solution (*A*; logarithmic scale) is proportional to the concentration of the compound measured in the solution (*C*), to the coefficient of absorption specific for the compound (*a*), and the light pathlength (*d*):

$$A = a \cdot d \cdot C$$

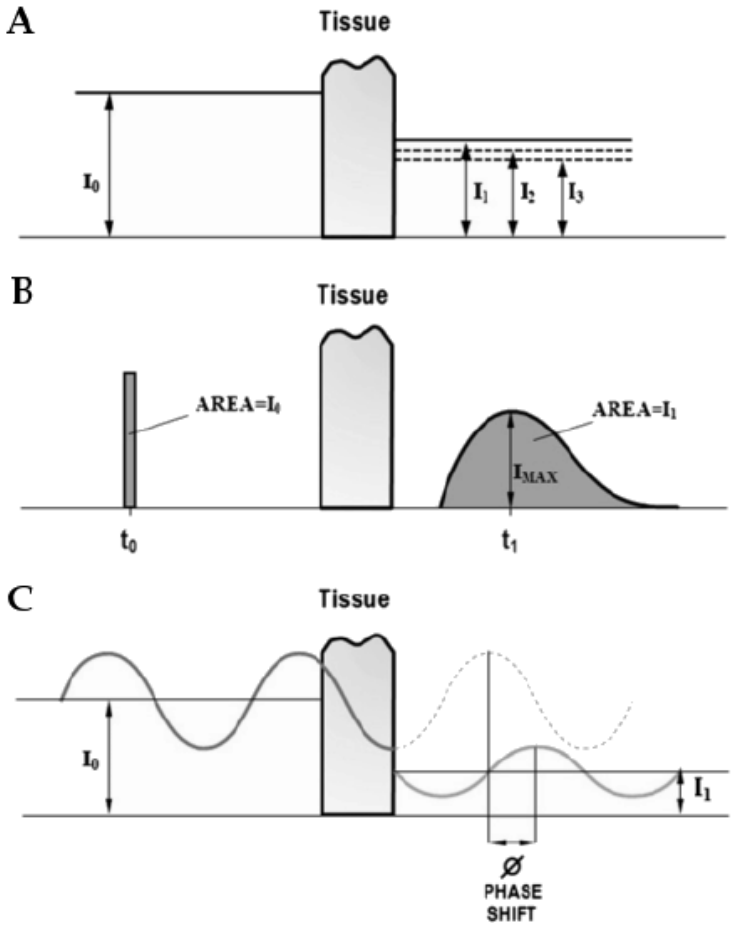

Figure 2-2. Schematic representation of three NIRS acquisition modalities: (A) Continuous wave, (B) Time resolved, and (C) Frequency resolved (from Bakker et al., 2012).

However, it has been demonstrated that the above equation is incorrect because it is applicable only if there is no optic diffusion in the solution (Sassaroli and Fantini 2004). In the event of light diffusion, the formula is modified as follows

$$A = a \cdot L \cdot C + X$$

In this formula, two new parameters have been added: *L* and *X*. Because of diffusion, light pathlength is not straightforward, so the real light pathlength (*L*)

increases with respect to physical light transmission (*d*). Furthermore, even in the case of absence of light absorption (i.e. $a = 0$), only a fraction of incident light can be detected as transmitted light. Hence, an attenuation factor *X* is introduced. Since *X* is unknown, *C* cannot be directly measured. In real measurements, *X* can be considered constant in time (t). Hence, *X* can be removed by subtracting *A*(t0) from *A*(t), and it provides the variation in concentration ΔC in the time interval t-t0, as described by the MBLL

$$\Delta A = a \cdot L \cdot \Delta C, \text{ hence } \Delta C = \Delta A/(a \cdot L)$$

Time-resolved systems generally employ a semiconductor or solid state laser to generate ultrashort pulses. Attenuation is measured by a time-correlated single photon counting, in which a photon counting detector detects and sorts the received photons by their time of arrival (Delpy and Cope 1997). In time domain spectrometers a light pulse of a few picoseconds long propagates in the tissue. Because of scattering, the timeline of photons exiting the tissues has a broad distribution, called temporal point spread function (TPSF). A typical tissue TPSF is characterized by a relatively rapidly rising intensity, peaking around 600-1000 ps and then a slow decay often several nanoseconds in duration (Chance, Nioka, et al. 1988). The main advantages of time domain spectrometers are the spatial resolution; the penetration depth and the accuracy in separating absorption and scattering effects. However, there are several disadvantages, including the sampling rate, the instrument size and the weight, the necessity for cooling, the lack of stabilization and the cost.

Frequency domain spectrometers generally employ a laser diode, LED or modulated white light sources. They measure the attenuation, phase shift and modulation depth of the exiting light by a photon counting detector or gain modulated area detector (Chance et al. 1990; Delpy and Cope 1997). In frequency domain spectrometers radio frequency modulated light propagates through tissue. The resulting signal is the Fourier transform of the TPSF, relating time domain results to frequency domain results. Therefore, the same information as measured with the time domain spectrometers can be found with the frequency domain spectrometers. The frequency domain spectrometers measure changes in intensity, phase and modulation using: (1) single wavelength and a fixed inter-optode distance, (2) multiple wavelengths and a fixed inter-optode distance, or (3) single

wavelength and multiple inter-optode distances. The main advantages of frequency domain spectrometers are the sampling rate and the relative accurate separation of absorption and scattering effects, and the main disadvantage is the penetration depth (Bakker et al. 2012; Delpy and Cope 1997).

2.4 The prefrontal cortex

The cortex of the anterior pole of the mammalian brain is commonly designated the prefrontal cortex (PFC) (J. Fuster 2008). It is defined as the part of the cerebral cortex that receives projections from the mediodorsal nucleus of the thalamus. Currently, PFC is one of the five most important topics in the field of neuroscience research (Yeung, Goto, and Leung 2017). The anatomical complexity of the PFC makes its functional homogeneity implausible. Furthermore, a unitary role for the PFC is also inconsistent with clinical findings in certain patients.

The entirety of the frontal cortex, including its prefrontal region, is "action cortex" in the broadest term. It is cortex devoted to action, whether skeletal movement, ocular movement, the expression of emotion, speech, or visceral control. The frontal cortex is "doer", whereas posterior cortex is "sensor" cortex. In recent years, it has become increasingly evident that PFC is involved in emotional and social behavior. Certain portions of this cortex, which are closely connected to limbic structures, are implicated in the control emotions and of the autonomic system. A complex system that includes prefrontal areas, the hypothalamus, the anterior thalamus, and the amygdala, appears essential for the evaluation of the emotional significance of environmental events and for decision making (S. M. Smith and Vale 2006). This evidence has provided with functional significance the connections between the prefrontal areas and those subcortical centers.

A large amount of experimental evidence indicates that PFC has few basic functions. These functions seem interrelated, mutually supporting and complementing one another. The three main functions of PFC are:

1) organizing actions in the time domain. Coherence and coordination of actions are essential to reach a goal, and they derive from the capacity of PFC to organize actions in time. Without organization, there is no execution of new behavior, no speech fluency, no higher reasoning, no creative activity.
2) executive functions, which essentially consist of the utilization of the neural substrate of permanent long-term memory. The substrate is utilized for the

acquisition of further executive memory and for the organization of behavior, reasoning, and language.

3) executive attention, which is indispensable for the two functions 1) and 2).

Organizing actions in the time domain consists of activating PFC with sensory areas in processing sensory information. For instance, in auditory system, PFC is activated in the same time or slightly after temporal lobes. Auditory system, including only primary auditory cortex, is not sufficient to percept audial temporal pattern, but information of frontal processing is required. PFC is also activated also during the processing of visual information. Concurrent activation of frontal and sensory cortices may relate to conscious awareness. EEG studies evidenced interaction between prefrontal regions and the rest of the brain. Probably, PFC plays a role in synchronizing rhythmic firing rate of neurons in various regions of brain. Many studies revealed the connections between the prefrontal region and other cortical areas implicated in sensory and motor processing (J. M. Fuster 2001). The disruption of various cortical interconnections was related to pathogenesis of neurological syndromes involving the higher integrative functions. Particularly, there are two class of frontal lobe syndromes: one class is characterized by loss of initiative, creativity, and concentration power, with a property of apathy and emotional blandness. In the second type, patients lost judgment, insight, and foresight. Furthermore, they do not seem to learn from experience, and impulsively stumble from one disastrous situation into another.

Executive function is essential for achieving a precise goal in a flexible and appropriate manner and is the product of the coordinated operation of various neural systems. Executive control permits: (1) to deal with novel tasks, (2) to properly interpret past events, (3) to interrupt an ongoing sequence of actions and initiate a new one, (4) to prevent inappropriate response, (5) to effectively switch from one task to another, (6) to correct errors. PFC performs executive functions by sending command signals, called top-down signaling, to other cerebral areas (Funahashi and Andreau 2013).

Executive attention has three components: (1) preparatory set, (2) working memory, and (3) inhibitory interference control. The three components are not executed directly from PFC, but PFC controls temporal organization of activities in other neural structures that participate in executive attention.

Preparatory set is the readying or priming of sensory and motor neural structures for the performance of an act contingent on a prior event, and thus the content of the working memory of that event.

Working memory is the memory in active state, that is the memory required for short-term performance. Daily activities, from keeping a telephone number in mind to considering alternative consequences of a moral dilemma rely on working memory. The content may be sensory, motor, or mixed. Working memory has a perspective toward recent past, preparatory set has a perspective toward recent future. Working memory is an attentional function that enables the on-line holding and mental manipulation of information. Working memory transforms information access from a sequential and disjunctive processes, where every event is classified into a separate cluster, to a conjunctive pattern where several selected clusters are connected into the stream of consciousness. Working memory plays a crucial role in shifting the focus from external events to internal representation, that is the thinking activity. The second function of working memory, the “manipulation” of the on-line information, is likely to play an important role in the reorganization of mental content (Stuss and Knight 2002).

Inhibitory control plays the role of enhancing and providing contrast to excitatory function. In PFC, inhibition is the mechanism by which, during the temporal organization of actions, sensory inputs and motor impulses that may impede action are considered. It is a critical component of attention, because inhibition selectively suppress interfering cognitive or emotional contents.

Chapter 3

Empirical mode decomposition and entropy-based metrics

3.1 Introduction

The traditional way of analysis of physiological systems has been based on linear system theory, even if many biomedical signals are apparently random or aperiodic in time. Traditionally, the randomness in biological signals has been ascribed to noise or interactions between very large numbers of constituent components (Akay 2000). However, it has been demonstrated that some physiological systems are characterized by nonlinearity: neurovascular coupling, for instance, showed nonlinearity between excitatory and inhibitory neuronal processes, due to the many feedback circuits of circulatory system. Also the neurovascular response to a cognitive task and somatosensory stimulation reveled nonlinear components in neurovascular coupling (E. E. Smith and Jonides 1997; Gsell et al. 2000; Rivadulla et al. 2011). Furthermore, traditional analysis of physiological systems is based on the hypothesis of stationarity. A random process (or signal) is said to be stationary in the strict sense if its statistics are not affected by a shift in the origin of time. Also, a random process is said to be stationary in the wide sense if its mean is a constant and its autocorrelation function depends only upon the difference (or shift) in time. Conversely, signals or processes that do not meet the conditions described above are called nonstationary. Stationary signals provide the same statistical measures for all the time course, or at least over the duration of observation, and the power spectral density (PSD) does not vary over time. As the Fourier spectra can only give meaningful interpretation to linear and stationary processes, its application to data from nonlinear and nonstationary processes may be

meaningfulness. Furthermore, probability distributions, which can represent global properties, imply stationarity in the population (Rangayyan 2015).

NIRS describes nonlinear processes and it cannot be considered stationary, nor in a wide sense (Caicedo 2012). Indeed, NIRS is characterized by time-varying chromophore concentration average (Molinari et al. 2013). Furthermore, it has been observed a phase shift between the oscillations in LF bandwidth in the blood oxygenation parameters (Obrig et al. 2000). Consequently, the traditional way of analysis based on linear system theory may be limiting. Nonlinearity and nonstationarity should be adequately analyzed with other techniques. In the past few decades, random behavior has been described in deterministic nonlinear systems. In this way, simple mathematical models allow to analyze and control physiological systems. The approach to revealing nonlinearity and nonstationarity is data-driven, rather than based on mathematical rules: in this way, the method of analysis is adaptive to the nature of the data, that is the definition of the components of a signals derives from the data, and it can be achieved by decomposing data in adaptive basis. (N. E. Huang and Wu 2008). A data-driven method of signal decomposition is the empirical mode decomposition (EMD), a part of the Hilbert-Huang Transform. EMD decomposes a signal into a finite number of simple functions, called Intrinsic Mode Functions (IMF).

In the present chapter, we introduce the traditional EMD and several algorithms developed to overcome its limitations. Subsequently, we introduce some entropy-based measures adopted to measure the complexity of the IMFs.

3.2 Empirical mode decomposition

3.2.1 Traditional EMD

The Hilbert-Huang transform (HHT) decomposes a signal to obtain instantaneous frequency. Differently from Fourier transform, HHT is an algorithm based on the characteristics of the data, rather than a theoretical approach (N. E. Huang and Wu 2008). Hence, unlike any other time-frequency techniques, it does not assume linearity as a requirement (Molinari et al. 2015). The fundamental part of HHT is the Empirical Mode Decomposition (EMD). The objective of EMD is identifying intrinsic oscillatory modes of a signal, called Intrinsic Mode Function (IMF). An IMF is a function that satisfies two conditions: (1) In the whole data set, the number of extrema and the number of zero crossings must either equal or differ at most by one; and (2) At any point, the mean value of the envelope defined by the local

maxima and the envelope defined by the local minima is zero. In summary, EMD is an iterative procedure to decompose a signal into a finite number of simple signals, the IMFs, and each IMF contains only one oscillatory mode (Yang and Yang 2009).

The traditional EMD algorithm is composed by three steps: the "sifting process" to compute an IMF, the computing of the new signal, and the iteration to compute all the IMF (Molinari et al. 2015; Rilling, Flandrin, and Es 2003; N. E. Huang et al. 1998).

The first step is the "sifting process". Given an arbitrary signal $x(t)$, the sifting process can be summarized as following:

1. identify all extrema of $x(t)$
2. interpolate with a cubic spline points between minima, ending up with the envelope $e_{min}(t)$. The same is applied to maxima, ending up with the envelope $e_{max}(t)$
3. compute the mean between the envelopes

$$m_1(t) = \frac{e_{min}(t) + e_{max}(t)}{2}$$

4. extract the detail

$$h_1(t) = x(t) - m_1(t)$$

An example of sifting process for a nonlinear signal is represented in **Figure 3-1**. At the end of the sifting process, the detail function $h_1(t)$ should meet the following criteria to be an IMF: it should be symmetrical and have positive maxima and negative minima. An IMF could be not obtained at the first iteration, since EMD is not a mathematically strict method. Hence, the sifting process is iterated until $h_1(t)$ meets the criteria to be the first IMF (**Figure 3-2**).

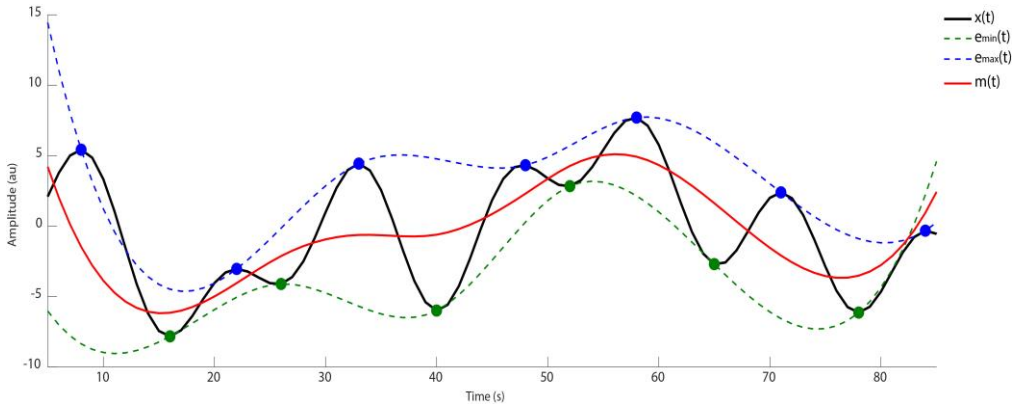

Figure 3-1. EMD decomposition process. For a nonlinear signal x(t) (black line) the maxima (blue dots) and minima (green dots) are computed. The envelop of maxima (dotted blue line) and the envelop of minima (dotted green line) are computed with a cubic spline. Finally, the mean of the envelopes (m(t), red line) is subtracted to x(t) to obtain the first IMF.

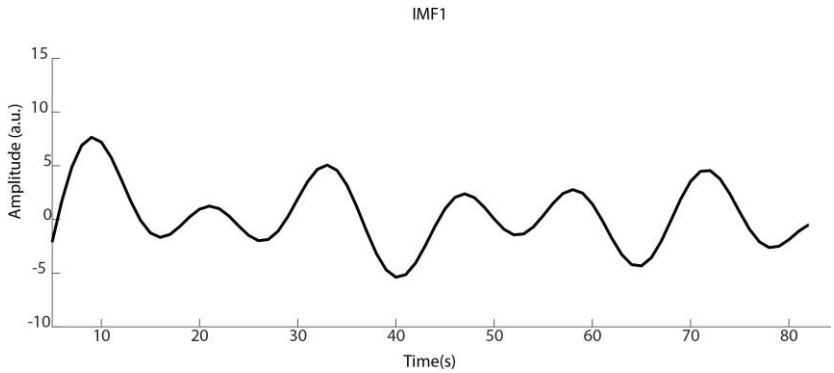

Figure 3-2. First IMF for the signal showed in Figure 3-1. It can be observed that the slow frequencies trend has been removed.

As a second step, the derived $h_1(t)$ is considered as the new signal and the mean of lower and upper envelopes m_{11} is computed. The new IMF is computed as

$$h_{11}(t) = h_1(t) - m_{11}(t)$$

The whole procedure is iterated to compute *k* IMF

$$h_{1k}(t) = h_{1(k-1)}(t) - m_{1k}(t).$$

To avoid obtaining IMF without any physical meaning, the normalized standard deviation (NSD) is imposed as a stop criterion. The iterations stop if the NSD between two consecutive IMF h_1 and $h_{1(k-1)}$

$$NSD = \frac{\sum_{t=1}^{T} \left| h_{1(k-1)}(t) - h_{1k}(t) \right|}{h_{1(k-1)}^2(t)}$$

is lower than a threshold (usually between 0.001 and 0.2).

3.2.2 Alternative EMD algorithms

The traditional EMD is affected by several limitations: since the sifting process is highly adaptive and extremes are interpolated with a cubic spline, it is unstable. It means that a small change in data (i.e. random noise) can lead to different IMFs (Lin, Wang, and Zhou 2009). This problem affects convergence of the sifting process, the orthogonality of IMFs, and other undefined problems. For this reason, new algorithms have been proposed to solve the principal issues of traditional EMD. It has been proposed to adopt B-spline rather than cubic spline to interpolate maxima and minima, and to exclude peaks at the extrema points, since they may diverge due to the instability of cubic interpolation. (Q. Chen et al. 2006). Furthermore, EMD may introduce some artificial peaks that may lead to meaningfulness IMFs. To avoid this problem, peak prominence threshold was introduced and generally ranges between the 20% and the 80% of the total length of the signal.

An alternative approach to the traditional EMD is the moving average based approach. In this approach, the mean of the extrema envelopes $m_1(t)$ is substituted

by a moving average (Lin, Wang, and Zhou 2009). Given a signal *x(t)*, at the iteration *n* it is masked with a fixed mask *a(x,t)* of length *l(x)*,

$$f_{n+1}(x) = f_n(x) - \int_{-l(x)}^{+l(x)} f_n(x+t)a(x,t)dt$$

The IMFs are now obtained via the same sifting algorithm, where the operator $m_{11}(t)$ is now replaced by $f(x)$. The moving average operator $a(x,t)$ is computed as an adaptive local weighted average. A simple class of filters with uniform mask is the double averaging filter:

$$a(t) = \frac{l-1+|t|}{(l+1)^2}, \qquad t = -l, -(l-1), \ldots, (l-1), l$$

The convergence of the sifting process has been established mathematically for uniform mask filters, where *a* and *l* are independent from *x* (Wang and Zhou 2012).

The iterative filtering EMD method is more stable under perturbation (i.e. random noise). Indeed, small changes in one segment of the data can lead to very different decompositions with traditional EMD, whereas the moving average based approach is more stable.

For extremely non-stationary time series, an adaptive EMD method better captures the non-stationary changes in the frequency and time domains. In the adaptive EMD, a moving average filter mask with nonuniform length is adopted. The length of the mask depends on the local density of the extrema, and it is computed as a multiple of the distance of subsequent local minima and maxima (Lin, Wang, and Zhou 2009).

If the signal *x(t)* has *k* local extreme points, and x_i denotes the position of the *i*-th local extreme point of *x(t)*, the filter mask length $l_n(x_i)$ is given by the difference between the extrema x_{i+1} and x_{i-1}

$$l_n(x_i) = x_{i+1} - x_{i-1}, \quad i = 2,3,\ldots, k\text{-}1$$

Once the lengths of the masks at the extreme are determined, the length of the filter mask for the intermediate points of the signal is obtained by interpolating the known filter length pairs (x_i, $l_n(x_i)$). However, the derived mask length may introduce high frequency oscillations, producing artifacts and diverging. To avoid these problems, the high frequency oscillations contained in $l_n(x)$ are filtered out.

Figure 3-3 shows an example of adaptive EMD for a strongly non-linear signal. Signal is obtained by the superposition of a chirp signal and an increasing monotonically curve (**Figure 3-3A**). Adaptive EMD adaptively changes the mask length from point to point. Hence, it decomposes correctly the signal and it separates the two components in a first IMF with the chirp signal (**Figure 3-3B**) and in a second IMF with a trend curve (**Figure 3-3C**).

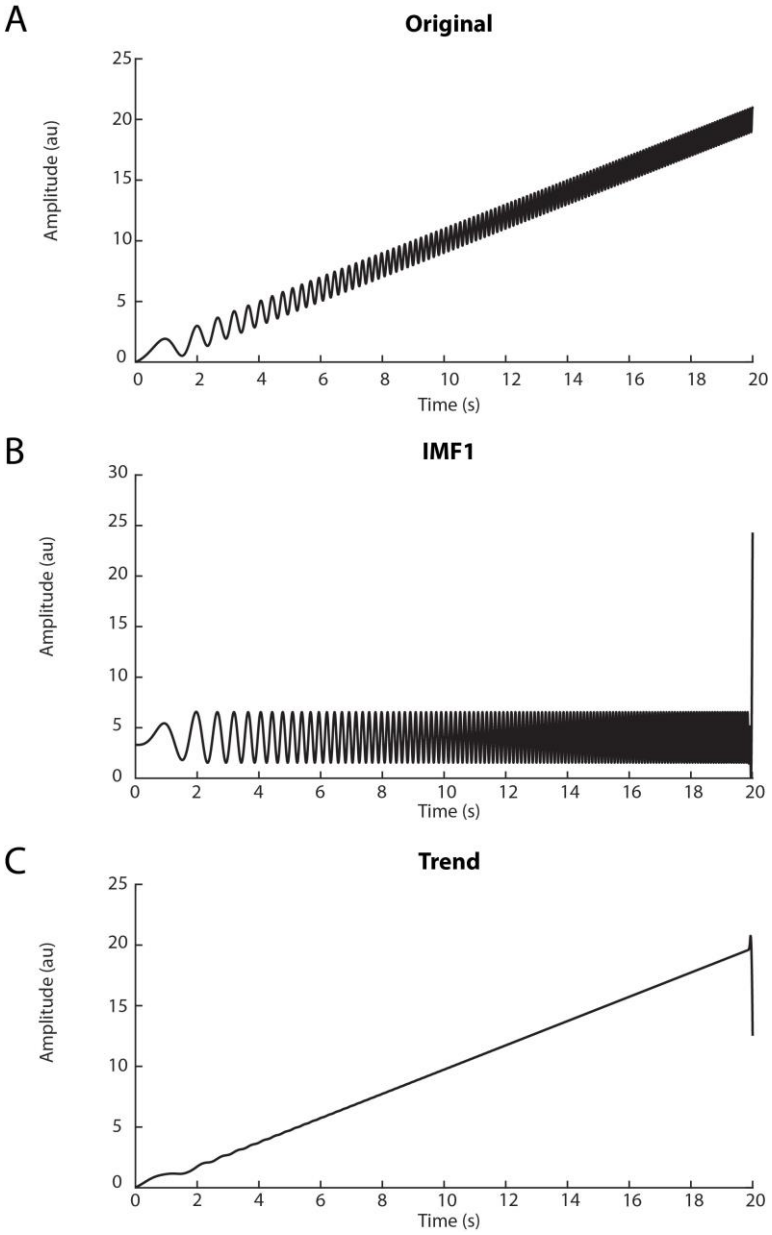

Figure 3-3. Adaptive EMD of a strongly nonlinear signal. (A) Original signal obtained from the superposition of a chirp signal and a linear trend. (B) and (C). The IMFs with the separate signals.

3.3 Entropy and entropy-based features

Entropy was introduced in thermodynamics by Clausius (1862) and Boltzmann (1896). The concept was applied by Shannon (Shannon 1948) and Jaynes (Jaynes 1957) to information theory to indicate the amount of unexpected data contained in a message. In the last decades, alternative entropy measures have been proposed and allowed the analysis of complex systems (Machado, Costa, and Quelhas 2011; Henriques et al. 2013).

3.3.1 Shannon entropy

Shannon defined the expression of entropy in theory of information from the expression for entropy in the theory of statistical mechanics established by Boltzmann in 1896 (Shannon 1948):

$$H = -K \sum_i p_i \log_b p_i$$

where K is a positive constant, p_i is the probability of a message m_i taken from the message space M, and b is the base of the logarithm used. Given a time series x(t), H measures the mean conditional uncertainty of the future $x(t+1)$ given the whole past $\ldots x(t-1), x(t)$. H may be interpreted as the average information taken over an information space, and it may vary between 0 and $\log_b$M. $H = 0$ means that the series is perfectly predictable from the past, whereas we obtain $H = \log_b$M if all values are independent and uniformly distributed. Hence, large H indicates high complexity (Bandt and Pompe 2002).

3.3.2 Sample Entropy

Since Shannon Entropy is affected by a bias caused by self-matching, Richman and Moorman developed another measure of time series regularity named Sample Entropy (SampEn) (Joshua S Richman et al. 2011). The SampEn is based on the temporal time series instead of relying on the PSD to capture "the rate generation of new information" (J S Richman and Moorman 2000). The new information is related to the degree of similarity between a sequence of length m (called

embedding dimension) and the same sequence extended by a time point *m+1* (Duran et al. 2013). The time series is used to derive vector sequences of length *m* (Pincus 2001; Pincus and Goldberger 1994), so that each vector sequence has the form:

$$u(n) = \{h_i(n), h_i(n+1), \dots, h_i(n+m-1)\}$$

where *h(1), h(2), …, h(N)* are the *N* samples of the time series. The distance between each vector segment and the others is computed by using the Chebyshev distance (Shieh and Tsai 2010). Given a distance threshold equal to *r* (generally varying between 10% and 20% of the time series standard deviation), each vector sequence is considered and the number of other segments with a distance lower than *r* is computed. This number, divided by the total number of vectors, indicates the probability $C_{n_i}^m$ of locating another vector not beyond the distance *r* from the considered vector $u(n_i)$. The overall conditional probability $\phi^m(r)$ is given by the sum over the total number of vector sequences:

$$\phi^m(r) = (N-m+1) \sum_{i=1}^{N-m+1} C_{n_i}^m(r)$$

The SampEn is then defined considering also the overall probability found for an embedding dimension equal to *m+1*; hence SampEn is defined as

$$SampEn(m, r, N) = -ln\left[\frac{\phi^m(r)}{\phi^{m+1}(r)}\right]$$

Figure 3-4 shows an example of SampEn for a generic time series, given *m*=2 and a generic positive tolerance *r*.

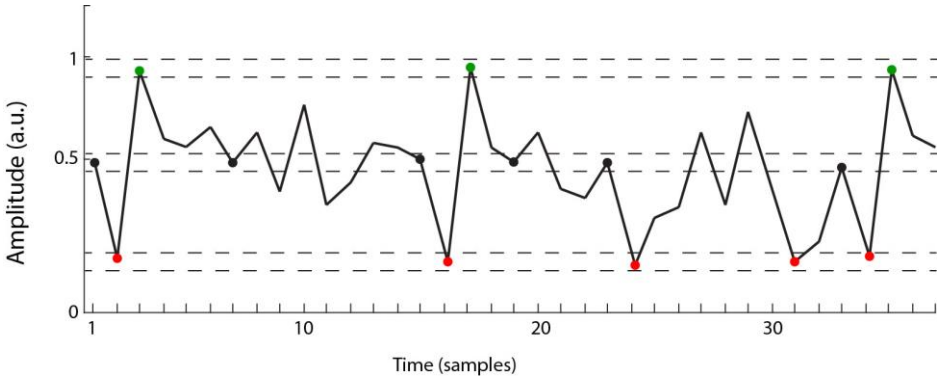

Figure 3-4. A generic time series of N points for the computation of SampEn for m=2 and a generic positive value r. Dotted horizontal lines indicate distance r around data points h(1), h(2), and h(3). Two data points of the time series match if the absolute distance between them is lower than r. Black filled dots represent data point matching with h(1). Similarly, red and green points match with h(2) and h(3) respectively. Consider the two components sequence (h(1), h(2)) and the three components sequence (h(1), h(2), h(3)). There are 4 sequences matching with sequence (h(1), h(2)), and three sequences matching with sequence (h(1), h(2), h(3)). Then, the number of matching sequences is repeated for the next two-components sequence (h(2), h(3)) and three components (h(2), h(3), h(4)). The calculation is repeated for the next N-m+1 sequences to compute the ratio between the number of two components sequences and the three components sequences. The negative natural logarithm of this ratio provides the SampEn of the time series. It indicates the probability that sequences that match each other for the first two data points will also match for the next point. (Modified from Costa, 2005).

3.3.3 Fuzzy Entropy

The Fuzzy Entropy (*FE*) is a measure of a time series regularity, and it is particularly suitable for short datasets. *FE* is defined as the negative natural logarithm of the conditional probability that two vectors similar for *m* points remain similar for the next *m + 1* points (W. Chen et al. 2007). *FE* takes origin from the concept of "fuzzy sets" introduced by Zadeh (Zadeh 1965). Zadeh's theory measures the degree to which a pattern belongs to a given class C. It introduces the "membership degree", a fuzzy function that assigns a value $\mu_C(x)$ to each point *x* by associating a real number in the range [0 1]. The higher the value of $\mu_C(x)$, the higher the membership grade of *x* in the set C. Fuzzy sets provide a scheme for handling a variety of problems in which a fundamental role is played by an indefiniteness arising more from a sort of intrinsic ambiguity than from a statistical variation (De Luca and Termini 1972). In *FE*, the concept of fuzzy sets is employed

by adopting a family of exponential membership functions $\exp(-(d_{ij}^m)^n/r))$, where *d* is the distance between two sequences *i* and *j* of length *m* and *n* and *r* are the tolerance and the gradient of the exponential function respectively. In *FE*, the two sequences of a time series are compared by measuring their distance, and the fuzzy measurement of two vectors similarity is based on their shapes. Fuzzy entropy has been widely adopted in EEG signal analysis to discriminate complexity of the EEG in neurological diseases (Cao et al. 2015), and to the analysis of complexity in heart rate (Zaylaa et al. 2015; Ji et al. 2015), surface electromyography (W. Chen et al. 2007; Xie, Guo, and Zheng 2010), and image processing (Di Zenzo, Cinque, and Levialdi 1998; Sil Kar and Maity 2016; Sokunbi et al. 2015).

A general *N* samples time series {μ(i), i = 1,…, N} forms a series of *m*-dimensional vectors by

$$X_m^i = \{u(i), u(i+1), \dots, u(i+m-1)\} - u_0(i),$$

where

$$u_0(i) = \frac{1}{m}\sum_{j=0}^{m-1} u(i+j)$$

The distance between the *i*-th and the *j*-th vectors X_i^m and X_j^m is defined as

$d_{ij}^m = d\left[X_i^m, X_j^m\right] = \max|u(i+k) - u_0(i) - (u(j+k) - u_0(i))|, (i, j = 1 \sim N - m + 1)$.

For certain vector X_i^m and given a tolerance *r* and gradient *n*, the similarity degree between the two vectors is determined by a fuzzy function

$$D_{ij}^m = \mu\left(d_{ij}^m, n, r\right) = \exp(-(d_{ij}^m/r)^n)$$

We define the overall conditional probability ϕ^m as the normalized sum of all the similarity degrees for a distance *m*

$$\phi^m(n,r) = \frac{1}{N-m}\sum_{i=1}^{N-m}\left(\frac{1}{N-m-1}\sum_{j=1,j\neq i}^{N-m} D_{ij}^m\right)$$

Similarly, we define ϕ^{m+1}

$$\phi^{m+1}(n,r) = \frac{1}{N-m}\sum_{i=1}^{N-m}\left(\frac{1}{N-m-1}\sum_{j=1,j\neq i}^{N-m} D_{ij}^{m+1}\right)$$

FE is defined as the negative natural logarithm of the deviation of ϕ^m from ϕ^{m+1}

$$FE(m,n,r,N) = ln\phi^m(n,r) - ln\phi^{m+1}(n,r)$$

There are three parameters that must be fixed for the calculation of *FE*. The first parameter *m* is the length of the sequences to be compared. A large *m* allows more detailed reconstruction of dynamic process, but a too large *m* requires a large dataset or a broad boundary, which may cause information loss. The other two parameters are the tolerance *r* and the gradient of the exponential function *n*. Similarly to *m*, too narrow parameters may be influenced by noise, whereas too broad a boundary may cause information loss. The value of *r* is recommended to be in the range 0.1-0.25 (Abásolo et al. 2006). Furthermore, due to the monotonicity and continuity of fuzzy membership functions, *FE* changes smoothly along with the change of the parameter *r*. The value of *n* should be a small positive integer such as 2 or 3. Indeed, when *n* tends to infinity, the exponential function $\exp(-(d_{ij}^m)^n/r$ is degenerated into Heaviside function, and the information at the boundary is lost (Cao et al. 2015). An example of exponential fuzzy function is

reported in **Figure 3-5**, where the effect of changing curvature parameters is also showed.

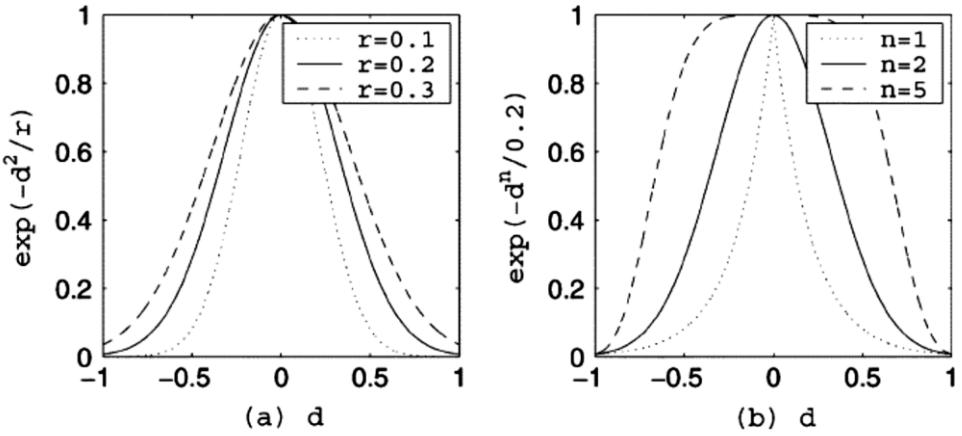

Figure 3-5. Exponential fuzzy function with different parameter choices. (a) Exponential function with fixed n=2 and r varying in the range 0.1-0.3. (b) Exponential function with fixed r = 0.2 and n varying between 1 and 5. For a certain distance between two vectors d, a value between 0 and 1 is given according to an exponential symmetric curve (from Chen 2007).

3.3.4 Permutation Entropy

The permutation entropy (*PE*) the complexity of a signal is determined by comparing the permutation patterns in the samples of the signal. This type of entropy is simple and robust towards noise (Bandt and Pompe 2002; X. Li, Ouyang, and Richards 2007). Also *PE* has been adopted as a complexity measure in several biosignal applications, particularly those related to EEG (Liang et al. 2015) and to reveal abnormalities in epilepsy (Zhu et al. 2014; Ferlazzo et al. 2014).

The computation of *PE* depends on the sequence length *e* and delay time τ. For a sequence of length *e*, a total number of *e!* permutations are possible. If *Bk* denotes the probability of occurrence of the *k*-th permutation pattern, then *PE* can be computed as

$$PE = -\sum_{k=1}^{e!} Bk\ log(Bk)$$

3.3.5 Hurst Exponent

The Hurst exponent (HE) aims to measure the presence/absence of long-range in a signal and dependence degree (Hurst 1951). Neurological studies evidenced that a change in the behavior of a physiological system causes a corresponding change in the HE. In the investigation of physiological systems, HE was used to discriminate between interictal and epileptic EEG (Geng et al. 2013) and to characterize the EEG in different sleep stages (Acharya U et al. 2005).

HE detects long-range dependency in the data and it relates to the autocorrelations of the time series. It varies between 0 and 1, and it provides information about long-range signal dependency. A HE next to 0 indicates random data (i.e. white noise), and HE < 0.5 indicates short-range dependency. A HE next to 1 indicates high long-range dependency (i.e. periodic signal). More generally, HE significantly greater than 0.5 means a long-term dependency of data. Normal signals are usually characterized by HE values that decrease as the system is normalizing its activity (Kannathal et al. 2005).

Given a time series *h(n)* of time length equal to *T*, the mean of the time series is computed and then subtracted by the time series itself. This produces a zero *mean* time series *h'(n)*. The cumulative deviation of *h'(n)* is then computed by summing up all the elements. Let's define *R* as the range of the cumulative deviation of *h'(n)* (*i.e.* the difference between the maximum and the minimum value) and *S* as the standard deviation of *h'(n)*. The HE is then defined as

$$HE = \frac{\log(R/S)}{\log(T)}$$

Chapter 4

Effect of Ocular Movements During Eye Movement Desensitization and Reprocessing (EMDR) Therapy: a Near-Infrared Spectroscopy Study[1]

4.1 Introduction

Eye Movement Desensitization and Reprocessing (EMDR) is a recent psychotherapy technique. It initially was born to treat patients suffering by post-traumatic stress disorder (PTSD), but nowadays EMDR is adopted to manage a wider range of clinical disturbs due to traumatic experiences (Fernandez I., Maxfield L. 2009).

EMDR, within a global therapeutic plan, adopts a standardized procedure composed by eight phases, with the aim of working on experiences and traumatic memories that cause actual disturbs. The main characteristics of EMDR is helping

[1] This chapter is based on the paper: Rimini, D., Molinari, F., Liboni, W. et al. PloS One (2016) 11(10): e0164379. https://doi.org/10.1371/journal.pone.0164379

the patient access the memory and metabolize it by asking the patient to focus on the most disturbing aspects of the memory (images, negative cognition, negative emotions, body sensation). In the meanwhile, a bilateral eye stimulation is induced. The natural mechanism of cerebral information processing is resumed by the alternating a rhythmic stimulation of cerebral hemispheres, obtained by means of eye movements (EM), and the recalling of the memory itself and its cognitive, behavioral and somatic elements (RECALL)(Zarghi, Zali, and Mehdi 2013). By EMDR, patient creates a more adaptive material that is integrated with traumatic memories. Therefore, the disturbing aspects of the memory are resolved. It allows to renovate cognitions in a more positive and adaptive way (Wilson, Tinker, and Becker 1995).

Currently, EMDR is recommended in the management of stress syndromes, such as PTSD (Shapiro and Maxfield 2002; World Health Organisation 2013). EMDR has been validated as an effective treatment for PTSD by American Psychological Association, based on empirical evidence obtained from researches conducted at the Department of Clinical Psychology of American Psychological Association (Fernandez I., Maxfield L. 2009). The International Society for Traumatic Stress Studies (ISTSS) classified EMDR as an efficient treatment for PTSD (Shalev et al. 2000). Furthermore, EMDR, together with CBT, has been declared the main treatment for PTSD (Ursano et al. 2004; CREST 2003). EMDR is also one of three methods to treat victims of terrorism (Bleich et al. 2002).

The physiological effects of EMDR have been explored by adopting a wide range of functional imaging techniques: nuclear imaging (Oh and Choi 2007), electroencephalography (EEG)(Pagani et al. 2012), and functional Magnetic Resonance Imaging (Herkt et al. 2014). All the studies evidenced modifications in the patterns of cerebral activity. These studies evidenced that the brain areas involved in EMDR are those involved in stress management: the so-called hypothalamus-pituitary-adrenal (HPA) axis (an articulated response network to a stressful condition which involves deep brain regions, such as hypothalamus and amygdala) and cortical areas, such as the prefrontal cortex (PFC) (Lupien et al. 2009). Nevertheless, one limitation of these studies is they investigated only pre- and post-treatment conditions.

By comparing a testing group performing the treatment with respect to a control group without eye movements evidenced the effect of ocular movements characterizing the EMDR protocol. Some specific studies aimed at exploring the difference between the use of EMDR with and without eye movements. Engelhard *et al.* showed that eye movement causes a decrease in arousal, flexibility in attention

and memory processing, as well as an improved semantic recalling (Engelhard et al. 2010). Lee and Cuijpers performed a meta-analysis of 15 clinical trials comparing EMDR with Vs. without eye movement and pointed out the beneficial effects of eye movement (C. W. Lee and Cuijpers 2013). However, these studies used self-reported measures as indicators of performance, without any functional investigation.

EMDR is a dynamic protocol in which the patient switch from a condition of eye movement to a providing feedback. To evaluate adequately the vasomotor response to the EMDR protocol, a neuroimaging technique with high temporal resolution is required. To this aim, NIRS is the suitable device because it allows to monitor PFC microcirculation in real time and during a therapy treatment. In this way autoregulation and neuronal activity can be effectively monitored. In a previous work on EMDR, NIRS established that O_2Hb decreases in the PFC during RECALL (Ohta ni et al. 2009).

The primary objective of the present study was to examine the effect of eye movement in PFC activity during an EMDR session, focusing on the modification in local hemodynamics. As a secondary endpoint, we explored the underlying complexity of the mechanisms of cerebral autoregulation induced by a response to EMDR stimulation. The study was conducted by comparing a treatment group with a control group: the first group received complete EMDR therapy with EM, whereas the second group received the same EMDR Protocol without the EM.

4.2 Material and Methods

4.2.1 Patients recruitment

We recruited twenty-one patients among the ones treated at “Un passo insieme” Foundation. They were randomly divided in two groups: a test group underwent the treatment with eye movements (wEM), and a control group performed the EMDR protocol without eye movements (woEM). wEM was constituted by 11 subjects (2 males, 9 females mean age 33.3 ± 6.34), woEM was constituted by 10 subjects (5 males, 5 females mean age 31.8 ± 5.60). All patients received all information about the aim and modalities of the study and all of them signed an informed consent. The study was approved by the Ethical Committee of the EMDR Italy Association.

We preliminary assessed recruited subjects with a battery of self-administered psychological tests: a Test Evaluation Checklist (TEC), an Impact of Event Score (IES) (Horowitz, Wilner, and Alvarez 1979), and a Symptom Checklist-90 (SCL-

90) (Derogatis and Cleary 1977). Afterwards, we assigned trauma severity to each subject, according to clinical history. We defined two levels of severity: major trauma (T), referring to all the events which may threaten life of the subject, such as natural disaster, or car accident, and minor trauma (t) referring to relational trauma, such as family conflicts, separations, betrayals, bullying.

4.2.2 EMDR Protocol

EMDR procedures have been designed to access dysfunctional experiences and stimulate a proper information elaboration. EMDR allows the transformation of information with an adaptive resolution, shifting the information to a more appropriate memory system. When information is completely elaborated, useful information is assimilated and the individual's memory structures are reorganized on the basis of the new information (Shapiro, Klaslow, and Maxfield 2007). On this basis, EMDR procedure adopts several instruments to recall memories and rework. Particularly, the eight fundamental EMDR components are (Greenwald 1999):

- *Images repertoire*: patient choices the most annoying images, or anyway the most characteristic, the most representative of the negative effect on the patient;
- *Negative cognition*: it is not just a description of the event, but the interpretation of the patient about himself that emerges from the memory. The characteristic of the negative cognition is that it remains after the traumatic event, and occasionally emerges in patient's lifespan;
- *Positive cognition*: like negative cognition, positive cognition is not a merely description, but rather an adaptive self-affirmation, more positive, and it represents the objective of the treatment, that is how patient sees himself. Some examples are: "I am a good person", "I can do it";
- *Emotion*: patient should externalize emotional reaction with respect to the chosen image of the memory. Some examples of the most frequent emotions are: sadness, fear, rage;
- *Validity of cognition scale (VOC)*: VOC represents a measurement of how much truthful the patient considers the positive information that should be installed during the treatment. VOC ranges from 1 (completely false) to 7 (completely true). The scale represents the progress of the patient during and after EMDR;
- *Subjective Units of Disturbance scale (SUD)*: SUD indicates the intensity of the felt disturbance. It measures how much intense is the negative emotion. SUD ranges from 1 (the emotion isn't distressing) to 10 (the worst

feeling you've ever had). It allows the patient and therapist to verify progresses obtained during and after EMDR;

- *Physical sensation*: it is considered an integrative part of the memory, since mnemonic traces are conserved in the body too. Affective states not adequately integrated survive in somatic states (van der Kolk 2005). Patient is asked to indicate where he feels physical sensation accomplishing the memory. The most frequent sensations are: nausea, tiredness, localized tension;
- *Ocular movements*: rapid eye movements allow the patient access to the memory-target, the elaboration and integration. They are induced by rhythmically moving fingers at a distance of 30-60 cm from the patient's face. If ocular movements are inadequate, other rhythmic stimulations can be adopted.

According to the original setting proposed by Shapiro (Shapiro 2001), EMDR is an eight-phases protocol. Each phase deals with a specific aspect of the treatment, even if it should be observed that each phase may affect the others.

Dworkin (Dworkin 2013) conceptualized the EMDR procedure in three stages, and the eight phases are distributed within:

Stage 1: evaluation and preparation

- Phase 1: understanding the case referring to the trauma (anamnesis and therapeutic plan)
- Phase 2: evaluation of patient's capacity of emotional tolerance and physical sensations awareness (patient preparation).

Stage 2: active work on trauma

- Phase 3: trauma activation (assessment)
- Phase 4: trauma elaboration (desensitization)
- Phase 5: linkage to an adaptive perspective (installation)
- Phase 6: intensive awareness of body sensations (body scan)

Stage 3: closure and reassessment

- Phase 7: debriefing (closure)
- Phase 8: reassessment

All the subjects received the entire EMDR protocol. The study focused specifically on phase 4 (desensitization). We compared the RECALL phases in which the subjects were recalling the event *per se* as well as the phase in which they were asked to focus on the worst image on the event itself (pre-RECALL): along

with eye movements in wEM groups and without eye movements in the woEM group.

4.2.3 NIRS data recording

A commercially NIRS device (NIRO-200NX, Hamamatsu Photonics K. K., Japan) equipped by two probes was adopted in our study. Each probe consisted of a photo - emitter and three infrared LED photo - detectors (peak wavelength nominally equal to 735, 810, and 850 nm). Before probes application, we carefully cleaned subject's frontal skin, to avoid the thin lipid film may reflect back part of the NIR energy. Probes were positioned bilaterally on the subject's forehead with detector placed medially with respect to the emitter. Receiver probe was placed 2 cm away from midline and 1 cm above the supraorbital ridge. **Figure 4.1** shows the probes placement with dotted line representing midline and supraorbital ridge.

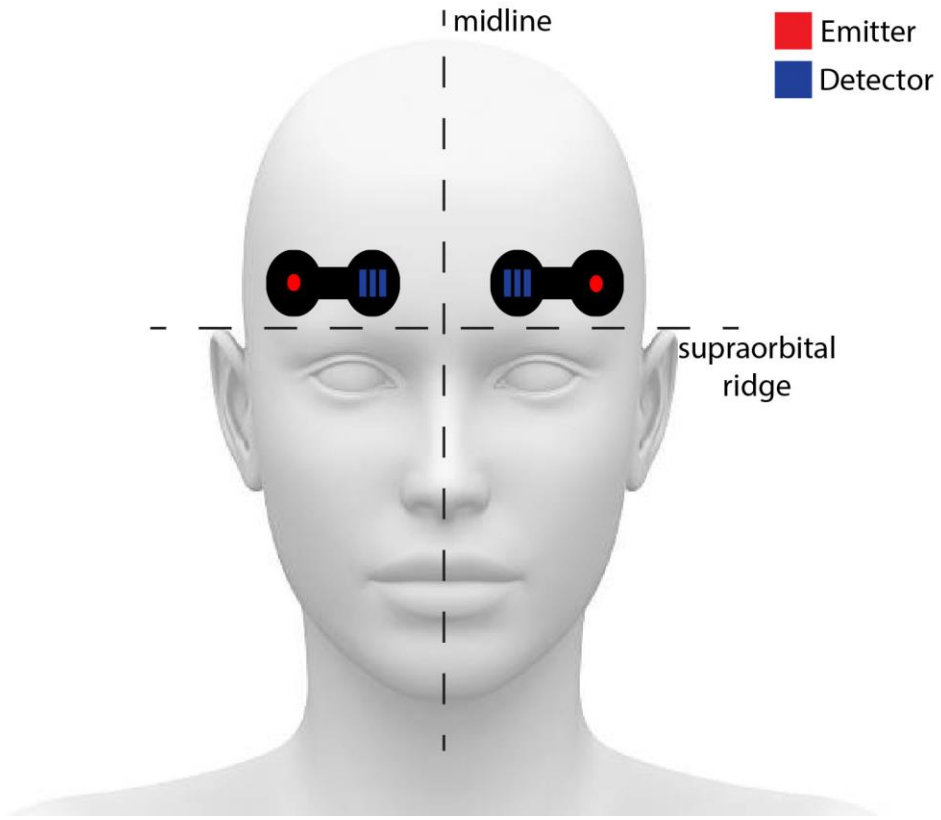

Figure 4-1. NIRS probes placement on patient forehead. Detectors are placed medially with respect to emitters. Detectors are placed 2 cm away from midline and 1 cm from supraorbital ridge.

Relative concentration of O_2Hb and HHb were continuously measured at a sampling frequency of 2 Hz. In addition, the adopted NIRS device measures the Total Oxygenation Index (TOI), and Tissue Hemoglobin Index (THI). TOI and THI represent the oxygen saturation of tissue hemoglobin and the relative concentration of total tissue hemoglobin, respectively. TOI provides information about mixed arterial - venous saturation, and it is a robust metric of tissue oxygen supply-demand balance (Waltz et al. 2015), whereas THI is representative of cerebral vasomotor reactivity (Rebet et al. 2015; Myers et al. 2009).

Differently from the O_2Hb and HHb, that are computed with the modified Beer-Lambert law (Owen-Reece et al. 1999), TOI and THI are measured by adopting the Spatially Resolved Spectroscopy (SRS). Indeed, the reliability of the NIRS measurements can be affected by confounding factors, such as high skin light absorption. For this reason, some recent NIRS devices introduced SRS technique to lower the effect of the confounding factors (Canova et al. 2011). In SRS, the slope of light attenuation versus distance is measured at a distant point from the light input using photon diffusion theory (S. Suzuki et al. 1999).

Since the apparent THI varies depending on tissue types and the geometry of the measured parts, the following normalized THI (nTHI), is measured:

$$nTHI(t) = \frac{THI(t)}{THI(0)} = \frac{cHB(t)}{cHb(0)}, \quad nTHI(1) = 0$$

nTHI represents the ratio of the current value to the initial value of total hemoglobin.

Each EMDR session was recorded with a digital video camera (DCS-900. D-LINK Corporation, Taiwan) placed behind the therapist and filming patient's eyes. The video and NIRS recording began synchronously. In this way, pre-RECALL and RECALL phases were individualized and separated.

4.2.4 Data analysis

Initially, for each subject, we identified the beginning of pre-RECALL and RECALL events from the recorded video and utilized them to separate the NIRS signals in the corresponding phases. Within each event, we preprocessed data: we adopted a low-pass filtering with a 16th order Chebyshev filter with a cut-off frequency of 250 mHz, followed by a fifth-order high-pass Chebyshev filter at 25 mHz. Within each pre-RECALL and RECALL, we normalized data to a 100 time points. Then, we computed the mean and the angular coefficient of the curves of O_2Hb, HHb, TOI, and nTHI. A positive angular coefficient indicates the parameter

is increasing, whereas a negative angular coefficient states for a diminishing parameter. For each subject and for each parameter, we computed the percentage of positive angular coefficients for pre-RECALL and RECALL separately.

NIRS signals were also analyzed in the frequency domain as slow frequency drifts convey autonomous nervous system information. We analyzed low frequency (LF) bandwidth. LF correlates to M-waves in the bandwidth of 60 to 140 mHz and represent vascular regulation of the autonomic nervous system. NIRS signal was analyzed with a time–frequency technique because of its nonstationarity. A time–frequency distribution belonging to Cohen class was computed, and a Choi–Williams distribution was adopted as kernel (Castiglioni 2005; Choi and Williams 1989)

$$D_{xx}(t,f) = \iiint_{-\infty}^{+\infty} x\left(t' - \frac{\tau}{2}\right) x^*\left(t' + \frac{\tau}{2}\right) g(\tau,\theta) \cdot e^{j2\pi\theta(t'-t)} e^{-j2\pi f\tau} dt' d\theta d\tau$$

where

$$g(\tau,\theta) = e^{\frac{\theta^2\tau^2}{\sigma}}$$

Scaling factor σ is the selectivity of the kernel and may vary from 0.1 to 10. We chose a value of 0.5, as it was low enough to attenuate interference terms, but it guaranteed a good representation of frequency components. Once $D_{xx}(t,f)$ was computed, power spectral density within LF bandwidth was extracted from CW distribution (Salvi et al. 2017).

After preprocessing, time and frequency domains parameters computing, NIRS signals of O_2Hb and HHb of pre-RECALL and RECALL intervals were decomposed using the Empirical Mode Decomposition (EMD) to obtain one intrinsic mode function (IMF1). We adopted an adaptive algorithm with the following parameters: normalized standard deviation threshold = 0.1, minimum peak prominence = 0.1, and order of the low pass filter for the nonuniform filter length = 100. Then, to measure signal complexity, we computed the Permutation Entropy (PE) and Fuzzy entropy (FE) of the obtained IMF1s (see **Chapter 3**).

We finally computed Relative Power (PIMF1) to measure the amount of spectral power associated to the IMF1. PIMF1 was computed as the ratio between the variance of IMF1 and the variance of the corresponding original signal *x*

$$PIMF1\ (\%) = \frac{var(IMF1)}{var(x)} \cdot 100$$

4.2.5 Statistical analysis

Trauma severity levels and previous EMDR experiences with NIRS parameters were correlated by means of a Pearson's Chi-Square test and the correlation ratio (η). We analyzed the efficacy of the EMDR treatment for wEM and woEM by comparing the VOC and SUD at the beginning and at the end of the treatment between wEM and woEM. Since they were score data, we adopted a Wilcoxon signed rank test to compare them.

As a primary endpoint, we analyzed NIRS time parameters to understand the main effects of eye movement on brain oxygenation. Firstly, we compared mean slope changes of O_2Hb, HHb, TOI, and nTHI during pre-RECALL/RECALL for wEM and woEM groups: for each parameter, a 2-way analysis of variance (ANOVA) was carried out, considering group (wEM, woEM) and hemisphere (right, left) as factors, and number of pre-RECALL/RECALL periods, trauma severity (t or T), and previous EMDR experiences (present or absent) as covariates. ANOVA analysis was exploited to select only variables that showed a statistically significant difference. The percentage of positive angular coefficients between wEM and woEM groups was compared by a two samples t-test, to explore different trends of the EMDR sessions. Finally, we performed a paired t-test to compare the different percentage of positive slopes of pre-RECALL/RECALL periods within the wEM and woEM groups. For all tests, we assumed a significance level α was set equal to 0.05, and all tests were performed considering different variance, since the two groups had different numerosity.

As a secondary endpoint, we performed a multivariate analysis to find the most important variables characterizing the NIRS patterns of complexity in EMDR therapy. We performed an unsupervised and supervised classification of collected variables.

The process starts with features selection and extraction: it is essential when dealing with systems characterized by many data and possible redundancy (Rosati, Balestra, and Molinari 2012; Molinari et al. 2014).

In multivariate analysis, we included two clinical features:

- *T*: trauma severity
- *N*: number of pre-RECALL/RECALL events

Also, for O_2Hb and HHb of right and left hemispheres, we included the following parameters:

- *M*: temporal mean of the original signal
- *PLF*: relative power in the low frequency band
- *PE*: permutation entropy of IMF1
- *FE*: fuzzy entropy of IMF1
- *PIMF1*: relative power of IMF1

In summary, we collected two clinical parameters and 5 parameters for 2 signals for 2 hemispheres, for an overall number of 22 parameters for each pre-RECALL and RECALL events.

As a first step of unsupervised classification, we removed collinear variables (Giustetto et al. 2010). To detect the most significant variables, we performed a one-way ANOVA. We considered group as independent variable (two levels: wEM, woEM) and the 22 parameters as independent variables. A parameter was considered significant in discriminating wEM from woEM if the ANOVA p-value was lower than 0.05. Afterwards, we performed an unsupervised learning by means of Principal Component Analysis (PCA). The difference between the coefficients of the most discriminant principal components wEM and woEM was tested by a two samples t-test.

We chose a multivariate analysis of variance (MANOVA) to perform a supervised classification of the two groups. By means of a MANOVA we performed a linear combination of the available parameters, to group the parameters into one, called Canonical Variable. To discriminate those variables responsible for the biggest part of the total variance, we performed a multivariate feature selection of the original 22 parameters. For each parameter, we performed a Wilk's lambda test:

$$\Lambda = \frac{|W|}{|W| + |B|}$$

where $|W|$ is the determinant of the within group variance matrix and $|B|$ is the between groups variance matrix. The returned value is between 0 and 1, and provides a measure of the mean differences between the groups: the smaller this value, the greater these differences. (Kshirsagar 2004). We chose, for the subsequent MANOVA analysis, the first 3 most significant variables (i.e. with the lowest Λ values).

4.3 Results

Initial and final SUD scores, and VOC scores are reported in **Table 4-I**. We found a significant difference in the final SUD between wEM and woEM patients (Wilcoxon signed rank test P = 0.03), but not a significant difference in the VOC values.

Two subjects (1 belonging to the wEM group and 1 woEM) were excluded from the analysis due to bad quality of NIRS registrations. **Table 4-II** summarizes the demographics of the remaining 10 wEM and 9 woEM subjects. No significant Pearson's Chi-Square coefficients (P > 0.1) and correlation ratio ($\eta < 0.32$) were found.

Table 4-I. VOC and initial and final SUD for wEM and woEM patients. P is the significance of the Wilcoxon signed rank test between the scores at the beginning and at the end of the therapy. *: P<0.05

	wEM	**woEM**	**P**
Initial SUD	7.95 ± 1.59	7.40 ± 1.43	0.41
Final SUD	0.10 ± 0.30	2.85 ± 3.56	0.03*
VOC	2.23 ± 1.50	2.60 ± 1.51	0.58

Table 4-II. Summary demographic data. Trauma severity has been categorized as low (t) or severe (T).

Case	Group	Sex	Age	Previous EMDR treatment	Trauma severity	Number of pre-RECALL - RECALL periods
1	wEM	F	40	No	t	20
2	wEM	F	25	Yes	T	25
3	wEM	F	34	No	T	8
4	wEM	F	41	No	T	6
5	wEM	F	24	Yes	T	13
6	wEM	F	37	No	T	9
7	wEM	F	31	Yes	t	17
8	wEM	F	41	No	T	22
9	wEM	F	29	Yes	t	12
10	wEM	M	31	Yes	t	16
11	woEM	F	29	Yes	T	8
12	woEM	F	25	Yes	t	5
13	woEM	M	34	Yes	T	27
14	woEM	M	42	Yes	t	13
15	woEM	F	31	No	T	12
16	woEM	M	35	Yes	t	21
17	woEM	F	38	No	T	16
18	woEM	M	28	No	T	8
19	woEM	M	25	Yes	t	11

4.3.1 wEM – woEM angular coefficients

Figure 4-2 shows the slope of O_2Hb and HHb curves of each patient averaged for pre-RECALL and RECALL. It can be noticed that in wEM O_2Hb slightly decreased during pre-RECALL, whereas it increased in RECALL. Indeed, in 7 out 10 subjects, O_2Hb diminished during pre-RECALL and it increased during RECALL. Conversely, HHb weakly increased in woEM during pre-RECALL, followed by a decrease in subsequent RECALL. A 2-way ANOVA evidenced a significant main effect of group (wEM vs woEM) on the mean slope of O_2Hb ($F_{(1,37)} = 7.6$, $P = 0.01$) and HHb ($F = 6.2$, $P = 0.02$) in pre-RECALL. As for the RECALL, a 2-way ANOVA revealed a significant effect of group on the slope of O_2Hb ($F = 7.274$, $P = 0.011$), and HHb ($F = 7.763$, $P < 0.01$). No further significant effect for hemisphere, or interaction between group and hemisphere were observed.

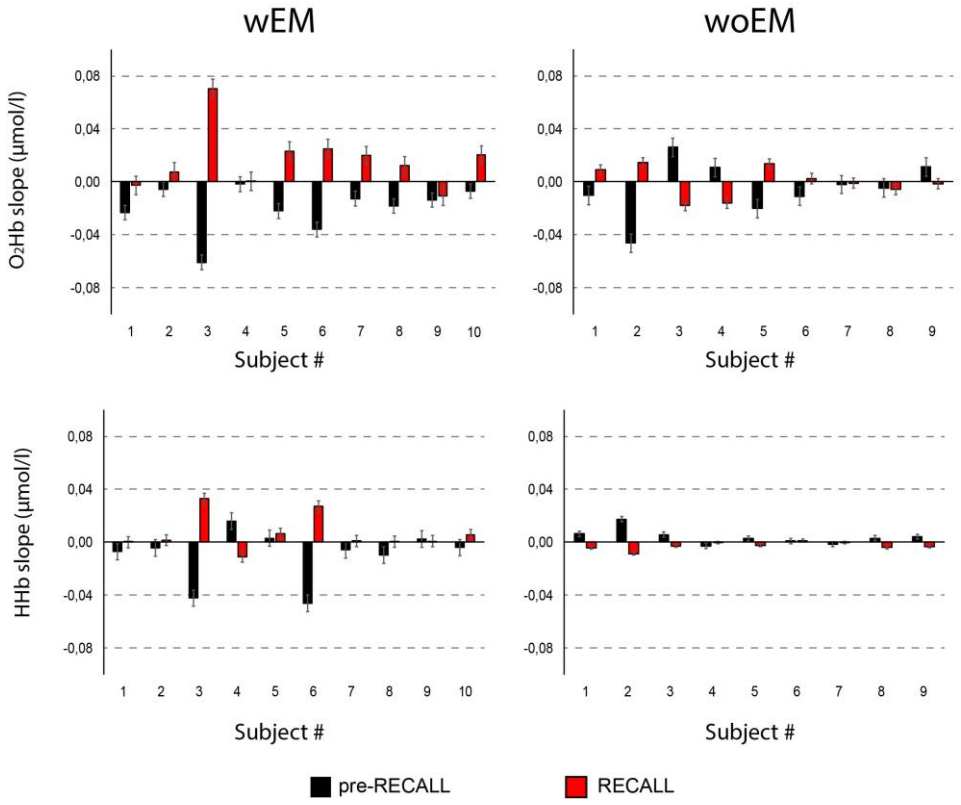

Figure 4-2. Right hemisphere O_2Hb and HHb slopes for pre-RECALL and RECALL. Subjects are numbered from 1 to 10 for wEM group and from 1 to 9 for woEM group. Data are reported as mean ± standard error.

4.3.2 wEM – woEM percentage of positive angular coefficients

We averaged O_2Hb and HHb values of left and right hemispheres, and we computed the percentage of positive angular coefficients for O_2Hb and HHb within pre-RECALL and RECALL. **Table 4-III** reports results of paired t-test of percentage of positive slopes of wEM with respect to woEM. It can be observed that both O_2Hb and HHb decreased during pre-RECALL, followed by an increase during RECALL. Particularly, two observations can be done: 1) during pre-RECALL, woEM subjects have a significant higher percentage of HHb positive angular coefficients than wEM subjects, and 2) during RECALL, woEM subjects have a significant lower percentage of positive angular coefficients with respect to wEM group. In woEM patients, the HHb increased during the simulated pre-RECALL more frequently than wEM subjects did, whereas during RECALL the mean concentration of HHb slightly went down.

Table 4-III. two-sample t-test of mean percentage of positive slopes of wEM and woEM groups

	Periods	Mean ± Ste	95% Confidence interval		Sig.
			Lower	Upper	
O_2Hb	pre-RECALL	-10.01 ± 9.71	-31.84	11.82	0.33
	RECALL	9.86 ± 7.48	-5.96	25.68	0.21
HHb	pre-RECALL	-21.48 ± 8.90	-40.19	-2.77	0.027*
	RECALL	19.28 ± 7.27	3.74	34.81	0.018*

* $P < 0.05$

We compared pre-RECALL and RECALL mean percentage of positive coefficients for O_2Hb and HHb. **Figure 4-3** shows the mean percentage of positive coefficients for each group and condition. Black bars represent pre-RECALL periods, red bars represent RECALL periods. In wEM patients, 27.26% of O_2Hb angular coefficients were positive, whereas 57.16% of O_2Hb angular coefficients were positive in RECALL events. A paired t-test of mean percentage positive angular coefficients showed that wEM subjects a significant higher percentage of positive coefficient of O_2Hb in RECALL than pre-RECALL (27.26% versus 57.16%, $P < 0.002$). Conversely, woEM group did not show statistically difference in O_2Hb between pre-RECALL and RECALL (34.24% versus 46.76%, $P > 0.4$). woEM subjects have a percentage of positive coefficient of HHb in pre-RECALL significatively higher

with respect to RECALL (68.02% versus 33.96%, P < 0.03), differently from wEM group (43.79% versus 55.32%, P = 0.39).

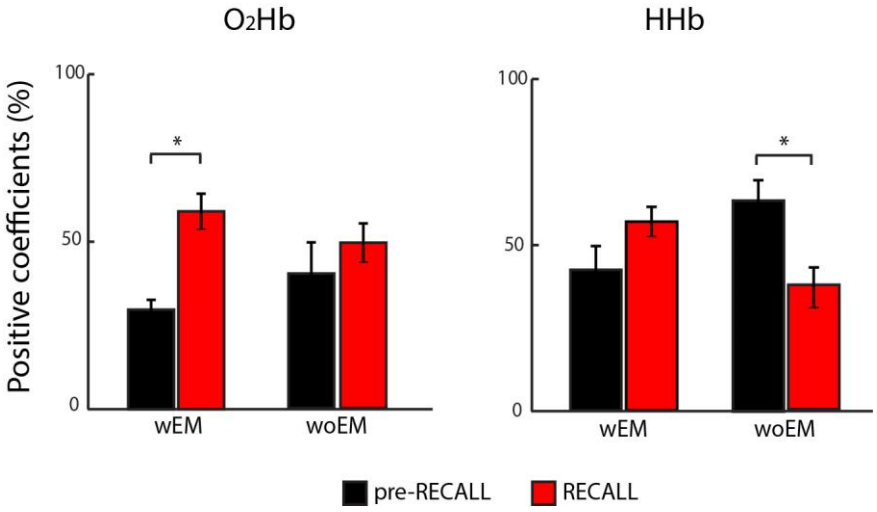

Figure 4-3. Mean percentage of positive angular coefficients of O_2Hb (A) and HHb (B) in pre-RECALL and RECALL periods for wEM and woEM groups. * : P < 0.05. Data are reported as mean ± standard error.

4.3.3 Unsupervised analysis - PCA

The most significant parameters for pre-RECALL and RECALL obtained from ANOVA are reported in **Table 4-IV**. It can be observed that Components are mainly related to frequency domain parameters. This result confirms the importance of vasomotricity and sympathetic action in the EMDR therapy. It can also be observed that number of repetitions, HHb mean concentration and complexity parameters provide a contribute in the separation of the two groups. Then, from raw data of the selected parameters, we computed the covariance matrix. From the covariance matrix, we obtained the eigenvalues for pre-RECALL and RECALL (**Figure 4-4**). It can be observed that, in both cases, two eigenvalues are higher than 1: hence, two components convey nearly all the variance of the original variables. Particularly, the first two components convey for the 71.66% and for the 63.59% of the total variance for the pre-RECALL and RECALL periods respectively.

Table 4-IV. Significant variables after ANOVA analysis. R stands for right hemisphere, L stands for Left hemisphere.

pre-RECALL		RECALL	
Variable	**Hemisphere**	**Variable**	**Hemisphere**
PLF O_2Hb	R	PLF O_2Hb	R
PLF HHb	R	PLF HHb	L
PLF O_2Hb	L	PE HHb	L
FE HHb	L	FE HHb	L
M HHb	L	M HHb	L
N		N	

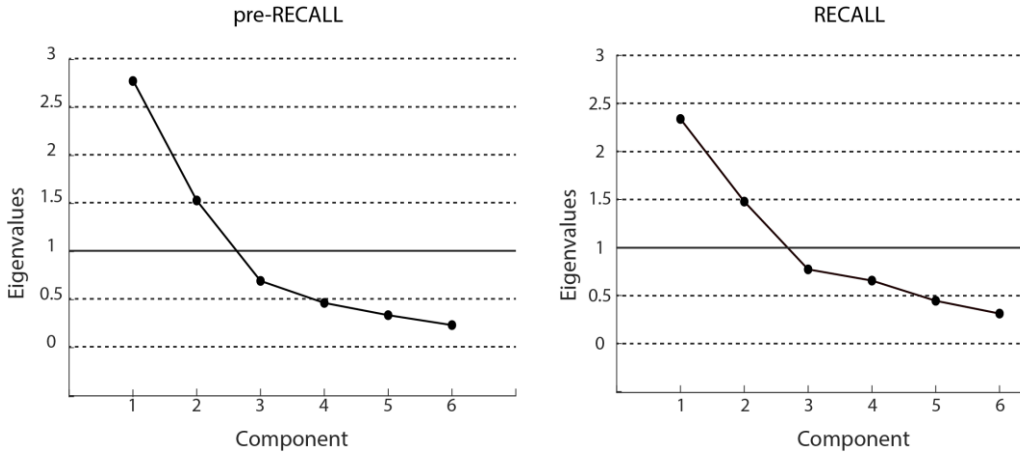

Figure 4-4. Eigenvalues applied to the dataset consisting of 6 variables for pre-RECALL (left panel) and RECALL (right panel) summarized in Table IV. The first two eigenvalues are higher than 1 (horizontal filled line). Therefore, these two eigenvalues were adopted to represent the subjects in a reduced domain of two principal components.

Figure 4-5 reports the subjects' distribution on the hyperplane formed by components 1 and 2. White circles represent wEM subjects, whereas black circles are the woEM subjects. The black continuous lines represent the projection of original variables on the hyperplane. It can be observed that PLF variables have positive components 1 and 2, and that first component well separates the two groups. **Table 4-V** reports the results of the t-test for the wEM versus woEM in pre-RECALL and RECALL periods. It can be noticed that Component 1 significantly separates the two groups in both pre-RECALL and RECALL periods.

Table 4-V. T-test comparing the scores of the Component 1 and Component 2 of wEM vs woEM groups in pre-RECALL and RECALL periods. The significance threshold is 0.05. First component significantly separates wEM from woEM subjects in both pre-RECALL and RECALL periods. Data are reported as mean ± standard deviation.

Period	Variable	wEM	woEM	p
pre-RECALL	Component 1	1.20 ± 1.25	-1.33 ± 0.82	<0.0001*
	Component 2	0.09 ± 1.54	-0.1 ± 0.86	0.75
RECALL	Component 1	0.82 ± 1.38	-0.91 ± 1.16	0.01*
	Component 2	0.25 ± 1.44	-0.28 ± 0.92	0.35

*: P<0.05

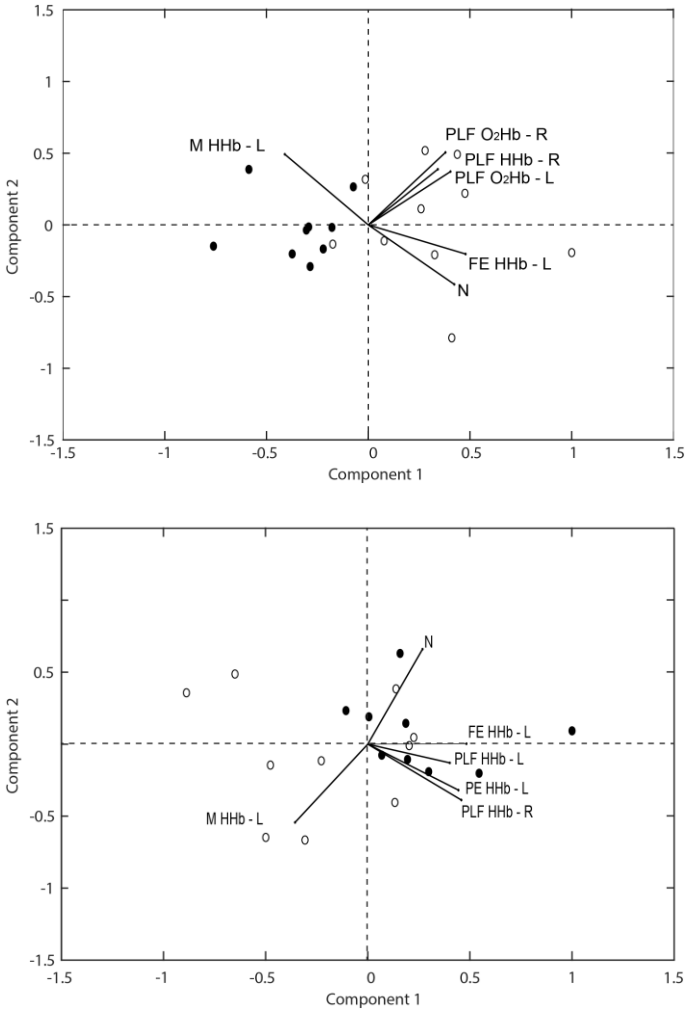

Figure 4-5. PCA representation of the subjects in the hyperplane of principal components 1 and 2. Top panel: pre-RECALL. Bottom panel: RECALL. White circles represent wEM subjects, black circles those in the woEM group. The black lines represent the projection of the original variables in the hyperplanes. In variable names, R stands for right hemisphere, L stands for Left hemisphere.

4.3.4 Supervised analysis – MANOVA

Table 4-VI reports the three variables with the most significant Λ for pre-RECALL and RECALL. It can be noticed that, in both cases, the power of HHb in LF band, FE of HHb, and the total number of repetitions are the most important variables. Table VI reports also the mean values of the most significant variables for wEM and woEM groups. It can be notices that wEM group has higher values of PLF and FE than woEM in pre-RECALL and RECALL periods. It may confirm that the vascular activity and the complexity of the physiological system during the EMDR therapy increases due to the eye movements. **Figure 4-6** represents the subjects in the hyperplane of the first and second Canonical Variables. MANOVA shows that the dimension of the space containing the two groups means is equal to 1, and that one Canonical Variable separates the two groups.

Table 4-VI. Most significant variables after Wilk's Lambda analysis. The values of the variables are reported as mean ± standard deviation. In variable names, R stands for right, L stands for left hemispheres.

Periods	Variable	wEM	woEM	Λ
pre-RECALL	PLF HHb - R	19.09 ± 6.44	11.99 ± 5.91	0.60
	FE HHb - L	0.014 ± 0.011	0.008 ± 0.013	0.69
	N	25.2 ± 11.6	16.2 ± 11.0	0.65
RECALL	FE HHb - L	0.025 ± 0.023	0.015 ± 0.015	0.85
	PLF HHb - L	20.80 ± 8.88	13.62 ± 6.70	0.84
	N	25.2 ± 11.6	16.2 ± 11.0	0.65

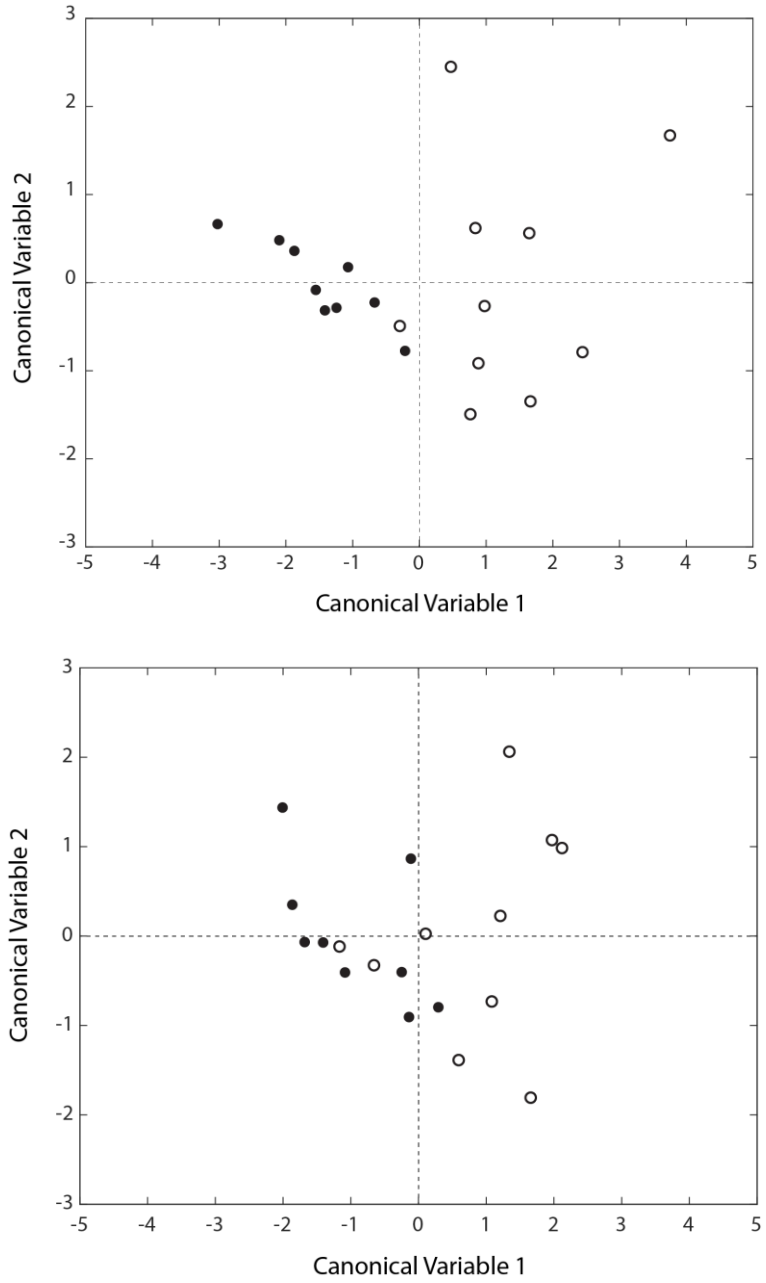

Figure 4-6. Representation of the subjects in the hyperplane of the first and second Canonical Variables. Upper panel shows the pre-RECALL periods, bottom panel represents the RECALL periods. The subjects of wEM group are represented with white markers. The subjects of the woEM group are represented with black markers. One Canonical Variable well separates the two groups.

4.4 Discussion

Our results showed different oxygenation of PFC and system physiology pattern in the case of EMDR therapy with ocular movements with respect to a control group without them. In wEM subjects, O_2Hb decreased during pre-RECALL, followed by an increase during RECALL. Conversely, in woEM subjects, we observed HHb increased during pre-RECALL, compensated by a decrease during RECALL. Finally, by considering descriptors of the complexity of the system physiology, we registered two different underlying patterns mainly due to a different sympathetic regulation.

Several functional studies have been performed to study effects of EMDR on cerebral activation. Pagani and colleagues found a pattern of resynchronization of cerebral EEG waves and an increase of interhemispheric connectivity during EMDR sessions (Pagani et al. 2012). Nuclear medicine was adopted to explore the CBF by comparing cerebral activation during exposure to the traumatic memory before and after therapy. It was showed that EMDR therapy induces a significant modification of neuropsychological condition and CBF. Several modifications were observed in areas involved in stress management belonging to HPA axis (Pagani et al. 2007). However, to the best of our knowledge, EMDR was investigated only in one study with NIRS (Ohta ni et al. 2009). Differently from the present work, Ohta ni and colleagues compared patients with and without eye movements after 2 to 10 EMDR sessions to explore the effect of therapy over time, whereas our work was limited to only one session. However, authors observed an improvement in brain perfusion for both patients with and without eye movement Hence, no clear association between EMDR and lateral PFC over-activity over the time can be deduced.

As a first result of interest of the present study, we observed a slight decrease of PFC microcirculation in the woEM group during the pre-RECALL period, as demonstrated by the decrease in HHb concentration. This phenomenon has been seldom reported in literature as negative BOLD response (NBR)(Mullinger et al. 2014). It is a not fully understood phenomenon, hence several hypothesis about underlying physiological mechanisms have been provided (Maggioni et al. 2015). One of the most reliable is that some brain regions require a raising in oxygen consumption due to the increase of their activity. Then, to satisfy its supply, oxygen is taken from contiguous areas, coinciding with monitored areas and where NBR is observed. In our recorded cases, slight but significant NBR in PFC has been recognized, maybe due to the raising of activity in closer brain areas which probably required a supplement consumption of oxygen.

Subjects in two groups, during the experimental protocol, dealt with an identical stressful condition, but with two different instruments to face it. Indeed, woEM subjects during RECALL were not focusing on a particular activity, so the resting state was theoretically the only activated network. Nevertheless, we suppose that subjects could feel in a stressful condition: while recalling the event, a traumatic memory emerged without resolution, and this could lead to the alteration of the network at rest. Subjects in wEM group showed an opposite behavior: during RECALL, they focused their attention on a secondary activity due to EM. It allowed the subjects to diminish their anxiety. The reduction in hardship was expressed in a differential modification of O_2Hb in PFC, since it increased significantly during RECALL, then decreased to lower values during pre-RECALL: therefore, by focusing on the particular activity of eye movement, activity shifts toward the areas highlighted by previous functional studies.

The study of complexity evidenced also an important role of frequency variables to define new variables in unsupervised and supervised learning. It is in good agreement with previous studies on EMDR, where a reduction in sympathetic activity (Schubert, Lee, and Drummond 2011) and mostly an increase in parasympathetic (Gunter and Bodner 2009) during pre-RECALL were reported, reinforcing the hypothesis that eye movements are dearousing.

4.5 Conclusion

We submitted two groups of subjects to EMDR therapy with and without eye movement respectively in order to observe the effects of cerebral hemodynamics, by assessing PFC with NIRS. Our outcomes revealed a different oxygenation pattern between pre-RECALL and RECALL periods in wEM group which is not observable in woEM. They evidenced a different hemodynamics induced by eye movements that may be helpful in resolving the stressful condition of trauma recalling.

Chapter 5

Cerebrovascular pattern improved by ozone autohemotherapy: an entropy-based study on multiple sclerosis patients[2]

5.1 Introduction

5.1.1 General overview of ozone therapy

Ozone is defined as a water-soluble molecule, chemically instable and with a strong oxidant power, composed by three atoms of oxygen and one odd electron. Oxygen-ozone therapy refers to the administration of an oxygen-ozone compound: concentration, quantity and modalities vary according to physio-pathological condition of the subject and to the purpose of the treatment. The only contraindications to ozone administration are: hyperthyroidism and deficit of Glucose-6-phosphate dehydrogenase (N. Smith et al. 2017).

One of the first applications of ozone in medicine was described by Leux Curtis in 1902 (Curtis 1902). In the paper, Curtis applied a combination of electricity, light, heat, and ozone to treat the phthisis of fifty patients suffering from

[2] This chapter is based on the paper: Molinari, F., Rimini, D., Liboni, W. et al. Med Biol Eng Comput (2017) 55: 1163. https://doi.org/10.1007/s11517-016-1580-z

tuberculosis, including several cases of consolidation of lung and twelve cases of tuberculous ulcer. The objective of this early study was "oxygenating the blood, destroying pathogenic organisms in the body, and eliminating the products of retrograde metabolism". Good results were obtained in nearly all the treated cases, with recovery of lung capacity and tuberculous infiltration resolution. Nowadays, ozone therapy is administered by autohemotherapy, subcutaneous and intra-articular injection, rectal, nasal and vaginal insufflation. The only dangerous administration is inhalation, because it would cause bronchospasm and the irritation of the mucous membranes. The way of administration, the quantity, and the concentration percentage of oxygen and ozone in the compound vary according to the pathology and condition of the patient ("WFOT's Review on Evidence Based Ozone Therapy" 2015).

According to Arthur C. Guyton, "blood is a functional whole and any pain, suffering or chronic illness is also caused by insufficient oxygenation at the cellular level" (Guyton and Hall 2005). It means that good functioning of physiological systems depends on the equilibrium between oxidant and antioxidant species. An imbalance of oxidant compounds, called oxidative stress, may be the cause or a consequence of a disease. Oxidative stress is the imbalance between pro-oxidant and free radicals versus antioxidant system. It is induced by chemical and physical agents or by mitochondrial metabolic disorders. Oxidative stress is considered the responsible of inflammation and several pathologies, including atherosclerosis, neoplasia, arterial hypertension, rheumatoid arthritis, neurodegenerative diseases, and aging (Flora 2007). Since ozone is an oxidant and free radical generator, it was considered harmful for the organism until the nineties of the last century. Indeed ozone, by reacting with unsaturated fatty acids and antioxidants, generates a transitory increase of reactive oxygen species (ROS) and Lipid Oxidation Products (LOPs). However, further studies evidenced a natural ozone release in human reactions. For instance, Marx and Bardi demonstrated that immunoglobulin exert the bactericidal action by freeing ozone (Marx 2002). Ozone therapy is based on a controlled oxidative stress generated by ozone. Within controlled blood volume and body compartments, oxygen-ozone compound induces a transitory increase of ROS and LOPs. ROS and LOPs increase glycolysis and mitochondrial and plasmatic antioxidant capacities, followed by all the consequent biological reactions (Velio Bocci 1995; Viebahn 1994; Velio Bocci et al. 2009; Muñoz 1993; Poppler et al. 1994; Simonetti, Liboni, and Molinari 2014). Particularly, LOPs interact with endothelium and activate NO synthetase: it induces NO release regulating vasodilation and inflammatory processes (Nakao et al. 2009; Pryor et al. 2006).

5.1.2 The action of ozone on microcirculation pathologies

Microcirculation is the thick network of small blood (capillaries, pre-capillaries, venule) and lymphatic vessels that allow the exchange of nutritious and cellular catabolites between blood and interstitial fluid. Vascular damage to the microcirculation vessels may vary according to the cause, entity, and location, and can be chronical or acute. Oxidative stress is one of the main risk factors, such as arterial hypertension, diabetes and insulin resistance, dyslipidemia, smoking, chronical inflammation, trauma.

Ozone in red blood cells increases glycolysis and adenosine triphosphate (ATP) production (Clavo et al. 2003). Furthermore, it has been demonstrated that ozone does not induces hemoglobin oxidation in methemoglobin. Indeed, by increasing membrane negative electric charge, it prevents erythrocyte adhesion to endothelium. Furthermore, by shortening lipid chain of cytoskeleton of red blood cells, it improves perfusion in microcirculation. Further researches demonstrated the antibody action and static virus of ozone (Agrillo et al. 2007; Marx 2002; Ohmine 2005; Madej et al. 2007).

Ozone eases blood flow, and reduces filterability, viscosity and platelet aggregation of red blood cells. In this way, ozone eases release of oxygen, stimulate release of growing factors, and rebalance cellular redox system (Valacchi and Bocci 1999; Giunta et al. 2001).

5.1.3 Ozone therapy in the multiple sclerosis

Multiple sclerosis (MS) is a disease of the central nervous system, characterized by multicentric inflammation, which causes neurodegeneration, and destruction of myelin (Trapp et al. 1998). MS is considered the major cause of neurological disability among young adults and affects approximately 2.5 million people worldwide. There are three different manifestations of MS: relapsing remitting, primary progressive, and secondary progressive. In most of MS patients, the disease course is relapsing remitting (MS-RR): it is characterized by acute relapses (demyelinating and inflammatory episodes) followed by periods of clinical remission. Nearly in 15% of MS patients it is characterized by the absence of remissions, and the disease course is primary progressive (Debouverie et al. 2008). Eventually, nearly 50-60% of MS-RR patients will progress to a very debilitating form of the disease, called secondary progressive, defined by sustained functional deterioration without periods of remission (Gaciasa and Casaccia 2013). Hence, clinical disability is a prominent feature of this disorder, as a result from axonal damage and neurodegeneration (Trapp and Nave 2008).

If the vascular implications of chronic venous insufficiency in MS are still debated (Morovic and Zamboni 2012; Dake 2012), the increased level of oxidative stress found in MS patients has been clearly demonstrated (Lu et al. 2000). Therefore, due to the inflammatory nature and oxidative stress in MS, ozone therapy is suitable to be an adjuvant treatment.

The quantification of vascular and metabolic cerebral effects of ozone therapy on patients is affected by cerebral autoregulation. In fact, cerebral autoregulation maintains a constant the level of oxygen which is supplied to the brain, independently with possible changes in the systemic oxygen saturation (Schytz et al. 2012). Therefore, complex methods and techniques are needed to investigate the cerebrovascular and metabolic effects of ozone therapy. Previous studies analysed the long-term effects of ozone autohemotherapy in MS patients and controls by using transcranial Doppler sonography and NIRS (Molinari et al. 2014; Lintas et al. 2013). Previous works well documented that ozone autohemotherapy increases the level of oxygen in the brain up to 1.5 hours after the reinfusion of the ozonized blood. We also demonstrated that, to avoid adverse vascular effects during ozone-autohemotherapy, oxygen-ozone compound should be administered slowly. Indeed, fast reinfusion causes vasoconstriction due to sympathetic and parasympathetic systems response (Rimini et al. 2016).

NIRS is generally adopted to monitor the changes in the concentrations of the oxygenated (O_2Hb) and reduced (HHb) haemoglobin in brain tissues (Elwell et al. 1994), thus providing vascular and flow related information. Some NIRS devices quantify brain metabolism by measuring the concentration changes of the cytochrome-c-oxidase. Cytochrome-c-oxidase is a biological enzyme and it is the terminal oxidase of the mitochondrial electron transport chain. Cytochrome-c-oxidase can be considered the pacesetter of mitochondrial oxidative metabolism and ATP synthesis, and its concentration is related to the level of mitochondrial activity of the neurons (Arnold 2012; Srinivasan and Avadhani 2012). We showed that the MS subjects increased the cytochrome-c-oxidase activity and concentration about 40 minutes after the end of the treatment. This result demonstrated the positive metabolic effect of ozone in reducing the level of oxidative stress and promoting brain metabolism (Molinari et al. 2014). However, due to the interaction with possible cofounding effects, such as skin light adsorption and low tissue concentration, newest NIRS devices do not measure cytochrome-c-oxidase anymore.

The NIRS signals, carry considerable information in the frequency domain as well. Obrig *et al.* showed that cerebral NIRS signals allow the evaluation of the cerebral vasomotor reactivity and autoregulation (Obrig et al. 2000). In our previous studies, we combined time and frequency analysis of NIRS signals in order to extract physiological information while trying to avoid the possible noise sources (Molinari et al. 2006; Molinari et al. 2015; Liboni et al. 2007). Furthermore, cerebral NIRS signals acquired when the subject is not in resting conditions might be nonstationary in nature; hence, ad-hoc time-frequency analysis should be used (Molinari et al. 2010; Liboni et al. 2007). Given the complex interaction between infrared light and tissues, NIRS signals are nonlinear in nature. Therefore, the time and time-frequency analysis might be insufficient to capture the subtle variations from the signals, whereas nonlinear techniques can provide more accurate information (Acharya, Molinari, et al. 2012; Molinari et al. 2013; Faust et al. 2012; Molinari et al. 2015).

In this chapter, we performed a linear and nonlinear analysis of cerebral NIRS signals acquired from MS patients and controls during major ozone autohemotherapy. The objective of the present work is assessing the effect of the ozone autohemotherapy on the cerebral pattern of MS patients even without monitoring the cytochrome-c-oxidase concentration. Furthermore, we also investigated the long term effect of ozone autohemotherapy in brain metabolism, by comparing autoregulation at the beginning of therapy, at the end of the therapy, and 24 hours after therapy.

5.2 Material and methods

5.2.1 Patients demographics

The experiment was conducted after having obtained the approval from the Review Institutional Board of the “Un Passo Insieme ONLUS Foundation” (Valdellatorre, Torino, Italy), of the “KAOS ONLUS Foundation” (Caselle Torinese, Torino, Italy), and of the Italian Society for the Oxygen and Ozone Therapy (SIOOT, Gorle (BG), Italy). The approved informed consent was read and explained to the subjects before the tests and they were required to sign it.

We recruited 10 subjects suffering from MS-RR, with a confirmed diagnosis of pathology whose onset was at least five years before. Two MS-RR subjects successfully underwent therapy, but interrupted the recording and did not reach the end of the monitoring. These two subjects were excluded from the analysis. Thus,

our sample group consists of 8 MS-RR (age: 40.2±3.9, 4 females) and 10 healthy controls (age: 60.1±4.2 years, 6 females). In MS-RR group, the years from the onset of the pathology were 7.3±3.3 years, the EDSS average score was in the range 1.5 – 3.5. All the subjects followed a therapy consisting in beta interferons injections, and corticosteroids administered in correspondence of attacks. In control group, we enrolled 10 volunteers without any neurological, metabolic, or cardiovascular disease. Heavy smoking and hypertension subjects were excluded.

5.2.2 Experimental protocol

The experiment was performed in two days. On day one, we administered major ozone-autohemotherapy and measured autoregulation before and after the therapy. On the second day, we only monitored autoregulation. Two end-points were analyzed: first end-point was assessing the effect of the ozone autohemotherapy on the cerebral pattern of MS patients even without monitoring the cytochrome-c-oxidase concentration. At this aim, we measured time and time-frequency entropy-based features within 7 windows of analysis. As a secondary end-point, we investigated long-term effects of ozone on microcirculation, by measuring cerebral autoregulation just before and up to 24 hours after the major ozone-autohemotherapy.

Cerebral oxygenation was monitored with NIRS from the forefront of the subjects. We adopted a NIRO200 device (Hamamatsu Photonics K.K., Japan), equipped by two probes, which consisted of a photo-detector and four infrared LED sources (wavelengths equal to 775, 810, 830 and 910 nm). Each probe was placed on the subject's forehead, 2 cm away from midline and 1 cm above the supraorbital ridge to avoid the sinuses (Molinari et al. 2006). The sampling frequency of the system was set to 2 Hz. The pre-processing consisted in a IIR digital 8^{th} order Butterworth band-pass filter, with lower frequency equal to 20 mHz and an upper bound set to 250 mHz.

5.2.3 Primary end-point: effect of ozone autohemotherapy on cerebral patterns

The major ozone autohemotherapy protocol consists of the following steps:

1. drowning of 240 grams of whole blood from the antecubital vein of the subjects by using SanO3 bags (Haemopharm, Milan, Italy);

2. mixing of the blood with 240 ml of O_2/O_3, composed by O_2 at 50%, with an O_3 concentration equal to 40 μg/ml (Medical 95 CPS, Multiossigen, Gorle (BG), Italy);
3. slow blood re-infusion in the same vein.

The subjects were asked to stay supine, keeping eyes closed and breathing normally. The NIRS device measured in real-time the concentration changes of the O_2Hb and HHb for both the hemispheres. Since we did not find any statistically significant difference in the concentration changes of the two hemispheres (paired Student's t-test; $p > 0.8$), we averaged the signals of the two hemispheres. Hence, for each subject, we recorded the O_2Hb and HHb concentrations. We analysed the acquired signals in 7 different time intervals, lasting 256 s each:

1. baseline recording;
2. blood drawing;
3. middle of reinfusion;
4. end (last 256 s) of reinfusion;
5. 40 minutes after reinfusion;
6. 1 hour after reinfusion;
7. 1.5 hours after the reinfusion.

We chose these analysis windows in order to observe specific event related and long-term changes. For each window and on each patient, we performed time domain analysis of the signals, by computing the average O_2Hb and HHb concentration within each observation windows.

The NIRS signals are characterized by a marked nonstationary nature and hence time-frequency analysis is required (Molinari et al. 2010; Molinari et al. 2014; Liboni et al. 2007). Within each monitoring window, we performed a time-frequency analysis and we computed a Choi-Williams (CW) distribution for O_2Hb and HHb (see **Chapter 5**) (Barry 1992; Molinari et al. 2010).

From the time-frequency representation, we computed the relative power of the low-frequency band (LF 40 mHz – 150 mHz): LF power was computed as the ratio between the power in the LF band over the total signal power (Obrig et al. 2000).

The Shannon Entropy (SE) is a measure derived from the field of information theory (Kumar, Kumar, and Kapur 1986). SE is based on the probability distribution; hence, to make it applicable in signal processing, the power spectral densities must be normalized. However, our signals are nonstationary, so, we

defined the SE based on the time-frequency representation $D_x(t,f)$ of the signals. Firstly, we normalized the power of the $D_x(t,f)$ as follows:

$$d_x(t,f) = \frac{D_x(t,f)}{\iint_{-\infty}^{+\infty} D_x(t,f)dtdf}$$

in order to make the overall power equal to 1. Then we defined the instantaneous SE as:

$$SE(t) = -\int_{-\infty}^{+\infty} d_x(t,f) \cdot \ln\big(d_x(t,f)\big)\ df$$

Figure 5-1 shows an example of time-frequency analysis for a representative subject. **Figure 5-1A** reports the O_2Hb concentration changes during the baseline recording of healthy subject. **Figure 5-1B** is its corresponding CW representation with function of time and frequency (grey box indicates LF band). **Figure 5-1C** reports the SE. The time course of the SE was averaged to compute a single value for each signal.

Within each window, we performed and Empirical Mode Decomposition (EMD) for the O_2Hb and HHb signals. From the EMD, we extracted the first three Intrinsic Mode Functions (IMFs) of O_2Hb and HHb signals, and, for each IMF, we computed two nonlinear metrics: Sample Entropy (SampEn) and Hurst Exponent (HE) (see **Chapter 3**).

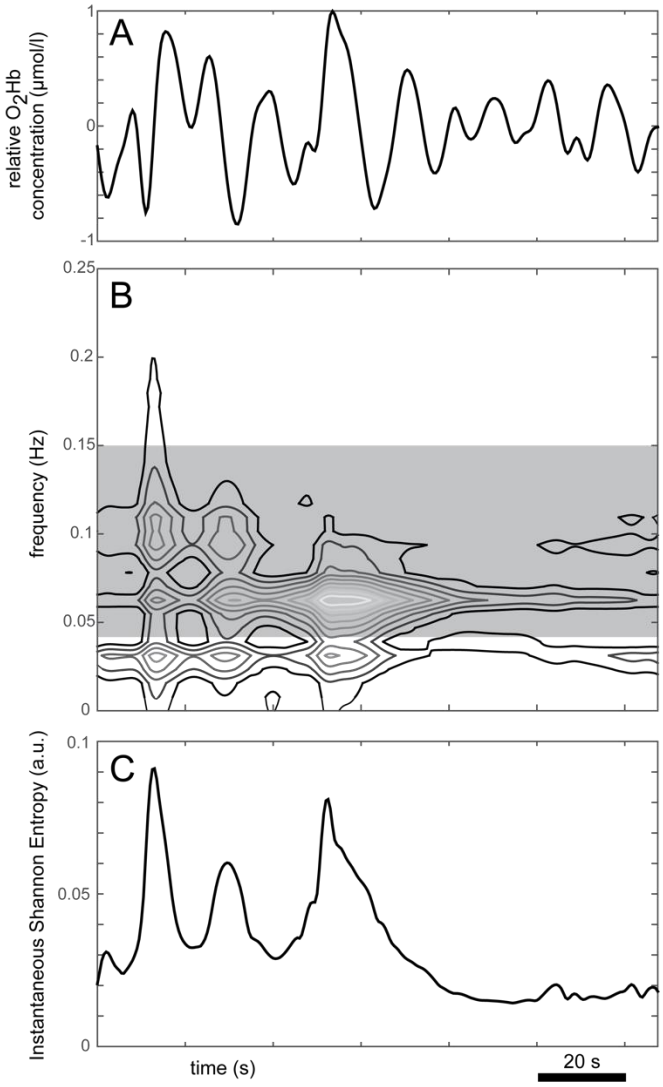

Figure 5-1. (A) Time course of the concentration of O_2Hb during baseline. (B) CW transform of the signal. The gray zone represents the LF band. The gray rectangle depicts the LF band. (C) Corresponding instantaneous SE derived from the CW transform. The time course of the SE was averaged to compute a single value for each signal.

5.2.4 Secondary end-point: short- and long-term effects of ozone on cerebral autoregulation

Autoregulation aims to maintain constant cerebral blood flow (CBF), despite the systemic pressure variation. It is essential maintaining CBF constant, in order to preserve brain activity and metabolic demand (Basso Moro et al. 2014). Hence, as a secondary end-point, we investigated how ozonetherapy affected autoregulation in healthy controls and MS patients. A good and easy-to-measure indicator of autoregulation is the modification of O_2Hb during apnea (Gersten 2015). Indeed, during apnea, to provide oxygen to the brain constantly, CNS activates an autoregulatory/hyperemia mechanism. During apnea, the relative pressure of CO_2 (P_{CO2}) increases, hence H^+ ions increases and pH decreases. To favor CO_2 removal, section of vessels increases (vasodilatation), with a consequent O_2Hb increase. Hence, ΔO_2Hb, the difference between the O_2Hb at baseline and O_2Hb at the end of apnea, was measured. Autoregulatory response was measured with the Breath Holding Index (BHI) (Molinari et al. 2006), computed as the ratio between the slope of O_2Hb concentration during apnea and the duration (in seconds) of apnea itself:

$$BHI = \frac{O_2\mathrm{Hb}_{\,BH} - O_2\mathrm{Hb}_{\,BASE}}{D_{BH}}$$

where O_2Hb_{BH} is mean O_2Hb concentration during the last 10 seconds of apnea, O_2Hb_{BASE} is O_2Hb mean concentration during the last 10 seconds before apnea, and D_{BH} is apnea duration.

We investigated how autoregulation varies at short- and long-term after ozonetherapy. The short-term autoregulation was measured during the experimental setup previously described (paragraph **5.2.3**). BHI was measured between the observation windows 1 and 2, and just after the observation window 7. As for the long-term autoregulation, a second NIRS monitoring was administered 24 hours after ending the first one. For the second NIRS monitoring, the experimental conditions were maintained as equal as possible to the first. Second monitoring consisted of a 5 minutes baseline recording, followed by a breath holding test. In summary, we measured BHI in three different periods: before ozone autohemotherapy (BHI_0), 1.5 hours after ozone autohemotherapy ($BHI_{1.5\text{-hours}}$), and 24 hours after ozone autohemotherapy ($BHI_{24\text{-hours}}$).

5.2.5 Statistical Analysis

Grouped data are expressed by mean ± SD. Data normality was tested by a Kolmogorov–Smirnov test, followed by a Student's t-test to check differences in the mean values. For all the tests, we adopted a confidence level of 95%.

As for the primary end-point, multivariate analysis of variance (MANOVA) was used to compare the entropy data among the two groups and their change from the beginning to the end of the major ozone autohemotherapy. The overall number of the original features was 98 for each subject, 14 for each analysis window. The 14 features were:

- SE of O_2Hb and HHb signals (2 features)
- SampEn and HE of the three IMFs from O_2Hb and HHb signals (12 features).

Feature reduction was performed by removing the variables that explained a statistically low amount of overall data variability by using the Wilk's lambda (el Ouardighi, el Akadi, and Aboutajdine 2007). The number of features decreased from 98 to 35 and the MANOVA was performed on these remaining variables. The original features that contributed the most to the canonical variables were considered as the most important to assess the changes in the cerebrovascular pattern induced by the ozone therapy and captured by NIRS.

As for the secondary end-point, BHI at the 3 time points were compared by an analysis of variance (ANOVA), with time point as a factor, and BHI measures (i.e. BHI_{0}, $BHI_{1.5\text{-hours}}$, $BHI_{24\text{-hours}}$) as dependent variables.

5.3 Results

5.3.1 Time Changes in Brain Oxygenation

Figure 5-2 depicts the average concentrations of O_2Hb (**Figure 5-2A**) and HHb (**Figure 5-2B**) signals. The concentrations are normalized and scaled with respect to the first window (baseline), which is thus zero valued. Controls are depicted in white, and MS are depicted in gray. In accordance to previous studies, we found that ozone autohemotherapy increased the level of brain oxygenation both in controls and MS subjects (Lintas et al. 2013; Molinari et al. 2014) (**Figure 5-2A**). However, it can be observed the MS subjects showed a decreasing concentration of O_2Hb, more evident in the 5-th window (40 minutes after the end of blood

reinfusion). Then the oxygen concentration raised and reached positive levels (compared to window 1) 1.5 hours after the end of blood reinfusion. Conversely, controls maintained positive O_2Hb concentration during the monitoring. This difference in the two groups might be explained by an increase in the oxygen consumption caused by the therapy on MS subjects. In fact, previous studies (Lintas et al. 2013; Molinari et al. 2014) showed that ozone therapy increased the level of mitochondrial activity, which lead to a higher oxygen consumption by neurons. Hence, a hypothesis is that the increase in the metabolic brain activity, occurring in MS subjects, lowered the overall O_2Hb concentration, despite the reinfusion of highly saturated blood. **Figure 5-2B** shows the same HHb concentration change in MS patients and controls. The numerical values of concentrations of O_2Hb and HHb are reported in **Table 5-I**. A Student's t-test evidenced no significant difference from zero in the concentration of O_2Hb and HHb (*i.e.* from the baseline; $p > 0.1$).

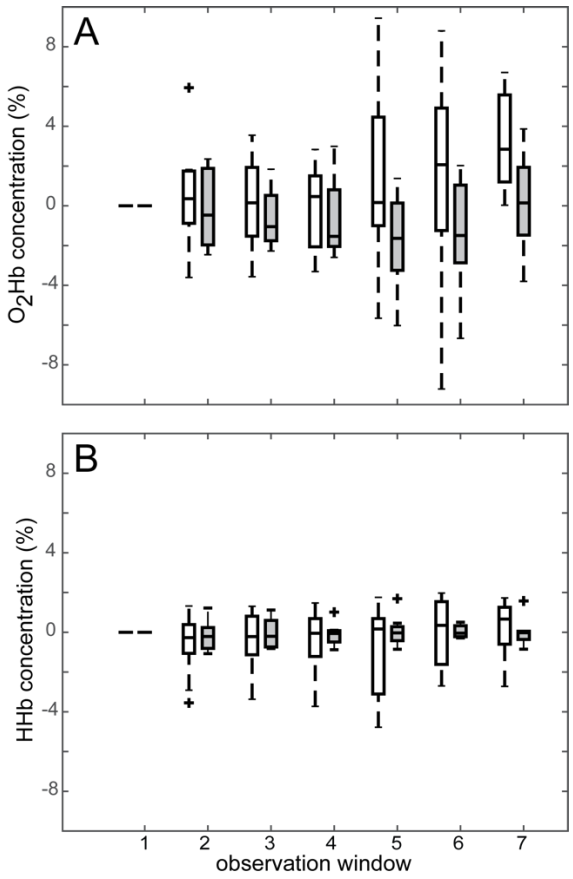

Figure 5-2. Boxplot showing the time evolution of the average concentration of O_2Hb (A) and HHb (B) in the seven analysis windows. All the values are normalized and scaled w.r.t. the first window. Controls are depicted in white, MS patients in gray. +: outlier values.

Table 5-I. Relative concentration of O_2Hb and HHb in the analysis windows. The first window (baseline) is taken as reference

Time interval window	Controls		MS-RR	
	O_2Hb (%)	*HHb (%)*	*O_2Hb (%)*	*HHb (%)*
Window 1	-	-	-	-
Window 2	0.362 ± 2.657	-0.633 ± 0.545	-0.151 ± 1.963	-0.180 ± 0.755
Window 3	0.029 ± 2.394	-0.386 ± 1.436	-0.625 ± 1.463	-0.050 ± 0.750
Window 4	-0.247 ± 2.126	-0.593 ± 1.716	-0.644 ± 2.002	-0.100 ± 0.574
Window 5	1.453 ± 4.549	-0.791 ± 2.223	-1.768 ± 2.474	0.062 ± 0.771
Window 6	1.334 ± 5.004	0.037 ± 1.766	-1.410 ± 2.882	0.045 ± 0.308
Window 7	1.997 ± 4.743	0.201 ± 1.449	0.160 ± 2.489	0.009 ± 0.715

5.3.2 Frequency Changes in NIRS Signals

Time-frequency analysis evidenced how the power associated in the LF band, representative of the vasomotor tone, changed during the therapy. **Figure 5-3** represents the changes in the LF power (normalized to the total power of the signal) of control and MS subjects during the therapy. It can be noticed that during blood drawing (window 2), the power in the LF band increased significantly compared to baseline ($p = 0.01$) for the O_2Hb signal of control subjects, and for the HHb signal of MS patients ($p = 0.02$). This effect is due to the vagal response to the needle insertion for blood drawing. In the rest of the therapy, we did not observe significant LF changes in the O_2Hb and HHb signals. **Table 5-II** summarizes the LF relative powers in the seven analysis windows.

Table 5-II. Relative power in the LF band for the O2Hb and HHb signals in the analysis windows.

Time interval window	Controls		MS-RR	
	O_2Hb (%)	*HHb (%)*	*O_2Hb (%)*	*HHb (%)*
Window 1	0.098±0.059	0.115±0.060	0.077±0.023	0.081±0.037
Window 2	0.231±0.219	0.163±0.128	0.142±0.115	0.159±0.115
Window 3	0.104±0.046	0.115±0.052	0.117±0.059	0.115±0.038
Window 4	0.119±0.096	0.102±0.033	0.096±0.052	0.097±0.031
Window 5	0.116±0.052	0.117±0.064	0.120±0.061	0.105±0.052
Window 6	0.126±0.085	0.091±0.030	0.113±0.083	0.080±0.029
Window 7	0.128±0.053	0.102±0.036	0.096±0.034	0.145±0.131

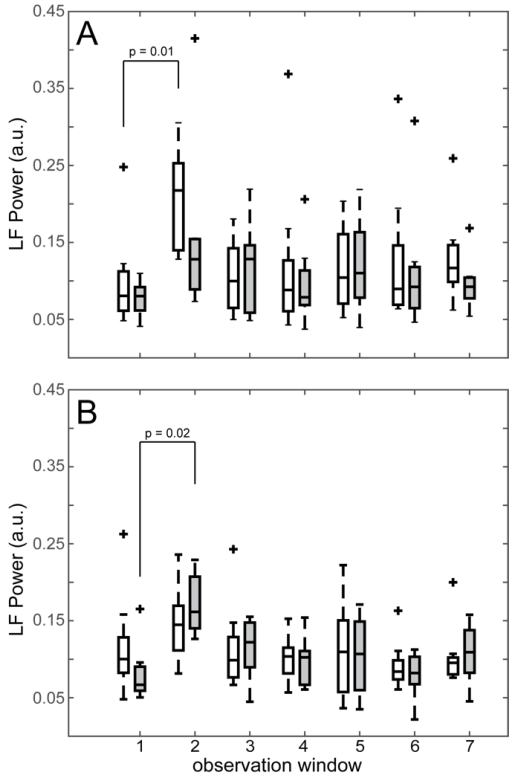

Figure 5-3. Changes in the power associated to the LF band compared to the overall signal power. Controls are depicted in gray, MS patients in white. The vertical bars superimposed to the histogram represent the standard error. (A) Power in the LF band for the O_2Hb. (B) Power in the LF band for the HHb. +: outlier values.

5.3.3 Signals' entropy and HE changes

The total of 98 descriptors of the signals in the analysis windows are reduced to 35 after the feature selection procedure with Wilk's Lambda test. These 35 features are considered as descriptive of the complexity of the cerebrovascular pattern of the subjects. The MANOVA is then applied to the set of 35 features per subject in order to evidence differences in the overall cerebrovascular patterns of MS patients versus controls. **Table 5-III** reports the statistical analysis results of three most discriminant features resulting from the Wilk's Lambda analysis. We considered three windows: window 1 (baseline), window 4 (end of blood reinjection) and window 7 (1.5 hours after blood reinjection). In all the three considered windows, the most significant features are the SampEn of first IMF obtained from HHb signal, the SampEn of the third IMF from O_2Hb signal, and HE of the first IMF from HHb signal. It can be observed that the entropy of the IMF is increasing as effect of ozone therapy, whereas the HE is decreasing. This result is observed on controls and on MS patients as well, although only for controls the increase in the SampEn of IMF3 from O_2Hb signal and HE of the IMF1 from HHb signal are statistically higher at the end of the monitoring compared to the baseline conditions ($p < 0.001$). The increase in the SampEn and decrease of the HE can be considered as indicators of increasing complexity of the physiological system under analysis.

Figure 5-4 reports the results of three IMFs extracted from the HHb signal of a MS subject. The left panel (**Figure 5-4A**) depicts the signal and its three IMFs during the baseline (1st window). The right panel (**Figure 5-4B**) depicts the signal and its IMFs at the end of the therapy (7th window). It can be noted that three IMFs show a markedly higher complexity at the end of the monitoring. More specifically, the IMF1 during baseline (**Figure 5-4A**) results in a quasi-periodic signal, clearly dominated by a single frequency. In this condition, it is expected that the entropy is low, due to the repeatability of the signal. Conversely, at the end of the ozone therapy (**Figure 5-4B**), the same IMF1 is characterized by random bursts of different amplitude and frequency, which make the signal less repeatable.

Figure 5-5 reports the representation of the subjects in the canonical plane of the first and second variables as computed by MANOVA for three different analysis windows: **Figure 5-5A** is relative to the baseline (window 1), **Figure 5-5B** is relative to the end of the blood reinjection (window 4), and **Figure 5-5C** to the end of the monitoring (window 7, approximately 1.5 hours after the end of the reinfusion). Control subjects are depicted as white squares, MS patients are depicted as black circles. In baseline condition (**Figure 5-5A**), the MANOVA analysis reveals that subjects can be considered coming from different groups ($p = 1.9 \cdot 10^{-4}$). In fact, the MANOVA dimension, which intuitively correspond to the number of variables sufficient to separate groups, is equal to 1. It can be noticed that the MS patients have a positive value of first canonical variable, whereas the controls have a negative one. At the end of the reinjection of the ozonized blood (**Figure 5-5B**), the dimension of the MANOVA is already lowered to zero ($p > 0.5$), thus indicating that subjects can be considered coming from the same group. Similarly, 1.5 hours after blood reinjection (**Figure 5-5C**), the MANOVA dimension is still zero and the MS patients and controls are superimposed ($p > 0.5$).

Table 5-III. Numerical values of the three most discriminant features in the 1st, 4th, and 7th analysis windows. The first three rows are relative to controls, the bottom three rows to the MS patients. Increasing values of sample entropy and decreasing values of the Hurst exponent are observable. * : p < 0.05

Group	Parameter	Window 1	Window 4	Window 7
Controls	SampEn IMF1 (HHb)	0.370±0.109	0.401±0.132	0.431±0.059
	SampEn IMF3 (O_2Hb)	0.201±0.057	0.244±0.098	0.266±0.091*
	HE IMF1 (HHb)	0.529±0.200	0.406±0.137	0.315±0.132*
MS-RR	SampEn IMF1 (HHb)	0.387±0.081	0.410±0.109	0.429±0.113
	SampEn IMF3 (O_2Hb)	0.281±0.104	0.287±0.073	0.318±0.076
	HE IMF1 (HHb)	0.518±0.156	0.471±0.148	0.408±0.184

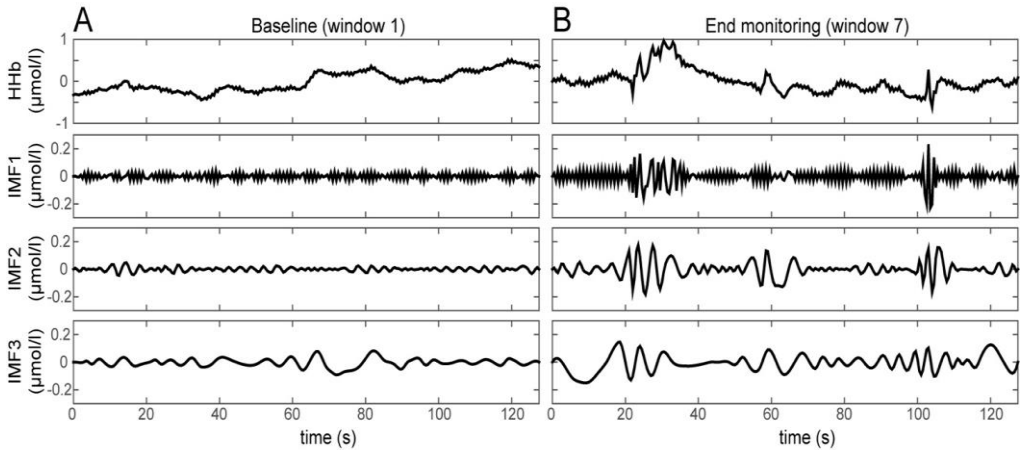

Figure 5-4. Results of the empirical mode decomposition applied to the HHb signal acquired in baseline conditions (A) and at the end of the monitoring (B) from a MS subject. The upper panels report the HHb time course; then the three IMFs are depicted. It can be observed that in panel (B) the IMFs are characterized by random bursts and changes, which make the signals less predictable.

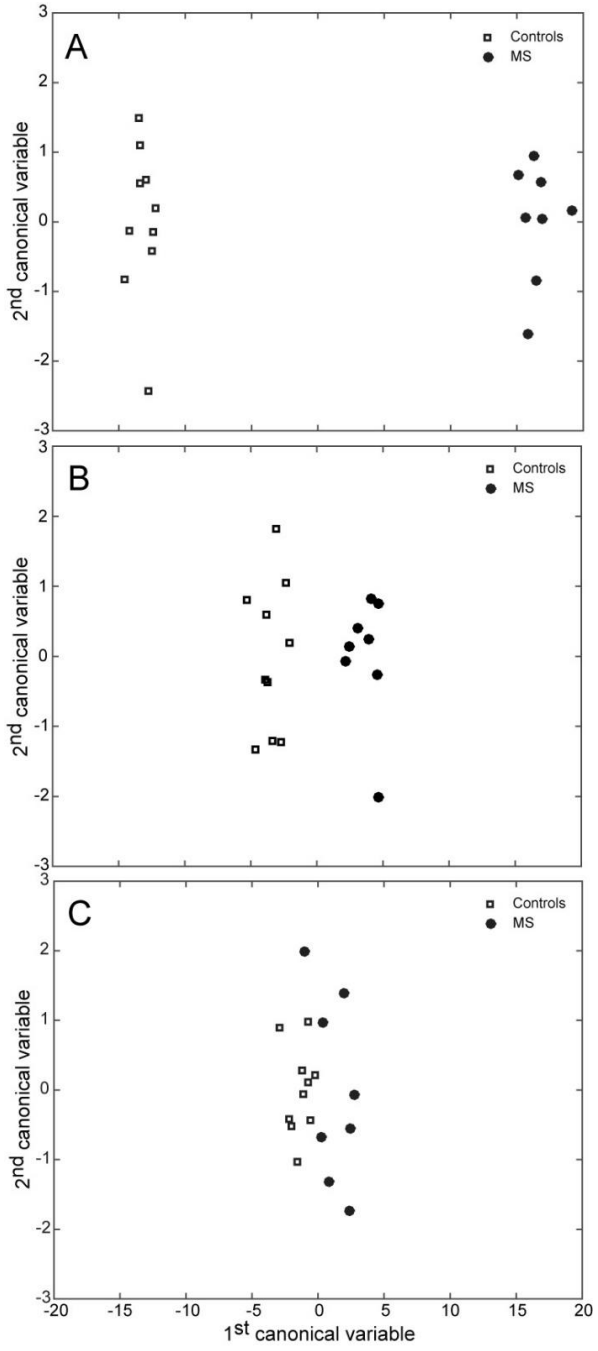

Figure 5-5. Representation of the MANOVA analysis for the subjects in three windows during therapy: (A) baseline (window 1); (B) end of the blood reinfusion (window 4); (C) end of monitoring (window 7). Controls are represented by white squares, MS patients by black circles. In (A) the subjects belong to two different groups ($p = 1.9 \cdot 10\text{-}4$), whereas in (B) and (C) the hypothesis that the subjects belong to the same group cannot be rejected ($p > 0.5$).

5.3.4 24 hours monitoring

As a secondary endpoint, we evaluated the effect of ozone therapy on cerebral autoregulation by computing BHI at three different time-points for Controls and SM-RR groups separately. Since no significant difference was found between left and right BHI for both groups and parameters ($p > 0.1$), the values were averaged between the two hemispheres.

Figure 5-6 shows the BHI in the three observation windows: at the beginning of ozone-therapy (BHI_0), at the end of therapy ($BHI_{1.5\text{-hours}}$), and 24 hours after the therapy ($BHI_{24\text{-hours}}$). BHI have been computed for the two groups separately and for O2Hb (top panels) and HHb (bottom panels). It can be observed that, for Control group, BHI O_2Hb 1.5 hours after reinjection is as half as the BHI at the beginning of therapy and 24 hours after therapy. Conversely, BHI in SM-RR group seems to not vary in the three observation time points. A one-way ANOVA evidenced a significative effect of time for BHI O_2Hb in Control group ($F = 5.12$, $p = 0.01$). BHI measured on HHb did not vary in both Control and SM-RR groups. In Control group, apnea duration was 23.8 ± 7.3 s at BHI_0, 28.3 ± 7.8 s at $BHI_{1.5\text{-hours}}$ and 24.3 ± 5.1 at $BHI_{24\text{-hours}}$. A one-way ANOVA evidenced a no significant difference in duration of apnea duration in the three observation windows. Conversely, time duration of apnea increased in SM-RR group at the end of ozone-therapy. Indeed, apnea duration was 20.5 ± 5.1 at BHI_0, 26.81 ± 6.4 at $BHI_{1.5\text{-hours}}$, and 26.8 ± 4.0 at $BHI_{24\text{-hours}}$. A one-way ANOVA evidenced a significative effect of time in apnea duration for SM-RR subjects ($F=3.74$, $p = 0.04$).

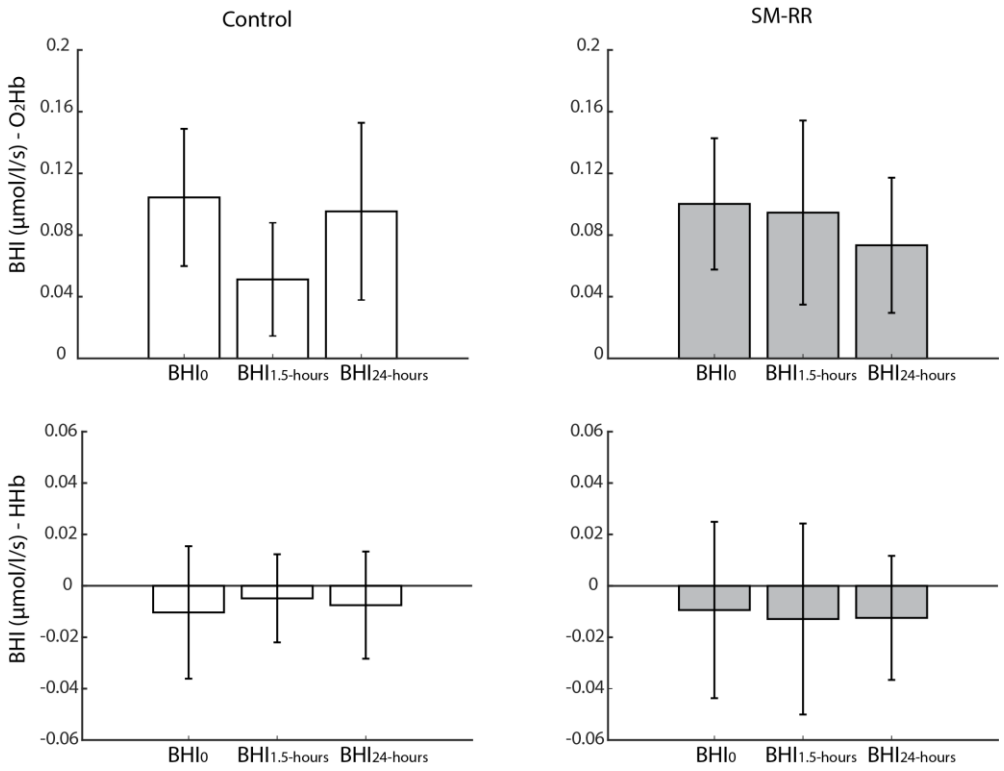

Figure 5-6. BHI values for O_2Hb (top) and HHb (bottom) for Control and SM-RR groups. BHI has been computed at three different time points: at the beginning of therapy (BHI_0), 1.5 hours after reinjection ($BHI_{1.5\text{-hours}}$), and 24 hours after therapy ($BHI_{24\text{-hours}}$).

5.4 Discussion

This chapter investigated the long-term effects of ozone therapy on cerebral circulation in MS patients compared to healthy controls. We administered major ozone autohemotherapy and we monitored the cerebral microcirculation up to 1.5 hours after the therapy by means of NIRS. We measured time, time-frequency and entropy-based features within 7 windows of interest. We observed that modification in concentration of O_2Hb and HHb were not significantly different between MS patients and healthy controls. However, entropy features evidenced different cerebrovascular patterns between MS patients and controls, and a different evolution during and after the therapy. Furthermore, we monitored cerebral circulation 24 hours after therapy and we compared the autoregulation capabilities of the two groups. We evidenced a different behaviour of MS patients from healthy controls, and different long-term effects of the ozone therapy on the two groups.

5.4.1 Primary end-point: effect of ozone autohemotherapy on cerebral patterns

In recent years, many studies evidenced positive effects of the oxygen and ozone therapy on a wide range of pathophysiological processes (H. Chen et al. 2008; Di Filippo et al. 2008), metabolism (Molinari et al. 2013), and organs (Velis Bocci, Zanardi, and Travagli 2011; Zaky et al. 2011; H. Chen et al. 2008). Certain studies focused on measuring ozone therapy efficacy at peripheral level. For instance, it was measured concentration changes of infective agents on the healing process (He and Ma 2015). Other studies showed how ozone autohemotherapy is effective in healing the leg of a patient with the post-surgical complications due to *staphylococcus aureus* infection causing a necrotic wound (Shah, Shyam, and Shah 2011). At a molecular level, Re *et al.* (Re et al. 2014) first demonstrated that ozone autohemotherapy helped the synthesis of proteins which collectively favoured cell survival.

However, there is still a lack of in-vivo evidence about the ozone action at the cerebral level. Indeed, there are several physiological limitations to non-invasively investigate the brain, including: autoregulation, that masks the most of vascular effects of therapies, and brain-blood barrier, that blocks the exchange of many chemical compounds between brain tissue and blood. Thus, many markers of inflammation, oxidation, and metabolic functions cannot be directly measured by blood samples. A few of studies adopted functional imaging to demonstrate ozone therapy efficacy. Wu and colleagues, by adopting diffusion tensor imaging, demonstrated the recovery of neurological function in acute cerebral infarction patients by reducing remote injury (Wu et al. 2016).

Previous studies showed that during ozone therapy, MS patients underwent an increase in the activity level of the cytochrome-c-oxidase of the brain tissues (Molinari et al. 2014; Lintas et al. 2013). The study is based on the spectral analysis of the NIRS signals by using a time-frequency approach. However, from a signal processing point of view, time-frequency transforms can only capture changes in the power distribution of the signals, but they cannot capture subtle changes in the signal. Hence, we integrated time and frequency analysis with nonlinear analysis of the NIRS signals.

In accordance to previous studies, the ozone therapy increased the overall level of tissue oxygenation (Clavo et al. 2004; Di Filippo et al. 2008; Molinari et al. 2014). Particularly, the oxygen increased more in controls than in MS patients (**Figure 2-A**). The latter group of subjects reached an increase in the level of oxygen concentration only at the end of the monitoring, about 1.5 hours after the end of the

reinfusion of the ozonized blood. This result might be explained by the metabolic boost induced by ozone. It is proved that MS patients are characterized by lower level of mitochondrial activity, possibly due to an oxidative damage to the DNA (Broadwater et al. 2011; Lu et al. 2000). Since ozone improved the level of mitochondrial activity (Molinari et al. 2014), it may be that the increment in the metabolic function of neurons caused an increase in the level of oxygen consumption. Therefore, just after the end of blood reinjection, the oxygen demand could have increased, thus leading to vascular response to increase the concentration at a later stage (about 1 hour after the end of the reinfusion). The analysis of the relative power in the LF band of the NIRS signals supports this consideration (**Figure 3**). It can be noticed a slight but not statistically significant increase in the LF relative power in the last three observation windows (compared to the window 1). The increase is more evident in the last window of the HHb signals analysis (**Figure 3-B**). Being the LF band a fingerprint of the vasomotor reactivity, this observation supports the hypothesis of increased metabolic demand by the brain cells, which triggers the cerebral autoregulation.

The nonlinear analysis of the NIRS signals structure showed that complexity of the cerebrovascular pattern increased during the therapy (**Table III**). Among all the descriptors used, the most significant are the SampEn of the first IMF of the HHb signals and the third IMF of the O_2Hb signals, along with the HE of the first IMF of the HHb signals. The first IMF obtained from EMD characterizes higher frequencies (**Figure 5**), whereas the third IMF lower frequencies. It is worth to observed that the most important feature for the MANOVA analysis is the SampEn of the first IMF of the HHb: it reveals a more complex structure indicating the rapid changes of the signal. Conversely, for the O_2Hb signal, we found that the structure of the signal changes in the third IMF. The third IMF is characterized by lower frequencies and higher amplitude compared to the first one. This result is in good accordance to the time changes reported by **Figure 2**: indeed, the HHb signal did not show major changes during the therapy, while the O_2Hb concentration changed considerably in both two groups. Therefore, the complexity and entropy-based analysis can capture subtle and more accurate differences in the overall cerebrovascular pattern, which are difficult to observe by time and/or time-frequency analysis alone.

We computed the SampEn and HE also on the raw NIRS signals. However, we did not find any significant difference of these descriptors when comparing controls to MS subjects, and when comparing the signals acquired on the same subjects in different windows. This may be due to the fact that the NIRS signals are a

combination of low amplitude and low frequency oscillations and of higher amplitude and higher frequency ones (Obrig et al. 2000). The computation of the structural characteristics of all the oscillations together, as in the raw NIRS signals, provides an "averaged" result, which is unable to capture the changes occurring during the therapy and the differences between controls and patients.

It is well known that the complexity of biosignals is linked to the state and properties of the underlying physiological system. In several studies, it is shown how the entropy of the EEG signal can be used to classify the sleep stages (Acharya et al. 2010), and identify (Acharya, Sree, et al. 2012) and predict (Martis et al. 2013) epileptic seizures. It is also shown that diabetes mellitus decreased the complexity of the EMG signals (Watanabe et al. 2012) of the subjects, and that physical activity helped to restore more complex muscular pattern in diabetic subjects (Molinari et al. 2013). Complexity of biosignals is usually connected to the unpredictability of the control mechanisms. In this case, since we are monitoring brain vascular and metabolic conditions, an increased entropy or decreased HE could be the effect of an increased level of control by means of cerebral autoregulation. Since the level of cerebral autoregulation is linked to the functional state of neurons, it can be hypothesized that, after a major ozone autohemotherapy, there is a boost in the metabolic and functional response of MS patients which brings the overall cerebrovascular pattern close to that of controls (**Figure 5**). The entropy of the NIRS signals increases in control subjects. Hence, we can conclude that the ozone autohemotherapy is beneficial to improve the overall cerebrovascular pattern of subjects.

Our study shows that changes in the cerebrovascular pattern cannot be properly observed by relying only on time and/or time-frequency analysis. Major changes in oxygen or carbon dioxide concentrations in the brain tissues are clearly linked to blood ozonisation and reinfusion. However, they cannot explain which are the positive effects of the therapy at a functional and molecular level. Therefore, more complex frameworks for data analysis are required. In this work, we have shown that EMD is an efficient tool for the analysis of the cerebral NIRS signals. Thus, the principal innovative contribution of this work is the demonstration that linear and non-linear NIRS signal analysis are needed for the characterization of the cerebrovascular pattern changes occurring after ozone autohemotherapy. This could have a direct impact in the numerical characterization of the cerebrovascular changes of subjects undergoing ozone therapy, and could lead to personalized and more effective therapies.

5.4.2 Secondary end-point: 24-hours effects of ozone on cerebral autoregulation

To the best of our knowledge, no study investigated long term effects of ozone therapy on cerebral autoregulation yet. We investigated the permanence of ozone effects on microcirculation up to 24 hours after the therapy. In our study, we evidenced that ozone-therapy induced a different autoregulation mechanism in the two groups. Indeed, we observed a lower BHI in Controls 1.5 hours after ozone-therapy, whereas it remained unchanged in SM-RR group 1.5 hours and 24 hours after ozone-therapy (**Figure 6**). To understand if BHI increased because apnea was shorter or because ΔO_2Hb, and so vasodilatation, increased, we compared the apnea duration in the three observation windows. Our analysis evidenced that, in healthy subjects, vasodilatation decreased after ozone-therapy: this is in good agreement with the increase of regional O_2Hb concentration (**Figure 2**). The hyperoxia after ozone-therapy improved autoregulation, in good agreement with previous studies (Rangel-Castilla et al. 2010; Nishimura et al. 2007). However, in this group of subjects, the effect of ozone exhausted 24 hours after the therapy. In SM-RR, we observed a different autoregulation mechanism. In fact, apnea duration increased significantly 1.5 hours after the ozone-therapy: since BHI remained constant, it means that vasodilatation was lower in the second apnea, after the therapy. The longer apnea duration may indicate that efficacy of autoregulation improved in SM-RR patients. Mostly, this different mechanism of autoregulation, differently from healthy subjects, persisted also 24 hours after the therapy. This demonstrates that the positive action of ozone is not limited just after the therapy, but produced a persistent improvement in cellular metabolism and reduced oxidative stress, at least up to 24 hours after the therapy.

5.4.3 Study limitations and further perspectives

A limitation of this study is the low number of enrolled subjects. However, being the protocol focused on the assessment of long-term effects of ozone therapy, it is difficult to find MS patients that can hold the NIRS monitoring for about three hours. NIRS requires continuous monitoring. An interruption in monitoring will cause a change in the optical coupling that introducing random variability in the signals. Another limitation is that the NIRS equipment we used did not measure the concentration changes of the cytochrome-c-oxidase. To the best of our knowledge, the only reliable biomarker of brain metabolism which can be non-invasively monitored is by NIRS signals. Nevertheless, we believe that our results documented an improvement in the cerebral pattern of the subjects, which also correlated with the subjective sensation of patients and clinical observations. Finally, the two groups are not exactly age-matched. We compared the cerebrovascular pattern of MS patients to a group of controls that was older. Actually, this was a specific

choice aimed at balancing the level of oxidative stress (with consequent reduction of the cytochrome-c-oxidase activity), which is typical of healthy brain cells during aging (Das and Muniyappa 2013). It would not have been proper to demonstrate a difference in the cerebral pattern of MS patients compared to healthy subjects of same age, since, in that case, the original level of cerebral oxidative stress would be very different. Elderly people show a progressive increase in the cerebral oxidative stress, which is physiological. Therefore, we believe that the ozone therapy is acting on this overt oxidative stress induced by MS, and by rebalancing it for a relatively long period (over 3h monitoring), we can document an increase in the O_2Hb consumption (indicating a metabolic boost).

5.5 Conclusion

In this study, we have analysed the changes in the cerebrovascular pattern of MS patients and normal subjects after a major ozone autohemotherapy. We have observed an increase in the complexity of the cerebrovascular pattern caused due to an increase in the metabolism. The changes in brain metabolism and oxygenation are monitored by a NIRS system. We have shown that time analysis of the NIRS signals is not able to explain the complex effects of ozone therapy. Hence, we have proposed non-linear and structural features to assess the functional cerebrovascular changes using NIRS signals.

Part II

Chapter 6

Background: from motor control problem to the muscle synergies definition

6.1 The motor control problem

The motor control problem refers to the actions that Central Nervous System (CNS) must take to transform a planned gesture into an action (Mussa-Ivaldi and Bizzi 2000). To achieve a motor task, CNS designs a map between accomplishing control signals and desired movements. A complex integration of inborn abilities, sensory information, and new strategies learning are the main aspects that CNS integrates in motor programs (Flash and Sejnowski 2001). Hence, motor control modifies movements in the event of motor learning, loads, or dynamic conditions (Ostry and Feldman 2003).

To translate motor plans into action, many elements must be integrated, such as positioning in space of the joints center of mass, and coordinating many muscles acting on the same joint (M. L. Latash, Scholz, and Schöner 2007).To accomplish the integration of these elements, CNS has to deal with the many degrees of freedom of musculoskeletal system (Bernstein 1967). This problem is referred to as motor redundancy, that is one task can be performed in many ways and involves mutually overlapping parts of the nervous system (Sporns and Edelman 1993). CNS finds the

optimal solution accomplishing a task, and it constantly corrects movement to reduce motor errors (M. L. Latash 2012). As an example, in a reaching task study, linear and curvilinear arm movements were compared. Investigators observed that, when the movement is linear, kinematics parameters (i.e. velocity, arm position) are constant. Conversely, in the case of curvilinear movements, variability in kinematics parameters raise (Abend, Bizzi, and Morasso 1982). Hence, for a given problem, there is no unique solution accomplishing a motor task. On the contrary, there are many possible solutions to allow biological systems to adapt to different conditions and environments.

6.2 The equilibrium point hypothesis and spinal force fields

Since musculoskeletal system is characterized by high redundancy, the way CNS optimizes movement and finds efficient solutions was explored. From the late ‘70s Bizzi and colleagues performed animal studies to investigate the influence of proprioceptive information on motor performance. In these studies, monkeys performed experiments in two conditions: in normal condition and without the sight of the arm (i.e. deafferented monkeys). Experiments consisted of reaching a target with the upper limb, and in repeating task after having moved the initial position. Surprisingly, deafferented monkeys performed as good as the animals in normal condition. The results demonstrated that motor tasks can be performed without proprioceptive information, that is likely adopted in optimizing movement. Therefore, there may be pre-built central patterns of neural impulses controlling limb movements (Polit and Bizzi 1978; Polit and Bizzi 1979). It was hypothesized that centrally generated commands modulate kinematic features, such as stiffness, rest-length and length-tension properties. CNS signals define a single equilibrium position of these features, which is continuously corrected with feedback corrections. Trajectories are generated by control signals determining the equilibrium-point position. Despite authors pointed out some criticisms of being a too simple theory for describing complex motor control tasks (Sainburg 2015), further studies formally enounced and adopted the equilibrium-point hypothesis to describe single joint and multi-joint arm movement, or speech movement (Shadmehr 1995; Perrier, Ostry, and Laboissière 1996).

The relationship between the equilibrium-point hypothesis and motor control was further explored. Indeed, it remained unclear if body movements were a mere sequence of equilibrium-points, or instead the same equilibrium-point was driven by descending neural commands over a trajectory. In the first case, only kinematic parameters were required to describe movement, otherwise equilibrium-point

hypothesis would be suitable to describe neural origin of motor control. In (Bizzi et al. 1984) the hypothesis that movements are produced by a sequence of equilibrium-points was rejected. Indeed, they observed that, after forcing a monkey's arm to the target, the arm did not remain there, but had the tendency to come back to the onset point. This result showed that muscular activation does not specify the force, but rather it causes the equilibrium shifting from onset position to the target. The equilibrium-point hypothesis represents a simplification of motor control, because CNS must compute only the difference between actual and target positions, without computing trajectory for all joints positions (Giszter, Mussa-Ivaldi, and Bizzi 1993). It was demonstrated that an interaction with nervous system is required. In (Bizzi, Mussa-Ivaldi, and Hogan 1986) the interaction with nervous system was proved. It was found that a gradual control signal exists and it drives the limb movement from an equilibrium point to another.

The equilibrium-point hypothesis in movement control was proved by electrophysiological studies of the spinal cord in deafferented frogs. Mostly, these studies demonstrated the modular nature of this kind of motor control (Giszter, Mussa-Ivaldi, and Bizzi 1993; Saltiel et al. 1998). In a series of experiments, authors electrically stimulated frog hindlimbs and mapped the force distribution for different hindlimb positions (**Figure 6-1**).

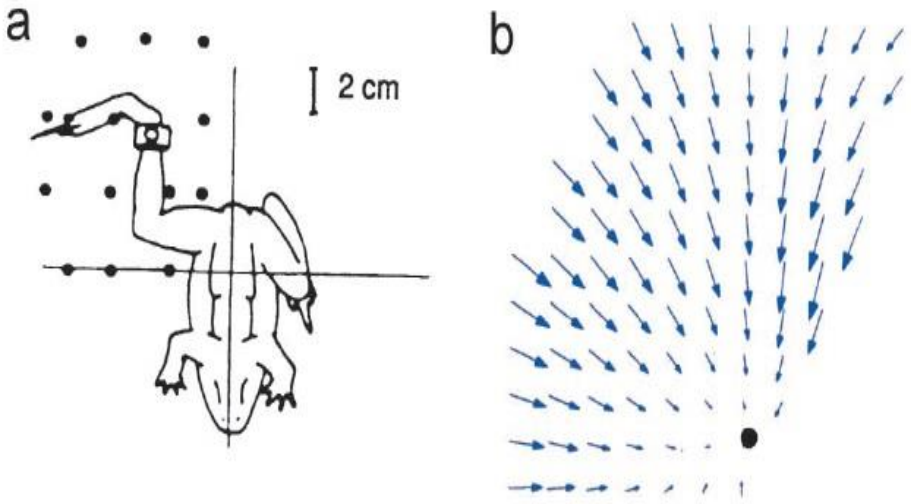

Figure 6-1. Fields of static forces associated with electrical stimulation of a spinal cord site in a deafferented frog. Forces were measured for different hindlimb's positions at the ankle level in two conditions: at resting state and after electrical stimulation of the spinal cord. (a) spatial locations of force recording; (b) force vector fields. Each arrow represents the vectoral summation between force vectors at resting state and after electrical stimulation condition respectively. It can be observed that vectors point towards an equilibrium-point (black filled dot) (from Bizzi et al., 2002).

Firstly, these studies proved that limb's movements are generated to direct force fields toward an equilibrium-point. Secondly, since frogs were deafferented, all forces were generated by neural circuits located at spinal level. Hence, these experiments demonstrated that motor control is generated and controlled by the circuitry located in the spinal cord. (Bizzi, Mussa-ivaldi, and Giszter 1991; Giszter, Mussa-Ivaldi, and Bizzi 1993). Also, they provided evidence for modular organization of motor control. In (Mussa-Ivaldi, Giszter, and Bizzi 1994), authors electrically stimulated several couples of frog hindlimb muscles in two ways: each muscle separately and both muscles together. By adopting the method of the force fields representation, authors observed that the force fields obtained stimulating two muscles together, was the vectoral summation of the individual responses **(Figure 6-2**). The linear behavior of hindlimbs was due to the force fields patterns shared by different muscles. Results demonstrated that CNS generates movements by superimposing motor primitives, or "modules", stored in neural circuits of spinal cord.

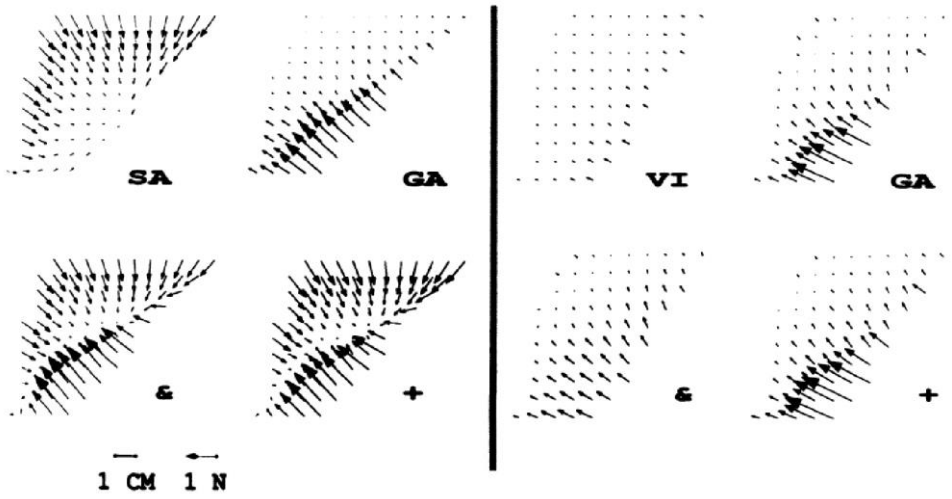

Figure 6-2. Linear superposition of electric fields of stimulation in frog's spinal cord for two couples of muscles. (Left) stimulus of sartorius (SA) and gastrocnemius (GA)(upper); co-stimulation of SA and GA (&) and vector sum (+). (Right) Stimulation of Vastus intermedius (VI) and GA (upper); co-stimulation of VI and GA (&) and vector sum (+). It can be observed that co-stimulation electric fields are the linear combination of the stimulation of the single muscles. (Copyright 1994 National Academy of Sciences).

6.3 Spinal motor modules and muscle synergies

A ‘‘module’’ is a functional unit of the spinal cord circuitry that generates a specific motor output. (D'Avella and Bizzi 1998). Modular hypothesis may simplify intermuscular coordination by enabling the nervous system to control muscles in group rather than controlling each muscle as a unit. In this way, CNS reduces the number of neural activation output controlled. This strategy may provide an efficient neural control solution that still maintains adequate flexibility to general task-specific muscle activity (Aoi and Funato 2016). Indeed, studies demonstrated that different motor tasks can be executed using the same motor modules and just varying the activation patterns (Bizzi et al. 2008; Chvatal and Ting 2013; d'Avella, Saltiel, and Bizzi 2003). Furthermore, it has been observed that a reaching task is better described by underlying motor plans rather than arm kinematic (Bizzi and Mussa-Ivaldi 1998; Thoroughman and Shadmehr 2000). Therefore, modules are recruited and flexibly combined by nervous system to control a variety of locomotor tasks (Fox et al. 2013).

Modules are largely controlled by brainstem and spinal neural networks (Tresch, Saltiel, and Bizzi 1999; Roh, Cheung, and Bizzi 2011). The circuitry in the spinal cord that specifies patterns of muscle activation are called Central Pattern

Generator (CPG) (Grillner 1981; Saltiel et al. 1998). They are assumed to be located within the spinal cord and they involve relatively small and autonomous neural networks (M. Latash and Zatsiorsky 2015). CPGs are hierarchically organized and separately control the locomotor rhythm and motor activity pattern (Aoi and Funato 2016). CPGs are modulated by sensory and reflex feedbacks within the spinal cord without descending or afferent inputs (Rossignol, Dubuc, and Gossard 2006; Forssberg, Grillner, and Halbertsma 1980; Giszter and Hart 2013). Afferent feedbacks are not required for generating basic locomotor pattern, but they are of critical importance in adapting and modulating the CPG action in the real situation (Rossignol, Dubuc, and Gossard 2006; Chvatal and Ting 2012). **Figure 6-3** schematizes how CPGs are modulated by supraspinal commands and interact with spinal interneurons to generate motor patterns (Rossignol, Dubuc, and Gossard 2006; Zehr 2005). In summary, CPGs generate rhythmic motor patterns to produce rhythmic activities without feedback information that peripheral nervous system can provide. Nonetheless, CPGs receive supraspinal control commands, which initiate motor programs, interacts with proprioceptive signals and correct motor patterns to interact properly with the environment (Haghpanah, Farahmand, and Zohoor 2017).

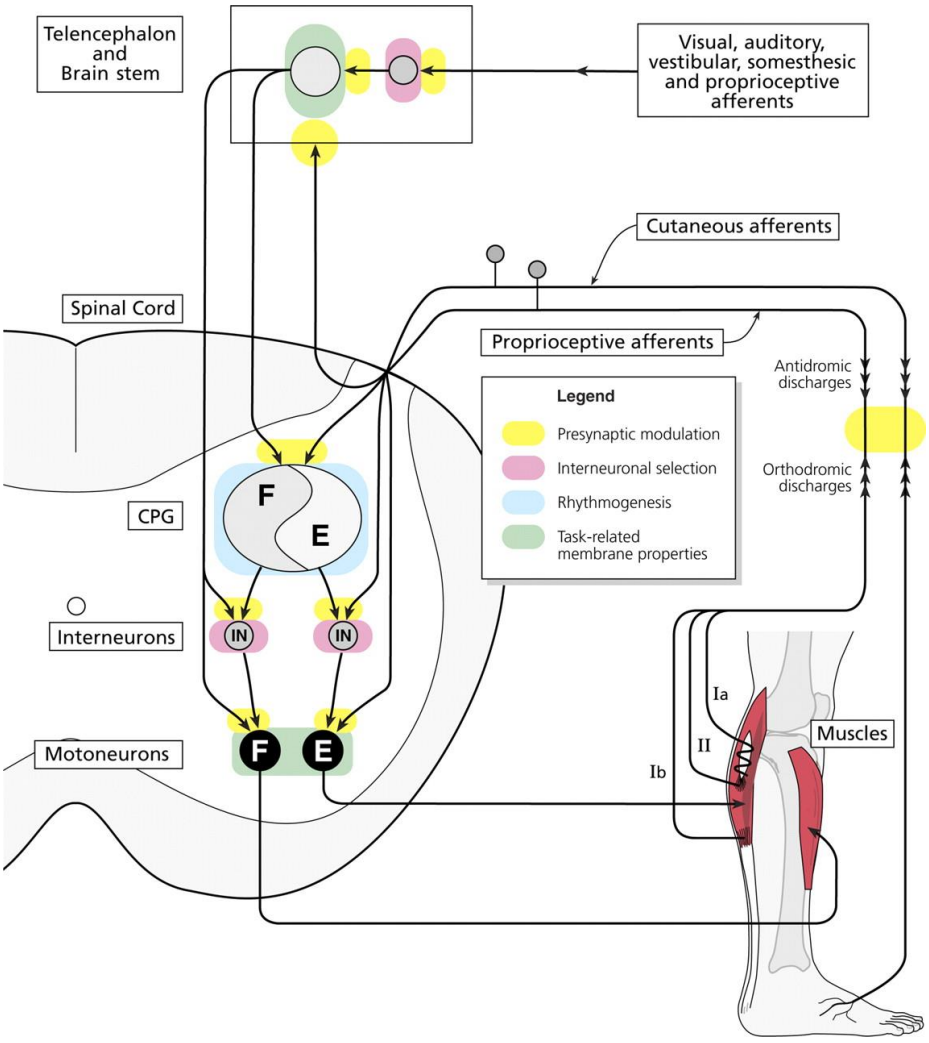

Figure 6-3. A schematic representation of motor patterns generation. Telencephalon and brain stem neural circuitry generate activation signals, and are continuously modulated by sensory and proprioceptive feedbacks. Supraspinal signals are sent to neuronal circuitry in the spinal cord to generate movement. CPGs generate rhythmic signals modulating motoneurons signaling on effector muscles. Interneurons are cyclically influenced by the CPG but are not part of the rhythm generation process itself of the CPG. Spinal circuitry is modulated by feedback information coming from proprioceptive and cutaneous reflex systems. F= flexor, E=extensor. (from Rossignol et al., 2006)

Motor output of modules produces a muscle synergy, a specific pattern of muscle activation (D'Avella and Bizzi 1998). Muscle synergies can be defined as basic patterns of muscle activation representing elementary components or building blocks for the generation of limb movements. This organization may help in

organizing movement by reducing degrees of freedom (Bizzi et al. 2008). The goal of muscle synergies is mapping high-level tasks into action (Torres-Oviedo and Ting 2010). Several studies proved the neurophysiological basis of muscle synergies directed by both supraspinal and afferent pathways to facilitate motor control. CNS selects the appropriate set of synergies from a larger pool, according to motor function (Barroso et al. 2014). In muscle synergies, a single command from CNS recruits several pools of α-motoneurons quasi-synchronously, as defined by modules, and activates several muscles. In modular control hypothesis, a given muscle synergy involves a basic activation pattern (temporal structure) and the weight of distribution (spatial structure) to different muscles (Lacquaniti, Ivanenko, and Zago 2012). Muscle synergies are shared by multiple muscles involved in each motor task (Lacquaniti, Ivanenko, and Zago 2012), and they represent the basic control signals required to generate the large repertoire of muscle-specific excitation needed for executing a specific motor task (Gonzalez-Vargas et al. 2015). **Figure 6-4** shows how supraspinal descending commands recruit motor modules located at spinal level to generate the muscle synergies to perform motor subtasks in human locomotion. Interneurons are supposed to play a role in assembling the synergies, by integrating supraspinal and CPGs commands, and drive them as a unit (Giszter 2015).

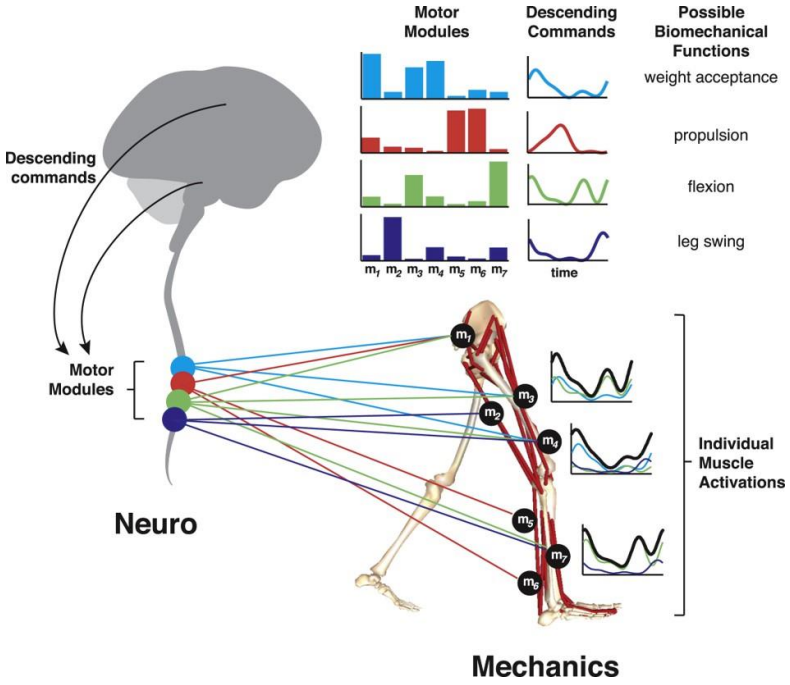

Figure 6-4. Scheme of muscle synergies formation for human locomotion. Supraspinal descending commands recruit motor modules, located at spinal level. From the combination of the motor modules with descending commands, the muscle synergies are generated. In this example, four motor modules are recruited to form four muscle synergies to describe motor subtasks of gait cycle. Individual muscle activations, recorded by EMG, are given by the linear combination of the four muscle synergies. In this manner, biomechanics behavior is fully described by nervous systems elements (from Ting et al., 2015).

Synergies can be thought of as a neural network organized at spinal or brainstem level, with each synergy specifying an invariant profile of activation for the motoneurons innervating a set of muscles (Cheung et al. 2009). Also, it has been proposed that subpopulations of pyramidal tract neurons act through the neuronal circuits in the spinal cord that produce the basic locomotor patterns (Drew, Kalaska, and Krouchev 2008). Besides the role of spinal cord and pyramidal tract neurons, also the motor cortex is involved in modulating the activity of muscle synergies. However, its role needs to be more defined. Indeed, fMRI studies demonstrated that motor cortical regions with significantly different functional connections, activate different muscle synergies (Rana et al. 2015). Other authors claimed that the major role of motor cortex may be inhibiting synergies to permit fractionated movements (Drew, Kalaska, and Krouchev 2008; Lemon and Griffiths 2005).

Modular architecture has been interpreted as a way for CNS to simplify motor control (Berniker et al. 2009; D'Avella et al. 2008; Cheung et al. 2005; Borzelli et al. 2013). Indeed, it was found that muscle synergies reduce dimensionality compared with independent muscle control (Bizzi et al. 2008; Zelik et al. 2014). However, it was also observed that modular strategies may not take into account more complex tasks, i.e. multi-joint movements, or fine movements (Zelik et al. 2014). The objective of simplifying motor control can be reached by sharing synergies across conditions or by mixing synergies to achieve more complex tasks. Also, synergies could be the same across tasks or can just adapt by modulating muscle weights or shifting descending command curves (Ivanenko, Poppele, and Lacquaniti 2004; Gonzalez-Vargas et al. 2015). For instance, cyclic tasks, such as pedaling or walking, showed high similarity of synergies (Barroso et al. 2014). Furthermore, it has been observed that certain cycling synergies can be obtained by combining walking synergies. Walking has been demonstrated sharing synergies with perturbated balance too (Anderson Souza Oliveira et al. 2013). Authors demonstrated that synergies recruited for perturbed walking are also recruited for perturbed balance. Furthermore, changes in the modular organization of walking affect both walking and balance function. All these findings demonstrate that CNS likely simplify motor control by adopting common strategies for different biomechanical context, for instance balance control during walking and static balance or by combining basilar synergies to perform more complex tasks.

Chapter 7

Muscle synergies extraction method

7.1 Blind source separation

Blind source separation (BSS) refers to the problem of recovering source signals from signal mixtures without or with a very limited information about the sources and the mixing process (Mirzal 2017). The term *blind* denotes a method based on output observation only (Comon and Jutten 2010). The goal of BSS is the estimation of physical sources and parameters of a mixing system. The objective is to find such a transformation or coding with a reliable physical meaning and interpretation (Cichocki et al. 2009).

Figure 7-1 schematize a general BSS problem decomposition. The system is composed by *I* sensors recording signal $y(t) = [y_1(t), y_2(t),\ldots, y_I(t)]$ coming from a *MIMO* (multiple input/multiple output) system, where *t* is a discrete time sample. These signals are usually a superposition (mixture) of *J* unknown source signals $x(t) = [x_1(t), x_2(t),\ldots, x_J(t)]$ and noises $e(t) = [e_1(t), e_2(t),\ldots, e_I(t)]$. The primary objective of decomposition methods is to estimate all the source signals $x_j(t)$, or part of them, only from output signals $y_i(t)$ (i.e. sensors or observations).

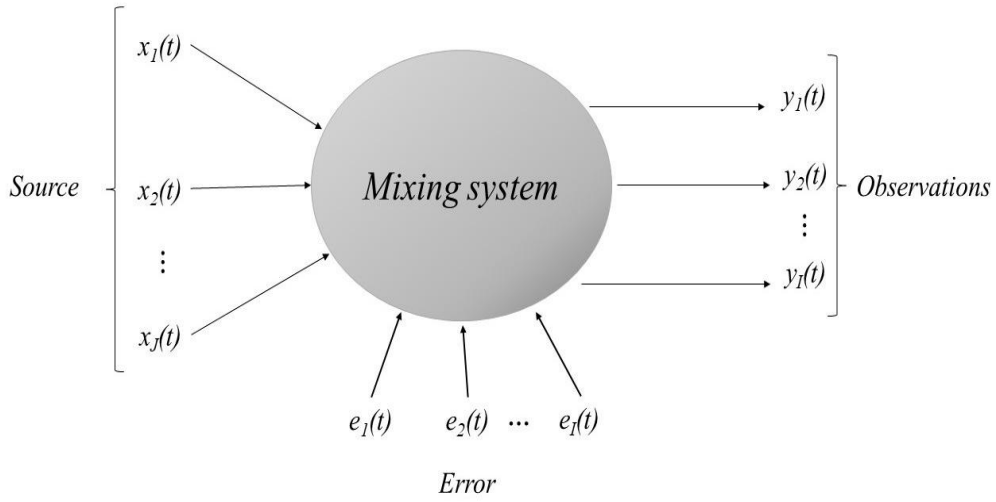

Figure 7-1. Scheme of a BSS system. Observations $[y_1(t), y_2(t),\ldots, y_I(t)]$ are the output of a mixing system where the source signals $[x_1(t), x_2(t),\ldots, x_J(t)]$ are unknown.

The simplest BSS model can be expressed algebraically in the form of matrix factorization. Given a set of observations $Y = [y_i(t)] = [y(1),\ldots,y(T)]$, source components are linked to the observations with the matrix factorization

$$Y = AX + E$$

where A represents the unknown basis matrix or mixing matrix, and E is a matrix representing errors or noises. $X = [x_j(t)] = [x(1), x(2),\ldots, x(T)]$ contains the latent (hidden) components giving the contribution of each basis vector, and T is the number of available samples. In general, the amount of source signals *J* is unknown and can be larger, equal or smaller than the number of observations *I* (Cichocki et al. 2009).

7.2 Basic Nonnegative Matrix Factorization algorithm

Non-Negative Matrix Factorization (NMF) decomposes a matrix of observations **V** into the product of two non-negative matrix factors **W** and **H** (**Figure 7-2**):

$$\boldsymbol{V}_{m\times t} \approx \boldsymbol{W}_{m\times n}\boldsymbol{H}_{n\times t}$$

where:

- **V** is the source matrix
- **W** and **H** are non-negative matrices of decomposition. They are the basis matrix and hidden components matrix of the BSS system.
- *n* represents the number of basis used to represent original matrix. It is a positive integer lower than m and t

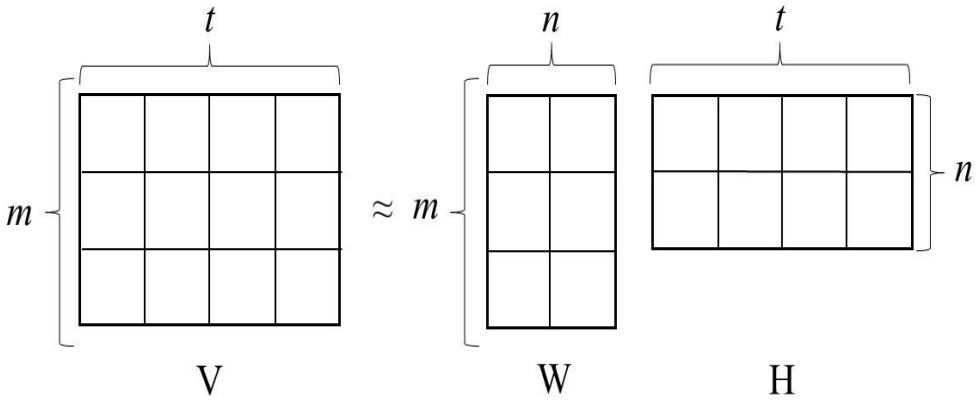

Figure 7-2. A schematic representation of NMF decomposition. A source matrix V, of dimensions m×t, is decomposed as a combination of non-negative matrices W, of dimension m×n, and H, of dimension n×t.

The objective of NMF is finding the pairs of matrices **W** and **H** which minimize the error of approximation. BSS methods based on Independent Component Analysis (ICA), the source components are not assumed to be independent.

Conversely, in NMF the only assumption is the non-negativity of the weight matrix **W** and the mixing matrix **H**. By disallowing negative entries in **W** and **H**, NMF implements a non-subtractive combination of parts to form a whole. Examples of NMF application are clustering textual data, face recognition, spectral analysis (Berry et al. 2007).

The basic NMF update algorithm is described in (D. D. Lee and Seung 1999; D. D. Lee and Seung 2001), and based on the work of Paatero (Paatero 1997). In the Lee and Seung NMF algorithm, a cost function is defined as the squared Euclidian distance between the source matrix **V** and factorization matrix **WH**:

$$D(V\|WH) = \frac{1}{2}\|V - WH\|^2$$

W and **H** are initialized with random non-negative values, before the iteration starts. Then, a multiplicative update algorithm with the mean squared error objective function is iteratively applied. The factors **W** and **H** are chosen to minimize the root-mean-squared error between **V** and **WH**. To avoid local minima, the algorithm is repeated several times, i.e. 20 times per dataset (Frère and Hug 2012).

7.3 Checking the quality of muscle synergies: the VAF criterion

To determine the decomposition of EMG matrix into the **WH** matrix, the matrix of experimental EMG need to be correlated with the matrix of reconstructed EMG. The comparison generally requires the Variance Accounted For (VAF, uncentered Pearson coefficient) of the overall EMG matrix reconstruction. VAF is defined as 1 - $\frac{SSE}{SST}$, where SSE (sum of squared error) is the unexplained data variation and SST (total sum of squares) is the total variation of data (Gizzi et al. 2011; Zelik et al. 2014). Practically, $\frac{SSE}{SST}$ is the ratio between the squared difference between the original and reconstructed EMG, and the squared original signal (Katherine M Steele, Rozumalski, and Schwartz 2015). VAF depends on the magnitude and the shape of the original and reconstructed datasets (Hagio, Fukuda, and Kouzaki 2015). Most of the studies select the number of synergies that provide at least 90 % of the VAF (Turpin et al. 2010; Frère and Hug 2012; Chvatal and Ting 2013; Zelik et al. 2014)(Serrancolí, Monllau, and Font-Llagunes 2016). VAF is generally evaluated globally over all muscles, but certain authors evaluated VAF for each

muscle individually as additional criterion (De Groote, Jonkers, and Duysens 2014). Certain authors measured the goodness of synergy approximation by calculating the multivariate R^2, where the SST is substituted by the summed squared residual from the mean normalized activation vector (de Rugy, Loeb, and Carroll 2013). However, VAF generally provided higher values than R^2.

7.4 Application of NMF to extract muscle synergies

Factorization techniques have been largely adopted in motor control studies to decompose patterned motor output into muscle synergies. Statistical and signal processing pattern separation methods such as NMF, ICA, Factor Analyses (FA), and Principal Component Analyses (PCA) have been widely used. (K. Suzuki, Nishida, and Mitsutomi 2014)(Tresch, Cheung, and d'Avella 2006). The advantage of these methods is to represent locally linear mechanisms adopted by CNS to adapt to the complex nonlinearities in the environment (Ting et al. 2015). These methods largely confirmed the construction mechanisms observed in spinal and decerebrate preparation physiology, with data collected in intact animal models and humans in freely moving conditions (Giszter 2015; Overduin et al. 2008; D'Avella and Lacquaniti 2013). Hart and Giszter, in an animal experiment, directly measured firing rate in the innervation zone of spinal motoneurons. They investigated how neural activity correlates with synergies obtained using ICA and with original EMG. They showed that firing rate shared higher mutual information with independent components than EMG. In this manner, they demonstrated that factorization techniques represent neuronal firing better than contraction of the single muscle (Hart and Giszter 2010; Delis, Chiovetto, and Berret 2010).

The fundamental assumption is that modular organization of neural systems can be deducted without regarding their origin, since only the features extracted from muscle activity during movement are necessary. In addition, factorization approach ignores the neurophysiological basis of the control patterns, such as neural output precision (Zelik et al. 2014). However, these methods only measure neural activity indirectly, and they may be influenced by physiological and non-physiological factors. For instance, cross-talk may generate or exaggerate a positive correlation among EMG records, and so introduce a bias in results (Ivanenko, Poppele, and Lacquaniti 2004). Hence, results of these decomposition methods have to be analyzed very carefully, being affected by several critical issues, as proponents and critics evidenced (Katherine M. Steele, Tresch, and Perreault 2013; Katherine Muterspaugh Steele, Tresch, and Perreault 2015).

In recent years, NMF has been widely adopted as a decomposition method since non-negativity constraints reflect spiking activity of neurons (Ting et al. 2015).

Many real-world data are nonnegative and the corresponding hidden components have a physical meaning only when nonnegative. In practice, nonnegative decomposition of data is often either desirable or necessary when the underlying components have a physical interpretation. NMF was selected since it provides robust estimates of EMG muscle coordination with no constraints on the correlation of activations across a broad range of motor tasks (Hayes et al. 2014). The sinusoidal-like basic activation patterns identified by the NMF model represent alternating bursts of activity (Danner et al. 2015).

Figure 7-3 shows an example of muscle synergies extracted for a representative healthy subject during walking. All the phases are reported in the figure: input EMG matrix, that represents the observation matrix (**Figure 7-3A**). Muscle synergies are reported in **Figure 7-3B**: muscle weightings are the basis function and activation signals are the hidden components of the BSS that describes motor control. Initially, the number of synergies is computed for a number of basis from 1 to the number of muscles recorded. Since muscle synergies aim to simplify motor control, the number of synergies is chosen lower that the number of muscles. Motor functions can be associated to each muscle synergy by observing muscle weights and activation signals. The VAF criterion is adopted to select a number of synergies conveying all the information (**Figure 7-3C**). In the reported example, VAF values increase from 80% (three synergies) to 88% (four synergies) up to 92% with five synergies. Hence, in this last case, original and reconstructed signals can be considered correlated more than 90%. **Figure 7-3D** shows that the signal reconstructed with five synergies well superimposes the original EMG signal. The biomechanical role of the extracted synergies can be derived by the most activated muscles and the timing of the activation signal. For instance, in the event of 3, 4, and 5 synergies, it can be observed a synergy involving muscles inserting on the hip and the knee: VM, TFL, GMD. By observing the activation signal, it can be noticed that these muscles are activated at the initial contact and in limb phase. It can be deduced that the biomechanical role of these synergies is hip and knee stabilizing during these phases. A fully detailed description of biomechanical role of muscle synergies during gait is presented in a next section (see Chapter 8).

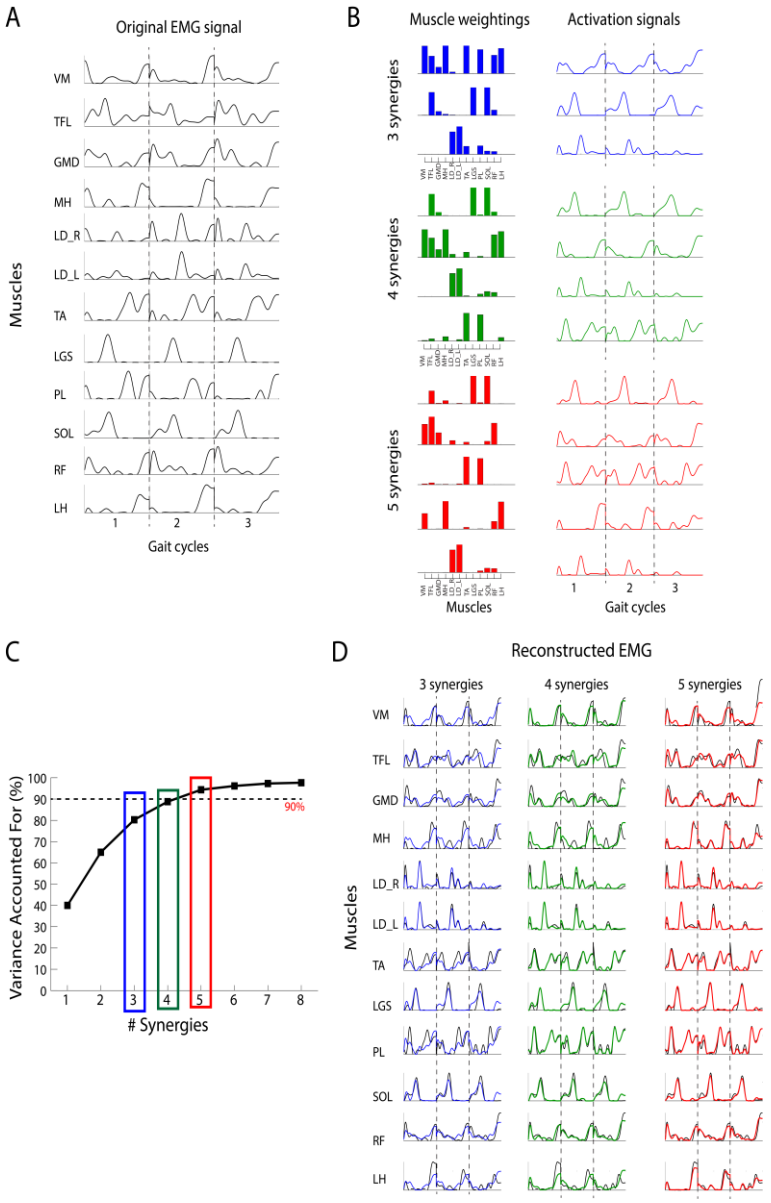

Figure 7-3. Example of muscle synergies extraction. Reported data are taken from 3 gait cycles of a representative healthy subject. (A) Original EMG for 12 muscles of the lower limb and the trunk after preprocessing (filtering, rectification, envelop). (B) Muscle synergies obtained with NMF. Muscle synergies are a linear combination of non-negative vectors of muscle weightings and activation signals. The number of synergies can vary from 1 to the number of muscles. In this case, muscle synergies are computer for 3,4, and 5 set of synergies. (C) For each synergy, the Variance Accounted For (VAF) measures the correlation between original EMG and data obtained from synergies (reconstructed EMG). In this case, 5 synergies reconstruct original EMG with a VAF>90%. (D) Superposition of original EMG (Black line) and reconstructed EMG with 3, 4, and 5 synergies.

Chapter 8

Muscle synergies during locomotion: consistency of muscle weights and activation signals[3]

8.1 Introduction

Human gait is characterized by intrinsic complexity due to the many subtasks that are repeated cyclically (Perry 1992). This complexity reflects in muscle activity: indeed, while lower limb kinematics remain invariant during locomotion, underlying muscle activity can vary greatly (Winter 1987; Di Nardo et al. 2015; Rosati et al. 2017). Electromyographic (EMG) studies demonstrated high degree of variability of the onset/offset EMG time intervals for individual muscles, according to subject, muscle, or task. For instance, it was demonstrated that forward versus backward locomotion modes show different EMG patterns, but the kinematics parameters were identical in both directions (Grasso, Bianchi, and Lacquaniti 1998). Similarly to locomotion, it was demonstrated that segmental kinematics waveforms remain unmodified across several postures, but kinetics parameters are corrected to maintain balance (Grasso, Zago, and Lacquaniti 2000).

[3] This chapter is based on the paper: Rimini D., Agostini V., Knaflitz M. Front. Hum. Neurosci (2017) 11. https:\\ 10.3389/fnhum.2017.00586

Despite muscle activity may vary, depending on many factors, early works demonstrated that the locomotion subtasks can be described by a few underlying muscle synergies that properly combine to generate the desired activation pattern (Davis and Vaughan 1993; Patla 1985; Ivanenko, Poppele, and Lacquaniti 2004). In each synergy, muscles are recruited at a certain degree (muscle weights) and at a precise percent of the gait cycle (GC), referred to as activation signals (Zehr 2005; Lacquaniti, Ivanenko, and Zago 2012; Danner et al. 2015). In recent years, several studies investigated the structure of muscle synergies in locomotion (Lacquaniti, Ivanenko, and Zago 2012). Many studies demonstrated that four (Gizzi et al. 2012; Ranganathan and Krishnan 2012; De Groote, Jonkers, and Duysens 2014) or five (Ivanenko, Poppele, and Lacquaniti 2004; Cappellini et al. 2006; McGowan et al. 2010), muscle synergies are good enough to describe locomotion. Muscle synergies have been demonstrated to be the same across subjects for different biomechanical tasks, such as in response to posture perturbation or during running (Chvatal and Ting 2013). However, it has been also demonstrated that the ability of muscle synergies to describe motor control depends on whether they can be adapted to specific task demands, for instance by integrating sensory feedback (Zelik et al. 2014). A simulation study showed the adaptability of muscle synergies to different conditions by simply scaling the mechanical output from modules associated with specific biomechanical subtasks (McGowan et al. 2010). Adaptability of muscle synergies has been confirmed in different gait conditions and demanding tasks. Early studies evidenced shared and specific muscle synergies, demonstrating that locomotor behaviors are mostly generated by a small number of centrally organized synergies, activated by central commands and modulated by sensory feedbacks (Cheung et al. 2005). Further studies observed that different subjects show similar muscle synergies, and that muscle synergies adapt to different walking speeds: indeed, it has been evidenced that muscle weights are velocity-dependent, whereas activation signals vary to a lesser extent across several locomotion speeds (Gonzalez-Vargas et al. 2015). Similar conclusions have been done by comparing synergies of several gait patterns during running: some synergies are shared among subjects, and they were similar across different running speeds and patterns. Finally, it has been proved that some muscle weights and activation signals may vary across gait patterns and speeds (Nishida et al. 2017). However, the robustness of both shared and subject-specific muscle synergies within a subject during a trial has not been investigated yet. The objective of the present work is exploring muscle synergies consistency during a locomotion task. We refer to as “intra-subject consistency”, that is the subject showing synergies with similar muscle weights and activation signals along the whole trial. It can be practically investigated by

comparing muscle synergies obtained by many consecutive GCs extracted during a single motor task.

To evaluate muscle synergies consistency, we extracted muscle synergies in a group of healthy subjects by adapting the factorization method NMF to the case of many GCs. We analyzed the muscle synergies at two levels: firstly, we clustered muscle synergies showing the same motor functions across subjects, called "shared synergies". Then, the remaining synergies were classified as "subject-specific". We quantified the consistency of muscle weights and activation signals for the shared and subject-specific synergies, and we analyzed them.

8.2 Material and Methods

8.2.1 Subjects

Twelve young healthy females (age: 24.6 ± 1.6 years, height: 164.1 ± 6.8 cm, body mass: 54.1 ± 5.7 kg) were recruited for the study. None of the subjects reported lower limb injuries or interventions, and none of them had neurological or musculoskeletal disorders that could compromise their gait. Participants signed a written informed consent before being enrolled in the study.

8.2.2 Recording system and signal acquisition

A multichannel system for gait analysis (STEP32, Medical Technology, Italy) was used to acquire the following data: 1) surface EMG, 2) foot-switch signals, 3) knee joint goniometry. Surface EMG probes had the following characteristics: single differential configuration, size 19 × 17 × 7 mm^3, 4-mm diameter Ag-disks, interelectrode distance 12 mm, CMRR over 126 Db. EMG signals were amplified to minimize, for each specific muscle, the quantization error; gain ranged from 60 dB to 86 dB. EMG probes were placed on 12 muscles of the dominant leg, defined according to (Sadeghi et al. 2000) and the trunk. Muscles were chosen on the trunk and around the hip, knee, and ankle joints (Netter 2014; Palastanga and Soames 2012): longissimus dorsii, at L4 level, right (LD_R), and left (LD_L), medial hamstring (MH), lateral hamstring (LH), tensor fasciae latae (TFL), gluteus medius (GMD), vastus medialis (VM), rectus femoris (RF), tibialis anterior (TA), lateral gastrocnemius (LGS), peroneus longus (PL), soleus (SOL). **Figure 8-1** reports the EMG probes positioning on trunk and lower limb.

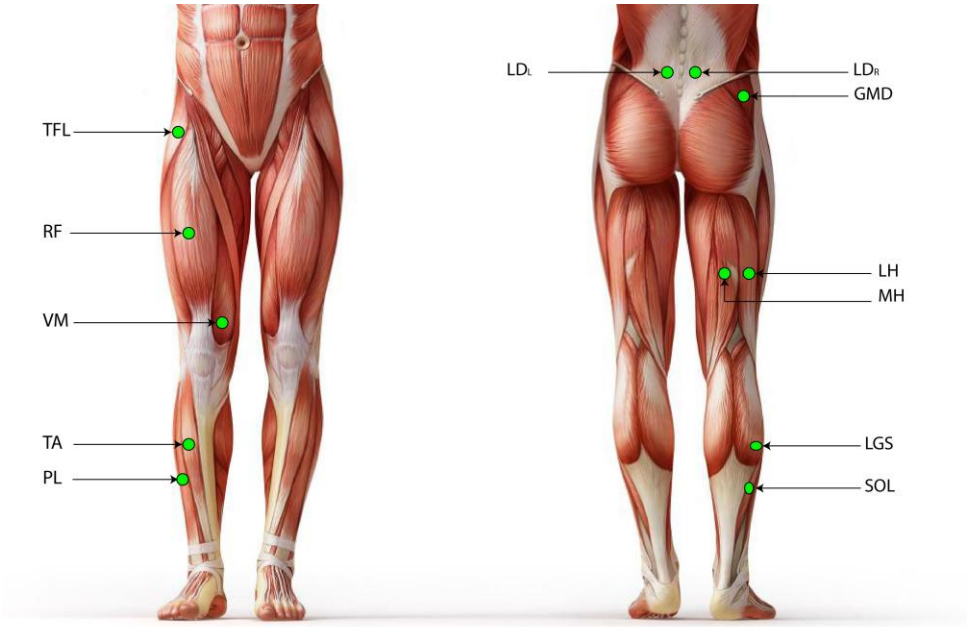

Figure 8-1. EMG probes positioning in lower limb and trunk.

Three thin foot-switches of size 10 × 10 × 0.5 mm^3, were placed under the foot in the following positions: under the heel, under the first and fifth metatarsal-heads. Knee joint kinematics were acquired bilaterally in the sagittal plane by means of electrogoniometers. All the data were acquired with a sampling frequency of 2000 Hz.

Once instrumented, subjects were instructed to walk barefoot back and forth over a straight pathway of 15 meters for 5 minutes (**Figure 8-2**). Subjects walked at a self-pacing rhythm with a constant speed in the A-B tract. The experimenter timed each subject's passage through the A-B tract. The average gait speed was defined as the total distance walked in a straight line divided by the total time required going through it (Agostini, Lo Fermo, et al. 2015).

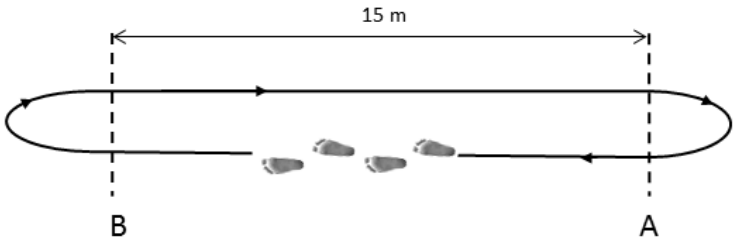

Figure 8-2. Schematic representation of the walking path. Subjects walked from point A to point B at their natural pace, then turned back and proceeded in the opposite direction.

8.2.3 Statistical gait analysis

Instrumented gait analysis studies the human walking by measuring body movements, body mechanics, and the activities of muscles (Whittle 2007). It provides quantitative, reliable, and repeatable measures of gait parameters and it allows to remove atypical gait patterns and GCs devoted to curve negotiation (Agostini and Knaflitz 2011).

Firstly, GCs were separated by using the foot-switches, which provide a four levels signal (Agostini, Balestra, and Knaflitz 2013). The foot-switches allow to individualize three sub-phases of the stance phase: Heel contact (H), Flat foot contact (F), and Push off (P). In normal gait, most of the GCs consist of sequence of the three sub-phases of stance, followed by the limb Swing (S) (Agostini, Balestra, and Knaflitz 2014). **Figure 8-3** shows the foot-switches configurations and four-levels signal of the HFPS gait pattern. Only GCs consisting of the sequence of H–F–P–S were considered, discarding other possible non-standard cycles.

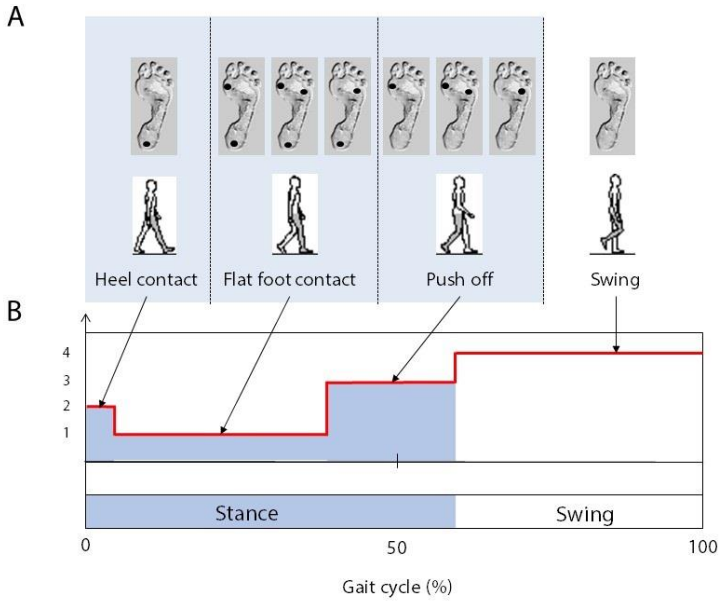

Figure 8-3. Scheme of HFPS foot switches signals sequence. (A): the timing of foot switches is reported for the gait phases. A black dotted circle indicates the switch is closed. (B): the four-levels signal obtained by the configurations of foot-switches. In the stance phase can be recorded three sub-phases, that are Heel-contact, Flat foot contact, and Push off.

Once non-standard gait patterns were removed, the knee range of motion and gait phases durations were exploited together to remove undesired strides relative to direction changes. A multivariate statistical procedure was adopted to discard strides related to curve negotiation, deceleration and acceleration before and after changing direction. In details, the following procedure was adopted (Di Nardo et al. 2017):

(1) a multivariate dataset is built with six variables: duration of H, F, P, and S gait-phases, and knee joint angles at 70 and 95% of GC;
(2) multivariate (Mahalanobis) distance between the value of each GC parameter and the average GC corresponding parameter is calculated;
(3) cycles that have a very high Mahalanobis distance with respect to the average GC are considered outlier and discarded. This is determined using a Hotelling t-test for multivariate data, choosing a confidence level $\alpha = 0.05$;
(4) average GC is re-calculated;

(5) previous steps are iterated until all outlier cycles are removed.

We assessed stride-to-stride variability by computing Coefficient of Variation (CV) of the stride time (Agostini, Lo Fermo, et al. 2015):

$$CV\ of\ stride\ time\ (\%) = \frac{standard\ deviation\ (stride\ time)}{mean\ (stride\ time)} \cdot 100$$

8.2.4 Muscle synergies extraction

GCs were concatenated prior to filtering, with the aim of attenuating the cutting artifact (Gizzi et al. 2015). Indeed, in concatenating consecutive GCs it can happen that they are not also contiguous, e.g. when they are separated by deceleration/acceleration or by other outlier cycles.

The EMG of each specific muscle was concatenated considering 10 consecutive HFPS GCs. To study the consistency of muscle synergies, *N* subgroups of 10 GCs each were generated: subgroup 1 contained the EMG signal of HFPS GCs from 1 to 10, subgroup 2 from 11 to 20, and so on. The last subgroup was discarded if it contained less than 10 GCs. An EMG matrix $M(t)$ of dimension m×n, where m was the number of muscles and n was the time points of 10 GCs, described each subgroup. After concatenation, the EMG signals were pre-processed before muscle synergies extraction. They were high-pass filtered at 35 Hz, demeaned, full-cycle rectified, and low-pass filtered at 12 Hz by a 5^{th} order Butterworth filter. Afterwards, EMG of each channel was normalized between 0 and 1 with respect to its global maximum, through the entire walk. Finally, the duration of each GC was resampled into 1000 time points (Clark et al. 2009).

For each subgroup, muscle synergies were extracted with Non-negative matrix factorization (NMF) (D. D. Lee and Seung 1999; Torres-Oviedo and Ting 2007). NMF models muscular activity as a linear combination of muscular synergies activated by time-varying coefficients:

$$\boldsymbol{M(t) = \sum_{k=1}^{K} C(t)_k W_k + e}$$

where $M(t)$ is the EMG signal, W_k are the weights of the linear combination, $C_k(t)$ are the recruiting coefficients that vary in time, and e is the residual error. W_k defines the k-synergy (k = 1,…,K), whereas $C_k(t)$ expresses the neural signal that controls the k-synergy (Ting and Chvatal 2010; Danner et al. 2015). Since the NMF algorithm was applied to each subgroup of 10 GCs, we obtained N sets of K muscle synergies, one for each subgroup. A reconstructed EMG is obtained as a linear combination of muscle synergies. The similarity between original EMG and the reconstructed EMG computed with NMF was evaluated by the Variance Account For (VAF). VAF expresses the amount of variation explicated by the model: the higher the VAF, the smaller the prediction error and, consequently, the better the model (Zar 2010). A minimum value of 90% for VAF was used to consider the quality of reconstruction quality acceptable (Barroso et al. 2014). Notice that, for each subgroup i, it may be required a different number of synergies K_i to accurately reconstruct the original signal. We chose the number of synergies K, common to all subgroups, in such a way as to obtain a VAF ≥ 90% for every subgroup. This requires calculating K as:

$$\boldsymbol{K = max(K_1, K_2, \dots, K_N)}$$

The k-means algorithm was adopted to order the synergies according to their weights W_k (Katherine Muterspaugh Steele, Tresch, and Perreault 2015). The number of k-means classes was set equal to K. Clusters were randomly initialized and 10000 permutations, repeated 5 times, were performed. The coefficient matrices C_k were ordered correspondingly.

8.2.5 Synergy consistency

We evaluated the intra-subject consistency of muscle synergies by quantifying the similarity of muscle weights and activation signals among subgroups of 10 concatenated GCs.
For each synergy, we adopted cosine similarity (*CS*) as a metric of similarity between two muscle weights vectors. The *CS* between two general subgroups i and j of a synergy k is the normalized scalar product

$$CS_k^{ij} = \frac{\boldsymbol{w}_k^i \cdot \boldsymbol{w}_k^j}{\|\boldsymbol{w}_k^i\|\|\boldsymbol{w}_k^j\|}$$

where w_k^i and w_k^j are the vectors of muscle weights of the *i*- and *j*-th subgroups, respectively. *CS* values range between 0 and 1: 0 indicates no similarity, whereas 1 demonstrates complete similarity (D'Avella and Bizzi 2005; Han and Kamber 2007).

The cross-correlation at zero time lag (*CC*) was adopted as a measure of similarity of activation signals (Godlove et al. 2016; Gizzi et al. 2011). *CC* is a measure of correlation, and can vary between -1 and 1. **Figure 8-4** resumes the entire experimental framework with the main four phases: data acquisition, statistical gait analysis, muscle synergies extraction, and consistency features computation.

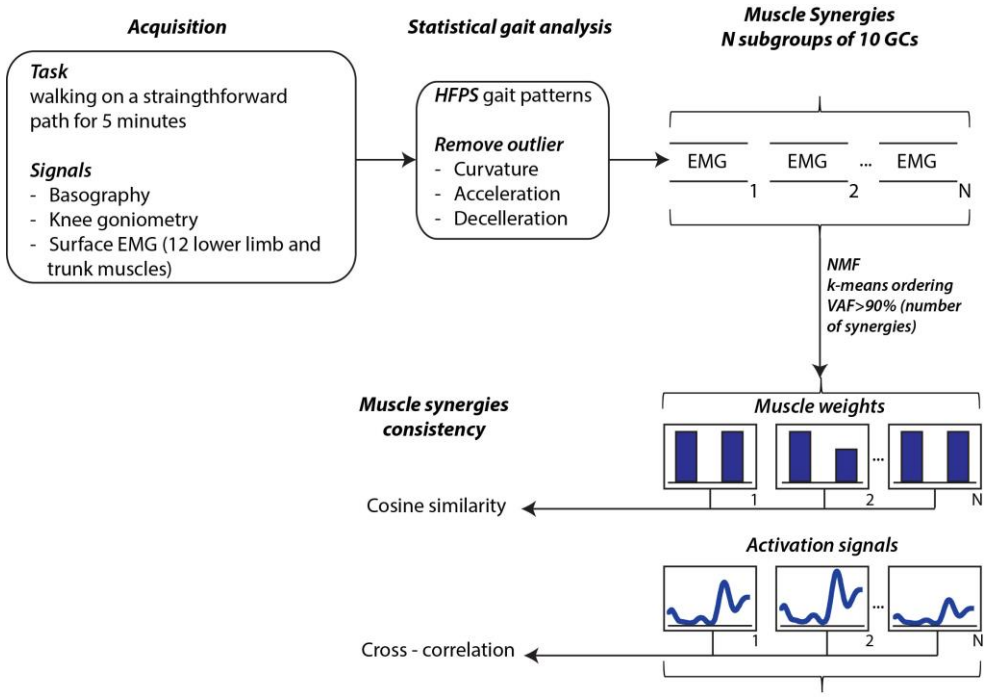

Figure 8-4. Scheme of the entire experimental processing, from data acquisition to muscle synergies parameters extraction.

8.2.6 Shared muscle synergies

Muscle synergies were divided in shared, across subjects, and subject-specific. To individualize shared muscle synergies, we randomly chose a reference subject *Sr*. We calculated *CS* between the weights of *Sr* and all the weights vectors of a general subject *Si*. The highest *CS* defined the first shared function between *Sr* and *Si*. This procedure was iterated for each weight vector of *Sr* to define the other shared functions with *Si*. We repeated the algorithm for all subjects. (Hagio, Fukuda, and Kouzaki 2015; Torres-Oviedo and Ting 2007).

8.2.7 Data analysis

For each synergy, we computed the average CS and CC across the GCs. For the shared synergies, we compared mean *CS* and *CC* values, to verify if motor functions were consistent to the same extent. Normality of *CS* and *CC* values were tested by means of a Kolmogorov-Smirnov test. Since data could not be assumed as normally distributed, we adopted a Kruskal-Wallis test followed by a post-hoc Fisher Least

Significant Difference (LSD) to test the difference in median between synergies of *CS* and *CC*. Significance level α was set at 0.05 for all tests. For the subject-specific synergies, we computed mean and standard deviation of *CS* and *CC* values.

8.3 Results

The twelve analyzed subjects walked at an average self-selected speed of 1.2 ± 0.1 m/s. On the average, 277 ± 11.5 GCs were recorded for each subject. After outlier removal, 181 ± 10 GCs were analyzed. CV of stride time was 1.76 ± 0.30 %, in good agreement with previous studies (Agostini, Lo Fermo, et al. 2015). Instead, EMG showed high stride-to-stride variability. **Figure 8-5** shows onset/offset activation intervals of the tibialis anterior muscle of a representative subject relative to 163 GCs of her walking trial. It can be observed a great variability of activation interval duration among GCs, particularly between 10% and 40% of the GC. It is worth to be observed that this is the residual variability after removing outlier GCs. Hence, variability due to direction and speed changes is not considered for the investigation of muscle synergies consistency. On average, 18 ± 1 subgroups of 10 concatenated GCs were available for each subject. Altogether, muscle synergies were extracted from 213 subgroups of 10 GCs.

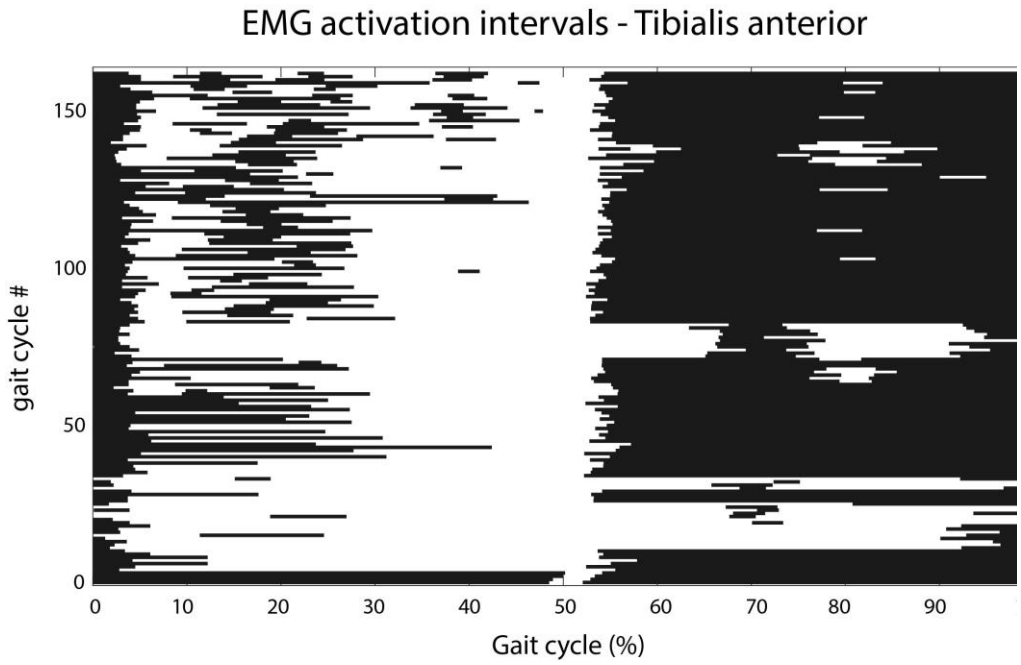

Figure 8-5. Onset/Offset EMG activation intervals of the tibialis anterior of a representative subject relative to 163 GCs of her walking trial. In each row, the black bars represent the EMG activation intervals within stride.

8.3.1 Number of extracted muscles synergies and analysis of synergy consistency

On the average 5.8 ± 0.6 muscle synergies were extracted for each subject. More specifically, 5 synergies were extracted in 3 subjects (VAF: 92.1% ± 0.6), 6 muscle synergies were extracted in 8 subjects (VAF: 92.1% ± 0.3) and 7 synergies were extracted in only 1 subject (VAF: 92.0%). An example of the number of synergies satisfying VAF > 90% criterion of each subgroup of GCs is reported in **Figure 8-6**. Dashed dotted line represents the number of synergies selected for the within-subject analysis.

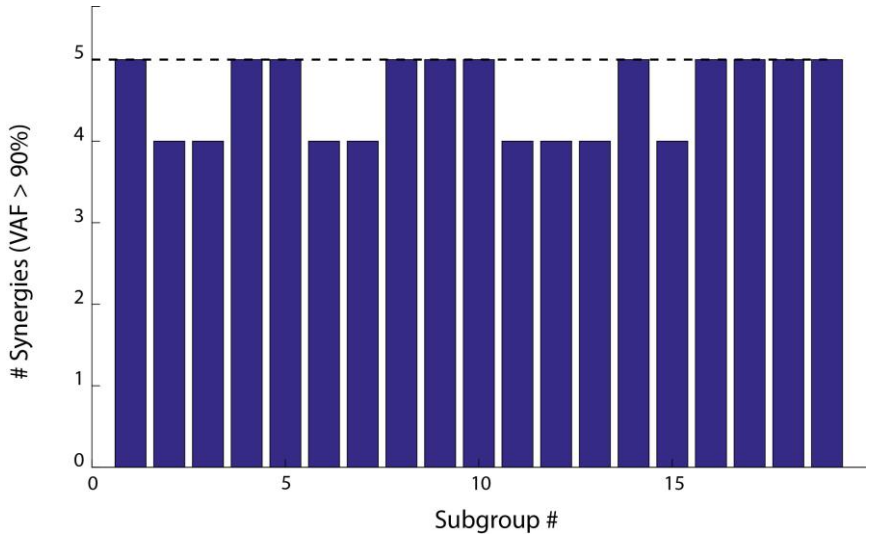

Figure 8-6. Number of synergies satisfying the VAF > 90% criterion of each subgroup of GCs for a representative subject.

Figure 8-7 reports the muscle synergies for a representative subject. The weights (**Figure 8-7A**) and coefficients (**Figure 8-7B**) of the muscle synergies are reported for each subgroup of 10 concatenated strides. It is evident that some synergies are very consistent among subgroups. As an example, synergy 2 is consistently dominated by muscles LGS, and SOL. In this case, these 2 muscles show a high value of weights (close to 1), similar among all subgroups, while the other muscles are scarcely represented (weights very close to zero). On the contrary, it can be observed that, in synergy 6, the contribution of the muscles is very variable. In some of the subgroups, weights are equal to 1 while in others they are zero. These observations are confirmed by the *CS* values reported in **Figure 8-7C**: *CS* is close to 1 in very consistent synergies (synergies 2, 3, and 5), while it decreases to 0.5 for the synergy 6 which is the least consistent. **Figure 8-7D** reports *CC* values for the activation signals. It can be observed that all activation signals are consistent across the task, with *CC* values above 0.8.

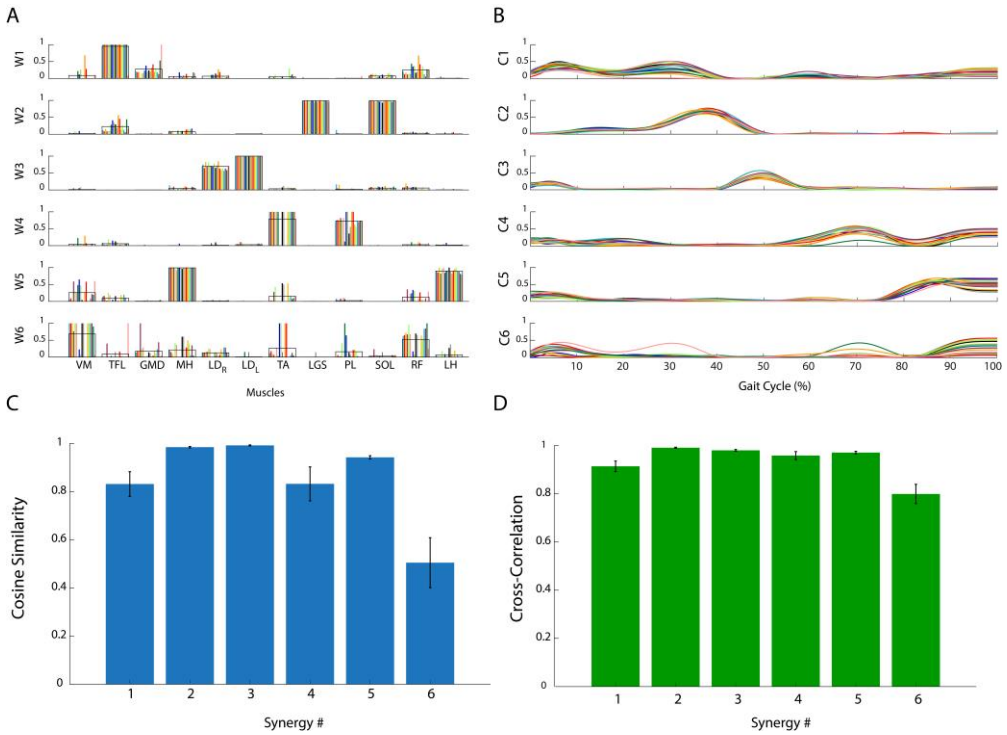

Figure 8-7. Analysis of the consistency of muscle synergies in a representative subject. (A) Muscle synergy weights: each bar represents weights of a subgroup of 10 concatenated GCs. The black line represents the average across bars. (B) Muscle synergy activation signals: each line represents activation signal of a subgroup of 10 concatenated GCs. (C) Cosine Similarity for the weights of each synergy. (D) Cross-Correlation coefficient for the activation signals of each synergy. Data are reported as mean ± standard error of the mean.

8.3.2 Shared motor functions and their muscle synergies consistency

We attributed biomechanical functions to muscle synergies by observing the involved muscles (weights > 0.5) and the timing of activation signals, according to the literature (Perry 1992; Winter 1987).

We found five motor functions shared by all the subjects, and we labeled them from F1 to F5 (**Figure 8-8**). Three shared motor functions were related to the generation of the cyclic pattern of gait (F2, F4, F5), while the remaining two functions aimed to stabilize body and control balance dynamically (F1, F3).

Function F1 was principally devoted to the hip joint stabilization. Muscle activation was found in the terminal swing and initial/mid-stance phases of gait.

TFL and GMD muscles, devoted to hip abduction and hip flexion, had weights above 0.5 and hence were predominant, while other muscles were activated to a lesser extent (weights below 0.5) and in a less repetitive manner.

Function F2 generated propulsion in mid and terminal stance phases of gait. Ankle plantarflexors muscles, LGS, PL, and SOL, had weights over 0.5 and hence were the most relevant to this function.

Function F3 controlled the trunk position in the frontal plane at the heel strike of the homolateral and contralateral foot. LD_R and LD_L muscles had weights above 0.5; other muscles, particularly PL and VM, were also activated to a lesser extent.

Function F4 slowed down the foot during first rocker and controls forefoot clearance during swing phase. This function was accomplished by the TA muscle, an ankle dorsiflexor, which had a weight close to 1.

Finally, function F5 decelerated the leg at the end of the swing phase. MH and LH muscles, whose principal motor function is knee flexion, were recruited with average weights above 0.5.

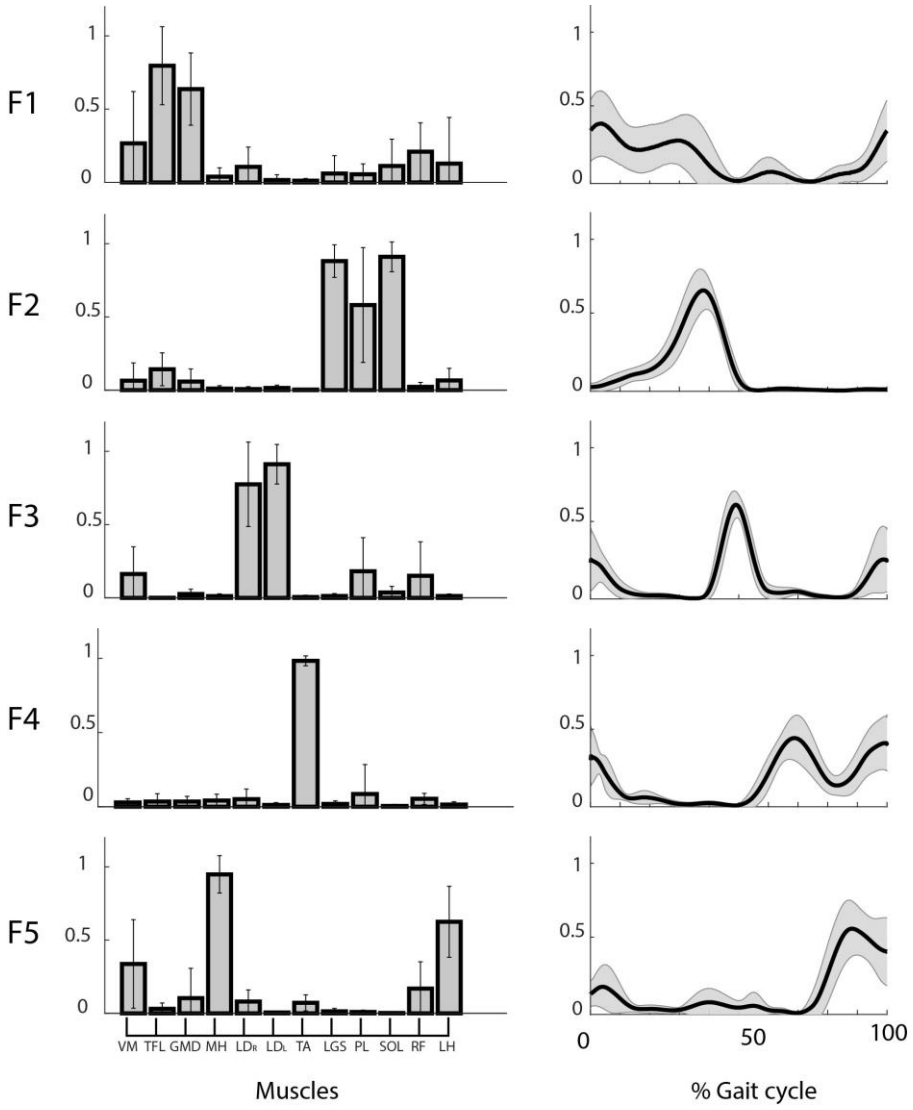

Figure 8-8. Weights (left) and coefficients (right) of the common muscle synergies across subjects. Muscle labels are reported below the weight plots. Data are reported as mean ± standard deviation.

Mean *CS* and *CC* values of the shared muscle synergies are reported in **Table 8-I**. It can be observed that all the values are above 0.90. No significant difference was found among *CS*, whereas a significant difference was found for *CC* values ($p = 0.17$ and $p=0.03$, respectively). A LSD post-hoc test evidenced a significant difference between *CC* activation signals of motor function F2 and motor functions F1 and F4.

Table 8-I. Cosine similarity for the weights and cross-correlation coefficients for the activation signals for the five shared muscle synergies. Data are reported as mean ± standard deviation.

	Motor Function				
	F1	*F2*	*F3*	*F4*	*F5*
Muscle weights (CS)	0.94 ± 0.07	0.97 ± 0.05	0.98 ± 0.06	0.95 ± 0.06	0.95 ± 0.06
Activation signals (CC)	0.96 ± 0.03	0.98 ± 0.02	0.98 ± 0.01	0.96 ± 0.03	0.97 ± 0.03

8.3.3 Characteristic subject-specific synergies

From 1 to 2 muscle synergies were characteristic of subjects. **Table 8-II** reports *CS*, *CC*, principal weights and biomechanical functions of the subject-specific synergies. More specifically, we found subject-specific synergies in 9 out of 12 subjects: 8 subjects showed 1 subject-specific synergy, while 1 subject showed 2 subject-specific synergies. Overall, we found 10 subject-specific synergies, with an average *CS* equal to 0.80 ± 0.20 and *CC* equal to 0.89 ± 0.14. VM was activated in 6 out 10 synergies, followed by GMD (5 out 10), RF (3 out 10), and TFL, LGS, SOL and (1 out 10). A motor function was assigned to each subject-specific synergy, similarly to the shared ones. The main motor functions aimed at decelerating leg at the heel strike and terminal swing phase.

Table 8-II. Intra-subject consistency of muscle weights and activation signals across subgroups of GCs, principal muscles recruited, and biomechanical functions of the subject-specific muscle synergies. Data are reported as mean ± standard deviation.

Subject	Consistency of motor functions		Principal muscles	Biomechanical function
	Muscle weights	***Activation signals***		
Subject #1	-	-	-	-
Subject #2	0.50 ± 0.22	0.80 ± 0.09	VM - RF	Stiff the knee at heel strike and the load acceptance phase
Subject #3	-	-	-	-
Subject #4	0.83 ± 0.08	0.91 ± 0.05	GMD - LGS - SOL	Stabilize hip joint and the foot at the heel strike
Subject #5	0.97 ± 0.01	0.99 ± 0.004	PL	Not defined
Subject #6	0.98 ± 0.03	0.99 ± 0.004	TFL - RF	Stabilize hip joint during swing
	0.74 ± 0.25	0.80 ± 0.17	VM	Not defined
Subject #7	0.49 ± 0.16	0.56 ± 0.09	GMD	Control the hip joint at heel strike and the end of the swing
Subject #8	0.99 ± 0.004	0.99 ± 0.004	VM - GMD - RF	Stiff the knee and control the hip joint at heel strike and the end of the swing
Subject #9	-	-	-	-
Subject #10	0.70 ± 0.17	0.87 ± 0.11	VM	Stiff the knee at heel strike and the end of the swing
Subject #11	0.96 ± 0.02	0.98 ± 0.01	VM - GMD	Stiff the knee and control the hip joint at heel strike and the end of the swing
Subject #12	0.97 ± 0.02	0.99 ± 0.01	VM - GMD	Stiff the knee and control the hip joint at heel strike and the end of the swing

Subjects #1, #3 and #9 showed no subject-specific synergies, but only shared synergies.

8.4 Discussion

In the present chapter we evaluated, in young adults, the consistency of muscle synergies during a 5-minutes walking trial. The trial was divided into subgroups of 10 concatenated GCs each. Then, we extracted muscle synergies from each subgroup of GCs. To quantify muscle synergies consistency, we adopted the cosine similarity metric, for the weights, and the cross-correlation, for the activation signals.

8.4.1 Methodological observations

It has been demonstrated that methodological choices affect the outcome of muscle synergies computation at each stage (Sartori et al. 2017). Particularly, the cut-off frequency of the low-pass filter is of paramount importance: a very low cut-off, such as 0.5 Hz, may oversmooth signal, whereas a very high cut-off, up to 20 Hz, introduces noise affecting muscle weights (Kieliba et al. 2018). Shuman et al. (B. R. Shuman, Schwartz, and Steele 2017) and Krogt et al. (Krogt et al. 2016) also evidenced the effect of low-pass filtering on the quality of extracted muscle synergies, expressed by the VAF: the higher the cut-off frequency is, the lower the VAF. It has been also observed that the higher the cut-off frequency of EMG envelop, the higher the amount of computed synergies (Hug et al. 2012). Hence, we choose a cut-off frequency of low-pass filter of 12 Hz, that is a good compromise between signal smoothing and introduced noise. Furthermore, it has been investigated how the unit variance scaling affects the EMG envelop (B. R. Shuman, Schwartz, and Steele 2017). Some works pointed out the number of strides and the difference between concatenating and averaging EMG (Anderson S Oliveira et al. 2014). Finally, extraction algorithms have been optimized to obtain more repeatable synergies and to reduce model error (Shourijeh, Flaxman, and Benoit 2015). We designed our study to limit the constraints to the walking: for this reason, we preferred natural pacing, since it has been demonstrated that constrained rhythm may influence the synergies with biomechanical constraints (Katherine Muterspaugh Steele, Tresch, and Perreault 2015). Similarly, we avoided shoed treadmill walking that may influence the synergies (Sloot, van der Krogt, and Harlaar 2014). The number of GCs within each subgroup was chosen to obtain a robust set of muscle synergies, that is enough subgroups of GCs to compute similarity across them. Experimental protocols generally adopt a few GCs to extract muscle synergies during walking. Most of the studies adopts 10 GCs (Ivanenko et al. 2003; Ivanenko, Poppele, and Lacquaniti 2004; Monaco, Ghionzoli, and Micera 2010; Chvatal and Ting 2012; Coscia et al. 2015; Haghpanah, Farahmand, and Zohoor 2017). However, there is a wide range of experimental protocol, where synergies are computed for 1 (Lencioni et al. 2016; Katherine Muterspaugh Steele, Tresch, and Perreault 2015) to a maximum of 20 GCs (Kim, Bulea, and Damiano

2016). It was demonstrated that, in healthy subjects, when calculated for small numbers of GCs the expected margin of error can change dramatically as a result of cycle-to-cycle variability. As the number of GCs increases, the margin of error decreases and stabilizes (B. Shuman et al. 2016). In addition, synergies extracted from 10 concatenated GCs are comparable with those obtained from more GCs (Anderson S Oliveira et al. 2014).

8.4.2 Five motor functions: coherence with literature and biomechanics

Overall, we found 5 to 7 muscle synergies per subject. Among these, five were shared by the entire sample, in good agreement with previous studies. Each synergy contributes to a precise biomechanical motor function, in good accordance with those described in previous works. For instance, (Lacquaniti, Ivanenko, and Zago 2012) reviews the motor functions described in previous works (Ivanenko, Poppele, and Lacquaniti 2004; Ivanenko, Poppele, and Lacquaniti 2006a; Cappellini et al. 2006). Motor function F1 is devoted to body support and load acceptance at heel contact, with a burst of activation at nearly 10% of GC and involves primarily hip and knee extensors. Synergies with the function of hip joint stabilization at initial contact were also found in (Zelik et al. 2014; Hagio, Fukuda, and Kouzaki 2015). Ankle plantar flexors constitute synergy F2, which contribute to body support, swing initiation and forward propulsion in late stance. Finally, a synergy dominated by TA muscle, with peak of activation signal at nearly 75% of GC, and a synergy decelerating the leg in late swing in preparation for heel contact were also found in previous studies (Coscia et al. 2015; Barroso et al. 2014). The difference across studies raises from the number and choice of muscles and the goodness of synergies criterion (B. Shuman et al. 2016).

8.4.3 Consistency of shared and subject-specific muscle synergies

Shared muscle synergies had *CS* and CC values close to 1. These high values indicate a good consistency of these synergies over the entire walking trial. Shared synergies represent biomechanical tasks cyclically repeated. They represent motor control strategies that remain consistent across many GCs.

In addition to the shared synergies, one or two subject-specific synergies were also found, in accordance with previous works (Chvatal and Ting 2012; Chvatal and Ting 2013). Subject-specific synergies were mainly present during two demanding phases of gait, which are heel strike and terminal swing. Recruited muscles suggest that these synergies were devoted to maintaining balance, a critical

end-point of motion control (Bauby and Kuo 2000). In fact, due to dynamic balance demand, locomotion is characterized by a high variability of the hip and knee angular moments (Winter 1995). Therefore, muscle synergies aimed at controlling the hip and knee joints may vary across subjects to optimize the balance task. It has also been demonstrated that foot contact is a challenging phase during gait, which requires an high degree of integration of internal models with sensory feedback inputs (van der Linden et al. 2007). This confirms the adaptability of muscle synergies, since they aim at adapting the global activity patterns to the kinetic and kinematic limb demands during locomotion (Ivanenko, Poppele, and Lacquaniti 2004). In most cases, subject-specific synergies had *CS* and *CC* close to 1, like shared ones. Subject-specific synergies, like shared ones, may refer to motor tasks that subjects execute cyclically, and, consequently, they are consistent during walking. It may be speculated that muscle synergy consistency reflects the contribution of lower motor neuron circuitries or the locomotion rhythmic signals produced by Central Pattern Generator (CPG) (Dimitrijevic, Gerasimenko, and Pinter 1998). However, some subject-specific synergies had a *CS* and *CC* value consistently lower, while others had undefined motor functions. Specific sensory inputs may play a role in these synergies (Cheung et al. 2005). It was demonstrated that synergies can vary due to obstacle negotiation, speed transitions or specific motor tasks (Cheung, D'Avella, and Bizzi 2009; Chvatal and Ting 2012; Hagio, Fukuda, and Kouzaki 2015). Furthermore, some researchers demonstrated that muscle synergies are influenced by step-related sensory feedback and biomechanical events of the GC (Ivanenko et al. 2003).

8.5 Conclusion

In this chapter, we described the method we adopted to extract muscle synergies in a 5-minutes walking trial. Secondly, we explored the intra-subject consistency of muscle synergies. We analyzed a sample of healthy young adults during a 5-minutes walking trial. We adopted cosine similarity yo measure consistency of muscle weights, and cross-correlation to measure consistency of activation signals. We found 5 synergies describing the same motor function in all subjects. These synergies showed a high degree of consistency. In addition, 9 out of 12 subjects showed also subject-specific synergies. Subject-specific muscle synergies were also consistent, although to a lesser extent. Our results confirm that CNS may adopt muscle synergies to effectively control human movement. Indeed, while motor output may vary, a set of basic functions are recruited cyclically, and they remain

unmodified during a repetitive task. This behavior could be verified at different speeds and for other cyclic movements, such as cycling or running.

Chapter 9

Muscle synergies of principal and secondary activations during gait

9.1 Introduction

Human locomotion is characterized by the cyclic repetition of biomechanical tasks with the aim of translating over a defined path with the less expenditure of energy. In (Basmajian and De Luca 1985), six major determinant of human gait are defined. However, human walking is quite more complex, because it requires the integration with sensory information and environment. For this reason, that are the basic constituents of the translation, but there are also adjunctive movements that seldom appear, but they are necessary for stability control and movement correction. This implies a modification in muscle activity, which reflects in different EMG activations. Therefore, two types of EMG activations can be defined: principal and secondary activations. Principal activations are the muscular activity required to generate movement. Secondary activations are generated by movements not necessary for the movement. The former describes movements repeated cyclically all Gait Cycles (GCs) and with a well-defined biomechanical function. The latter, are less repeatable across GCs and their function is auxiliary to the movement and less repeatable. To obtain principal and secondary activations, many consecutive GCs are required. Then, activation intervals of each GC are given as input of a classifier, which defines the principal and secondary activation intervals (Rosati et al. 2017; Agostini and Knaflitz 2011).

However, motor control strategies of walking activation patterns have been not analyzed yet. The objective of the present chapter is investigating if different

activation patterns are controlled by different neural circuits, that is if they recruit different motor modules or if they are controlled differently by supraspinal commands. For this reason, we investigated a sample of healthy subjects performing a walking task. Then, principal and secondary activations were computed from EMG, and corresponding muscle synergies were extracted. In this way, muscle synergies relative to three modalities were available. We call Principal Synergies (PS) the muscle synergies obtained from EMG corresponding to principal activation intervals. Similarly, we call Secondary Synergies (SS) the muscle synergies obtained from EMG corresponding to secondary activations. Finally, we call Original Synergies (OS) the muscle synergies obtained from original EMG, disregarding the activation intervals. We hypothesize that principal and secondary activations have different neural control mechanism. Furthermore, since secondary activations are occasional and repeatable to a lesser degree than principal activations, we hypothesize that SS are very different from PS in muscle weights and activation signals.

9.2 Material and methods

The dataset of the walking session relative to twelve healthy subjects (All females, right side dominant; mean age 24.58 ± 1.62; mean body mass index 20.07 ± 1.79) fully described in **Chapter 8** was adopted for this section. Briefly, subjects were instructed to walk at a self-selected pace for 5 minutes, maintaining a constant walking velocity. They walked back and forth over a 10-m pathway. EMG from 12 muscles of the trunk and the dominant leg were recorded and preprocessed. After data acquisition, we identified onset and offset of GCs by an automatic algorithm (Agostini, Balestra, and Knaflitz 2014). Then, outlier GCs, including acceleration, deceleration, and turning in correspondence of direction changes, were discarded.

9.2.1 Principal and secondary activations algorithm

Principal activations were extracted from each muscle individually. We computed principal activations intervals with the Clustering for Identification of Muscle Activation Patterns (CIMAP), a hierarchical dendrogram clustering algorithm described in (Rosati et al. 2017).

EMG is preprocessed before computing principal activations, and the following steps are performed:

- separate each GC and normalize to 1000 time points
- select a specific gait pattern (H-F-P-S)

detect activation intervals by means of a double threshold algorithm. The algorithm detects when EMG signal is above the background-noise level (ON) or when it is below (OFF) (Bonato, D'Alessio, and Knaflitz 1998). An activation interval *j* begins at the timing points ON_j and ends at OFF_j.

CIMAP algorithm is divided in three parts: dataset preparation, clustering algorithm, and extraction of principal activations.

Dataset preparation consists of pooling together strides with similar activation modality, that is activations with the same number of ON/OFF timing points. Datasets with less than 50 GCs are excluded from the analysis.

GCs of each dataset are clustered with a hierarchical dendrogram clustering algorithm. Initially, each GC is a single-element cluster. In an iterative manner, for a general cluster A with *m* ON/OFF timing points, the centroid is computed as the mean of ON and OFF timing points of the GCs inside the cluster, normalized by the number of GCs:

$$CLC_A = \frac{1}{|A|}\sum_{a_i \in A} a_i = \{\overline{ON_1}, \overline{OFF_1}, \dots, \overline{ON_j}, \overline{OFF_j}, \dots, \overline{ON_m}, \overline{OFF_m}\}$$

Then, the two closest clusters A and B are merged in the same cluster. L-infinity norm is adopted as a measure of similarity between two clusters A and B:

$$d(CLC_A, CLC_B) = \max(\max_m(ON_A - ON_B), \max_m(OFF_A - OFF_B))$$

The rule to select the final number of clusters is defined to have clusters with a comparable number of elements, a small intra-cluster variability, and a great distance between clusters. The intra-cluster variability is computed as the Euclidian distance between each GC within the cluster and the cluster centroid. At each level *k* of the dendrogram, two clusters A and B are merged in a cluster A∪B, and an

index R_k is computed. R_k is the ratio between intra-cluster variability of the new cluster A∪B and the maximum between the intra-cluster variability of the two original clusters A and B. To have a reasonable number of clusters, R_k is computed only for the last 20% of iterations. k is identified as the maximum R_k, and the final number of clusters is k - 1.

Finally, principal activations common to all datasets are computed for each muscle. A cluster centroid is computed for each cluster. The principal activations are given by the intersection of the clusters centroids. **Figure 9-1** shows an example of activation intervals of tibialis anterior muscle for a representative subject. In this case, GCs have been divided in two datasets with 2 and 3 activation intervals. The CIMAP algorithm clustered GCs into a) 3 clusters with 2 activations and b) 4 clusters with 3 activations. Overall, 7 clusters were created. Clusters centroids are computed, and the principal activations are the intersection of the clusters centroids. Otherwise, activations are labeled as secondary activations.

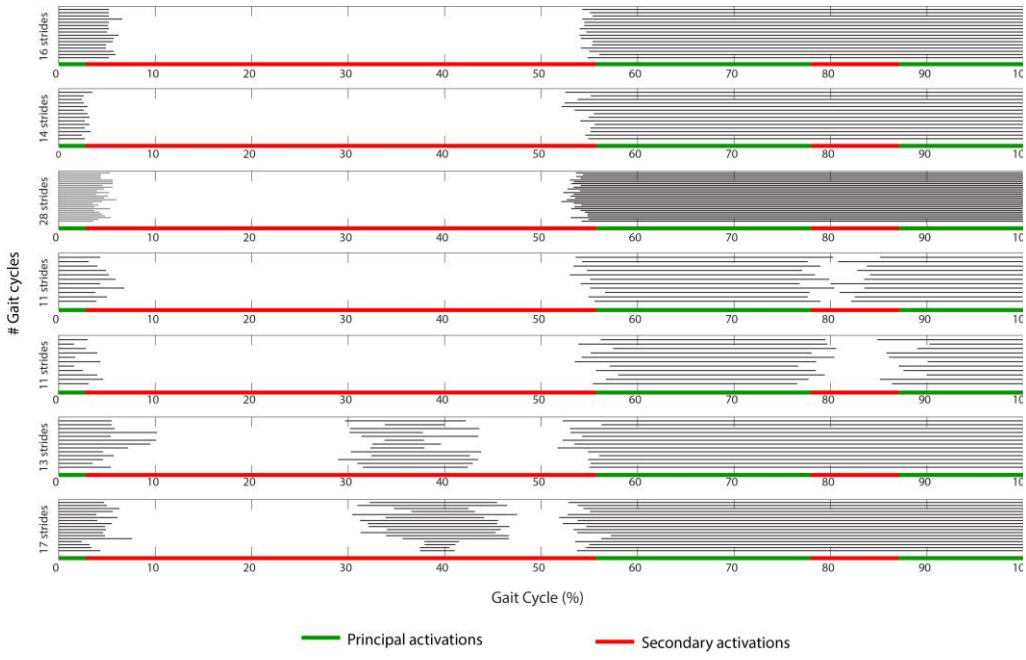

Figure 9-1. Results of CIMAP clustering algorithm for tibialis anterior muscle of a representative subject. Each grey bar represents the activation interval in percent of GC. Activation intervals are clustered according to number and duration of onset/offset intervals. Principal activations (green bar) are those common to all clusters prototypes extracted with the CIMAP algorithm, while secondary activations (red bar) are those present only in a subset of clusters.

Once we obtained principal and secondary activations for each muscle, we computed three binary masks, in order to collect the EMG within the specified activation interval:

- a mask equal to one everywhere, for to the original EMG;
- a mask with one in correspondence of principal activations, zero elsewhere;
- a mask with one in correspondence of secondary activations, zero elsewhere.

Before masks superposition, EMG of each channel was scaled from 0 to 1 according to the maximal activation within muscle, and each GC was normalized to 1000-time points. Then, we multiplied the binary masks with the EMG of the corresponding muscle. Where a mask was one, the signal remained unmodified, elsewhere the signal was set to zero. **Figure 9-2** shows an example of the three masks superposed to the EMG of the tibialis anterior for a representative GC. We repeated the masking with all muscles. Hence, we obtained the following three EMG matrices: a first one, with original EMG (EMG_{OS}), a second one with principal activations (EMG_{PS}), and a third EMG matrix with the bursts of the secondary activations (EMG_{SS}).

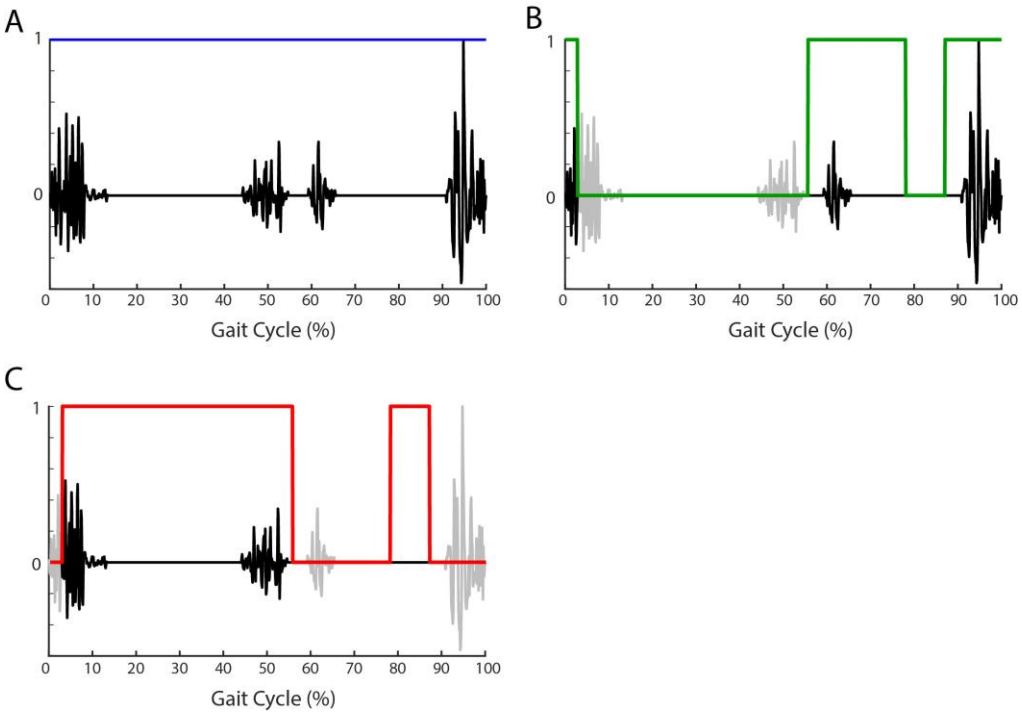

Figure 9-2. Example of activation masks applied to the EMG of a representative GC. The mask for original (blue line, panel A), principal activations (green line, panel B), and secondary activations (red line, panel C), are superimposed to the EMG of the tibialis anterior. Black line represents the EMG included in the mask, grey line represents the EMG excluded for the specified activation modality.

We pre-processed the three EMG matrices in the same way: they were high-pass filtered at 35 Hz, then demeaned, rectified, and low-pass filtered at 12Hz.

Muscle synergies were extracted from each EMG matrix with the methods fully described in **Chapter 8** (see paragraph 8.2). Briefly, we divided each EMG matrix (i.e EMG_{OS}, EMG_{PS}, and EMG_{SS}) in subgroups of 10 GCs each. For each subgroup, we extracted muscle synergies with NMF method. Hence, for a subject with N subgroups of 10 GCs, N sets of muscle synergies were computed. The goodness of fit of the data reconstruction using these synergies was quantified by the Variance Accounted For (VAF), defined as 100 × uncentered Pearson's correlation coefficient. For each modality, we selected a number of synergies accounting for at least 90% of the overall data variability (Chvatal et al. 2011). Since every subgroup may satisfy the VAF > 90% criterion with a different number of synergies, a further criterion was added: we choose the maximum number of synergies satisfying the

VAF > 90% criterion among the N subgroups. In this way, an equal number of synergies was obtained for each subgroup of each subject, and, contemporary, the VAF > 90% criterion was satisfied.

9.2.2 Data analysis

We compared the constitution, flexibility and biomechanical role of muscle synergies obtained from the three modalities: OS, PS, and SS. We tested normality of the data distribution in the analyzed subsets by means of a Shapiro-Wilks test, and we choose an α level of 0.05 for all tests.

We compared the number of synergies and the reconstruction VAF. Due to categorical nature of the number of synergies, we compared the number of synergies satisfying the VAF>90% criterion by means of a Wilcoxon Signed Rank test (Hayes et al. 2014). We compared VAF by means of a one-way ANOVA (factor: modality, three levels: OS, PS, SS) followed by post-hoc tests with Bonferroni correction, as the VAF distributions in the three modalities were not different from normal.

Flexibility is the feature of a muscle synergy to adapt to different motor tasks: the more flexible it is, the more the motor tasks it describes (M. L. Latash, Scholz, and Schöner 2007). Flexibility of two sets of muscle synergies can be compared in this manner: given a matrix EMG_1, it can be decomposed in the product of matrices of weights W_1 and coefficients curves C_1. The goodness of synergy modelization is described by the VAF computed between the original EMG and reconstructed data matrix:

$$VAF_1 = 1 - \frac{(EMG_1 - W_1C_1)^2}{EMG_1^2}$$

Similarly, the same description can be done for a matrix EMG_2 and synergies W_2C_2 with a goodness of modelization described by VAF_2.

To describe the flexibility of synergies of EMG_1, the cross-VAF can be computed as

$$VAF_{12} = 1 - \frac{(EMG_2 - W_1C_1)^2}{EMG_2^2}$$

where VAF_{12} represents the flexibility of synergies W_1C_1 to describe the motor task corresponding to EMG_2. Similarly,

$$VAF_{21} = 1 - \frac{(EMG_1 - W_2C_2)^2}{EMG_1^2}$$

describes the flexibility of synergies obtained from motor task EMG_2 (Fox et al. 2013).

We analyzed flexibility of muscle synergies by computing the within-subject cross-VAF. Iteratively, we used the synergies computed for one subgroup of GCs to reconstruct the EMG matrices of all the other subgroups. The following procedure was adopted to analyze intra-subject flexibility. N sets of synergies were available, each one corresponding to 10 GCs. For a subgroup of GCs *i,* we computed the reconstruction signal W_iC_i. Then, we obtained the cross-VAF with respect to the EMG of the remaining N-1 GCs. We repeated this procedure iteratively to obtain a cross-VAF for all the subgroups. Finally, the cross-VAF values were averaged across subgroups to obtain the within-subject flexibility. We computed cross-VAFs for OS, PS, and SS synergies, and they were compared by means of a one-way ANOVA, followed by post-hoc test if necessary.

We also analyzed consistency of muscle synergies, that is how well they describe the basic motor patterns (Clark et al. 2010). We adopted cosine similarity to compare muscle weights, and zero-lag cross-correlation to compare activation signals among subgroups of a subject (Gizzi et al. 2011). To compute the cosine similarity, the same number of synergies was required. We computed the cosine similarity iteratively among the N subgroups and for all the synergies between each pair of synergies. Finally, the average cosine similarities were compared with a paired-t test to test the null hypothesis the consistency of muscle synergies remained unaltered before and after principal activations calculation. The same procedure and statistical test was performed for the cross-correlation of activation signals. Cosine

similarity and cross-correlation were compared among the three modalities by means of a one-way ANOVA with factor modalities (three levels: OS, PS, SS), followed by post hoc analyses of pairwise comparisons when required.

Finally, we analyzed the number of dominant muscles of muscle weights of each synergy for PS and SS. A muscle was considered dominant in a synergy if it was within the 20% of the maximum weight (Katherine M. Steele, Tresch, and Perreault 2013). Like the number of synergies, we considered the number of muscles as categorical data. Then, the number of dominant weights was compared between PS and SS by means of a Wilcoxon signed-rank test.

9.3 Results

Across all participants, an average number of 181.17±10.19 GCs were analyzed. Subjects walked at a mean velocity of 1.18±0.10 m/s, with a cadence of 54.91±2.29 cycles/min. Overall, we observed nearly the same synergies extracted from EMG_{OS} and EMG_{PS}, but a better flexibility and stability came out after computing principal activations. On the contrary, muscle synergies obtained from EMG_{SS} were very different from those obtained from EMG_{OS} and EMG_{PS}, which may be indicative of a different neural origin.

9.3.1 Muscle synergies of a representative subject

Figure 9-3 shows muscle synergies for a representative subject. It reports synergies obtained from original EMG (**Figure 9-3A**) and synergies after principal activations filtering (**Figure 9-3B**). Overall, it can be observed that muscle weights were more uniform in amplitude in PS than OS. For instance, in $W3_{OS}$ there is a great variability in LGS and SOL recruitment. Conversely, in $W1_{PS}$ all the ankleflexors muscles are recruited equally. In addition, activation curves improved after principal activations filtering, particularly during the stance phase. Indeed, PS show coefficient curves that are nearly identical for all subgroups, whereas activation curves from $C1_{OS}$ to $C3_{OS}$ varied greatly in amplitude and shape. First and second synergies OS mixed in a single synergy PS ($W1_{PS}$ and $C1_{PS}$), which is formed by hip abductors TFL and GMD and, to a lesser extent, ankleflexors LGS and SOL and describes load acceptance.

Figure 9-4 shows muscle synergies obtained from secondary activations, SS, for the same representative subject. It can be observed that much more synergies than OS and PS are required to satisfy VAF>90% criterion. Furthermore, the most of synergies are dominated by only one muscle, and rarely from two muscles. Finally, it can be noticed that the amplitude of activation signals for SS is lower than PS and OS.

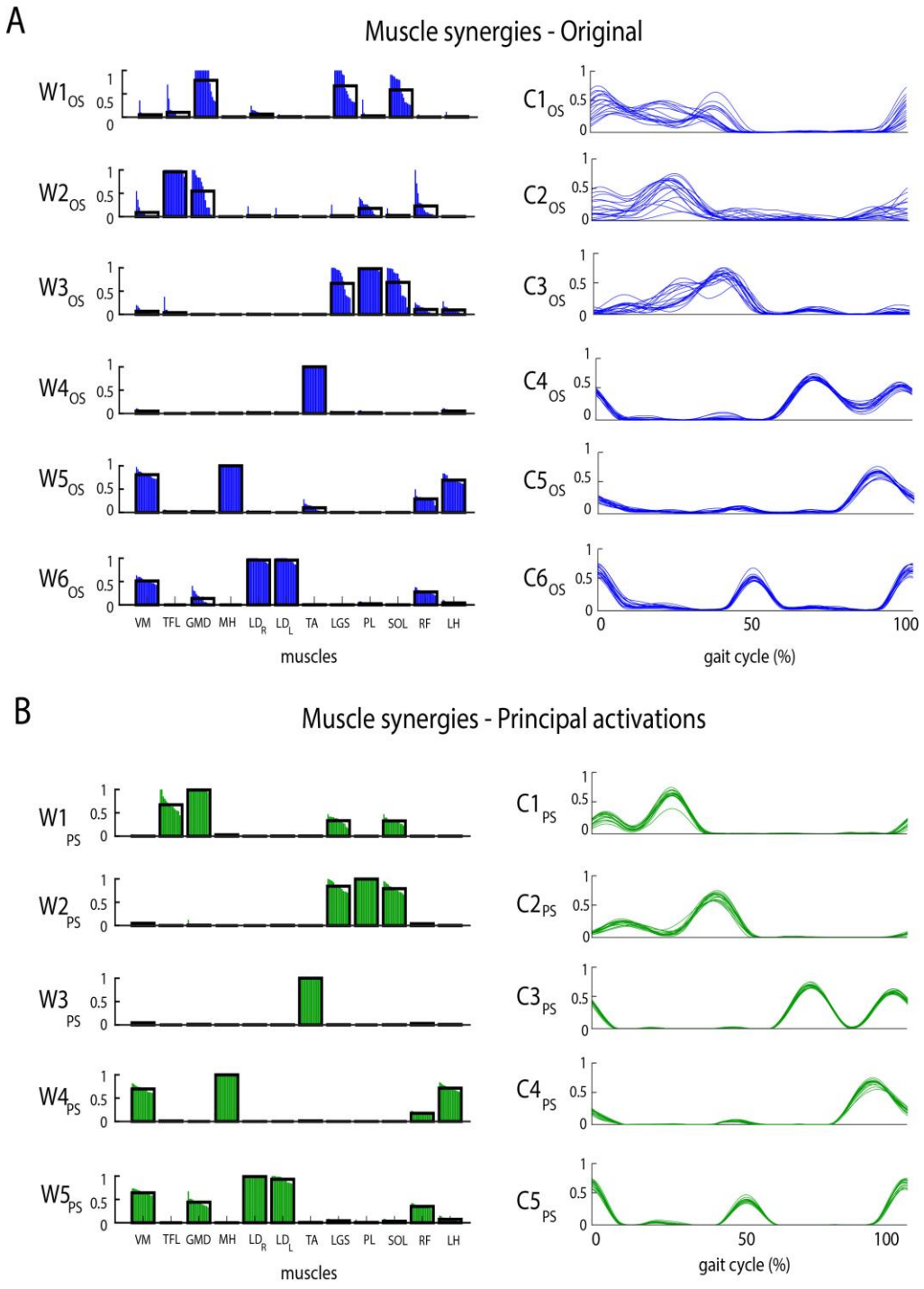

Figure 9-3. Muscle weights and activation signals for a representative subject. (A) muscle synergies obtained from original EMG signal. (B) muscle synergies obtained after principal activations processing. Black lines represent mean weights across subgroups of GCs.

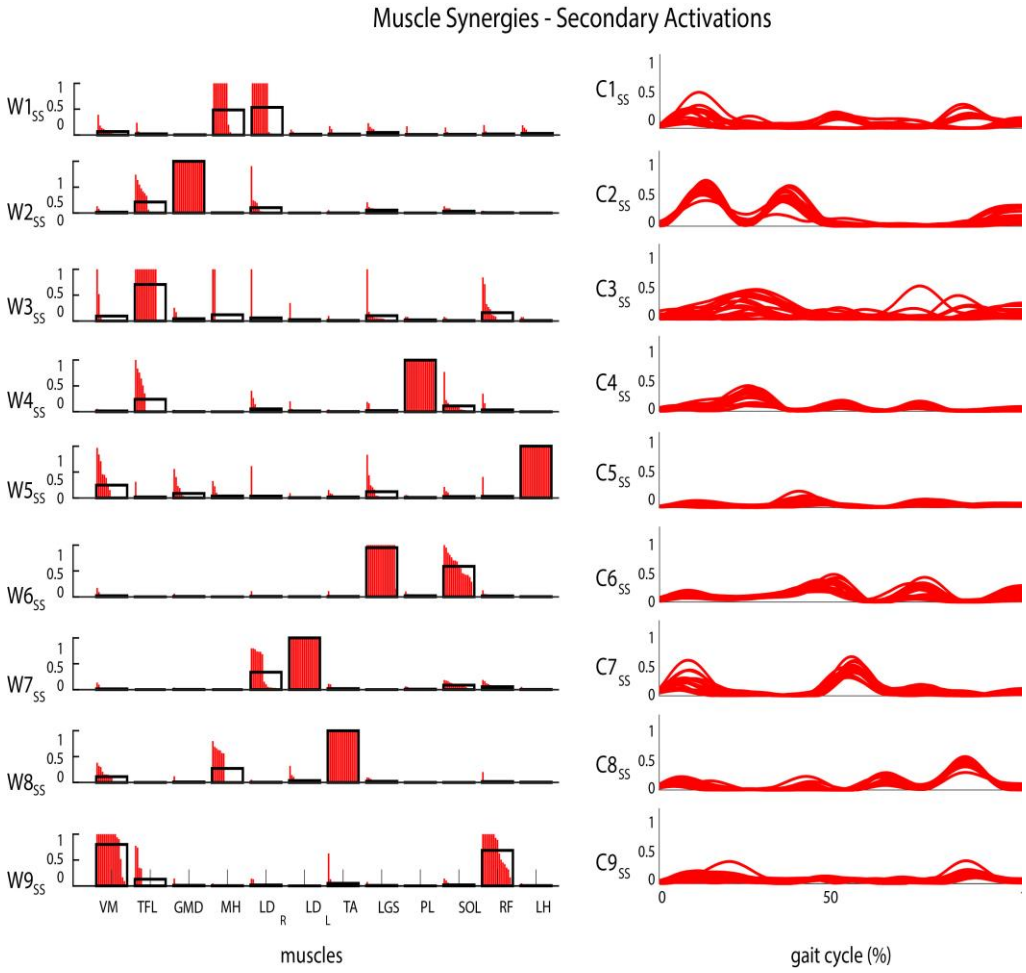

Figure 9-4. Secondary activations muscle synergies for a representative subject. One to two muscles are recruited within each muscle weight vector (Left), and activation signal have low amplitude (Right). Black lines represent mean weights across subgroups of GCs.

Muscle synergies consistency in the three modalities has been evaluated by measuring cosine similarity of muscle weights and cross-correlation of activation signals. Consistency measures of the synergies of the representative subject are reported in **Figure 9-5**. It can be observed that PS have the best consistency in both muscle weights and activation signals across subgroups of GCs (**Figure 9-5B**). Conversely, OS show a lower degree of consistency, particularly in the stance phase (**Figure 9-5A**, synergies W1-W3 and C1-C3). However, cosine similarity and cross-correlation remained above 0.8 in all the synergies. Finally, **Figure 9-5C** shows cosine similarity and cross-correlation for the synergies obtained from

secondary activations only, SS. It can be observed that muscle synergies consistency decreased dramatically. In both stance and swing phases it can be observed that muscle weights and activation signals varied over time. For SS, differently from OS and PS, it can be noticed that certain synergies had consistency mean values of cosine similarity and cross-correlation well below 0.5 (W1ss, W2ss) and 0.7 (C1ss and C3ss) respectively. They indicate a large amount of synergies of subgroups of GCs with very low levels of consistency with other subgroups.

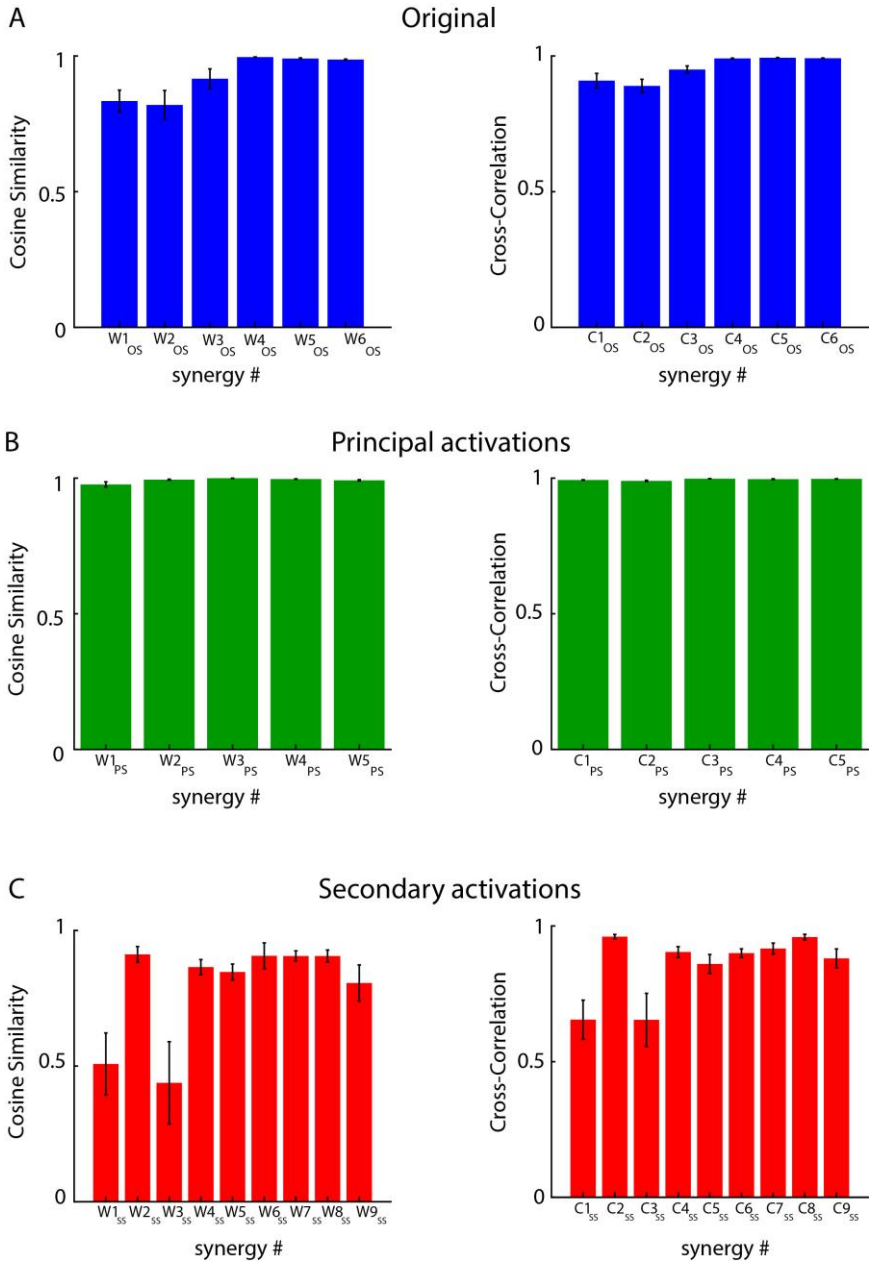

Figure 9-5. Muscle synergies consistency measurements for the representative subject. For the muscle weights, it has been adopted cosine similarity (Left panel), while for the activation signals it has been adopted zero lag cross-correlation (Right panel). Consistency measurements have been reported for OS (A), PS (B), and SS (C) Data are reported as mean ± standard error. Each bar represents the mean consistency measurement between the same synergy of all subgroups of GCs. Measures have been labeled according to the muscle weights vectors or activation signals (Figure 9-3 and Figure 9-4).

9.3.2 Number of synergies and reconstruction VAF

On the average, each subject satisfied the VAF>90% criterion with 5.6 ± 0.5 synergies OS, whereas with principal activations EMG 5.0 ± 0.5 synergies PS and with secondary activations 8.8 ± 0.6 SS were extracted. In details, 7 subjects had one less synergy when principal activations were extracted, while in 5 subjects OS and PS had the same number of synergies. A Kruskal-Wallis test showed a significant difference in the number of synergies among the three modalities OS, PS, SS. A post-hoc test indicated a significative difference between the ranks of OS and PS ($p = 0.01$), between PS and SS ($p = 0.02$), and OS and SS ($p = 0.02$). A one-way ANOVA showed no statistical difference for the mean reconstruction VAF of the extracted synergies (VAF 92.1 ± 0.5 OS, 92.2 ± 1.1 PS and 91.52 ± 0.3 SS, $p = 0.05$).

9.3.3 Number of muscles within synergies

We compared the composition of PS and SS, by comparing the number of dominant muscles. For PS and SS, we determined the amount of dominant muscles. Then, we divided synergies in two groups: synergies with less than 2 dominant muscles (1-2 group) and synergies with more than three muscles (3+). **Table 9-I** reports the number of synergies of PS and SS modalities divided according to the number of dominant muscles. It can be observed that the most of SS were dominated by 1-2 muscles. On the other hand, the PS modality showed, on the average, an equal number of synergies with 1-2 and 3+ dominant muscles for each synergy. A Wilcoxon signed rank test showed a significative difference in the number of dominant muscles between the PS and SS modalities for both 1-2 and 3+ groups ($p < 0.0001$).

Table 9-I. Number of synergies according to the number of dominant muscles for PS and SS modalities. Data are reported as mean ± standard deviation.

	Number of synergies		
	Total	***1-2 muscles***	***3+ muscles***
PS	5.0 ± 0.6	2.5 ± 0.9	2.5 ± 0.7
SS	8.4 ± 1.2	8.0 ± 2.0	0.4 ± 0.9

9.3.4 Synergies flexibility and consistency

We computed cross-VAF to evaluate within-subject flexibility of muscle synergies. **Figure 9-6** shows the distribution of the within-subject cross-VAF. It can be observed that cross-VAF PS is slightly higher than OS. It may indicate that PS are more repeatable within-subject than OS. On the average, cross-VAF improved by 7.0%, from a minimum of 4.6% to 12.8%. Only in one subject (S6) cross-VAF of PS decreased by 16%. A Kruskal-Wallis test showed a significant difference in the median cross-VAF among the three modalities ($p<0.0001$). A Wilcoxon signed rank test indicated a significative difference of median cross-VAF between OS and PS ($p = 0.03$), between PS and SS ($p<0.0001$), and between OS and SS ($p<0.0001$).

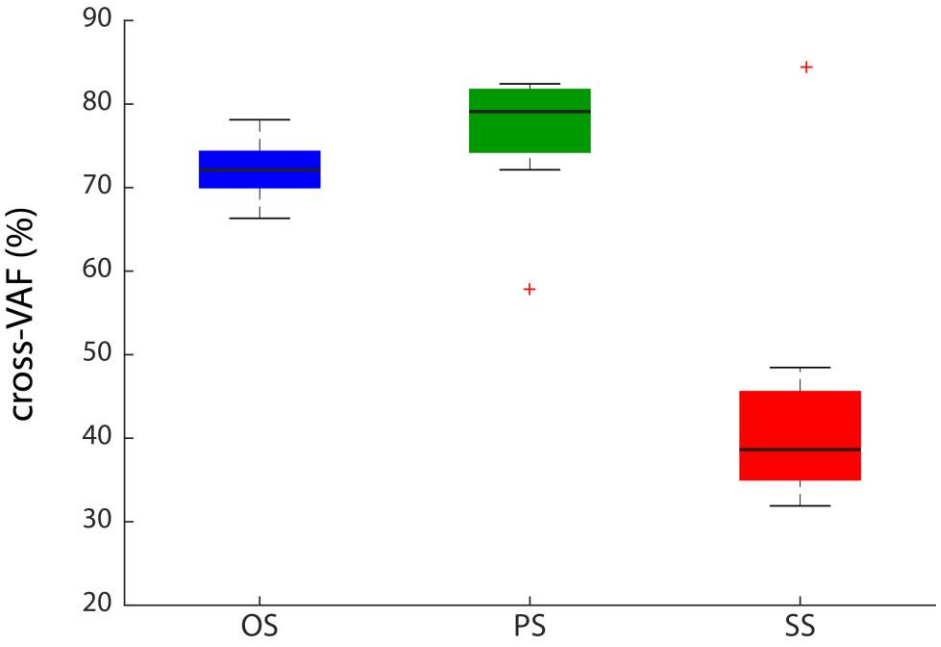

Figure 9-6. Within-subject cross-VAF for synergies obtained from original EMG (OS), principal activation (PS), and secondary activation (SS). +: outlier subject.

We compared consistency of the three modalities by computing the cosine similarity of muscle weights and cross-correlation of activation signals. On the average, PS had the highest cosine similarity (0.98 ± 0.03), whereas OS and SS had a lower cosine similarity, equal to 0.93 ± 0.06 and 0.82 ± 0.07 respectively. A one-way ANOVA showed a significant difference in the mean cosine similarity of muscle weights between the three modalities ($F = 29.18$, $p<0.0001$). A post-hoc paired t-test evidenced also a significative difference in the cosine similarity of PS from OS ($T = -3.31$, $p = 0.007$), PS from SS ($T = 7.6$, $p < 0.0001$), and OS from SS

($T = 5.33$, $p = 0.0002$). As for the cross-correlation, muscle synergies showed the same trends of consistency across GCs. Indeed, PS had the higher mean cross-correlation, equal to 0.99 ± 0.01, whereas OS and SS showed a value of cross-correlation equal to 0.96 ± 0.03 and 0.88 ± 0.03 respectively. A post-hoc paired t-test evidenced also a significative difference in the cross-correlation of PS from OS ($T = -3.85$, $p = 0.002$), PS from SS ($T = 14.94$, $p < 0.0001$), and OS from SS ($T = 9.21$, $p < 0.0001$).

9.4 Discussion

In recent years, many studies evidenced that walking task is not achieved by repeating the same motor patterns cyclically, but there are several patterns of muscular activation. For instance, it has been observed that LGS activates not only during midstance as ankle flexor (Perry 1992; Sutherland 2001), but also in the pre-swing, to correct foot position in heel strike preparation (Agostini et al. 2010; Di Nardo, Ghetti, and Fioretti 2013). It has also been observed that extra activations of GMD appear between terminal stance and pre-swing, probably with the function of hip abduction when the hip is unloaded (Agostini et al. 2014). Other studies evidenced that children affected by hemiplegic cerebral palsy may have different patterns of muscular activation, even if classified in the same Winter class (Agostini, Nascimbeni, et al. 2015). All these results demonstrate the richness of muscular activation patterns during gait. This richness is mainly due to the redundancy of skeletal-muscle system, because a motor task can be accomplished by adopting one among many possible solutions (Bernstein 1967; Abend, Bizzi, and Morasso 1982; Sharif Razavian, Mehrabi, and McPhee 2015).

More recently, it has been developed a novel algorithm that, in an automatic way, classifies activation patterns on the base of onset and offset instant times of muscular activity. It allows to separate the more frequent muscular activation patterns from those that seldom appear. In this manner, two kind of activation patterns with different biomechanical roles emerged for each muscle: principal activations, that allow the movement execution, and secondary activations, that have auxiliary functions (Rosati et al. 2017).

The present work aimed to understand if different activation patterns are controlled with a different neural organization. For this reason, muscle synergies were computed for principal and secondary activations separately. Muscle synergies were obtained by applying a factorization algorithm to the EMG signal, to compute vectors of muscle weights and curves of activation signals (Torres-Oviedo and Ting 2007). In this way, muscle synergies put in evidence the functional

groups of muscles coded at spinal level, and the supraspinal signals that synchronize the activation of the specific muscle group (Ivanenko, Poppele, and Lacquaniti 2006b; Bizzi et al. 2002). The criterion we adopted to choose the number of synergies of each subject, that is guaranteeing a VAF>90% for each set of synergies, allowed to obtain synergies that well reconstruct the starting data, without significant difference among the modalities (see Paragraph 8.3.1). Furthermore, by recording nearly two hundred GCs during a single task, we could measure consistency and flexibility of muscle synergies, that may indicate how synergies are repeatable and independent from the motor task.

The main outcome of the present work is that different muscular activations need different neuronal activation. Indeed, our results demonstrated that PS and SS were significantly different in all the measured parameters. PS were constituted by a few motor modules with three or more muscles each. On the contrary, SS were formed by many motor modules with less muscles than PS. In our study, we limited the analysis of the number of dominant muscles per synergy only to PS and SS because we were interested to determine if there were different muscle recruitment between the two modalities. Furthermore, the study of PS and SS evidenced how nervous system integrates the two modalities to adapt and optimize movement. Indeed, we observed that SS accomplished selective tasks, through prolonging or anticipating PS. For instance, certain subjects needed to improve stability in the stance to swing transition. To this aim, the bilateral activation of trunk muscles in late-stance, as defined by PS, was followed by a SS of the contralateral muscle. The same mechanism may be devoted to increase stability in leg control at the heel strike. This behavior can be observed in the synergies obtained for the representative subject we reported in Results section (**Figure 9-4** and **Figure 9-5**).

It has been hypothesized that muscle synergies represent motor control of the CNS (Roh, Cheung, and Bizzi 2011; Bizzi and Cheung 2013; Ting et al. 2015). Neural circuits located in the spinal cord drive muscular activations during locomotion while intermediating between descending signals and peripheral sensory information (Monaco, Ghionzoli, and Micera 2010). Previous studies evidenced that task-specific synergies could raise to adapt to motor control, indicating that synergies may depend on intended action (de Rugy, Loeb, and Carroll 2013; Sharif Razavian, Mehrabi, and McPhee 2015). Also (McGowan et al. 2010) evidenced flexible weightings may be required, with substantial changes in mechanical demands. Nevertheless, it remains unclear if synergies represent the activity of nervous system, or rather, they represent the constraints of articular joints to the accomplishment of motor task (Aoi and Funato 2016; McGowan et al. 2010).

In this sense, we observed that, according to the motor function, different neuronal control mechanisms may coexist. As for the PS, we observed muscle synergies very similar to those generally reported in the literature (Cappellini et al. 2006; Lacquaniti, Ivanenko, and Zago 2012; Chvatal and Ting 2013). Otherwise, in the SS modality, we cannot talk of motor modules really, because each synergy accounted for one or two muscles only. The very low amplitude of SS activation signals reinforces this hypothesis. Furthermore, PS are highly repeatable within subject, whereas there is high variability in SS, as results of consistency and flexibility demonstrated. We suppose that SS may not represent synergies coded at the spinal level, but rather be sensitive responses managed at a peripheral level. In summary, nervous system seems to manage differently the motor tasks during the same GC. This could be interpreted as an optimization strategy that nervous system adopts for motor control: motor tasks that are frequently repeated are stored at spinal level as motor modules, whereas task-specific adjustments, requiring secondary activations, may be only a peripheral reflex. Our results imply that results obtained from muscle synergies during gait may be affected by the secondary activations. To properly study the framework of neural control of gait, principal activations only are required, whereas secondary activations should be discarded if not of specific interest.

9.5 Conclusion

In this chapter, we analyzed the muscle synergies of principal and secondary muscle activations during gait. We computed the principal and secondary activation intervals by means of CIMAP algorithm and we extracted muscle synergies associated to the original EMG signal and the two different activation modalities. The main outcome of this work is that different gait patterns are originated by different neural control mechanisms. Indeed, results we obtained evidenced significant difference between PS and SS in terms of composition, flexibility, and consistency. We found that PS had a few muscle synergies composed by many muscles and large activation curves. Conversely, SS had many synergies with one or two muscles and activation curves close to zero. Furthermore, we found significant differences between synergies obtained from raw EMG and PS. Our results demonstrate that activation patterns are controlled differently by nervous system: it seems that only principal activations are originated by motor modules, whereas secondary activations may be only peripheral reflexes acted to adjust movement to the biomechanical task

.

Chapter 10

Clinical cases of muscle synergies analysis in lower back pain patients after one-month physiotherapy rehabilitation

10.1 Introduction

Lower Back Pain (LBP) is an acute or chronic pain in the lumbar or sacral regions, which may be associated with muscular-ligamentous sprains and strains, intervertebral disk displacement, and other conditions (Parker and Parker 2004). LBP is classified as being specific or nonspecific. Specific LBP is caused by specific patho-physiological mechanisms, such as infections, inflammations, osteoporosis, rheumatoid arthritis, fracture or tumor. However, the vast majority of patients are labelled as having nonspecific LBP, which is defined as symptoms without a clear specific cause (van Middelkoop et al. 2010). Furthermore, it could be an accompanying pain of spine disorders such as sciatica (El Barzouhi et al. 2014; Jones, Pandit, and Lavy 2014). LBP is generally a long-term experience pain with significant recurrence, rather than a single case episode (Campbell et al. 2013). The lifetime prevalence of LBP is reported to be as high as 84%, and best estimates suggest that the prevalence of chronic LBP is about 23%, with 11–12% of the population being disabled by it (Balagué et al. 2012). Treatments of LBP generally

include pharmacological treatment, surgical intervention, transcutaneous electrical stimulation, and physical therapies such as spinal manipulations (Herndon, Zoberi, and Gardner 2015). A very recent review showed that LBP is related to hip, trunk and spine strength imbalances and low flexibility levels, but there is no evidence that the normalization of these variables may reduce pain and functionally improve subjects with LBP (Victora Ruas and Vieira 2017).

Little is known about the gait abnormalities of people suffering from this pathology (Lamoth et al. 2006). It has been observed that LBP patients adapt gait pattern at the trunk level (Y. P. Huang et al. 2011). An excessive foot pronation during gait in women suffering from LBP has been viewed, which may indicate a role of the foot position in the LBP (Menz et al. 2013). A particular gait alteration that has been observed is the stiffed-leg walking: it means that LBP patients have the tendency of to walk with the knee extended during the load acceptance phase (Agostini et al. 2009; Müller, Ertelt, and Blickhan 2015). The correction of this alteration is of great importance, because walking is a daily activity, but it requires a reeducation to the normal gait.

It has been evidenced that muscle synergies may be helpful in designing rehabilitation therapies (McMorland, Runnalls, and Byblow 2015), for instance as a tool for monitoring the recovery of the physiological muscle recruitment (Safavynia, Torres-Oviedo, and Ting 2011; Ting et al. 2015). Therefore, muscle synergies have been sometimes adopted to evaluate therapies. For instance, some previous works adopted muscle synergies to show the effect of gait rehabilitation in persons suffering by multiple sclerosis (Jonsdottir et al. 2015) and in the rehabilitation of the upper limb of stroke patients (Urra, Casals, and Jané 2014).

The present chapter is a pilot study with the objective of investigating how rehabilitation of LBP patients with stiffed-leg walking may affect their motor control strategies. A group of LBP patients were evaluated with a brief walking trial. Then, we enrolled a small subgroup of patients with stiffed-leg walking. Enrolled patients underwent a one-month physiotherapy to reduce the stiffness of the leg and to correct the trunk posture. Before and after the physiotherapy, we analyzed the muscle synergies extracted during a walking trial. Muscle synergies were extracted and analyzed with the methods we developed and described in the previous chapters. In details, we analyzed muscle synergies only for principal activations, computed as described in **Chapter 9**. We adopted the experimental protocol and muscle synergies extraction procedure described in **Chapter 8**.

10.2 Material and methods

10.2.1 Participants and experimental setup

Participants were recruited from the Rehabilitation Division of IRCCS San Camillo Hospital, Torino (Italy) across the hospital population with diagnosis of chronic LBP. Patients with comorbidity of neurological or vascular disease, BMI > 30, non-autonomous or aided walking were excluded from the study. Hence, eights patients (2 males and 6 females, age 59 ± 6.5 years, BMI 22.15 ± 1.5) were included in the study. The experimental protocol was approved by the local ethical committee and all participants gave their written informed consent to be included in the study.

The flow chart in **Figure 10-1** resumes the phases of this study. The work was divided into three phases: a preliminary assessment session, to enroll eligible patients (Enrollment). At the end this session, three out the 8 patients met the criteria to be enrolled in the rehabilitative protocol (see next Section). The selected three patients were analyzed with gait analysis in order to investigate muscle synergies before (Pre-treatment) and after one-month rehabilitation (Post-treatment).

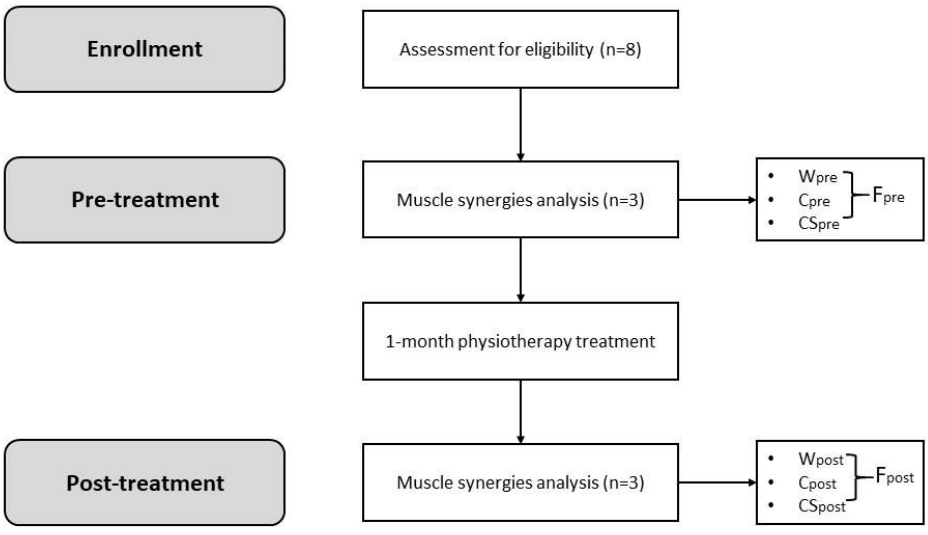

Figure 10-1. Flow chart of the study. At each stage, n patients were analyzed.

10.2.2 Enrollment

The enrollment stage consisted of recording a walking session, to compute the goniometry of the knee during walking. Subjects were equipped with a system for the gait analysis (STEP32, Medical Technology, Italy). Signals were acquired at 2 kHz. The system recorded: foot-switches signals, for timing the gait cycle, and knee joint angle curves in the sagittal plane. Foot-switch signals were acquired by three thin switches (size $10 \times 10 \times 0.5$ mm^3; activation force: 3N) placed beneath the heel, the first, and fifth metatarsal-heads of each barefoot sole. Knee joint kinematics in the sagittal plane was collected, bilaterally, by electrogoniometers (accuracy: 0.5°) placed on the lateral side of each lower limb.

After sensors positioning, subjects were asked to walk at self-selected speed back and forth over a straight pathway of 15 meters for 2 minutes.

Foot-switches signals were adopted for timing the gait cycles and removing outlier gait cycles, i.e. with abnormal timing, like those relative to deceleration, acceleration, and reversing (Agostini, Balestra, and Knaflitz 2013). Gait cycles were then normalized at 1000-time points.

Knee joint kinematic of the right leg was recorded for each gait cycle and averaged across gait cycles. To evaluate the knee kinematic at the initial contact, two parameters were computed: the angle of heel contact at initial stride (a_i), and angle of the peak of first knee flexion (a_p). For the two parameters, we set the following thresholds to define extended knee at initial contact: 1) $a_i < 5$ degrees, 2) $a_p < 10$ degrees, and 3) $a_p - a_i < 5$ degrees. The stiffed-leg walking condition was met if at least one of the three conditions were not satisfied, and the subject was considered eligible for the rehabilitation phases. **Figure 10-2** shows an example of measured parameters in two reference subjects, one with normal knee parameters (**Figure 10-2A**), and a second one with extended knee at the initial contact (**Figure 10-2B**).

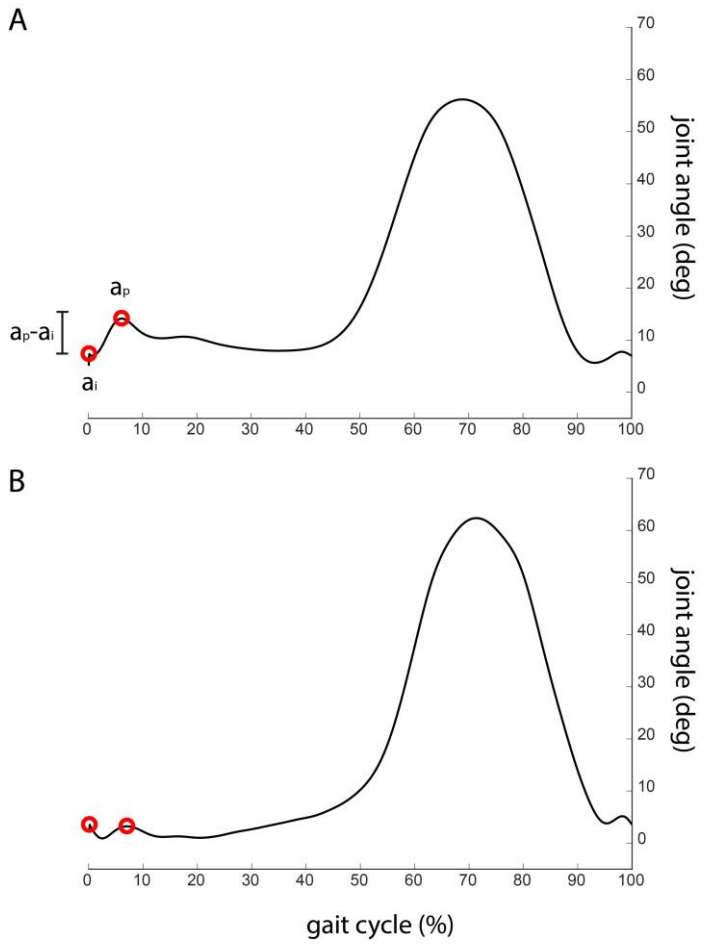

Figure 10-2. Comparison of knee joint kinematic between good (A) and stiff-legged (B) initial contact. Black line is the mean knee joint goniometry of all recorded gait cycles. 2-A reports the parameters adopted to define knee extension at initial contact: a_i is the angle at initial contact, a_p is the peak angle at first extension, and a_p - a_i is the difference between the two parameters.

10.2.3 Physiotherapy protocol

The enrolled subjects underwent a one-month physiotherapy treatment. The treatment lasted 4 weeks, 3 days a week. Patients were assessed before and after the treatment period with the following scales:

- Numeric Pain Rating Scale (NPRS): a unidimensional measure of pain intensity in adults. It assigns a value from 1 (minimum pain) to 10 (maximum pain) to quantify pain (Rodriguez 2001; Hawker et al. 2011);

- Body chart: patient is asked to localize painful body parts on a human body scheme. Pain is quantified by means of NPRS and sorted by patient according to relevance. There is no range, but the evaluation is based on the number of individualized painful points;
- Oswestry Low Back Pain Disability Questionnaire: it provides a subjective percentage score of disability in daily living activities. The scores range from 0 (no pain at the moment) to 5 (the pain is the worst imaginable at the moment). The Oswestry Disability Index (ODI) is the percentage of marked disability points over the total available points (Fairbank JC, Couper J, Davies JB 1980);
- Physiotherapy evaluation according to Clarkson criteria (Clarkson 2012).

The rehabilitative protocol consisted of two sets of exercises: the first aimed at recovering LBP, the second to correct stiffed-leg walking.

- Rehabilitative exercises for LBP were defined as follows:
- to prevent lumbar pain
- to improve passive and active range of movement of lumbar spine and basin
- Selective recruitment of stabilizing muscles of the lumbar spine during AAII and AASS activities
- Selective recruitment of Longissimus dorsii muscle

As for the stiffed-leg walking, the protocol aimed:

- To improve knee flexion perception in initial contact and load acceptance phases
- To improve knee stabilization in flexion-extension phase

10.2.4 Muscle synergies

Muscle synergies were extracted from a walking session before the rehabilitation (pre-treatment) and from another walking session at the end of the rehabilitation period (post-treatment). Experimental protocol and muscle synergies extraction methods were the same as described elsewhere (see Material and Methods in **Chapter 8** and **Chapter 9**) and briefly resumed here.

Subjects walked on a straightforward 10-meters path for 5 minutes. Electromyography (EMG) from the right lower limb, foot-switches signals, and

knee goniometry in the sagittal plane were recorded. Gait cycles were segmented by using foot-switches and knee goniometry and outlier cycles were filtered out. Afterwards, principal activations were extracted by using the CIMAP algorithm described in (Rosati et al. 2017). EMG was preprocessed and gait cycles were divided in 10-gait cycles subgroups. Muscle synergies were extracted from EMG matrix for each subgroup separately by using non-negative matrix factorization, as introduced by (D. D. Lee and Seung 1999), and applied to EMG by (Ting and Macpherson 2005; McKay and Ting 2008). An overall variance accounted for (VAF, uncentered Pearson Coefficient), adopted to quantify the goodness of the matching between measured and reconstructed EMG, was set to 90% to choose the suitable number of synergies. Afterwards, to compare synergies between subgroups, synergies were ordered with K-means clustering. K was set equal to the number of extracted synergies, and clustering was repeated five times with different random initial clusters for selecting the solution with the lowest within-cluster sums of point-to-centroid distance. For a given 10-cycle subgroup *i*, synergies were permutated in order to minimize the distance of a synergy with respect to the centroid of the synergies of the other subgroups.

We obtained a set of muscle synergies for the pre-treatment and another one for the post-treatment analysis. Pre-treatment synergies were characterized by vectors of muscle weights W_{pre} and coefficients C_{pre}. Post-treatment synergies were characterized by vectors of muscle weights W_{post} and coefficients C_{post} (**Figure 10-1**). *CS* was adopted to measure the within-subject similarity of weight vectors. *CS* was computed between each pair of muscle weight vectors of each subgroup of gait cycles. Then, it was averaged across subgroups. We obtained a mean *CS* pre-treatment (CS_{pre}) and post-treatment (CS_{post}).

10.2.5 Data analysis

To individualize the main motor functions of the synergies of LBP patients, we selected the best matching synergies with a set of reference synergies. Reference synergies were the synergies we obtained from a sample of twelve healthy controls previously computed (see Chapter 8). At this purpose, we computed the mean muscle weights and activation signals across the subgroups of gait cycles for each synergy of LBP patients. Afterwards, we adopted the following procedure for comparing synergies of LBP with reference synergies. We selected a reference synergy; them, we compared the reference muscle weights with the muscle weights of a LBP patient by computing the cosine similarity between them ($CS_{LBP\text{-}Control}$).

We iterated the comparison for each LBP synergy. We selected the LBP synergy with the highest $CS_{LBP\text{-}Control}$, since it shared the motor function with the reference synergy. An example of comparison between two good-matching synergies between reference (black line) and LBP (red line) is reported in **Figure 10-3**. In this case, the mean similarity of muscle weights and activation signals between LBP and the reference is 0.98. This procedure was repeated iteratively for all the reference synergies to define all the functions. In summary, we collected 5 synergies pre-treatment and 5 synergies post-treatment for each LBP patients. These synergies were the best matching with reference synergies of healthy controls previously extracted, hence they described precise motor functions.

To verify an improvement of muscle synergies after rehabilitation, we compared the VAF, the number of synergies, and the *CS* of the pre-treatment synergies with those of the post-treatment synergies. All statistical tests were performed at a significance level of 0.05. We tested the normality of the VAF and *CS* parameters with a Kolmogorov-Smirnov test. Since not all the datasets followed a normal distribution, we adopted non parametric tests to perform the statistical analysis.

First, we performed a Wilcoxon rank sum test to test the null hypothesis that the reconstruction VAF of pre- and post-treatment are samples from continuous distributions with equal medians. The same test was adopted to compare the number of synergies with VAF>90 pre-treatment and post-treatment.

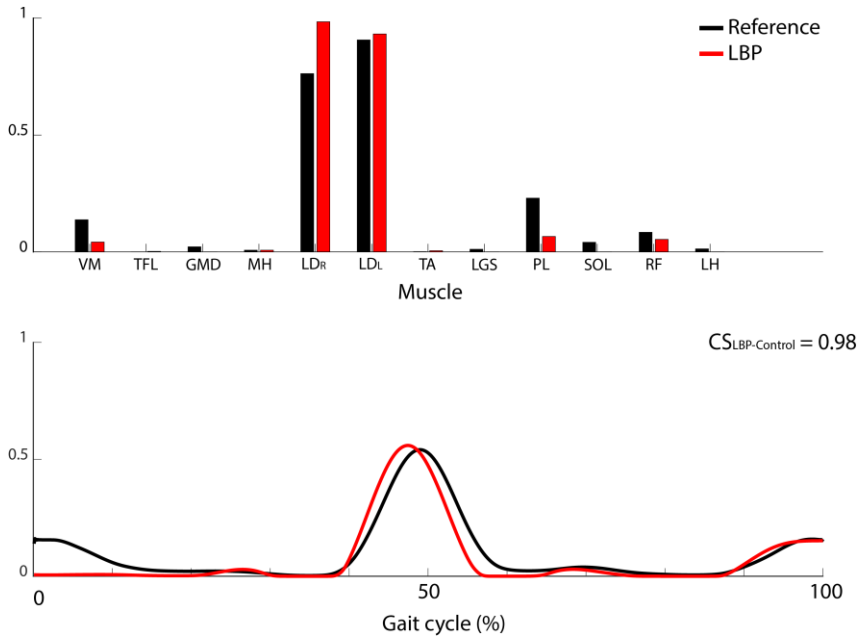

Figure 10-3. Comparison between reference synergy (black) and a representative LBP subject (red). Top figure reports the muscle weights and bottom the activation signals. A good similarity between the two synergies reflects in the high cosine similarity (*$CS_{LBP\text{-}Control}$* = 0.98).

10.3 Results

10.3.1 Enrollment

Knee joint parameters at the enrollment stage are reported in **Table 10-I**. Patients have been labelled from S1 to S8. Four patients showed at least one parameter under the threshold (i.e. extended leg at initial contact) and so they resulted recruitable for the rehabilitation stage. This result is in accordance with previous study, since near the half of investigated subjects suffering from LBP showed extended knee at initial contact during gait (Agostini et al. 2009). They had the following knee joint kinematics parameters: patients S3, S4, and S5 showed an angle of impact lower than 4 degrees. Patient S7 had a_i and a_p over threshold, but the difference between the two angles was lower than 5 degrees. Subject S4 renounced to continue the study, hence three subjects were enrolled to undergo the rehabilitation: S3, S5, and S7 (Mean age 62.67 ± 4.73, weight 55.67 ± 5.86 kg, height 162 ± 4.62 cm).

Table 10-I. Results of the knee joint kinematic of the patients investigated during enrollment stage. Each subject is labelled progressively from S1 to S8. For each subject, the following parameters are reported: angle at initial contact (a_i), peak angle at first knee extension (a_p), knee excursion at first extension (a_p - a_i), and knee range of motion (ROM). In last column, it is reported if the subject met the threshold criteria to be enrolled in the following stages.

Subject	age	sex	knee ROM (mean ± std dev)	a_i (deg)	a_p (deg)	$a_p - a_i$ (deg)	recruitable
S1	59	F	52.30 ± 2.30	7.34	14.14	6.80	no
S2	66	F	57.05 ± 3.92	8.23	18.89	10.66	no
S3	59	F	61.42 ± 4.97	3.51*	3.22*	-0.29*	yes
S4	67	M	57.88 ± 1.15	3.52*	8.09*	4.57*	yes
S5	68	F	43.74 ± 2 29	3.30*	7.33*	4.03*	yes
S6	77	F	45.51 ± 1.49	9.65	17.09	7.45	no
S7	61	F	54.49 ± 1.36	15.02	20.11	5.09*	yes
S8	64	M	57.96 ± 2.89	7.17	13.95	6.78	no

*: under threshold.

10.3.2 Rehabilitation

Table 10-II shows the results of the scales before and after rehabilitation. It can be observed that scores of the three subjects improved after the rehabilitation.

Table 10-II. Results of the physiotherapy tests adopted to evaluate patients in pre-treatment and post-treatment phases.

Subject	pre-tratment			post-treatment		
	Body chart	*NPRS*	*Oswerty*	*Body chart*	*NPRS*	*Oswerty*
S3	3	4	16	1	2	10
S5	1	6	20	1	3	16
S7	2	3	38	1	2	30

Figure 10-4 shows the mean knee joint angle of the three LBP patients measured before and after the rehabilitative treatment. Red line represents the mean pre-treatment knee joint angle, blue line represents the post-treatment knee joint angle. Black circles indicate knee angle at the initial contact (a_i) and peak angle at first knee extension (a_p). S3 and S5 modified markedly the knee joint angle profile after the treatment, whereas S7 maintained the same knee joint profile. In details, it can be observed that a_p and a_p - a_i of S3 were under threshold at pre-treatment: in fact, their amplitudes were 6.6 and 2.9 degrees respectively. After the treatment, a_p raised over the threshold of 10 degrees, with an amplitude of 14.5 degrees. Therefore, a_p - a_i increased nearly to the threshold, with an amplitude of 4.7 degrees. In patient S5, a_i and a_p were under threshold at the pre-treatment, with an amplitude of 4.3 and 4.0 degrees respectively. Angle amplitude raised to 6.1 and 11 degrees after the treatment. Finally, S7 showed a_i and a_p above threshold before and after the treatment, whereas a_p - a_i remained under the threshold of 5 degrees.

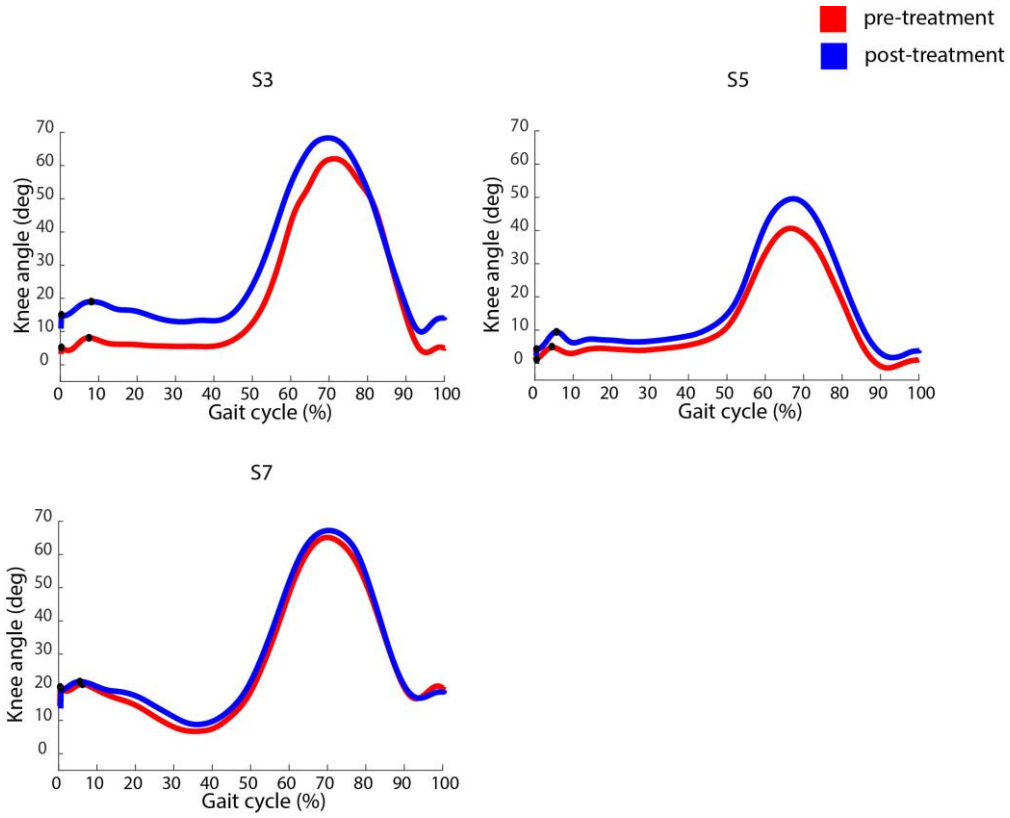

Figure 10-4. Mean knee joint angle pre-treatment (red) and post-treatment (blue) in the LBP patients. Black circles indicate knee angle at the initial contact and peak angle at first knee extension.

10.3.3 Muscle synergies

Table 10-III shows gait parameters for the three subjects before and after treatment. It can be observed that subject S5 had gait parameters lower than the other two patients, particularly the number of gait cycles and gait velocity.

Table 10-III. Gait parameters obtained from gait analysis before and after rehabilitative treatment.

Subject	pre-treatment			post-treatment		
	cadence (cyc/min)	*number gait cycles*	*velocity (m/s)*	*cadence (cyc/min)*	*number gait cycles*	*velocity (m/s)*
S3	50.7	148	1.05 ± 0.07	57.2	207	1.12 ± 0.07
S5	45.6	83	0.69 ± 0.05	49.0	60	0.84 ± 0.04
S7	54.1	166	1.05 ± 0.03	50.3	143	1.25 ± 0.08

VAF reconstruction from 3 to 8 muscle synergies are reported in **Figure 10-5**. It can be observed VAF values increased after rehabilitation, which demonstrated an improvement in quality of muscle synergies. S3 showed the best improvement, because VAF post-treatment was higher than VAF pre-treatment for all the set of synergies. By contrast, S5 showed nearly the same VAF post-treatment with respect to pre-treatment. Eventually, S7 VAF post-treatment was higher than pre-treatment, even if to less extent than S3. It can also be observed that, by averaging the VAF of the synergies of all subgroups of gait cycles, the number of synergies to overcome the threshold of VAF > 90 varied before pre-treatment and post-treatment for S3 patient. Indeed, S3 required 7 synergies to reconstruct original signal before treatment (VAF 92.71 ± 1.17), which reduced to 5 synergies after treatment (VAF 91.23 ± 0.55). By contrast, S5 and S7 satisfied the VAF > 90 criterion to reconstruct original EMG signal with the same number of synergies before and after rehabilitation, that are 7 and 5 synergies respectively.

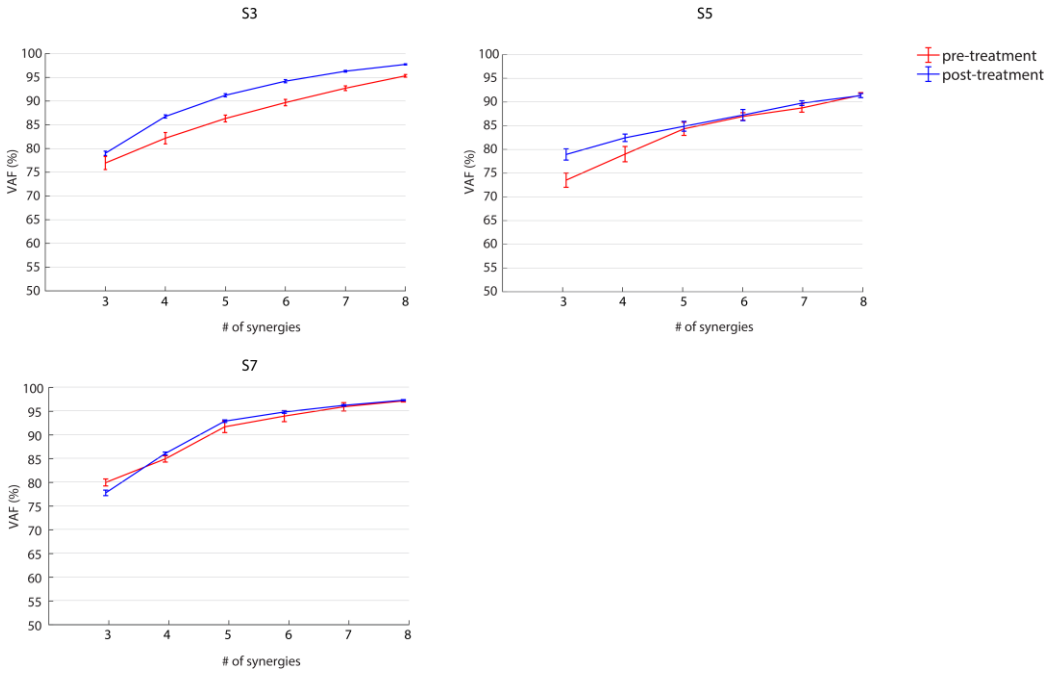

Figure 10-5. VAF of the synergies for the patients submitted to rehabilitation before (red line) and after (blue line) rehabilitation. Data are reported mean ± standard error.

Significance of the Wilcoxon rank sum test for VAF from 3 to 8 synergies is reported in **Table 10-IV**. It can be observed that S3 significantly improved VAF for all the sets of synergies, whereas S5 and S7 just for the synergies explaining the lowest VAF.

Table 10-IV. P-values for the Wilcoxon rank sum test for VAF pre-treatment vs. post-treatment when 3 to 8 synergies are adopted to reconstruct original EMG signal.

Subject	# of synergies					
	3	*4*	*5*	*6*	*7*	*8*
S3	0.008*	0.000*	0.000*	0.000*	0.000*	0.000*
S5	0.001*	0.013*	0.345	0.755	0.181	1.000
S7	0.001*	0.009*	0.026*	0.659	1.000	0.274

*:P<0.05

The five muscle synergies representing the motor functions of the three LBP patients and healthy controls group are reported in **Figure 10-6**. Motor functions of LBP patients before (red) and after treatment (blue) are compared with reference synergies of healthy subjects (green). Overall, rehabilitation caused a modification in the recruitment of muscles in the weights vectors, whereas activation signals remained unmodified. Synergies recruiting longissimi dorsii (F3), which described the motor function devoted to trunk stabilization at terminal stance, showed the most relevant modification in weight vector. Indeed, it can be noticed that in the pre-treatment analysis all LBP patients recruited only one muscle, whereas both of longissimi dorsii were recruited after treatment. Particularly, LD_R in S3 increased from 0.14 to 1. Patient S5 also augmented LD_R recruitment, from 0.14 to 0.8. S7 increased LD_L recruitment from 0.06 to 0.5. S3 patient modified also F1 weights, where TFL, VM, and LH where recruited after treatment. S5 varied synergy F2, by increasing recruitment of PL muscle. Furthermore, in F4, recruited SOL and TA muscles in the post-treatment, whereas it recruited only TA in pre-treatment. Finally, S7 maintained unaltered weights of 4 out 5 synergies. Activation signals remained unmodified in the most of synergies after treatment, in both timing and amplitude. Only two main modifications can be observed: in F1 of patient S3, the peak of activation curve shifted from the midstance phase to the early stance. In F5 post-treatment of S5, a predominant activity during stance and terminal swing can be evidenced. Peak amplitude of activation signals pre-treatment and post-treatment are close to peak amplitude of healthy subjects. However, it can be observed that peak amplitude of F3 pre-treatment and post-treatment in S5 is lower than healthy subjects.

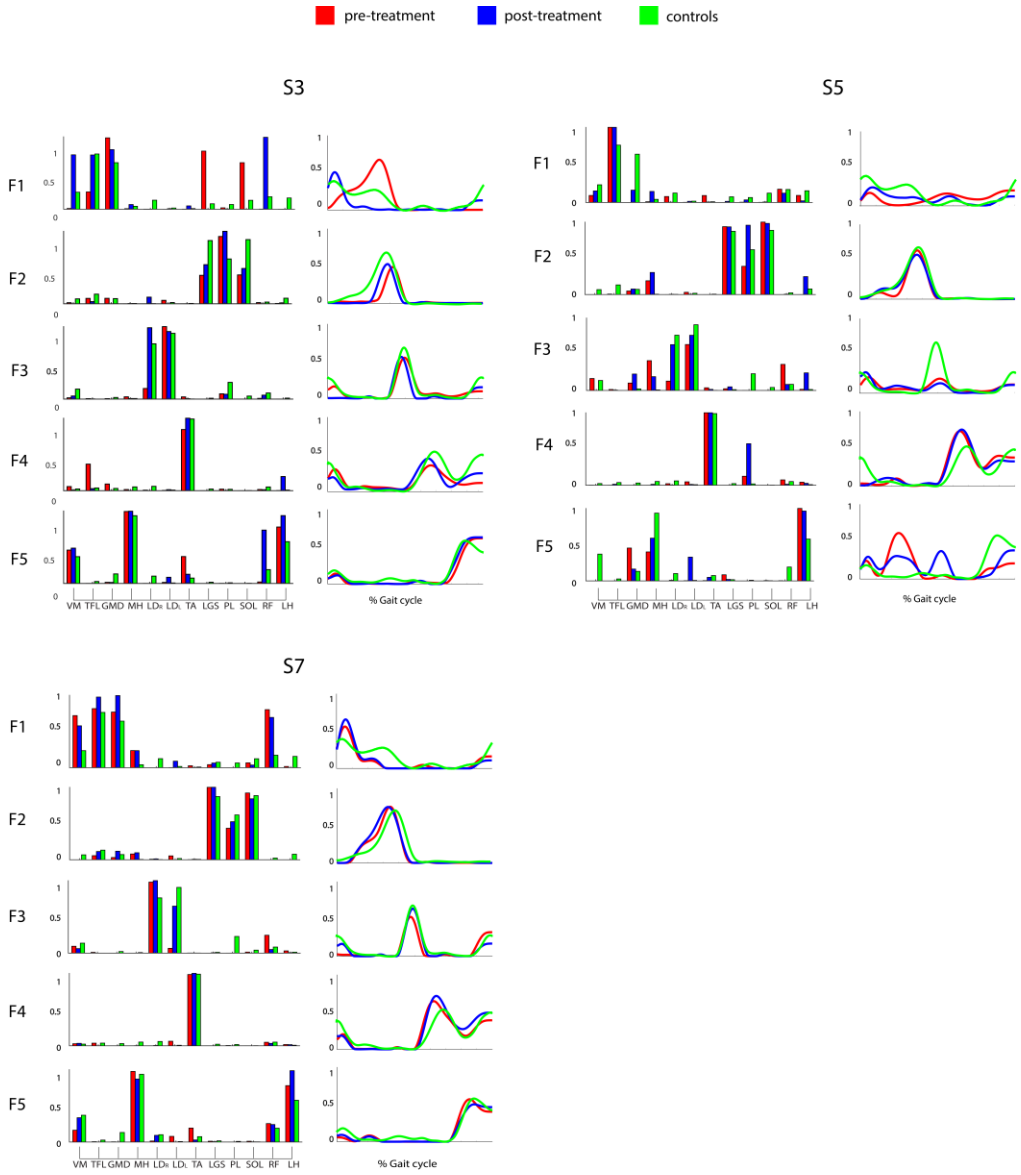

Figure 10-6. Muscle weights and activation signals for the motor functions of the three LBP subjects before (red line) and after (blue line) rehabilitation. Data are compared with muscle synergies of healthy controls (green line).

Within-subject *CS* of the three patients pre- and post-treatment is pictured in **Figure 10-7**. Each bar represents the averaged *CS* between each pair of subgroups of gait cycles. It can be observed an overall improvement of *CS* between pre-treatment and post-treatment stages. Significance of the difference of *CS* before and after treatment have been compared by a Wilcoxon rank sum test. Significance of Wilcoxon test is reported in **Table 10-V**. Median *CS* significantly improved for all the synergies of S3 and S7, while 3 out 5 synergies of S5 had significant improvement.

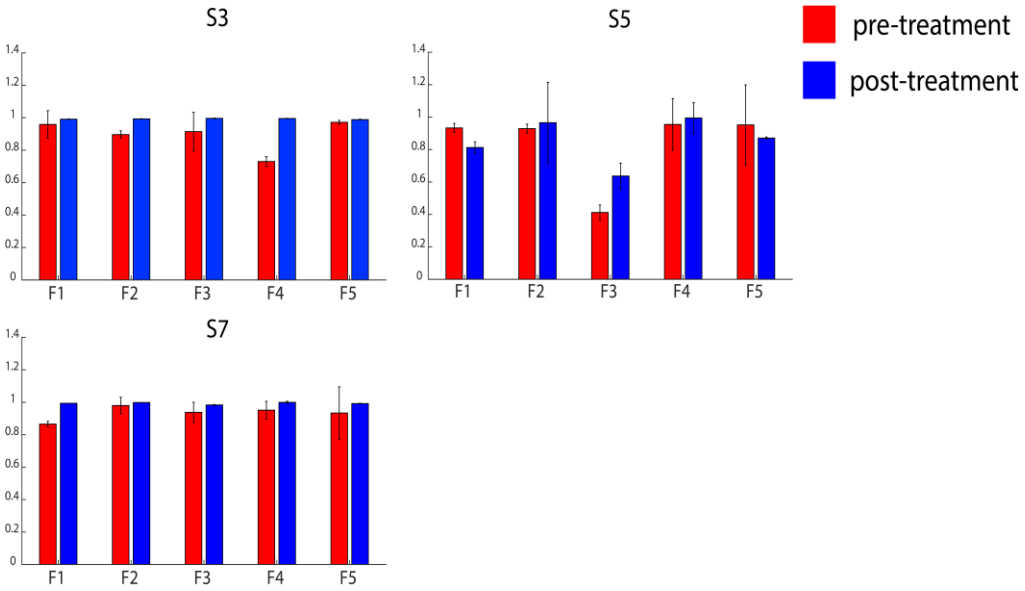

Figure 10-7. CS of the motor functions of the three patients before (red) and after (blue) the rehabilitation.

Table 10-V. Wilcoxon rank sum test p-values for CS pre- and post-treatment.

Subject	Synergies				
	F1	*F2*	*F3*	*F4*	*F5*
S3	0.000*	0.000*	0.000*	0.000*	0.033*
S5	0.073	0.343	0.073	0.003*	0.149
S7	0.000*	0.000*	0.046*	0.000*	0.000*

*: $p<0.05$

10.4 Discussion

The objective of the present chapter was verifying the efficacy of a physiotherapy treatment to correct the stiffed-leg walking in patients suffering from LBP by analyzing muscle synergies. To this end, we performed a screening session to enroll a small group with a stiffed-leg walking. To verify the efficacy of physiotherapy on rearranging neuromuscular control of gait, we analyzed muscle synergies before and after one month of physiotherapy. Our results demonstrated that patients improved kinematic parameters and muscle synergies. In detail, we observed a recovery of functional groups of recruited muscles.

Several studies analyzed the kinematic of gait in patients suffering from LBP. Huang and colleagues observed a larger pelvis rotation and lower relative phase between pelvis and thorax horizontal rotations (Y. P. Huang et al. 2011). It was observed that LBP patients show the tendency to walk with the knee extended during the load acceptance phase. It was also observed that, after treatment, this tendency diminished (Agostini et al. 2009). The same conclusion was made by Müller and colleagues: they observed that in chronic non-specific LBP patients the knee joint angle at initial contact was more extended with respect to healthy controls during level and uneven walking (Müller, Ertelt, and Blickhan 2015). Furthermore, several studies have been performed on posture in LBP. Jacobs and colleagues studied postural response to perturbation in LBP patients. They evidenced that patients had a broader baseline than healthy controls. In addition, the response to perturbation was more likely a modulation of baseline rather than an activation burst. This was observed at the levels of erector spinae, internal and external oblique, and gastrocnemius. Further studies evidenced a reduced and delayed response, that may indicate an altered neuromuscular response (Cholewicki et al. 2005).

Nevertheless, at which level the neuromuscular alteration is, it was not investigated yet. In this sense, muscle synergies may provide a useful tool. In the muscle synergies model, functional muscle activation patterns are used to reliably produce motor functions during natural motor behavior. They represent a set of subtasks that nervous system can flexibly combine to produce complex and natural movements. Muscle synergies are muscle co-activation necessary to coordinate body segments. A single neural command can recruit a muscle synergy to reliably produce the motor subtask. It means that muscle synergies may reflect a general principle of neural control, and they may better characterize a patient's motor deficit and/or compensations and assess degree of flexibility and adaptability.

Effectiveness of rehabilitative treatment can be evidenced by observing modification of evaluation scales (**Table 10-II**) and knee joint angle profile (**Figure 10-4**). Scores describing pain demonstrated that patients' pain reduced, as well as difficulties in daily living activities. Knee kinematics demonstrated that, after the rehabilitation, S3 and S5 reduced markedly leg stiffening at initial contact: indeed, initial contact angle and peak at first knee flexion moved above the thresholds. It can be noticed that knee joint angle values are different at enrollment and pre-treatment. This can be due to the different experimental conditions, since equipment and trial duration were different. However, knee angles were under threshold at the enrollment and pre-treatment. Hence, the analysis of physiotherapy scales and knee kinematics demonstrated the efficacy of rehabilitative treatment in stiffed leg gait, and results in muscle synergies can be ascribed to this improvement.

A first result of this work is the evidence of altered of muscle synergies in stiffed-leg walking. To the best of our knowledge, this pathological walking was not described with muscle synergies yet. We observed that the number of synergies and the activation signals remained substantially unmodified with respect to healthy synergies, but muscle weights were recruited not functionally. Furthermore, this is also the first essay of describing LBP walking with muscle synergies. Only one previous study named muscle synergies in LBP (Jacobs et al. 2011). However, the muscle synergies were referred to as centrally organized response patterns, rather than functional groups of muscles that combine to generate motor patterns.

From a clinical point of view, three aspects of synergies are of relevance to be analyzed: the number, the structure, and the recruitment of synergies. Firstly, the number of synergies indicates the number of independent subtasks that can be performed. Furthermore, it has been proposed that the number of synergies may be an index of complexity of motor control (Clark et al. 2010; Frère and Hug 2012; Kim, Bulea, and Damiano 2016). Structure of synergies affects muscle coordination patterns and could reflex changes in neural connectivity and excitability. Finally, recruitment affects timing and force of the motor subtask, that may result in abnormal motor patterns. For instance, there can be an anomalous recruitment in the event of deficiency of motor cortex inhibition. Previous studies evidenced an alteration in at least one of the aforementioned aspects (Safavynia, Torres-Oviedo, and Ting 2011). In this work, we observed that stiffed-leg walk patients had an alteration in the structure of muscle synergies, and that the rehabilitation protocol recovered it to a functional one. Furthermore, an improvement in the consistency of synergies could be also indicative of a recovery of the structure of synergies to be more functional. Indeed, by recovering functional synergies which execute a

cyclic motor task, they better reflect the action of Central Pattern Generators in generating rhythmic movements.

Several limitation of this study need to be addressed. First, in this pilot study, the small and heterogeneous sample size limits the ability to generalize results. However, subjects showed similar improvement in consistency and modules recruitment. A second limitation is in a slight gait speed difference between pre- and post-treatment evaluation. Since patients adopted a self-selected speed, they choose the most comfortable. Previous studies evidenced that speed may affect muscle synergies, particularly in activation curves profile (Clark et al. 2010; Buurke et al. 2016). However, it was showed that locomotor activation patterns remain the same across speeds, and that muscle weightings change according to biomechanical requirements. In our study, the difference in the speed between pre- and post-treatment were very subtle and they were considered not influencing the muscle synergies. Furthermore, the speed of LBP patients was comparable with the speed of healthy controls on the average (see chapter 8). Finally, we performed our analysis on principal activations only, without considering secondary activations. Since secondary activations are extra muscular activations due to, for instance, body balance or walking scheme adaption, the subsequent muscle synergies may represent reflexes rather motor control strategies of the central nervous system. Hence LBP patients, by adapting walking scheme to pathological conditions, may show additional or merging muscle synergies obtained from secondary activations. Future developments should involve the analysis of a larger cohort of LBP patients and the analysis of muscle synergies obtained from secondary activations.

10.5 Conclusion

We investigated the muscle synergies in a small group of subjects suffering from LBP with stiffed-leg walking. We preliminary analyzed the gait in a group of LBP patients, then we recruited those with at least one of these characteristics: small angle at initial contact, small angle at first knee extension, and small difference between the two angles. Three patients were enrolled from an initial sample of eight subjects. A one-month of rehabilitation was administered to the enrolled patients, and we investigated muscle synergies during a five-minute overgound walking before and after the rehabilitation. We computed muscle synergies for the principal activations during gait and we compared the number, the quality and the consistency of synergies. We observed an alteration in the consistency and quality of muscle synergies before rehabilitation. Furthermore, we observed an altered

composition of muscle weights vectors with respect to healthy muscle synergies. All these parameters slightly improved after the rehabilitation. Our results demonstrated how LBP may affect the recruitment of muscles in the generation of movement during gait and that rehabilitation can effectively recover muscle synergies composition. Muscle synergies can be an effective instrument to evaluate gait abnormalities in stiffed-leg walking and they can better address the rehabilitation protocol to recover muscle synergies.

Chapter 11

Conclusions

This thesis aimed to investigate two aspects of CNS: nonlinear features of cerebrovascular patterns and motor control strategies described by means of muscle synergies. In the first part of the thesis, we analyzed NIRS signals with nonlinear techniques. We adopted well known entropy metrics translated from information theory to characterize the complexity and periodicity of biosignals. Our results demonstrate that nonlinear characteristics of biosignals cannot be ascribed only to randomness. Conversely, we evidenced that nonlinearity are characteristics of physiological systems and that they may vary with different stimuli (Chapter 4) or in pathological conditions (Chapter 5).

In the second part of the work, we investigated the motor control strategies adopted by CNS. Muscle synergies can effectively describe motor control. In muscle synergies model, a muscular activation is the combination of fixed muscle weights and time varying activation signal. Muscle synergies codify movement as a few motor modules, stored in spinal cord, activated by a central command signal. We investigated walking activity, because it is a movement characterized by defined patterns. Despite walking is considered a repetitive movement, it is characterized by a richness of walking patterns, and kinetic and kinematic features may vary from stride to stride. This richness of walking patterns reflects the redundancy of musculoskeletal system and the adaptability to many factors, including the environment, energy consumption, or pathological conditions. To properly record the variability of walking, many gait cycles must be recorded and properly analyzed. In this thesis, we explored the motor control strategies underlying the variability of walking patterns.

We explored two new aspects: the consistency of muscle synergies during a single walking trial (Chapter 8) and the muscle synergies associated to principal and secondary activations (Chapter 9). To this aim, we recorded a 5 minutes walking trial in a group of healthy subjects. Statistical gait analysis was exploited to remove atypical gait, such as turning points, acceleration and deceleration. We observed two groups of synergies: a first group was constituted by five muscle synergies common to all subjects and were related to the execution of the movement. These synergies well matched with the typical phases of gait and were devoted to movement generation and balance. A second group of synergies was constituted by one or two synergies per subject. They were devoted to extra activity during gait, particularly balance control in challenging phases, such as leg control during swing or load acceptance. These synergies were consistent, that is they appeared cyclically in nearly all investigated phases. The consistency of muscle synergies well reflects the movement generation of CPGs. As a secondary work, we investigated muscle synergies associated to principal and secondary activations. Principal activations are those related to movement generation, secondary activations are supplementary activation to improve movement efficacy, such as balance or speed control. We investigated if different walking patterns are generated to different muscle synergies. We compared muscle synergies constitution (i.e. number of muscles), consistency, and flexibility. Our results evidenced a great difference between the muscle synergies of the two motor patterns. Indeed, gait patterns of principal activations are associated to few muscle synergies with many muscles per synergy, great amplitude of activation signal. By contrast, secondary activations are constituted by many synergies with one or two muscles per synergy, and with a very low signal amplitude. Furthermore, muscle synergies of principal activations are very repeatable and flexible during a walking trial, whereas muscle synergies of secondary activations are less flexible and consistent. These results confirm that: (1) muscle synergies well reflect CNS motor control and CPGs activity, and (2) walking is not a simple cyclic movement, hence CNS may adapt according to several factors, including pathological conditions, or environment. Principal activations are effectively controlled by CNS, by adapting a few sets of modules stored in spinal cord. However, muscle synergies also record muscle patterns that may be recruited at the peripheral level and that not reflect CNS control. Hence, this type of synergies should be removed because they may mask the effective CNS control. Finally, we explored muscle synergies in a small group of LBP patients with stiffed-leg walking as a pilot study, before and after rehabilitation (Chapter 10). The methods of analysis previously described (i.e. muscle synergies computation during a prolonged walking trial and principal

activations) were applied to a small group of patients. Our results demonstrated how LBP may affect the recruitment of muscles in generating the movement during gait and that rehabilitation can effectively recover muscle synergies composition. Muscle synergies can be an effective instrument to evaluate gait abnormalities in stiffed-leg walking and they can better address the rehabilitation protocol to recover muscle synergies.

This second part of the thesis also is affected by several limitations. A first limitation is methodological. Non-negative matrix factorization with fixed muscle weights and time-varying activation curves was considered for the analysis. Several studies were carried out to improve the reliability of muscle synergies, such as developing algorithms of time-varying muscle weights vectors or optimization methods. Furthermore, only one walking scheme was investigated, that is normal walking. Future works should be addressed to cover all the variability of human locomotion, by considering speed, obstacles, or direction change.

There are many directions that future works may adopt in the noninvasive analysis of biosignals related to CNS. Novel entropy metrics could be adopted to characterize cerebrovascular system. Furthermore, new methods may be implemented to extract features from NIRS signal. Finally, feature extracted from NIRS and muscle synergies analysis could be adopted to improve design of rehabilitative devices or brain-computer interfaces, in order to reduce disturbing noise and recover as much as possible human abilities.

References

Abásolo, D., R. Hornero, P. Espino, D. Álvarez, and J. Poza. 2006. “Entropy Analysis of the EEG Background Activity in Alzheimer’s Disease Patients.” *Physiological Measurement* 27 (3): 241–53. doi:10.1088/0967-3334/27/3/003.

Abend, W, Emilio Bizzi, and Pietro Morasso. 1982. “Human Arm Trajectory Formation.” *Brain* 105: 331–48.

Acharya, U. Rajendra, Filippo Molinari, S. Vinitha Sree, Subhagata Chattopadhyay, Kwan Hoong Ng, and Jasjit S. Suri. 2012. “Automated Diagnosis of Epileptic EEG Using Entropies.” *Biomed Signal Process Control* 7 (4). Elsevier Ltd: 401–8. doi:10.1016/j.bspc.2011.07.007.

Acharya, U. Rajendra, S. Vinitha Sree, AP Alvin, R Yanti, and JS. Suri. 2012. “Application of Non-Linear and Wavelet Based Features for the Automated Identification of Epileptic EEG Signals.” *International Journal of Neural Systems* 22 (2). World Scientific Publishing Company: 1–14. doi:10.1142/S0129065712500025.

Acharya, U Rajendra, Eric Chern-Pin Chua, Kuang Chua Chua, Lim Choo Min, and Toshiyo Tamura. 2010. “Analysis and Automatic Identification of Sleep Stages Using Higher Order Spectra.” *International Journal of Neural Systems* 20 (6). World Scientific Publishing Company: 509–21. doi:10.1142/S0129065710002589.

Acharya U, Rajendra, Oliver Faust, N Kannathal, TjiLeng Chua, Swamy Laxminarayan, R.A. McCarthy, E.K. Warrington, et al. 2005. “Non-Linear Analysis of EEG Signals at Various Sleep Stages.” *Computer Methods and Programs in Biomedicine* 80 (1). Elsevier: 37–45. doi:10.1016/j.cmpb.2005.06.011.

Agostini, Valentina, Gabriella Balestra, and Marco Knaflitz. 2013. “Segmentation and Classification of Gait Cycles.” *IEEE Transactions on Neural Systems and Rehabilitation Engineering : A Publication of the IEEE Engineering in Medicine and Biology Society* PP (99): 1. doi:10.1109/TNSRE.2013.2291907.

———. 2014. “Segmentation and Classification of Gait Cycles.” *IEEE Trans Neural Syst Rehabil Eng* 22 (5): 946–52. doi:http://dx.doi.org/10.1109/TNSRE.2013.2291907.

Agostini, Valentina, Daria Ganio, Katia Facchin, Luciano Cane, Susana Moreira Carneiro, and Marco Knaflitz. 2014. "Gait Parameters and Muscle Activation Patterns at 3, 6 and 12 Months after Total Hip Arthroplasty." *J Arthroplasty* 29 (6): 1265–72. doi:10.1016/j.arth.2013.12.018.

Agostini, Valentina, and Marco Knaflitz. 2011. "Statistical Gait Analysis." In *Distributed Diagnosis and Home Healthcare*, edited by U. Rajendra Acharya, Filippo Molinari, Toshiyo Tamura, D Subbaram Naidu, and jasjit S Suri, 99–121.

Agostini, Valentina, Francesco Lo Fermo, Giuseppe Massazza, and Marco Knaflitz. 2015. "Does Texting While Walking Really Affect Gait in Young Adults?" *J Neuroeng Rehabil* 12 (1): 86. doi:10.1186/s12984-015-0079-4.

Agostini, Valentina, A. Nascimbeni, A. Gaffuri, P. Imazio, M. G. Benedetti, and M. Knaflitz. 2010. "Normative EMG Activation Patterns of School-Age Children during Gait." *Gait and Posture* 32 (3). Elsevier B.V.: 285–89. doi:10.1016/j.gaitpost.2010.06.024.

Agostini, Valentina, A. Nascimbeni, A. Gaffuri, and Marco Knaflitz. 2015. "Multiple Gait Patterns within the Same Winters Class in Children with Hemiplegic Cerebral Palsy." *Clinical Biomechanics* 30: 908–14. doi:http://dx.doi.org/10.1016/j.clinbiomech.2015.07.010.

Agostini, Valentina, MP M.P. Schieroni, M. Siccardi, M. Campagnoli, and Marco Knaflitz. 2009. "Gait Characteristics of Persons with Chronic Low Back Pain." *Gait Posture* 30 (S1): S28. doi:http://dx.doi.org/10.1016/j.gaitpost.2009.07.011.

Agrillo, Allesandro, Claudio Ungari, Fabio Filiaci, Paolo Priore, and Giorgio Iannetti. 2007. "Ozone Therapy in the Treatment of Avascular Bisphosphonate-Related Jaw Osteonecrosis." *The Journal of Craniofacial Surgery* 18 (5): 1071–75. doi:10.1097/scs.0b013e31857261f.

Akay, Metin, ed. 2000. *Nonlinear Biomedical Signal Processing, Volume 2: Dynamic Analysis and Modeling*. Wiley-IEEE Press.

Ances, B M, D F Wilson, Joel H Greenberg, and J A Detre. 2001. "Dynamic Changes in Cerebral Blood Flow, O2 Tension, and Calculated Cerebral Metabolic Rate of O2 During Functional Activation Using Oxygen Phosphorescence Quenching." *J Cereb Blood Flow Metab* 21 (5): 511–16. doi:10.1097/00004647-200105000-00005.

Aoi, Shinya, and Tetsuro Funato. 2016. "Neuromusculoskeletal Models Based on the Muscle Synergy Hypothesis for the Investigation of Adaptive Motor

Control in Locomotion via Sensory-Motor Coordination." *Neurosci Res* 104. Elsevier Ireland Ltd and Japan Neuroscience Society: 88–95. doi:10.1016/j.neures.2015.11.005.

Arnold, Susanne. 2012. "The Power of Life-Cytochrome c Oxidase Takes Center Stage in Metabolic Control, Cell Signalling and Survival." *Mitochondrion*. doi:10.1016/j.mito.2011.05.003.

Bakker, Akke, Brianne Smith, Philip Ainslie, and Kurt Smith. 2012. "Near-Infrared Spectroscopy." In *Applied Aspects of Ultrasonography in Humans*, 65–88. InTech. doi:10.5772/32493.

Balagué, Federico, Anne F. Mannion, Ferran Pellisé, and Christine Cedraschi. 2012. "Non-Specific Low Back Pain." *The Lancet* 379 (9814): 482–91. doi:10.1016/S0140-6736(11)60610-7.

Bandt, Christoph, and Bernd Pompe. 2002. "Permutation Entropy: A Natural Complexity Measure for Time Series." *Physical Review Letters* 88 (17): 174102. doi:10.1103/PhysRevLett.88.174102.

Barroso, Filipe O., Diego Torricelli, Juan C. Moreno, Julian Taylor, Julio Gomez-Soriano, Elisabeth Bravo-Esteban, Stefano Piazza, Cristina Santos, and José L. Pons. 2014. "Shared Muscle Synergies in Human Walking and Cycling." *J Neurophysiol* 112 (8): 1984–98. doi:10.1152/jn.00220.2014.

Barry, Daniel T. 1992. "Fast Calculation of the Choi-Williams Time-Frequency Distribution." *IEEE Trans Sig Proc* 40 (2): 450–55. doi:10.1109/78.124957.

Basmajian, John V, and Carlo J De Luca. 1985. *Muscles Alive: Their Functions Revealed by Electromyography*. Edited by Williams & Wilkins. Fifth edit. Williams & Wilkins.

Basso Moro, Sara, Silvia Bisconti, Makii Muthalib, Matteo Spezialetti, Simone Cutini, Marco Ferrari, Giuseppe Placidi, and Valentina Quaresima. 2014. "A Semi-Immersive Virtual Reality Incremental Swing Balance Task Activates Prefrontal Cortex: A Functional near-Infrared Spectroscopy Study." *NeuroImage* 85. Elsevier Inc.: 451–60. doi:10.1016/j.neuroimage.2013.05.031.

Bauby, Catherine E., and Arthur D. Kuo. 2000. "Active Control of Lateral Balance in Human Walking." *J Biomech* 33 (11): 1433–40. doi:10.1016/S0021-9290(00)00101-9.

Berniker, Max, Anthony Jarc, Emilio Bizzi, and Matthew C. Tresch. 2009. "Simplified and Effective Motor Control Based on Muscle Synergies to

Exploit Musculoskeletal Dynamics." *Proc Natl Acad Sci U S A* 106 (18): 7601–6. doi:10.1073/pnas.0901512106.

Bernstein, Nikolaj A. 1967. *The Co-Ordination and Regulation of Movements*. First edit. Pergamon Press Ltd.

Berry, Michael W, Murray Browne, Amy N Langville, V Paul Pauca, and Robert J Plemmons. 2007. "Algorithms and Applications for Approximate Nonnegative Matrix Factorization." *Computational Statistics & Data Analysis* 52 (June 2006): 155–73. doi:10.1016/j.csda.2006.11.006.

Bizzi, Emilio, N. Accornero, W. Chapple, and Neville Hogan. 1984. "Posture Control and Trajectory Formation During Arm Movement." *J Neurosci* 4 (11): 2738–44. doi:6502202.

Bizzi, Emilio, and Vincent C. K. Cheung. 2013. "The Neural Origin of Muscle Synergies." *Front Comput Neurosci* 7 (April): 1–6. doi:10.3389/fncom.2013.00051.

Bizzi, Emilio, Vincent C.K. Cheung, Andrea D'Avella, Philippe Saltiel, and Matthew C. Tresch. 2008. "Combining Modules for Movement." *Brain Research Reviews* 57 (1). NIH Public Access: 125–33. doi:10.1016/j.brainresrev.2007.08.004.

Bizzi, Emilio, Andrea D'Avella, Philippe Saltiel, and Matthew C. Tresch. 2002. "Modular Organization of Spinal Motor Systems." *The Neuroscientist* 8 (5): 437–42. doi:10.1177/107385802236969.

Bizzi, Emilio, F. A. Mussa-Ivaldi, and N. Hogan. 1986. "Regulation of Multi-Joint Arm Posture and Movement." *Progress in Brain Research* 64 (C): 345–51. doi:10.1016/S0079-6123(08)63428-7.

Bizzi, Emilio, and Ferdinando A Mussa-Ivaldi. 1998. "Neural Basis of Motor Control and Its Cognitive Implications." *Trends in Cognitive Sciences* 2 (3): 97–102. doi:10.1016/S1364-6613(98)01146-2.

Bizzi, Emilio, Ferdinando A Mussa-ivaldi, and Simon Giszter. 1991. "Computations Underlying the Execution of Movement : A Biological Perspective." *Science* 253 (5017): 287–91.

Bleich, A, M Kother, I Kutz, and A Shalev. 2002. "Guidelines for the Assessment and Professional Intervention with Terror Victims in the Hospital and in the Community." Jerusalem, Israel.

Boas, David A., Clare E. Elwell, Marco Ferrari, and Gentaro Taga. 2014. "Twenty Years of Functional near-Infrared Spectroscopy: Introduction for the Special

Issue." *NeuroImage* 85. Elsevier Inc.: 1–5. doi:10.1016/j.neuroimage.2013.11.033.

Bocci, Velio. 1995. "Ozone Therapy Today." In *12th World Congress of Intern.Ozone Ass.*, 13–27. Lille.

Bocci, Velio, Emma Borrelli, Valter Travagli, and Iacopo Zanardi. 2009. "The Ozone Paradox: Ozone Is a Strong Oxidant as Well as a Medical Drug." *Medicinal Research Reviews* 29 (4): 646–82. doi:10.1002/med.20150.

Bocci, Velis, Iacop Zanardi, and Valter Travagli. 2011. "Ozone: A New Therapeutic Agent in Vascular Diseases." *Am J Cardiovasc Drugs* 11 (2): 73–82. doi:10.2165/11539890-000000000-00000.

Bonato, Paolo, Tommaso D'Alessio, and Marco Knaflitz. 1998. "A Statistical Method for the Measurement of Muscle Activation Intervals from Surface Myoelectric Signal during Gait." *IEEE Trans Biomed Eng* 45 (3): 287–99. doi:10.1109/10.661154.

Borzelli, Daniele, Denise J. Berger, Dinesh K Pai, and Andrea D'Avella. 2013. "Effort Minimization and Synergistic Muscle Recruitment for Three-Dimensional Force Generation." *Front Comput Neurosci* 7 (December): 186. doi:10.3389/fncom.2013.00186.

Broadwater, Laurie, Ashish Pandit, Robert Clements, Sausan Azzam, Jonathan Vadnal, Michael Sulak, V. Wee Yong, Ernest J. Freeman, Roger B. Gregory, and Jennifer McDonough. 2011. "Analysis of the Mitochondrial Proteome in Multiple Sclerosis Cortex." *Biochimica et Biophysica Acta - Molecular Basis of Disease* 1812 (5): 630–41. doi:10.1016/j.bbadis.2011.01.012.

Bunce, Scott C., Meltem Izzetoglu, Kurtulus Izzetoglu, Banu Onaral, and Kambiz Pourrezaei. 2006. "Functional near-Infrared Spectroscopy: An Emerging Neuroimaging Modality." *IEEE Eng Med Biol* 25 (August): 54–62. doi:10.1109/MEMB.2006.1657788.

Buurke, Tom J.W., Claud J.C. Lamoth, Lucas H.V.Der Van Woude, and A. Rob Den Otter. 2016. "Synergistic Structure in the Speed Dependent Modulation of Muscle Activity in Human Walking." *PLoS ONE* 11 (4): 1–19. doi:10.1371/journal.pone.0152784.

Caicedo, Alexander. 2012. "Detection of Cerebral Autoregulation by near-Infrared Spectroscopy in Neonates: Performance Analysis of Measurement Methods." *J Biomed Opt* 17 (11): 117003. doi:10.1117/1.JBO.17.11.117003.

Campbell, Paul, Nadine E. Foster, Elaine Thomas, and Kate M. Dunn. 2013.

"Prognostic Indicators of Low Back Pain in Primary Care: Five-Year Prospective Study." *Journal of Pain* 14 (8). Elsevier Ltd: 873–83. doi:10.1016/j.jpain.2013.03.013.

Canova, D, S Roatta, D Bosone, and G Micieli. 2011. "Inconsistent Detection of Changes in Cerebral Blood Volume by near Infrared Spectroscopy in Standard Clinical Tests." *J Appl Physiol* 110 (6): 1646–55. doi:10.1152/japplphysiol.00003.2011.

Cao, Yuzhen, Lihui Cai, Jiang Wang, Ruofan Wang, Haitao Yu, Yibin Cao, and Jing Liu. 2015. "Characterization of Complexity in the Electroencephalograph Activity of Alzheimer's Disease Based on Fuzzy Entropy." *Chaos* 25 (8). doi:10.1063/1.4929148.

Cappellini, Germana, Yuri P Ivanenko, Richard E Poppele, and Francesco Lacquaniti. 2006. "Motor Patterns in Human Walking and Running." *J Neurophysiol* 95 (6): 3426–37. doi:10.1152/jn.00081.2006.

Castiglioni, Paolo. 2005. "Choi-Williams Distribution." In *Encyclopedia of Biostatistics*. Chichester, UK: John Wiley & Sons, Ltd. doi:10.1002/0470011815.b2a12012.

Chance, Britton, J S Leigh, H Miyake, D S Smith, S Nioka, R Greenfeld, M Finander, K Kaufmann, W Levy, and M Young. 1988. "Comparison of Time-Resolved and -Unresolved Measurements of Deoxyhemoglobin in Brain." *Proc Natl Acad Sci U S A* 85 (14): 4971–75. doi:10.1073/pnas.85.14.4971.

Chance, Britton, M Maris, J Sorge, and M Z Zhang. 1990. "A Phase Modulation System for Dual Wavelenght Difference Spectroscopy of Haemoglobin Deoxygenation in Tissue." *Proc.SPIE* 1204: 481–91.

Chance, Britton, Shoko Nioka, Jane Kent, Kevin McCully, Michael Fountain, Robert Greenfeld, and Gary Holtom. 1988. "Time-Resolved Spectroscopy of Hemoglobin and Myoglobin in Resting and Ischemic Muscle." *Anal Biochem* 174 (2): 698–707. doi:10.1016/0003-2697(88)90076-0.

Chance, Britton, Z Zhuang, C UnAh, C Alter, and L Lipton. 1993. "Cognition-Activated Low-Frequency Modulation of Light Absorption in Human Brain." *Proc Natl Acad Sci U S A* 90 (April): 3770–74. doi:10.1073/pnas.90.8.3770.

Chen, Hui, Bianzhi Xing, Xiuheng Liu, Bingyan Zhan, Jiangqiao Zhou, Hengcheng Zhu, and Zhiyuan Chen. 2008. "Ozone Oxidative Preconditioning Inhibits Inflammation and Apoptosis in a Rat Model of Renal Ischemia/reperfusion Injury." *Eur J Pharmacol* 581 (3): 306–14. doi:10.1016/j.ejphar.2007.11.050.

Chen, Qiuhui, Norden Huang, Sherman Riemenschneider, and Yuesheng Xu. 2006. "A B-Spline Approach for Empirical Mode Decompositions." *Advances in Computational Mathematics* 24 (1–4): 171–95. doi:10.1007/s10444-004-7614-3.

Chen, Weiting, Zhizhong Wang, Hongbo Xie, and Wangxin Yu. 2007. "Characterization of Surface EMG Signal Based on Fuzzy Entropy." *IEEE Trans Neural Syst Rehabil Eng* 15 (1): 266–72. doi:10.1109/TNSRE.2007.897025.

Cheung, Vincent C. K., Andrea D'Avella, Matthew C Tresch, and Emilio Bizzi. 2005. "Central and Sensory Contributions to the Activation and Organization of Muscle Synergies during Natural Motor Behaviors." *J Neurosci* 25 (27): 6419–34. doi:10.1523/JNEUROSCI.4904-04.2005.

Cheung, Vincent C. K., Lamberto Piron, Michela Agostini, Stefano Silvoni, Andrea Turolla, and Emilio Bizzi. 2009. "Stability of Muscle Synergies for Voluntary Actions after Cortical Stroke in Humans." *Proc Natl Acad Sci U S A* 106 (46): 19563–68. doi:10.1073/pnas.0910114106.

Cheung, Vincent C K, Andrea D'Avella, and Emilio Bizzi. 2009. "Adjustments of Motor Pattern for Load Compensation via Modulated Activations of Muscle Synergies during Natural Behaviors." *J Neurophysiol* 101 (3): 1235–57. doi:10.1152/jn.01387.2007.

Choi, Hyung Ill, and William J. Williams. 1989. "Improved Time-Frequency Representation of Multicomponent Signals Using Exponential Kernels." *IEEE Trans Acoust* 37 (6): 862–71. doi:10.1109/ASSP.1989.28057.

Cholewicki, J, SP Silfies, RA Shah, HS Greene, NP Reeves, K Alvi, and B Goldberg. 2005. "Delayed Trunk Muscle Reflex Responses Increase the Risk of Low Back Injuries." *Spine (Phila Pa 1976)* 30 (23): 2614–20.

Chvatal, Stacie A., and Lena H Ting. 2012. "Voluntary and Reactive Recruitment of Locomotor Muscle Synergies during Perturbed Walking." *J Neurosci* 32 (35): 12237–50. doi:10.1523/JNEUROSCI.6344-11.2012.

———. 2013. "Common Muscle Synergies for Balance and Walking." *Front Comput Neurosci* 7 (May): 48. doi:10.3389/fncom.2013.00048.

Chvatal, Stacie A., Gelsy Torres-Oviedo, Seyed A. Safavynia, and Lena H Ting. 2011. "Common Muscle Synergies for Control of Center of Mass and Force in Nonstepping and Stepping Postural Behaviors." *J Neurophysiol* 106 (2): 999–1015. doi:10.1152/jn.00549.2010.

Cichocki, Andrzej, Rafal Zdunek, Anh Huy Phan, and Shun-Ichi Amari. 2009. *Nonnegative Matrix and Tensor Factorizations*. First Edit. John Wiley & Sons, Ltd.

Clark, David J., Lena H Ting, Felix E Zajac, Richard R. Neptune, and Steven A. Kautz. 2010. "Merging of Healthy Motor Modules Predicts Reduced Locomotor Performance and Muscle Coordination Complexity Post-Stroke." *J Neurophysiol* 103 (2): 844–57. doi:10.1152/jn.00825.2009.

Clark, David J., Lena H Ting, Felix E Zajac, Richard R. Neptune, Steven A. Kautz, Richard R. Neptune, and Steven A. Kautz. 2009. "Merging of Healthy Motor Modules Predicts Reduced Locomotor Performance and Muscle Coordination Complexity Post-Stroke." *J Neurophysiol* 103 (2): 844–57. doi:10.1152/jn.00825.2009.

Clarkson, Hazel M. 2012. *Musculoskeletal Assessment: Joint Motion and Muscle Testing*. 3 Edition. Wolters Kluwer.

Clavo, Bernardino, Juan L. Pérez, Laura López, Gerardo Suárez, Marta Lloret, Victor Rodríguez, David Macías, et al. 2004. "Ozone Therapy for Tumor Oxygenation: A Pilot Study." *Evidence-Based Complementary and Alternative Medicine* 1 (1): 93–98. doi:10.1093/ecam/neh009.

Clavo, Bernardino, Juan L Pérez, Laura López, Gerardo Suárez, Marta Lloret, Victor Rodríguez, David Macías, et al. 2003. "Effect of Ozone Therapy on Muscle Oxygenation." *Journal of Alternative and Complementary Medicine (New York, N.Y.)* 9 (2): 251–56. doi:10.1089/10755530360623365.

Comon, Pierre, and Christian Jutten. 2010. *Handbook of Blind Source Separation. Independent Component Analysis and Applications*. First Edit. Academic Press.

Coscia, Martina, Vito Monaco, Chiara Martelloni, Bruno Rossi, Carmelo Chisari, and Silvestro Micera. 2015. "Muscle Synergies and Spinal Maps Are Sensitive to the Asymmetry Induced by a Unilateral Stroke." *J Neuroeng Rehabil* 12 (1). ??? 1–16. doi:10.1186/s12984-015-0031-7.

CREST. 2003. *The Management of Post Traumatic Stress Disorder In Adults*. Edited by Social Services and Public Safety. Belfast.

Curtis, G. Lenox. 1902. "The Influence of Electric Ozonation upon Disease." *New York Medical Journal* 75: 91–94.

D'Avella, Andrea, and Emilio Bizzi. 1998. "Low Dimensionality of Supraspinally Induced Force Fields." *Proc. Natl. Acad. Sci. USA* 95 (13): 7711–14.

doi:10.1073/pnas.95.13.7711.

———. 2005. “Shared and Specific Muscle Synergies in Natural Motor Behaviors.” *Proc Natl Acad Sci U S A* 102 (8): 3076–81. doi:10.1073/pnas.0500199102.

D’Avella, Andrea, Laure Fernandez, Alessandro Portone, and Francesco Lacquaniti. 2008. “Modulation of Phasic and Tonic Muscle Synergies with Reaching Direction and Speed.” *J Neurophysiol* 100 (3): 1433–54. doi:10.1152/jn.01377.2007.

D’Avella, Andrea, and Francesco Lacquaniti. 2013. “Control of Reaching Movements by Muscle Synergy Combinations.” *Front Comput Neurosci* 7 (April): 1–7. doi:10.3389/fncom.2013.00042.

d’Avella, Andrea, Philippe Saltiel, and Emilio Bizzi. 2003. “Combinations of Muscle Synergies in the Construction of a Natural Motor Behavior.” *Nature Neuroscience* 6 (3): 300–308. doi:10.1038/nn1010.

Dake, Michael D. 2012. “Chronic Cerebrospinal Venous Insufficiency and Multiple Sclerosis: History and Background.” *Tech Vasc Interv Radiol* 15 (2): 94–100. doi:10.1053/j.tvir.2012.02.002.

Danner, Simon M., Ursula S. Hofstoetter, Brigitta Freundl, Heinrich Binder, Winfried Mayr, Frank Rattay, and Karen Minassian. 2015. “Human Spinal Locomotor Control Is Based on Flexibly Organized Burst Generators.” *Brain* 138 (October): 577–88. doi:10.1093/brain/awu372.

Das, Kumuda C, and Harish Muniyappa. 2013. “Age-Dependent Mitochondrial Energy Dynamics in the Mice Heart: Role of Superoxide Dismutase-2.” *Exp Gerontol* 48 (9): 947–59. doi:10.1016/j.exger.2013.06.002.

Davies, David J., Zhangjie Su, Michael T. Clancy, Samuel J. E. Lucas, Hamid Dehghani, Ann Logan, and Antonio Belli. 2015. “Near-Infrared Spectroscopy in the Monitoring of Adult Traumatic Brain Injury: A Review.” *Journal of Neurotrauma* 44 (0): 150417112024001. doi:10.1089/neu.2014.3748.

Davis, Brian L, and Christopher L Vaughan. 1993. “Phasic Behavior of EMG Signals during Gait: Use Ofmultivariate Statistics.” *J Electromyogr Kinesiol* 3 (1): 51–60. doi:doi.org/10.1016/1050-6411(93)90023-P.

De Groote, Friedl, Ilse Jonkers, and Jacques Duysens. 2014. “Task Constraints and Minimization of Muscle Effort Result in a Small Number of Muscle Synergies during Gait.” *Front Comput Neurosci* 8 (September): 1–11. doi:10.3389/fncom.2014.00115.

De Luca, A., and S. Termini. 1972. “A Definition of a Nonprobabilistic Entropy in the Setting of Fuzzy Sets Theory.” *Information and Control* 20 (4): 301–12. doi:10.1016/S0019-9958(72)90199-4.

de Rugy, Aymar, Gerald E. Loeb, and Timothy J. Carroll. 2013. “Are Muscle Synergies Useful for Neural Control?” *Front Comput Neurosci* 7 (March): 1–13. doi:10.3389/fncom.2013.00019.

Debouverie, M., S. Pittion-Vouyovitch, S. Louis, and F. Guillemin. 2008. “Natural History of Multiple Sclerosis in a Population-Based Cohort.” *European Journal of Neurology* 15 (9): 916–21. doi:10.1111/j.1468-1331.2008.02241.x.

Delis, Ioannis, Enrico Chiovetto, and Bastien Berret. 2010. “On the Origins of Modularity in Motor Control.” *J Neurosci* 30 (22): 7451–52. doi:10.1523/JNEUROSCI.1562-10.2010.

Delpy, D. T., and M. Cope. 1997. “Quantification in Tissue near-Infrared Spectroscopy.” *Philos Trans R Soc Lond B Biol Sci* 352 (1354): 649–59. doi:10.1098/rstb.1997.0046.

Derogatis, L R, and P A Cleary. 1977. “Factorial Invariance across Gender for the Primary Symptom Dimensions of the SCL-90.” *Br J Soc Clin Psychol* 16 (4): 347–56. doi:10.1111/j.2044-8260.1977.tb00241.x.

Di Filippo, C., R. Marfella, P. Capodanno, F. Ferraraccio, L. Coppola, M. Luongo, L. Mascolo, et al. 2008. “Acute Oxygen-Ozone Administration to Rats Protects the Heart from Ischemia Reperfusion Infarct.” *Inflammation Research* 57 (10): 445–49. doi:10.1007/s00011-008-7237-0.

Di Nardo, Francesco, Giacomo Ghetti, and Sandro Fioretti. 2013. “Assessment of the Activation Modalities of Gastrocnemius Lateralis and Tibialis Anterior during Gait: A Statistical Analysis.” *J Electromyogr Kinesiol* 23 (6). Elsevier Ltd: 1428–33. doi:10.1016/j.jelekin.2013.05.011.

Di Nardo, Francesco, Alessandro Mengarelli, Elvira Maranesi, Laura Burattini, and Sandro Fioretti. 2015. “Assessment of the Ankle Muscle Co-Contraction during Normal Gait: A Surface Electromyography Study.” *J Electromyogr Kinesiol* 25 (2). Elsevier Ltd: 347–54. doi:10.1016/j.jelekin.2014.10.016.

Di Nardo, Francesco, Alessandro Mengarelli, Annachiara Strazza, Valentina Agostini, Marco Knaflitz, Laura Burattini, and Sandro Fioretti. 2017. “A New Parameter for Quantifying the Variability of Surface Electromyographic Signals during Gait: The Occurrence Frequency.” *J Electromyogr Kinesiol* 36. Elsevier Ltd: 25–33. doi:10.1016/j.jelekin.2017.06.006.

Di Zenzo, Silvano, Luigi Cinque, and Stefano Levialdi. 1998. “Image Thresholding Using Fuzzy Entropies.” *IEEE Transactions on Systems, Man, and Cybernetics, Part B: Cybernetics* 28 (1): 15–23. doi:10.1109/3477.658574.

Dimitrijevic, Milan R, Yuri Gerasimenko, and Michaela M Pinter. 1998. “Evidence for a Spinal Central Pattern Generator in Humans.” *Ann N Y Acad Sci* Nov 16 (860): 360–76. doi:10.1111/j.1749-6632.1998.tb09062.x.

Drew, Trevor, John Kalaska, and Nedialko Krouchev. 2008. “Muscle Synergies during Locomotion in the Cat: A Model for Motor Cortex Control.” *J Physiol* 586 (5): 1239–45. doi:10.1113/jphysiol.2007.146605.

Duran, Nicholas D., Rick Dale, Christopher T. Kello, Chris N.H. Street, and Daniel C. Richardson. 2013. “Exploring the Movement Dynamics of Deception.” *Frontiers in Psychology* 4 (MAR): 1–16. doi:10.3389/fpsyg.2013.00140.

Dworkin, Mark. 2013. *EMDR and the Relational Imperative: The Therapeutic Relationship in EMDR Treatment*. Routledge.

El Barzouhi, Abdelilah, Carmen L A M Vleggeert-Lankamp, Bas F. Van Der Kallen, Geert J. Lycklama À Nijeholt, Wilbert B. Van Den Hout, Bart W. Koes, and Wilco C. Peul. 2014. “Back Pain’s Association with Vertebral End-Plate Signal Changes in Sciatica.” *Spine Journal* 14 (2): 225–33. doi:10.1016/j.spinee.2013.08.058.

el Ouardighi, A., A. el Akadi, and D. Aboutajdine. 2007. “Feature Selection on Supervised Classification Using Wilks Lambda Statistic.” In *2007 International Symposium on Computational Intelligence and Intelligent Informatics*, 51–55. IEEE. doi:10.1109/ISCIII.2007.367361.

Elwell, C. E., M. Cope, A. D. Edwards, J. S. Wyatt, D. T. Delpy, and E. O R Reynolds. 1994. “Quantification of Adult Cerebral Hemodynamics by near-Infrared Spectroscopy.” *J Appl Physiol* 77 (6): 2753–60.

Engelhard, Iris M., Marcel A. van den Hout, Wilco C. Janssen, and Jorinde van der Beek. 2010. “Eye Movements Reduce Vividness and Emotionality of ‘ Flashforwards.’” *Behaviour Research and Therapy* 48 (5). Elsevier Ltd: 442–47. doi:10.1016/j.brat.2010.01.003.

Fairbank JC, Couper J, Davies JB, O’Brien JP. 1980. “The Oswestry Low Back Pain Disability Questionnaire.” *Physiotherapy* 66 (8): 271–73. https://www.ncbi.nlm.nih.gov/pubmed/6450426.

Faust, O, U R Acharya, F Molinari, S Chattopadhyay, and T Tamura. 2012. “Linear and Non-Linear Analysis of Cardiac Health in Diabetic Subjects.” *Biomed*

Signal Process Control 7 (3): 295–302. doi:10.1016/j.bspc.2011.06.002.

Ferlazzo, Edoardo, Nadia Mammone, Vittoria Cianci, Sara Gasparini, Antonio Gambardella, Angelo Labate, Maria Adele Latella, et al. 2014. "Permutation Entropy of Scalp EEG: A Tool to Investigate Epilepsies. Suggestions from Absence Epilepsies." *Clinical Neurophysiology* 125 (1). International Federation of Clinical Neurophysiology: 13–20. doi:10.1016/j.clinph.2013.06.023.

Fernandez I., Maxfield L., Shapiro F. 2009. "Eye Movement Desensitization and Reprocessing (EMDR)." In *Psicotraumatologia. Fondamenti E Strumenti Operativi*, edited by Michele Giannantonio, 370. Milano: Centro Scientifico Editore.

Ferrari, Marco, Karl H Norris, and Michael G Sowa. 2012. "Medical near Infrared Spectroscopy 35 Years after the Discovery." *J Near Infrared Spec* 20: vii–ix. doi:10.1255/jnirs.xxx.

Flash, Tamar, and Terrence J Sejnowski. 2001. "Computational Approaches to Motor Control." *Curr Opin Neurobiol* 11 (6): 655–62.

Flora, SJ. 2007. "Role of Free Radicals and Antioxidants in Health and Disease." *Cell Mol Biol* 53 (1): 1–2. https://www.ncbi.nlm.nih.gov/pubmed/17535753.

Forssberg, H., S. Grillner, and J. Halbertsma. 1980. "The Locomotion of the Low Spinal Cat. I. Coordination within a Hindlimb." *Acta Physiol Scand* 108 (3): 269–81. doi:10.1111/j.1748-1716.1980.tb06534.x.

Fox, E.J., Tester N.J., S.A. Kautz, D.R. Howland, David J. Clark, and C. Garvan. 2013. "Modular Control of Varied Locomotor Tasks in Children with Incomplete Spinal Cord Injuries." *J Neurophysiol* 110 (6): 1415–25. doi:10.1152/jn.00676.2012.

Frère, Julien, and François Hug. 2012. "Between-Subject Variability of Muscle Synergies during a Complex Motor Skill." *Front Comput Neurosci* 6 (December): 99. doi:10.3389/fncom.2012.00099.

Funahashi, Shintaro, and Jorge Mario Andreau. 2013. "Prefrontal Cortex and Neural Mechanisms of Executive Function." *J Physiol* 107 (6). Elsevier Ltd: 471–82. doi:10.1016/j.jphysparis.2013.05.001.

Fuster, Joaquín. 2008. *The Prefrontal Cortex*. Fourth Edi. San Diego, CA: Academic Press. https://www.elsevier.com/books/the-prefrontal-cortex/fuster/978-0-12-373644-4.

Fuster, Joaquín M. 2001. "The Prefrontal Cortex - An Update: Time Is of the

Essence." *Neuron* 30 (2): 319–33. doi:10.1016/S0896-6273(01)00285-9.

Gaciasa, Mar, and Patrizia Casaccia. 2013. "Promoting Return of Function in Multiple Sclerosis: An Integrated Approach." *Mult Scler Relat Disord* 2 (4): 312–26. doi:doi:10.1016/j.msard.2013.04.002.

Geng, Shujuan, Weidong Zhou, Qi Yuan, Dongmei Cai, and Yanjun Zeng. 2013. "EEG Non-Linear Feature Extraction Using Correlation Dimension and Hurst Exponent." *http://dx.doi.org/10.1179/1743132811Y.0000000041*. Taylor & Francis.

Gersten, Alexander. 2015. "Probing Brain Oxygenation with Near Infrared Spectroscopy (NIRS) — The Role of Carbon Dioxide and Blood Pressure." *Infrared Spectroscopy - Anharmonicity of Biomolecules, Crosslinking of Biopolymers, Food Quality and Medical Applications*. doi:10.5772/59113.

Giszter, Simon F. 2015. "Motor Primitives-New Data and Future Questions." *Curr Opin Neurobiol* 33. Elsevier Ltd: 156–65. doi:10.1016/j.conb.2015.04.004.

Giszter, Simon F., and Corey B. Hart. 2013. "Motor Primitives and Synergies in the Spinal Cord and after Injury-the Current State of Play." *Ann N Y Acad Sci* 1279 (1): 114–26. doi:10.1111/nyas.12065.

Giszter, Simon F., Ferdinando a. Mussa-Ivaldi, and Emilio Bizzi. 1993. "Convergent Force Fields Organized in the Frog's Spinal Cord." *J Neurosci* 13 (2): 467–91.

Giunta, R., A. Coppola, C. Luongo, A. Sammartino, S. Guastafierro, A. Grassia, L. Giunta, L. Mascolo, A. Tirelli, and L. Coppola. 2001. "Ozonized Autohemotransfusion Improves Hemorheological Parameters and Oxygen Delivery to Tissues in Patients with Peripheral Occlusive Arterial Disease." *Annals of Hematology* 80 (12): 745–48. doi:10.1007/s002770100377.

Giustetto, Pierangela, William Liboni, Ornella Mana, Gianni Allais, Chiara Benedetto, and Filippo Molinari. 2010. "Joint Metabonomic and Instrumental Analysis for the Classification of Migraine Patients with 677-MTHFR Mutations." *Open Med Inform J* 4: 23–30. doi:10.2174/1874431101004020023.

Gizzi, Leonardo, Jørgen Feldbæk Nielsen, Francesco Felici, Juan C. Moreno, José L. Pons, and Dario Farina. 2012. "Motor Modules in Robot-Aided Walking." *J Neuroeng Rehabil* 9: 76. doi:10.1186/1743-0003-9-76.

Gizzi, Leonardo, Silvia Muceli, Frank Petzke, Deborah Falla, D Farina, and UG Kersting. 2015. "Experimental Muscle Pain Impairs the Synergistic Modular

Control of Neck Muscles." Edited by François Hug. *PLoS ONE* 10 (9). Public Library of Science: e0137844. doi:10.1371/journal.pone.0137844.

Gizzi, Leonardo, Jørgen Feldbæk Nielsen, Francesco Felici, Yuri P Ivanenko, and Dario Farina. 2011. "Impulses of Activation but Not Motor Modules Are Preserved in the Locomotion of Subacute Stroke Patients." *J Neurophysiol* 106 (1): 202–10. doi:10.1152/jn.00727.2010.

Godlove, Jason, Tanuj Gulati, Ben Dichter, Edward Chang, and Karunesh Ganguly. 2016. "Muscle Synergies after Stroke Are Correlated with Perilesional High Gamma." *Ann Clin Transl Neurol* 3 (12): 956–61. doi:10.1002/acn3.368.

Gonzalez-Vargas, Jose, Massimo Sartori, Strahinja Dosen, Diego Torricelli, Jose L. Pons, Dario Farina, Yun Wang, et al. 2015. "A Predictive Model of Muscle Excitations Based on Muscle Modularity for a Large Repertoire of Human Locomotion Conditions." *Front Comput Neurosci* 9 (October). Springer Berlin Heidelberg: e0140161. doi:10.3389/fncom.2015.00121.

Grasso, R, L Bianchi, and Francesco Lacquaniti. 1998. "Motor Patterns for Human Gait: Backward versus Forward Locomotion." *J Neurophysiol* 80 (4): 1868–85.

Grasso, R, M Zago, and F Lacquaniti. 2000. "Interactions between Posture and Locomotion: Motor Patterns in Humans Walking with Bent Posture versus Erect Posture." *J Neurophysiol* 83 (1): 288–300.

Greenwald, Ricky. 1999. *Eye Movement Desensitization Reprocessing (EMDR) in Child and Adolescent Psychotherapy*. Jason Aronson, Inc.

Grillner, Sten. 1981. "Control of Locomotion in Bipeds, Tetrapods, and Fish." In *Handbook of Physiology Vol. 2 Part 2*, edited by V.B. Brooks, 1179–1236. American Physiological Society. doi:10.1002/cphy.cp010226.

Gsell, Willy, Christelle De Sadeleer, Yannick Marchalant, Eric T. MacKenzie, Pascale Schumann, and François Dauphin. 2000. "The Use of Cerebral Blood Flow as an Index of Neuronal Activity in Functional Neuroimaging: Experimental and Pathophysiological Considerations." *J Chem Neuroanat* 20 (3–4): 215–24. doi:10.1016/S0891-0618(00)00095-8.

Gunter, Raymond W., and Glen E. Bodner. 2009. "EMDR Works . . . But How? Recent Progress in the Search for Treatment Mechanisms." *Journal of EMDR Practice and Research* 3 (3): 161–68. doi:10.1891/1933-3196.3.3.161.

Guyton, Arthur, and John Hall. 2005. *Textbook of Medical Physiology*. Elsevier. https://www.elsevier.com/books/textbook-of-medical-physiology/hall/978-0-

7216-0240-0.

Haghpanah, Seyyed Arash, Farzam Farahmand, and Hassan Zohoor. 2017. "Modular Neuromuscular Control of Human Locomotion by Central Pattern Generator." *J Biomech* 0 (0). Elsevier: 2157–63. doi:10.1016/j.jbiomech.2017.01.020.

Hagio, Shota, Mizuho Fukuda, and Motoki Kouzaki. 2015. "Identification of Muscle Synergies Associated with Gait Transition in Humans." *Front Neurosci* 9 (February): 1–12. doi:10.3389/fnhum.2015.00048.

Han, Jiawei, and Micheline Kamber. 2007. *Data Mining: Concepts and Techniques*. Edited by Jim Gray. *Intelligent Systems Reference Library*. Second Edi. Vol. 12. Elsevier Science. doi:10.1007/978-3-642-19721-5.

Hart, Corey B, and Simon F Giszter. 2010. "A Neural Basis for Motor Primitives in the Spinal Cord." *J Neurosci* 30 (4): 1322–36. doi:10.1523/JNEUROSCI.5894-08.2010.

Hawker, Gillian A., Samra Mian, Tetyana Kendzerska, and Melissa French. 2011. "Measures of Adult Pain: Visual Analog Scale for Pain (VAS Pain), Numeric Rating Scale for Pain (NRS Pain), McGill Pain Questionnaire (MPQ), Short-Form McGill Pain Questionnaire (SF-MPQ), Chronic Pain Grade Scale (CPGS), Short Form-36 Bodily Pain Scale (SF." *Arthritis Care and Research* 63 (SUPPL. 11): 240–52. doi:10.1002/acr.20543.

Hayes, Heather B., Stacie A. Chvatal, Margaret A. French, Lena H Ting, and Randy D. Trumbower. 2014. "Neuromuscular Constraints on Muscle Coordination during Overground Walking in Persons with Chronic Incomplete Spinal Cord Injury." *Clin Neurophysiol* 125 (10). International Federation of Clinical Neurophysiology: 2024–35. doi:10.1016/j.clinph.2014.02.001.

He, Chao, and Xuanpeng Ma. 2015. "Distal Fallopian Tube Recanalization Using Ozone Treatment: A Clinical Study in Two Hundred Tubal Obstruction Chinese Patients." *International Journal of Clinical and Experimental Medicine* 8 (2): 2958–61.

Henriques, Teresa, Hernâni Gonçalves, Luís Antunes, Mara Matias, João Bernardes, and Cristina Costa-Santos. 2013. "Entropy and Compression: Two Measures of Complexity." *Journal of Evaluation in Clinical Practice* 19 (6): 1101–6. doi:10.1111/jep.12068.

Herkt, Deborah, Visal Tumani, Georg Grön, Thomas Kammer, Arne Hofmann, and Birgit Abler. 2014. "Facilitating Access to Emotions: Neural Signature of EMDR Stimulation." *PLoS ONE* 9 (8): e106350.

doi:10.1371/journal.pone.0106350.

Herndon, CM, KS Zoberi, and BJ Gardner. 2015. “Common Questions about Chronic Low Back Pain.” *American Family Physician* 91 (10): 708–14. http://www.scopus.com/inward/record.url?eid=2-s2.0-84929254686&partnerID=tZOtx3y1.

Horowitz, M, N Wilner, and W Alvarez. 1979. “Impact of Event Scale: A Measure of Subjective Stress.” *Psychosomatic Medicine* 41 (3): 209–18. doi:10.1097/00006842-197905000-00004.

Hoshi, Yoko, and M Tamura. 1993a. “Dynamic Multichannel near-Infrared Optical Imaging of Human Brain Activity.” *J Appl Physiol* 75 (8750–7587 LA–eng PT–Journal Article RN–0 (Hemoglobins) SB–IM): 1842–46. http://www.ncbi.nlm.nih.gov/entrez/query.fcgi?db=pubmed&cmd=Retrieve&dopt=AbstractPlus&list_uids=8282640.

Hoshi, Yoko, and Mamoru Tamura. 1993b. “Detection of Dynamic Changes in Cerebral Oxygenation Coupled to Neuronal Function during Mental Work in Man.” *Neuroscience Letters* 150 (1): 5–8. doi:10.1016/0304-3940(93)90094-2.

Huang, Norden E, Zheng Shen, Steven R Long, Manli Wu Wu, Hsing H Shih, Quanan Zheng, Nai-Chyuan Yen, Chao Chi Tung, and Henry H Liu. 1998. “The Empirical Mode Decomposition and the Hilbert Spectrum for Nonlinear and Non-Stationary Time Series Analysis.” *Proc. R. Soc. Lond. A* 454: 903–95.

Huang, Norden E, and Zhaohua Wu. 2008. “A Review on Hilbert-Huang Transform : Method and Its Applications.” *Reviews of Geophysics* 46 (2007): 1–23. doi:10.1029/2007RG000228.1.INTRODUCTION.

Huang, Yun Peng, Sjoerd M. Bruijn, Jian Hua Lin, Onno G. Meijer, Wen Hua Wu, Hamid Abbasi-Bafghi, Xiao Cong Lin, and Jaap H. Van Dieën. 2011. “Gait Adaptations in Low Back Pain Patients with Lumbar Disc Herniation: Trunk Coordination and Arm Swing.” *European Spine Journal* 20 (3): 491–99. doi:10.1007/s00586-010-1639-8.

Hug, François, Nicolas a. Turpin, Sylvain Dorel, and Arnaud Guével. 2012. “Smoothing of Electromyographic Signals Can Influence the Number of Extracted Muscle Synergies.” *Clin Neurophysiol* 123 (9): 1895–96. doi:10.1016/j.clinph.2012.01.015.

Hurst, H E. 1951. “Long-Term Storage Capacity of Reservoirs.” *Trans. Amer. Soc. Civil Eng.* 116: 770–808.

Ivanenko, Yuri P, Renato Grasso, Myrka Zago, Marco Molinari, Giorgio Scivoletto, Vincenzo Castellano, Velio Macellari, and Francesco Lacquaniti. 2003. “Temporal Components of the Motor Patterns Expressed by the Human Spinal Cord Reflect Foot Kinematics.” *J Neurophysiol* 90 (5): 3555–65. doi:10.1152/jn.00223.2003.

Ivanenko, Yuri P, R E Poppele, and F Lacquaniti. 2006a. “Spinal Cord Maps of Spatiotemporal Alpha-Motoneuron Activation in Humans Walking at Different Speeds.” *J Neurophysiol* 95 (2): 602–18. doi:10.1152/jn.00767.2005.

Ivanenko, Yuri P, Richard E Poppele, and Francesco Lacquaniti. 2004. “Five Basic Muscle Activation Patterns Account for Muscle Activity during Human Locomotion.” *J Physiol* 556: 267–82. doi:10.1113/jphysiol.2003.057174.

———. 2006b. “Motor Control Programs and Walking.” *Neuroscientist* 12 (4): 339–48. doi:10.1177/1073858406287987.

Jacobs, Jesse V, Sharon M Henry, Stephanie L Jones, Juvena R Hitt, and Janice Y Bunn. 2011. “A History of Low Back Pain Associates with Altered Electromyographic Activation Patterns in Response to Perturbations of Standing Balance.” *J Neurophysiol* 106 (5): 2506–14. doi:10.1152/jn.00296.2011.

Jaynes, E. T. 1957. “Information Theory and Statistical Mechanics.” *The Physical Review* 106 (4): 620–30.

Ji, Lizhen, Peng Li, Ke Li, Xinpei Wang, and Changchun Liu. 2015. “Analysis of Short-Term Heart Rate and Diastolic Period Variability Using a Refined Fuzzy Entropy Method.” *BioMedical Engineering OnLine* 14 (1): 64. doi:10.1186/s12938-015-0063-z.

Jobsis, F. 1977. “Noninvasive, Infrared Monitoring of Cerebral and Myocardial Oxygen Sufficiency and Circulatory Parameters.” *Science* 198 (4323): 1264–67. doi:10.1126/science.929199.

Jones, Luke D., Hemant Pandit, and Christopher Lavy. 2014. “Back Pain in the Elderly: A Review.” *Maturitas* 78 (4). Elsevier Ireland Ltd: 258–62. doi:10.1016/j.maturitas.2014.05.004.

Jonsdottir, Johanna, Tiziana Lencioni, Elisa Gervasoni, Alessandro Crippa, Marco Rovaris, Maurizio Ferrarin, A Montesano, and Davide Cattaneo. 2015. “Influence of Gait Rehabilitation on Muscle Synergies and Their Activation Profiles in Persons Affected by Multiple Sclerosis.” *Gait Posture* 42S (2015). Elsevier B.V.: S21.

Kannathal, N., U. Rajendra Acharya, C.M. Lim, and P.K. Sadasivan. 2005. "Characterization of EEG—A Comparative Study." *Computer Methods and Programs in Biomedicine* 80 (1): 17–23. doi:10.1016/j.cmpb.2005.06.005.

Kato, T, A Kamei, S Takashima, and T Ozaki. 1993. "Human Visual Cortical Function during Photic Stimulation Monitoring by Means of near-Infrared Spectroscopy." *J Cereb Blood Flow Metab* 13 (3): 516–20. doi:10.1038/jcbfm.1993.66.

Kieliba, Paulina, Peppino Tropea, E. Pirondini, Martina Coscia, Silvestro Micera, and Fiorenzo Artoni. 2018. "How Are Muscle Synergies Affected by Electromyography Pre-Processing?" *IEEE Transactions on Neural Systems and Rehabilitation Engineering* 26 (4): 882–93. doi:10.1109/TNSRE.2018.2810859.

Kim, Yushin, Thomas C. Bulea, and Diane L. Damiano. 2016. "Novel Methods to Enhance Precision and Reliability in Muscle Synergy Identification during Walking." *Front Neurosci* 10 (September): 1–12. doi:10.3389/fnhum.2016.00455.

Krogt, Marjolein Van Der, Laura Oudenhoven, Annemieke Buizer, Annet Dallmeijer, Nadia Dominici, and Jaap Harlaar. 2016. "The Effect of EMG Processing Choices on Muscle Synergies before and after BoNT-A Treatment in Cerebral Palsy." *Gait & Posture* 49S. Elsevier B.V.: 31. doi:10.1016/j.gaitpost.2016.07.095.

Kshirsagar, Anant M. 2004. "Wilks's Lambda Criterion." In *Encyclopedia of Statistical Sciences*, 1–5. John Wiley & Sons, Inc. doi:10.1002/0471667196.ess1388.pub2.

Kumar, U., V. Kumar, and J. N. Kapur. 1986. "Normalized Measures of Entropy." *International Journal of General Systems* 12 (1): 55–69. doi:10.1080/03081078608934927.

Lacquaniti, Francesco, Yuri P Ivanenko, and Myrka Zago. 2012. "Patterned Control of Human Locomotion." *J Physiol* 590: 2189–99. doi:10.1113/jphysiol.2011.215137.

Lamoth, Claudine J.C., Andreas Daffertshofer, Onno G. Meijer, and Peter J. Beek. 2006. "How Do Persons with Chronic Low Back Pain Speed up and Slow Down?" *Gait Posture* 23 (2): 230–39. doi:http://dx.doi.org/10.1016/j.gaitpost.2005.02.006.

Latash, Mark L. 2012. "The Bliss of Motor Abundance." *Exp Brain Res* 217 (1): 1–5. doi:10.1007/s00221-012-3000-4.

Latash, Mark L, John P Scholz, and Gregor Schöner. 2007. “Toward a New Theory of Motor Synergies.” *Motor Control* 11: 276–308. doi:10.1017/CBO9781107415324.004.

Latash, Mark, and Vladimir Zatsiorsky. 2015. *Biomechanics and Motor Control*. First Edit. Elsevier. doi:10.1016/b978-0-12-800384-8.00009-0.

Lee, Christopher William, and Pim Cuijpers. 2013. “A Meta-Analysis of the Contribution of Eye Movements in Processing Emotional Memories.” *Journal of Behavior Therapy and Experimental Psychiatry* 44 (2). Elsevier Ltd: 231–39. doi:10.1016/j.jbtep.2012.11.001.

Lee, Daniel D, and H Sebastian Seung. 1999. “Learning the Parts of Objects by Non-Negative Matrix Factorization.” *Nature* 401 (6755): 788–91. doi:10.1038/44565.

———. 2001. “Algorithms for Non-Negative Matrix Factorization.” *Adv Neural Inf Process Syst*, no. 1: 556–62. doi:10.1109/IJCNN.2008.4634046.

Lemon, Roger N., and James Griffiths. 2005. “Comparing the Function of the Corticospinal System in Different Species: Organizational Differences for Motor Specialization?” *Muscle and Nerve* 32 (3): 261–79. doi:10.1002/mus.20333.

Lencioni, Tiziana, Johanna Jonsdottir, Davide Cattaneo, Alessandro Crippa, Elisa Gervasoni, Marco Rovaris, Emilio Bizzi, and Maurizio Ferrarin. 2016. “Are Modular Activations Altered in Lower Limb Muscles of Persons with Multiple Sclerosis during Walking? Evidence from Muscle Synergies and Biomechanical Analysis.” *Front Neurosci* 10 (December): 1–14. doi:10.3389/fnhum.2016.00620.

León-Carrion, José, Jesús Damas-López, Juan Francisco Martín-Rodríguez, José Maria Domínguez-Roldán, Francisco Murillo-Cabezas, Juan Manuel Barroso y Martin, and M. Rosario Domínguez. 2008. “The Hemodynamics of Cognitive Control: The Level of Concentration of Oxygenated Hemoglobin in the Superior Prefrontal Cortex Varies as a Function of Performance in a Modified Stroop Task.” *Behav Brain Res* 193 (2): 248–56. doi:10.1016/j.bbr.2008.06.013.

Li, Lin Z., Loet Leydesdorff, Shoko Nioka, Nannan Sun, and Eugene Garfield. 2014. “Citation Analysis of the Scientific Publications of Britton Chance in ISI Citation Indexes.” *J Innov Opt Health Sci* 7 (2): 1430003. doi:10.1142/S1793545814300031.

Li, Xiaoli, Gaoxian Ouyang, and Douglas A. Richards. 2007. “Predictability

Analysis of Absence Seizures with Permutation Entropy." *Epilepsy Research* 77 (1): 70–74. doi:10.1016/j.eplepsyres.2007.08.002.

Liang, Zhenhu, Yinghua Wang, Xue Sun, Duan Li, Logan J. Voss, Jamie W. Sleigh, Satoshi Hagihira, and Xiaoli Li. 2015. "EEG Entropy Measures in Anesthesia." *Frontiers in Computational Neuroscience* 9 (February): 1–17. doi:10.3389/fncom.2015.00016.

Liboni, W, F Molinari, G Allais, O Mana, E Negri, G Grippi, C Benedetto, G D'Andrea, and G Bussone. 2007. "Why Do We Need NIRS in Migraine?" *Neurol Sci* 28 Suppl 2 (May): S222-4. doi:10.1007/s10072-007-0782-4.

Lin, Luan, Yang Wang, and Haomin Zhou. 2009. "Iterative Filtering As an Alternative Algorithm for Empirical Mode Decomposition." *Advances in Adaptive Data Analysis* 1 (4): 543–60. doi:10.1142/S179353690900028X.

Lintas, G, F Molinari, V Simonetti, M Franzini, and W Liboni. 2013. "Time and Time-Frequency Analysis of near-Infrared Signals for the Assessment of Ozone Autohemotherapy Long-Term Effects in Multiple Sclerosis." *Conf Proc IEEE Eng Med Biol Soc* 2013 (January): 6171–74. doi:10.1109/EMBC.2013.6610962.

Lu, Fengmin, Mary Selak, John O'Connor, Sidney Croul, Carlos Lorenzana, Catalin Butunoi, and Bernadette Kalman. 2000. "Oxidative Damage to Mitochondrial DNA and Activity of Mitochondrial Enzymes in Chronic Active Lesions of Multiple Sclerosis." *Journal of the Neurological Sciences* 177 (2): 95–103. doi:10.1016/S0022-510X(00)00343-9.

Lupien, Sonia J, Bruce S McEwen, Megan R Gunnar, and Christine Heim. 2009. "Effects of Stress throughout the Lifespan on the Brain, Behaviour and Cognition." *Nature Reviews. Neuroscience* 10 (6): 434–45. doi:10.1038/nrn2639.

Machado, J.a. Tenreiro, António C. Costa, and Maria Dulce Quelhas. 2011. "Entropy Analysis of the DNA Code Dynamics in Human Chromosomes." *Computers & Mathematics with Applications* 62 (3). Elsevier Ltd: 1612–17. doi:10.1016/j.camwa.2011.03.005.

Madej, Paweł, Andrzej Plewka, Janusz A. Madej, Danuta Plewka, Wojciech Mroczka, Krzysztof Wilk, and Zuzanna Dobrosz. 2007. "Ozone Therapy in Induced Endotoxemic Shock. II. The Effect of Ozone Therapy upon Selected Histochemical Reactions in Organs of Rats in Endotoxemic Shock." *Inflammation* 30 (3–4): 69–86. doi:10.1007/s10753-007-9023-5.

Maggioni, Eleonora, Erika Molteni, Claudio Zucca, Gianluigi Reni, Sergio Cerutti,

Fabio M. Triulzi, Filippo Arrigoni, and Anna M. Bianchi. 2015. “Investigation of Negative BOLD Responses in Human Brain through NIRS Technique. A Visual Stimulation Study.” *NeuroImage* 108. Elsevier Inc.: 410–22. doi:10.1016/j.neuroimage.2014.12.074.

Martis, Roshan Joy, U Rajendra Acharya, Jen Hong Tan, Andrea Petznick, Louis Tong, Chua Kuang Chua, and Eddie Yin Kwee Ng. 2013. “Application of Intrinsic Time-Scale Decomposition (ITD) to EEG Signals for Automated Seizure Prediction.” *International Journal of Neural Systems* 23 (5). World Scientific Publishing Company: 1350023. doi:10.1142/S0129065713500238.

Marx, J. 2002. “Antibodies Kill by Producing Ozone.” *Science* 298: 1319. doi:10.1126/science.298.5597.1319.

McGowan, Craig P., Richard R. Neptune, David J. Clark, and Steven A. Kautz. 2010. “Modular Control of Human Walking: Adaptations to Altered Mechanical Demands.” *J Biomech* 43 (3). Elsevier: 412–19. doi:10.1016/j.jbiomech.2009.10.009.

McKay, J. Lucas, and Lena H Ting. 2008. “Functional Muscle Synergies Constrain Force Production during Postural Tasks.” *J Biomech* 41 (2): 299–306. doi:10.1016/j.jbiomech.2007.09.012.

McMorland, Angus J. C., Keith D. Runnalls, and Winston D. Byblow. 2015. “A Neuroanatomical Framework for Upper Limb Synergies after Stroke.” *Front Neurosci* 9 (February): 1–6. doi:10.3389/fnhum.2015.00082.

Menz, Hylton B., Alyssa B. Dufour, Jody L. Riskowski, Howard J. Hillstrom, and Marian T. Hannan. 2013. “Foot Posture, Foot Function and Low Back Pain: The Framingham Foot Study.” *Rheumatology (United Kingdom)* 52 (12): 2275–82. doi:10.1093/rheumatology/ket298.

Mirzal, Andri. 2017. “NMF versus ICA for Blind Source Separation.” *Advances in Data Analysis and Classification* 11 (1): 25–48. doi:10.1007/s11634-014-0192-4.

Molinari, Filippo, U. Rajendra Acharya, Roshan Joy Martis, Riccardo De Luca, Giuliana Petraroli, and William Liboni. 2013. “Entropy Analysis of Muscular near-Infrared Spectroscopy (NIRS) Signals during Exercise Programme of Type 2 Diabetic Patients: Quantitative Assessment of Muscle Metabolic Pattern.” *Comput Methods Programs Biomed* 112 (3). Elsevier Ireland Ltd: 518–28. doi:10.1016/j.cmpb.2013.08.018.

Molinari, Filippo, Roshan Joy Martis, U. Rajendra Acharya, Kristen M. Meiburger, Riccardo De Luca, Giuliana Petraroli, and William Liboni. 2015. “Empirical

Mode Decomposition Analysis of near-Infrared Spectroscopy Muscular Signals to Assess the Effect of Physical Activity in Type 2 Diabetic Patients." *Computers in Biology and Medicine* 59 (April): 1–9. doi:10.1016/j.compbiomed.2015.01.011.

Molinari, Filippo, William Liboni, Gianfranco Grippi, and Emanuela Negri. 2006. "Relationship between Oxygen Supply and Cerebral Blood Flow Assessed by Transcranial Doppler and near-Infrared Spectroscopy in Healthy Subjects during Breath-Holding." *J Neuroeng Rehabil* 3: 16. doi:10.1186/1743-0003-3-16.

Molinari, Filippo, Samanta Rosati, William Liboni, Emanuela Negri, Ornella Mana, Gianni Allais, and Chiara Benedetto. 2010. "Time-Frequency Characterization of Cerebral Hemodynamics of Migraine Sufferers as Assessed by NIRS Signals." *Eurasip Journal on Advances in Signal Processing* 2010 (1): 459213. doi:10.1155/2010/459213.

Molinari, Filippo, Vincenzo Simonetti, M Franzini, S Pandolfi, F Vaiano, L Valdenassi, and William Liboni. 2014. "Ozone Autohemotherapy Induces Long-Term Cerebral Metabolic Changes in Multiple Sclerosis Patients." *Int J Immunopathol Pharmacol* 27 (3): 379–89. http://www.ncbi.nlm.nih.gov/pubmed/25280029.

Monaco, Vito, Alessio Ghionzoli, and Silvestro Micera. 2010. "Age-Related Modifications of Muscle Synergies and Spinal Cord Activity during Locomotion." *J Neurophysiol* 104 (4): 2092–2102. doi:10.1152/jn.00525.2009.

Morovic, Sandra, and Paolo Zamboni. 2012. "CCSVI Is Associated with Multiple Sclerosis." *Neurological Research*. doi:10.1179/1743132812Y.0000000035.

Müller, Roy, Thomas Ertelt, and Reinhard Blickhan. 2015. "Low Back Pain Affects Trunk as Well as Lower Limb Movements during Walking and Running." *J Biomech* 48 (6). Elsevier: 1009–14. doi:10.1016/j.jbiomech.2015.01.042.

Mullinger, K J, S D Mayhew, a P Bagshaw, R Bowtell, and S T Francis. 2014. "Evidence That the Negative BOLD Response Is Neuronal in Origin: A Simultaneous EEG-BOLD-CBF Study in Humans." *NeuroImage* 94. Elsevier B.V.: 263–74. doi:10.1016/j.neuroimage.2014.02.029.

Muñoz, a. 1993. "Design and Analysis of Studies of the Health Effects of Ozone." *Environmental Health Perspectives* 101 Suppl (December): 231–35. doi:10.1289/ehp.93101s4231.

Mussa-Ivaldi, Ferdinando A., Simon F. Giszter, and Emilio Bizzi. 1994. "Linear

Combinations of Primitives in Vertebrate Motor Control." *Proc. Natl. Acad. Sci. USA* 91 (16): 7534–38. doi:10.1073/pnas.91.16.7534.

Mussa-Ivaldi, Ferdinando A, and Emilio Bizzi. 2000. "Motor Learning through the Combination of Primitives." *Phil Trans R Soc Lond B* 355 (1404): 1755–69. doi:10.1098/rstb.2000.0733.

Myers, Dean, Michelle McGraw, Mark George, Kristine Mulier, and Greg Beilman. 2009. "Tissue Hemoglobin Index: A Non-Invasive Optical Measure of Total Tissue Hemoglobin." *Critical Care* 13 (SUPPL. 5). doi:10.1186/cc8000.

Nakao, Atsunori, Ryujiro Sugimoto, Timothy R Billiar, and Kenneth R McCurry. 2009. "Therapeutic Antioxidant Medical Gas." *Journal of Clinical Biochemistry and Nutrition* 44 (1): 1–13. doi:10.3164/jcbn.08-193R.

Netter, Frank H. 2014. *Atlas of Human Anatomy*. Edited by John Hansen, Brion Benninger, Jennifer Brueckner-Collins, Todd M. Hoagland, and R. Shane Tubbs. 6th Editio. Philadelphia, PA: Saunders Elsevier.

Nishida, Koji, Shota Hagio, Benio Kibushi, Toshio Moritani, and Motoki Kouzaki. 2017. "Comparison of Muscle Synergies for Running between Different Foot Strike Patterns." *PLoS ONE* 12 (2): e0171535. doi:10.1371/journal.pone.0171535.

Nishimura, N, K Iwasaki, Y Ogawa, and S Shibata. 2007. "Oxygen Administration, Cerebral Blood Flow Velocity, and Dynamic Cerebral Autoregulation." *Aviat Space Environ Med.* 78 (12): 1121–27. https://www.ncbi.nlm.nih.gov/pubmed/18064916.

Obrig, Hellmuth, Markus Neufang, Rüdiger Wenzel, Matthias Kohl, Jens Steinbrink, Karl Einhäupl, and Arno Villringer. 2000. "Spontaneous Low Frequency Oscillations of Cerebral Hemodynamics and Metabolism in Human Adults." *NeuroImage* 12 (6): 623–39. doi:10.1006/nimg.2000.0657.

Oh, Dong-Hoon, and Joonho Choi. 2007. "Changes in the Regional Cerebral Perfusion After Eye Movement Desensitization and Reprocessing: A SPECT Study of Two Cases." *Journal of EMDR Practice and Research* 1 (1): 24–30. doi:10.1891/1933-3196.1.1.24.

Ohmine, Seiga. 2005. "Investigation of the Mechanisms of Ozone-Mediated Viral Inactivation." *All Theses and Dissertations*. Brigham Young University. http://scholarsarchive.byu.edu/etd/597.

Ohta ni, Toshiyuki, Koji Matsuo, Kiyoto Kasai, Tadafumi Kato, and Nobumasa Kato. 2009. "Hemodynamic Responses of Eye Movement Desensitization and

Reprocessing in Posttraumatic Stress Disorder." *Neuroscience Research* 65 (4): 375–83. doi:10.1016/j.neures.2009.08.014.

Oliveira, Anderson S, Leonardo Gizzi, Dario Farina, and Uwe G Kersting. 2014. "Motor Modules of Human Locomotion: Influence of EMG Averaging, Concatenation, and Number of Step Cycles." *Front Neurosci* 8 (May): 335. doi:10.3389/fnhum.2014.00335.

Oliveira, Anderson Souza, Priscila Brito Silva, Morten Enemark Lund, Leonardo Gizzi, Dario Farina, and Uwe Gustav Kersting. 2013. "Effects of Perturbations to Balance on Neuromechanics of Fast Changes in Direction during Locomotion." *PLoS ONE* 8 (3): 1–13. doi:10.1371/journal.pone.0059029.

Ostry, david J, and Anatol G Feldman. 2003. "A Critical Evaluation of the Force Control Hypothesis in Motor Control." *Exp Brain Res* 221: 275–88. doi:10.1007/s00221-003-1624-0.

Overduin, S. A., A. D'Avella, J. Roh, and Emilio Bizzi. 2008. "Modulation of Muscle Synergy Recruitment in Primate Grasping." *Journal of Neuroscience* 28 (4): 880–92. doi:10.1523/JNEUROSCI.2869-07.2008.

Owen-Reece, H, M Smith, C E Elwell, and J C Goldstone. 1999. "Near Infrared Spectroscopy." *Br J Anaesth* 82 (3): 418–26. doi:10.1038/nrn2330.

Paatero, Pentti. 1997. "Least Squares Formulation of Robust Nonnegative Factor Analysis." *Chemometr Intell Lab* 37 (1): 23–35. doi:doi.org/10.1016/S0169-7439(96)00044-5.

Pagani, Marco, Giorgio Di Lorenzo, Anna Rita Verardo, Giampaolo Nicolais, Leonardo Monaco, Giada Lauretti, Rita Russo, et al. 2012. "Neurobiological Correlates of EMDR Monitoring - An EEG Study." *PLoS ONE* 7 (9): 1–12. doi:10.1371/journal.pone.0045753.

Pagani, Marco, Göran Högberg, Dario Salmaso, Davide Nardo, Orjan Sundin, Cathrine Jonsson, Joaquim Soares, et al. 2007. "Effects of EMDR Psychotherapy on 99mTc-HMPAO Distribution in Occupation-Related Post-Traumatic Stress Disorder." *Nuclear Medicine Communications* 28 (10): 757–65. doi:10.1097/MNM.0b013e3282742035.

Palastanga, Nigel, and Roger Soames. 2012. *Anatomy and Human Movement: Structure and Function*. 6th Editio. London, United Kingdom: Elsevier Health Sciences.

Parker, James N, and Phillip M Parker, eds. 2004. *Lower Back Pain: A Medical Dictionary, Bibliography, and Annotated Research Guide to Internet*

References. ICON Group International, Inc.

Patla, Aftab E. 1985. “Some Characteristics of EMG Patterns during Locomotion: Implications for the Locomotor Control Process.” *J Mot Behav* 17 (4): 443–61. doi:dx.doi.org/10.1080/00222895.1985.10735360.

Patterson, Michael S, Britton Chance, and B C Wilson. 1989. “Time Resolved Reflectance and Transmittance for the Non- Invasive Measurement of Tissue Optical Properties.” *Applied Optics* 28 (12): 2331–36. doi:10.1364/AO.28.002331.

Perrier, Pascal, David J Ostry, and Rafael Laboissière. 1996. “The Equilibrium Point Hypothesis and Its Application to Speech Motor Control.” *Journal of Speech, Language, and Hearing Research* 39 (2): 365–78.

Perry, Jacquelin. 1992. *Gait Analysis. Normal and Pathological Function*. First edit. SLACK Incorporated.

Pincus, S M. 2001. “Assessing Serial Irregularity and Its Implications for Health.” *Annals of the New York Academy of Sciences* 954 (December): 245–67.

Pincus, S M, and A L Goldberger. 1994. “Physiological Time-Series Analysis: What Does Regularity Quantify?” *The American Journal of Physiology* 266 (4 Pt 2): H1643-56.

Polit, Andres, and Emilio Bizzi. 1978. “Processes Controlling Arm Movements in Monkeys.” *Science* 201 (8): 1235–37.

———. 1979. “Characteristics of Motor Programs Underlying Arm Movements in Monkeys.” *J Neurophysiol* 42 (1): 183–94.

Poppler, CG, X Duan, AR Buckpitt, and KE Pinkerton. 1994. “Dose-Dependent Tolerance to Ozone: IV. Site-Specific Elevation in Antioxidant Enzymes in the Lungs of Rats Exposed for 90 Days or 20 Months.” *Toxicology and Applied Pharmacology* 127 (1). doi:doi.org/10.1006/taap.1994.1146.

Pryor, Wa William A, Kn Kendall N Houk, Christopher S Foote, Jon M Fukuto, Louis J Ignarro, Giuseppe L Squadrito, and Kelvin J A Davies. 2006. “Free Radical Biology and Medicine: It’s a Gas, Man!” *Am J Physiol Regul Integr Comp Physiol* 291 (3): R491-511. doi:10.1152/ajpregu.00614.2005.

Rana, Manku, Moheb S Yani, Skulpan Asavasopon, Beth E Fisher, and Jason J Kutch. 2015. “Brain Connectivity Associated with Muscle Synergies in Humans.” *J Neurosci* 35 (44): 14708–16. doi:10.1523/JNEUROSCI.1971-15.2015.

Ranganathan, R., and C. Krishnan. 2012. “Extracting Synergies in Gait: Using EMG Variability to Evaluate Control Strategies.” *J Neurophysiol* 108 (5): 1537–44. doi:10.1152/jn.01112.2011.

Rangayyan, Rangaraj M. 2015. *Biomedical Signal Analysis, 2nd Edition*. Wiley-IEEE Press. http://eu.wiley.com/WileyCDA/WileyTitle/productCd-0470911395.html.

Rangel-Castilla, Leonardo, Lucia Rivera Lara, Shankar Gopinath, Paul R. Swank, Alex Valadka, and Claudia Robertson. 2010. “Cerebral Hemodynamic Effects of Acute Hyperoxia and Hyperventilation after Severe Traumatic Brain Injury.” *Journal of Neurotrauma* 27 (10): 1853–63. doi:10.1089/neu.2010.1339.

Re, Lamberto, Gregorio Martínez-Sánchez, Marica Bordicchia, Giuseppe Malcangi, Antonella Pocognoli, Miguel Angel Morales-Segura, John Rothchild, and Armando Rojas. 2014. “Is Ozone Pre-Conditioning Effect Linked to Nrf2/EpRE Activation Pathway in Vivo? A Preliminary Result.” *Eur J Pharmacol* 742 (November): 158–62. doi:10.1016/j.ejphar.2014.08.029.

Rebet, Olivier, Marc-Olivier Fischer, Guillaume Zamparini, Jean-Louis Gérard, Jean-Luc Fellahi, and Jean-Luc Hanouz. 2015. “Near-Infrared Spectroscopy Hemoglobin Index Measurement During Fluid Challenge: A Prospective Study in Cardiac Surgery Patients.” *J Cardiothorac Vasc Anesth* 29 (4). Elsevier: 924–29. doi:10.1053/j.jvca.2015.01.013.

Richman, J S, and J R Moorman. 2000. “Physiological Time-Series Analysis Using Approximate Entropy and Sample Entropy.” *American Journal of Physiology. Heart and Circulatory Physiology* 278 (6): H2039–49.

Richman, Joshua S, J Randall Moorman, Motoo Yamauchi, Shinji Tamaki, Masanori Yoshikawa, Yoshinobu Ohnishi, Hiroshi Nakano, et al. 2011. “Physiological Time-Series Analysis Using Approximate Entropy and Sample Entropy.” *Cardiovascular Research*, 2039–49.

Rilling, Gabriel, Patrick Flandrin, and Paulogonçal Es. 2003. “On Empirical Mode Decomposition and Its Algorithms.” *IEEE-EURASIP Workshop on Nonlinear Signal and Image Processing* 3: 8–11. doi:10.1109/ICASSP.2008.4518437.

Rimini, Daniele, Filippo Molinari, William Liboni, Vincenzo Simonetti, and Marianno Franzini. 2016. “The Speed of Reinfusion Affects the Vascular System during Ozone Major Autohemotherapy.” *Ozone Therapy* 1 (6477): 56–60. doi:10.4081/ozone.2016.6477.

Rivadulla, Casto, Carmen de Labra, Kenneth L. Grieve, and Javier Cudeiro. 2011.

"Vasomotion and Neurovascular Coupling in the Visual Thalamus in Vivo." *PLoS ONE* 6 (12). doi:10.1371/journal.pone.0028746.

Rodriguez, S. Carmen. 2001. "Pain Measurement in the Elderly: A Review." *Pain Management Nursing* 2 (2): 38–46. doi:doi.org/10.1053/jpmn.2001.23746.

Roh, J., V. C. K. Cheung, and Emilio Bizzi. 2011. "Modules in the Brain Stem and Spinal Cord Underlying Motor Behaviors." *J Neurophysiol* 106 (3): 1363–78. doi:10.1152/jn.00842.2010.

Rosati, Samanta, Valentina Agostini, Marco Knaflitz, and Gabriella Balestra. 2017. "Muscle Activation Patterns during Gait: A Hierarchical Clustering Analysis." *Biomedical Signal Processing and Control* 31: 463–69. doi:10.1016/j.bspc.2016.09.017.

Rosati, Samanta, Gabriella Balestra, and Filippo Molinari. 2012. "Feature Selection Applied To the Time-Frequency Representation of Muscle Near-Infrared Spectroscopy (Nirs) Signals: Characterization of Diabetic Oxygenation Patterns." *Journal of Mechanics in Medicine and Biology* 12 (4). doi:10.1142/S0219519412400131.

Rossignol, Serge, Réjean Dubuc, and Jean-Pierre Gossard. 2006. "Dynamic Sensorimotor Interactions in Locomotion." *Physiological Reviews* 86 (1): 89–154. doi:10.1152/physrev.00028.2005.

Sadeghi, Heydar, Paul Allard, Fran??ois Prince, and Hubert Labelle. 2000. "Symmetry and Limb Dominance in Able-Bodied Gait: A Review." *Gait Posture* 12 (1): 34–45. doi:10.1016/S0966-6362(00)00070-9.

Safavynia, Seyed A., Gelsy Torres-Oviedo, and Lena H Ting. 2011. "Muscle Synergies: Implications for Clinical Evaluation and Rehabilitation of Movement." *Topics in Spinal Cord Injury Rehabilitation* 17 (1): 16–24. doi:10.1310/sci1701-16.

Sainburg, Robert L. 2015. "Should the Equilibrium Point Hypothesis (EPH) Be Considered a Scientific Theory?" *Motor Control* 19 (2): 142–48. doi:10.1123/mc.2014-0056.

Sakatani, Kaoru, Yuxiao Xie, Wemara Lichty, Sunwei Li, and Huancong Zuo. 1998. "Language-Activated Cerebral Blood Oxygenation and Hemodynamic Changes of the Left Prefrontal Cortex in Poststroke Aphasic Patients." *Stroke* 29 (7): 12–14. doi:10.1161/01.STR.29.7.1299.

Sakatani, K, Y Xie, W Lichty, S Li, and H Zuo. 1998. "Language-Activated Cerebral Blood Oxygenation and Hemodynamic Changes of the Left

Prefrontal Cortex in Poststroke Aphasic Patients: A near-Infrared Spectroscopy Study." *Stroke; a Journal of Cerebral Circulation* 29 (7): 1299–1304.

Saltiel, Philippe, Matthew C Tresch, Emilio Bizzi, Philippe Saltiel, Matthew C Tresch, and Emilio Bizzi. 1998. "Spinal Cord Modular Organization and Rhythm Generation : An NMDA Iontophoretic Study in the Frog." *J Neurophysiol* 80: 2323–39.

Salvi, Massimo, Daniele Rimini, Filippo Molinari, Gianni Bestente, and Alberto Bruno. 2017. "Effect of Low-Level Light Therapy on Diabetic Foot Ulcers: A near-Infrared Spectroscopy Study." *J Biomed Opt* 22 (3): 38001. doi:10.1117/1.JBO.22.3.038001.

Sartori, Massimo, Leonardo Gizzi, Vincent C K Cheung, Carolynn Patten, Caitlin L Banks, Mihir M Pai, Theresa E Mcguirk, and Benjamin J Fregly. 2017. "Methodological Choices in Muscle Synergy Analysis Impact Differentiation of Physiological Characteristics Following Stroke." *Front Comput Neurosci* 11 (August): 1–12. doi:10.3389/fncom.2017.00078.

Sassaroli, Angelo, and Sergio Fantini. 2004. "Comment on the Modified Beer-Lambert Law for Scattering Media." *Phys Med Biol* 49 (14): 255–57. doi:10.1088/0031-9155/49/14/N07.

Scholkmann, Felix, Stefan Kleiser, Andreas Jaakko Metz, Raphael Zimmermann, Juan Mata Pavia, Ursula Wolf, and Martin Wolf. 2014. "A Review on Continuous Wave Functional near-Infrared Spectroscopy and Imaging Instrumentation and Methodology." *NeuroImage* 85: 6–27. doi:10.1016/j.neuroimage.2013.05.004.

Schubert, Sarah J., Christopher W. Lee, and Peter D. Drummond. 2011. "The Efficacy and Psychophysiological Correlates of Dual-Attention Tasks in Eye Movement Desensitization and Reprocessing (EMDR)." *Journal of Anxiety Disorders* 25 (1). Elsevier Ltd: 1–11. doi:10.1016/j.janxdis.2010.06.024.

Schytz, Henrik W., Song Guo, Lars T. Jensen, Moshe Kamar, Asaph Nini, Daryl R. Gress, and Messoud Ashina. 2012. "A New Technology for Detecting Cerebral Blood Flow: A Comparative Study of Ultrasound Tagged NIRS and 133Xe-SPECT." *Neurocritical Care* 17 (1): 139–45. doi:10.1007/s12028-012-9720-2.

Serrancolí, Gil, Joan C. Monllau, and Josep M. Font-Llagunes. 2016. "Analysis of Muscle Synergies and Activation-Deactivation Patterns in Subjects with Anterior Cruciate Ligament Deficiency during Walking." *Clin Biomech (Bristol, Avon)* 31. Elsevier Ltd: 65–73.

doi:10.1016/j.clinbiomech.2015.09.019.

Shadmehr, Reza. 1995. “The Equilibrium Point Hypothesis for Control of Movements.” In *Handbook of Brain Theory and Neural Networks*, edited by MA Arbib, 370–72. MIT Press.

Shah, Prasham, Ashok K Shyam, and Sambhav Shah. 2011. “Adjuvant Combined Ozone Therapy for Extensive Wound over Tibia.” *Indian Journal of Orthopaedics* 45 (4): 376–79. doi:10.4103/0019-5413.80332.

Shalev, A. Y., M. J. Friedman, E. B. Foa, and T. M. Keane. 2000. “Integration and Summary.” In *Effective Treatments for PTSD: Practice Guidelines from the International Society for Traumatic Stress Studies*, edited by E. A. Foa and T. M. Keane, M. J, Frie, 359–79. Guilford Press. https://www.guilford.com/books/Effective-Treatments-for-PTSD/Foa-Keane-Friedman-Cohen/9781609181499/reviews.

Shannon, Claude E. 1948. “A Mathematical Theory of Communication.” *The Bell System Technical Journal* 27 (July 1928): 379–423. doi:10.1145/584091.584093.

Shapiro, Francine. 2001. *Eye Movement Desensitization and Reprocessing (EMDR) Therapy, Third Edition: Basic Principles, Protocols, and Procedures*. 2nd Editio. The Guilford Press.

Shapiro, Francine, F. W. Klaslow, and Louise Maxfield. 2007. *Handbook of EMDR and Family Therapy Processes*. First Ed. Wiley.

Shapiro, Francine, and Louise Maxfield. 2002. “Eye Movement Desensitization and Reprocessing.” *Encyclopedia of Psychoterapy*.

Sharif Razavian, Reza, Naser Mehrabi, and John McPhee. 2015. “A Model-Based Approach to Predict Muscle Synergies Using Optimization: Application to Feedback Control.” *Front Comput Neurosci* 9 (October): 121. doi:10.3389/FNCOM.2015.00121.

Shieh, Min Zheng, and Shi Chun Tsai. 2010. “Decoding Frequency Permutation Arrays under Chebyshev Distance.” *IEEE Transactions on Information Theory* 56 (11): 5730–37. doi:10.1109/TIT.2010.2069253.

Shourijeh, Mohammad S., Teresa E. Flaxman, and Daniel L. Benoit. 2015. “An Approach for Improving Repeatability and Reliability of Non-Negative Matrix Factorization for Muscle Synergy Analysis.” *J Electromyogr Kinesiol* 26. Elsevier Ltd: 1–8. doi:10.1016/j.jelekin.2015.12.001.

Shuman, Benjamin, Marije Goudriaan, Lynn Bar-On, Michael H. Schwartz, Kaat

Desloovere, and Katherine M. Steele. 2016. “Repeatability of Muscle Synergies Within and Between Days for Typically Developing Children and Children With Cerebral Palsy.” *Gait Posture* 45. Elsevier B.V.: 127–32. doi:10.1016/j.gaitpost.2016.01.011.

Shuman, Benjamin R., Michael H. Schwartz, and Katherine M. Steele. 2017. “Electromyography Data Processing Impacts Muscle Synergies during Gait for Unimpaired Children and Children with Cerebral Palsy.” *Front Comput Neurosci* 11 (June): 1–9. doi:10.3389/fncom.2017.00050.

Sil Kar, Sudeshna, and Santi P. Maity. 2016. “Retinal Blood Vessel Extraction Using Tunable Bandpass Filter and Fuzzy Conditional Entropy.” *Computer Methods and Programs in Biomedicine* 133. Elsevier Ireland Ltd: 111–32. doi:10.1016/j.cmpb.2016.05.015.

Simonetti, Vincenzo, William Liboni, and Filippo Molinari. 2014. “Why Ozone Therapy in Multiple Sclerosis?” *Revista Española de Ozonoterapia* 4 (1): 51–68.

Sloot, L. H., M. M. van der Krogt, and J. Harlaar. 2014. “Self-Paced versus Fixed Speed Treadmill Walking.” *Gait Posture* 39 (1). Elsevier B.V.: 478–84. doi:10.1016/j.gaitpost.2013.08.022.

Smith, Edward E., and John Jonides. 1997. “Working Memory: A View from Neuroimaging.” *Cognitive Psychology* 33 (1): 5–42. doi:10.1006/cogp.1997.0658.

Smith, NoelL, AnthonyL Wilson, Jason Gandhi, Sohrab Vatsia, and SardarAli Khan. 2017. “Ozone Therapy: An Overview of Pharmacodynamics, Current Research, and Clinical Utility.” *Medical Gas Research* 7 (3): 212. doi:10.4103/2045-9912.215752.

Smith, Sean M., and Wylie W. Vale. 2006. “The Role of the Hypothalamic-Pituitary-Adrenal Axis in Neuroendocrine Responses to Stress.” *Dialogues in Clinical Neuroscience* 8 (4): 383–95. doi:10.1038/nrendo.2011.222.

Sokunbi, Moses O., George G. Cameron, Trevor S. Ahearn, Alison D. Murray, and Roger T. Staff. 2015. “Fuzzy Approximate Entropy Analysis of Resting State fMRI Signal Complexity across the Adult Life Span.” *Medical Engineering & Physics* 37 (11). Elsevier Ltd: 1082–90. doi:10.1016/j.medengphy.2015.09.001.

Sporns, Olaf, and Gerald M Edelman. 1993. “Solving Bernstein’s Problem: A Proposal for the Development of Coordinated Movement by Selection.” *Child Dev* 64 (4): 960–81. doi:10.1111/j.1467-8624.1993.tb04182.x.

Srinivasan, Satish, and Narayan G. Avadhani. 2012. “Cytochrome c Oxidase Dysfunction in Oxidative Stress.” *Free Radical Biology and Medicine* 53 (6). Elsevier: 1252–63. doi:10.1016/j.freeradbiomed.2012.07.021.

Steele, Katherine M., Matthew C. Tresch, and Eric J. Perreault. 2013. “The Number and Choice of Muscles Impact the Results of Muscle Synergy Analyses.” *Front Comput Neurosci* 7 (August): 1–9. doi:10.3389/fncom.2013.00105.

Steele, Katherine M, Adam Rozumalski, and Michael H Schwartz. 2015. “Muscle Synergies and Complexity of Neuromuscular Control during Gait in Cerebral Palsy.” *Dev Med Child Neurol*, n/a-n/a. doi:10.1111/dmcn.12826.

Steele, Katherine Muterspaugh, Matthew C. Tresch, and Eric J. Perreault. 2015. “Consequences of Biomechanically Constrained Tasks in the Design and Interpretation of Synergy Analyses.” *J Neurophysiol* 113 (January): jn.00769.2013. doi:10.1152/jn.00769.2013.

Strangman, Gary, David A. Boas, and Jeffrey P. Sutton. 2002. “Non-Invasive Neuroimaging Using near-Infrared Light.” *Biol Psychiatry* 52 (7): 679–93. doi:10.1016/S0006-3223(02)01550-0.

Stuss, Donald T., and Robert T. Knight. 2002. *Principles of Frontal Lobe Function*. Oxford Scholarship Online. doi:10.1093/acprof:oso/9780195134971.001.0001.

Sutherland, David H. 2001. “The Evolution of Clinical Gait Analysis Part I: Kinesiological EMG.” *Gait Posture* 14 (1): 61–70. doi:10.1016/S0966-6362(01)00100-X.

Suzuki, Keisuke, Yusuke Nishida, and Kazuhiko Mitsutomi. 2014. “Association between Muscle Synergy and Stability during Prolonged Walking.” *J Phys Ther Sci* 26 (10): 1637–40. doi:10.1589/jpts.26.1637.

Suzuki, Susumu, Sumio Takasaki, Takeo Ozaki, and Yukio Kobayashi. 1999. “Tissue Oxygenation Monitor Using NIR Spatially Resolved Spectroscopy.” In *Proc. SPIE 3597, Optical Tomography and Spectroscopy of Tissue III*. doi:10.1117/12.356862.

Tamura, M, O Hazeki, S Nioka, Britton Chance, and DS Smith. 1988. “The Simultaneous Measurements of Tissue Oxygen Concentration and Energy State by near-Infrared and Nuclear Magnetic Resonance Spectroscopy.” *Adv Exp Med Biol* 222: 359–63. https://www.ncbi.nlm.nih.gov/pubmed/3364259.

Thoroughman, K A, and R Shadmehr. 2000. “Learning of Action Trough Adaptative Combination of Motor Primitives.” *Nature* 407 (6805): 742–47.

doi:10.1038/35037588.Learning.

Ting, Lena H, Hillel J Chiel, Randy D Trumbower, Jessica L Allen, J. Lucas McKay, Madeleine E Hackney, and Trisha M Kesar. 2015. “Neuromechanical Principles Underlying Movement Modularity and Their Implications for Rehabilitation.” *Neuron* 86 (1). Elsevier Inc.: 38–54. doi:10.1016/j.neuron.2015.02.042.

Ting, Lena H, and Stacie A. Chvatal. 2010. “Decomposing Muscle Activity in Motor Tasks: Methods and Interpretation.” In *Motor Control*, edited by F Danion and Mark L. Latash, 102–38. New York: Oxford University Press. doi:10.1093/acprof:oso/9780195395273.003.0005.

Ting, Lena H, and Jane M Macpherson. 2005. “A Limited Set of Muscle Synergies for Force Control during a Postural Task.” *J Neurophysiol* 93 (1): 609–13. doi:10.1152/jn.00681.2004.

Torres-Oviedo, Gelsy, and Lena H Ting. 2007. “Muscle Synergies Characterizing Human Postural Responses.” *J Neurophysiol* 98 (4): 2144–56. doi:10.1152/jn.01360.2006.

———. 2010. “Subject-Specific Muscle Synergies in Human Balance Control Are Consistent Across Different Biomechanical Contexts.” *J Neurophysiol* 103 (6): 3084–98. doi:10.1152/jn.00960.2009.

Trapp, Bruce D., and Klaus-Armin Nave. 2008. “Multiple Sclerosis: An Immune or Neurodegenerative Disorder?” *Annual Review of Neuroscience* 31 (1): 247–69. doi:10.1146/annurev.neuro.30.051606.094313.

Trapp, Bruce D., John Peterson, Richard M. Ransohoff, Richard Rudick, Sverre Mörk, and Lars Bö. 1998. “Axonal Transection in the Lesions of Multiple Sclerosis.” *Engl J MEd* 338 (5): 278–85. doi:10.1056/NEJM199801293380502.

Tresch, Matthew C., P Saltiel, and Emilio Bizzi. 1999. “The Construction of Movement by the Spinal Cord.” *Nature Neuroscience* 2 (2): 162–67. doi:10.1038/5721.

Tresch, Matthew C, Vincent C K Cheung, and Andrea d’Avella. 2006. “Matrix Factorization Algorithms for the Identification of Muscle Synergies: Evaluation on Simulated and Experimental Data Sets.” *J Neurophysiol* 95 (4): 2199–2212. doi:10.1152/jn.00222.2005.

Turpin, Nicolas A, A. Guével, A. Dossat, S. Durand, and F. Hug. 2010. “Recognition of Muscle Functional Organisation in Rowing by Synergy

Identification." *Comput Methods Biomech Biomed Engin* 13 (sup1): 141–42. doi:10.1080/10255842.2010.495876.

Urra, O, A Casals, and R Jané. 2014. "Synergy Analysis as a Tool to Design and Assess an Effective Stroke Rehabilitation." In *Conf Proc IEEE Eng Med Biol Soc*, 3550–53.

Ursano, RJ, C Bell, S Eth, M Friedman, A Norwood, B Pfefferbaum, JD Pynoos, et al. 2004. "Practice Guideline for the Treatment of Patients with Acute Stress Disorder and Posttraumatic Stress Disorder." *Am J Psychiatry* 161 (11 Suppl): 3–31.

Valacchi, G, and Velio Bocci. 1999. "Studies on the Biological Effects of Ozone: 10. Release of Factors from Human Endothelial Cells." *Mediators of Inflammation* 8 (4–5): 205–9. doi:10.1080/09629359990360.

van der Kolk, Bessel. 2005. "Developmental Trauma Disorder: Toward a Rational Diagnosis for Children with Complex Trauma Histories." *Psychiatric Annals* 35 (5): 401–8.

van der Linden, M H, D S Marigold, F J Gabreels, and J Duysens. 2007. "Muscle Reflexes and Synergies Triggered by an Unexpected Support Surface Height during Walking." *J Neurophysiol* 97 (5): 3639–50. doi:10.1152/jn.01272.2006.

Van Haren, Robert M., Mark L. Ryan, Chad M. Thorson, Nicholas Namias, Alan S. Livingstone, and Kenneth G. Proctor. 2013. "Bilateral near-Infrared Spectroscopy for Detecting Traumatic Vascular Injury." *Journal of Surgical Research* 184 (1): 526–32. doi:10.1016/j.jss.2013.03.090.

van Middelkoop, M, S M Rubinstein, A P Verhagen, R W Ostelo, B W Koes, and M W van Tulder. 2010. "Exercise Therapy for Chronic Nonspecific Low-Back Pain." *Best Pract Res Clin Rheumatol* 24 (2). Elsevier Ltd: 193–204. doi:10.1016/j.berh.2010.01.002.

Victora Ruas, Cassio, and Adriane Vieira. 2017. "Do Muscle Strength Imbalances and Low Flexibility Levels Lead to Low Back Pain? A Brief Review." *J Funct Morphol Kinesiol* 2 (3): 29. doi:10.3390/jfmk2030029.

Viebahn, Renate. 1994. *The Use of Ozone in Medicine: A Practical Handbook*. 2nd Editio. Haug.

Villringer, A., J. Planck, C. Hock, L. Schleinkofer, and U. Dirnagl. 1993. "Near Infrared Spectroscopy (NIRS): A New Tool to Study Hemodynamic Changes during Activation of Brain Function in Human Adults." *Neuroscience Letters*

154 (1–2): 101–4. doi:10.1016/0304-3940(93)90181-J.

Villringer, Arno, and Hellmuth Obrig. 2002. “Near-Infrared Spectroscopy and Imaging.” In *Brain Mapping: The Methods (Second Edition)*, edited by Arthur W Toga and John C Mazziotta, 141–58. Elsevier. doi:doi.org/10.1016/B978-012693019-1/50008-3.

von Siebenthal, K, G Bernert, and P Casaer. 1992. “Near-Infrared Spectroscopy in Newborn Infants.” *Brain Dev* 14 (3): 135–43. https://www.ncbi.nlm.nih.gov/pubmed/1514651.

Waltz, Xavier, Marie Dominique Hardy-Dessources, Nathalie Lemonne, Danièle Mougenel, Marie Laure Lalanne-Mistrih, Yann Lamarre, Vanessa Tarer, et al. 2015. “Is There a Relationship between the Hematocrit-to-Viscosity Ratio and Microvascular Oxygenation in Brain and Muscle?” *Clinical Hemorheology and Microcirculation* 59 (1): 37–43. doi:10.3233/CH-131742.

Wang, Yang, and Zhengfang Zhou. 2012. “On the Convergence of Iterative Filtering Empirical Mode Decomposition.” In *Excursions in Harmonic Analysis, Volume 2*, edited by Travis D. Andrews, Radu Balan Okoudjou, John J. Benedetto, and Wojciech CzajaKasso A., 157–72. Birkhäuser, Boston. doi:https://doi.org/10.1007/978-0-8176-8379-5.

Watanabe, Kohei, Toshiaki Miyamoto, Yoji Tanaka, Kazuhito Fukuda, and Toshio Moritani. 2012. “Type 2 Diabetes Mellitus Patients Manifest Characteristic Spatial EMG Potential Distribution Pattern during Sustained Isometric Contraction.” *Diabetes Res Clin Pract* 97 (3): 468–73. doi:10.1016/j.diabres.2012.03.004.

“WFOT’s Review on Evidence Based Ozone Therapy.” 2015. http://www.wfoot.org/wp-content/uploads/2016/01/WFOT-OZONE-2015-ENG.pdf.

Whittle, Michael W. 2007. *Gait Analysis: An Introduction*. 4th Editio. Elsevier Health Sciences.

Wilson, S. A., R. H. Tinker, and L. A. Becker. 1995. “Eye Movement Desensitization and Reprocessing (EMDR) Treatment for Psychologically Traumatized Individuals.” *Journal of Consulting and Clinical Psychology* 63 (6): 928–37. doi:dx.doi.org/10.1037/0022-006X.63.6.928.

Winter, David A. 1987. *The Biomechanics and Motor Control of Human Gait*. Waterloo, Ontario, Canada: University of Waterloo Press.

———. 1995. “Human Balance and Posture Control during Standing and

Walking." *Gait Posture* 3 (4): 193–214. doi:10.1016/0966-6362(96)82849-9.

World Health Organisation. 2013. "Guidelines for the Management of Conditions Specifically Related to Stress." Geneva.

Wu, Xiao-na, Tao Zhang, Jun Wang, Xiao-yan Liu, Zhen-sheng Li, Wei Xiang, Wei-qing Du, et al. 2016. "Magnetic Resonance Diffusion Tensor Imaging Following Major Ozonated Autohemotherapy for Treatment of Acute Cerebral Infarction." *Neural Regeneration Research* 11 (7): 1115. doi:10.4103/1673-5374.187046.

Xie, Hong Bo, Jing Yi Guo, and Yong Ping Zheng. 2010. "Fuzzy Approximate Entropy Analysis of Chaotic and Natural Complex Systems: Detecting Muscle Fatigue Using Electromyography Signals." *Annals of Biomedical Engineering* 38 (4): 1483–96. doi:10.1007/s10439-010-9933-5.

Yang, Zhihua, and Lihua Yang. 2009. "A New Definition of the Intrinsic Mode Function." *Engineering and Technology* 60 (8620): 822–25. http://citeseerx.ist.psu.edu/viewdoc/download?doi=10.1.1.193.338&rep=rep1&type=pdf.

Yeung, Andy W. K., Tazuko K. Goto, and W. Keung Leung. 2017. "At the Leading Front of Neuroscience: A Bibliometric Study of the 100 Most-Cited Articles." *Front Hum Neurosci* 11 (July): 1–15. doi:10.3389/fnhum.2017.00363.

Zadeh, L. A. 1965. "Fuzzy Sets." *Information and Control* 8 (3): 338–53. doi:10.1016/S0019-9958(65)90241-X.

Zaky, Saad, Sherif Ebrahiem Kamel, Magda Shahata Hassan, Nadia Abdel Sallam, Mohamad Ahmad Shahata, Shaaban Redwan Helal, and Heba Mahmoud. 2011. "Preliminary Results of Ozone Therapy as a Possible Treatment for Patients with Chronic Hepatitis C." *J Altern Complement Med* 17 (3): 259–63. doi:10.1089/acm.2010.0016.

Zar, Jerrold H. 2010. *Biostatistical Analysis*. 5thed. Upper Saddle River, New Jersey: Pearson.

Zarghi, Afsaneh, Alireza Zali, and Tehranidost Mehdi. 2013. "Methodological Aspects of Cognitive Rehabilitation with Eye Movement Desensitization and Reprocessing (EMDR)." *Basic Clin Neurosci.* 4 (1): 97–103.

Zaylaa, Amira, Souad Oudjemia, Jamal Charara, and Jean Marc Girault. 2015. "N-Order and Maximum Fuzzy Similarity Entropy for Discrimination of Signals of Different Complexity: Application to Fetal Heart Rate Signals." *Computers in Biology and Medicine* 64. Elsevier: 323–33.

doi:10.1016/j.compbiomed.2015.03.006.

Zehr, E Paul. 2005. “Neural Control of Rhythmic Human Movement: The Common Core Hypothesis.” *Exerc Sport Sci Rev* 33 (1): 54–60. http://www.ncbi.nlm.nih.gov/pubmed/15640722%5Cnhttp://journals.lww.com/acsm-essr/Abstract/2005/01000/Neural_Control_of_Rhythmic_Human_Movement__The.10.aspx.

Zelik, Karl E, Valentina La Scaleia, Yuri P Ivanenko, and Francesco Lacquaniti. 2014. “Can Modular Strategies Simplify Neural Control of Multidirectional Human Locomotion?” *J Neurophysiol* 111 (8): 1686–1702. doi:10.1152/jn.00776.2013.

Zhu, Guohun, Yan Li, Peng (Paul) Wen, and Shuaifang Wang. 2014. “Classifying Epileptic EEG Signals with Delay Permutation Entropy and Multi-Scale K-Means.” In *Signal and Image Analysis for Biomedical and Life Sciences*, edited by Wang D. Sun C., Bednarz T., Pham T., Vallotton P., Signal and, 143–57. Springer, Cham. doi:doi.org/10.1007/978-3-319-10984-8_8.